FATIGUE CRACKING OF BITUMINOUS PAVING MIXTURES

JOHN MADDISON READ



A dissertation submitted to the University of Nottingham
for the Degree of Doctor of Philosophy

University of Nottingham, Department of Civil Engineering

May, 1996

To Jane

ACKNOWLEDGEMENTS AND DECLARATION

I would like to thank all those people who helped, encouraged and generally cajoled me into writing this thesis, without their efforts it would certainly never have been completed.

I am forever in the debt of Professor S.F.Brown and Professor P.S.Pell, my supervisors, who's enthusiasm and energy meant they were always there with encouragement, and constructive criticism, whenever required. I would also like to thank Todd and Mike who worked with me for nearly 4 years without losing their minds, a feat which nobody else has ever achieved, and Dr. N.H.Thom with whom I had many fruitful discussions and from whom I learnt much. Over the latter stages of this project I had many interesting and stimulating talks with Dr. A.C.Collop, and for this I thank him. I would also like to mention all the researchers of the Pavement and Geotechnics Research Group with whom, over numerous cups (or buckets) of tea, I had lots of discussions (or sometimes arguments) from which I feel I learnt a great deal.

The experimental work would have been impossible without the tremendous amount of hard work by Ehsan and Shane and the mechanical wizardry of Denis and to them I would like to say the biggest thankyou of all. Keith Cooper, the Chief Experimental Officer, who guided me at the beginning and taught me much before he retired was an inspiration to me and for that I am extremely grateful. I would also like to thank all the other technical staff who have helped me along the way, especially Barry Broderick.

This work was funded by the Environmental and Physical Sciences Research Council (EPSRC), the Department of Transport, Cooper Research Technology Limited, Esso Petroleum Company Limited, Foster Yeoman Limited, Mobil Oil Company Limited, Nynas Bitumen, Shell Bitumen, SWK Pavement Engineering Limited, Tarmac Roadstone Limited Wimpey Environmental Limited, the Worshipful Company of

Paviors, the County Surveyor's Society and the Rees Jeffreys Road fund, and I am grateful for their generous support. I would also like to mention all the people at the various County Council Laboratories who managed to help me immensely even though they had no financial means to do so.

Finally, let me thank all those who have assisted me in some way but have not been specifically mentioned above.

The work described in this dissertation was carried out at the University of Nottingham, Department of Civil Engineering between June 1992 and September 1995. This dissertation is the result of my own work, except where specific reference has been made to the work of others. No part of the work has been, or is currently being, submitted for any degree, diploma or other qualification.

ABSTRACT

This dissertation is concerned with the fatigue cracking of bituminous paving mixtures. It considers both the life to crack initiation and the life for crack propagation, including the development of a method for calculating the number of wheel load applications to either critical or failure condition.

The development and subsequent validation of the Indirect Tensile Fatigue Test (ITFT) are described. Both the repeatability and reproducibility of the method are examined as well as its correlation with two other fatigue test methods. The test is shown to be a suitable method for measuring the life to crack initiation of bituminous paving mixtures as well as being an economically viable test.

Poisson's ratio for bituminous paving mixtures is examined showing that, provided at least 500 conditioning pulses are used in order to achieve steady state conditions, 0.35 is an appropriate value. Prior to these early load applications Poisson's ratio is shown to be variable and often in excess of 0.50, an explanation of which is given in detail.

Crack propagation was experimentally simulated using beams of material with a crack initiated on the underside. The work shows that the rate of crack propagation can be described by a power relationship between the stiffness of the mixture and the number of cycles to failure, which is mixture and binder dependent. A general equation is developed which allows the critical and failure lives of bituminous pavements to be calculated and these are compared to two traditional pavement design methods, giving equivalent results for unmodified mixtures but, giving more realistic results for polymer modified mixtures. Image analysis of the cracks demonstrates that they propagate around coarse aggregate trying to separate it from the matrix and that they travel in the straightest line possible between the point of crack initiation and the point of applied load.

CONTENTS

ACKNOWLEDGEMENTS AND DECLARATION iii
ABSTRACT v
CONTENTS vi
LIST OF FIGURES x
LIST OF PLATES xvii
LIST OF TABLES xviii

Chapter 1 Introduction

1.1 A Brief History of UK Roads 1.1
1.2 Analytical Pavement Design 1.5
1.3 Bituminous Materials 1.7
1.3.1 Asphalt Mixture Types 1.10
1.3.2 Macadam Mixture Types 1.12
1.4 Material Properties 1.15
1.4.1 Stiffness 1.16
1.4.2 Permanent Deformation 1.16
1.4.3 Fatigue Cracking 1.18
1.5 References 1.19

Chapter 2 Background

2.1 Introduction 2.1
2.2 Test Methods for Fatigue 2.2
2.3 Factors Affecting Fatigue 2.12
2.3.1 Stresses Induced in a Pavement 2.12
2.3.2 Mode of Loading 2.13
2.3.3 Loading Waveform 2.15
2.3.4 Rest Periods 2.17

2.3.5 Mixture Variables 2.18
2.4 Fatigue Relationships 2.21
2.5 Use of Fatigue Relationships 2.24
2.6 Summary 2.25
2.7 References 2.26

Chapter 3 Indirect Tensile Fatigue

3.1 Introduction 3.1
3.2 Analysis of the ITFT 3.3
3.3 Equipment Development 3.10
3.3.1 Hardware Development 3.10
3.3.2 Software Development 3.12
3.4 Stiffness Modulus 3.15
3.5 Fatigue Test Methods 3.24
3.5.1 Trapezoidal Cantilever 3.24
3.5.2 Uniaxial Tension Compression 3.25
3.5.3 Indirect Tensile Fatigue Testing 3.26
3.6 ITFT Protocols 3.27
3.7 Main Test Programme 3.29
3.8 Additional Test Programme 3.33
3.8.1 Repeatability of the ITFT 3.33
3.8.2 Reproducibility of the ITFT 3.33
3.8.3 Practical Use of the ITFT 3.34
3.8.4 Contractual Use of the ITFT 3.34
3.8.5 Further Validation of the ITFT 3.39
3.9 References 3.39

Chapter 4 Results of the Indirect Tensile Fatigue Testing

4.1 Introduction 4.1
4.2 Initial Findings 4.1
4.3 Results of the Main Test Programme 4.3

4.4 Repeatability of the ITFT 4.11
4.5 Reproducibility of the ITFT 4.16
4.6 Practical Use of the ITFT 4.24
4.7 Further Validation of the ITFT 4.29
4.8 Additional Results 4.35
4.9 Summary of Results 4.39
4.10 References 4.42

Chapter 5 Poisson's Ratio

5.1 Introduction 5.1
5.2 Test Programme 5.8
5.3 Results 5.9
5.3.1 Aluminium Cube 5.12
5.3.2 Aluminium Core 5.14
5.4 Summary 5.16
5.5 References 5.16

Chapter 6 Crack Propagation

6.1 Introduction 6.1
6.2 Fracture Mechanics 6.3
6.3 Image Analysis 6.10
6.4 Pilot Test Programme 6.11
6.4.1 Results 6.12
6.5 Main Test Programme 6.17
6.6 References 6.22

Chapter 7 Results of the Crack Propagation Test Programme

7.1 Introduction 7.1
7.2 Image Analysis 7.1
7.3 Analysis of Crack Propagation Data 7.5
7.4 Summary 7.9

7.5 References 7.11

Chapter 8 Practical Application of Research Results

8.1 Introduction 8.1

8.2 Mixture Design 8.1

8.3 Pavement Evaluation 8.2

8.4 Pavement Design 8.4

8.5 References 8.11

Chapter 9 Discussion and Conclusions

9.1 Introduction 9.1

9.2 Indirect Tensile Fatigue 9.1

9.3 Poisson's Ratio 9.5

9.4 Crack Propagation 9.7

Chapter 10 Recommendations for Future Research

10.1 Indirect Tensile Fatigue 10.1

10.2 Poisson's Ratio 10.1

10.3 Crack Propagation 10.2

Appendix A Protocols

Appendix B Data for ITFT Work

Appendix C Data for the Poisson's Ratio Work

Appendix D Data for Crack Propagation Test Programme

Appendix E Crack Propagation Photographs

LIST OF FIGURES

1.1 Schematic Demonstrating the Different Construction Practises of Telford (top) and M^{c}Adam (bottom) 1.2

1.2 Comparison of Gap Graded and Continuously Graded Mixtures 1.9

1.3 30/14 Hot Rolled Asphalt 1.11

1.4 Idealised Stone Mastic Asphalt 1.12

1.5 Typical 20mm Dense Bitumen Macadam Demonstrating the Continuous Grading 1.13

1.6 Typical 20mm Porous Asphalt Showing the Aggregate Skeleton without a Bitumen/Sand/Filler Matrix 1.14

1.7 Typical 20mm Asphaltic Concrete 1.15

1.8 Visco-elastic Deformation Response to Applied Loading 1.17

1.9 Visco-elastic Response to Millions of Wheel Loadings 1.17

2.1 Schematic demonstrating the Main Forms of Fatigue Test: (a) Two Point Bending; (b) Four Point Bending; (c) Four Point Bending; (d) Rotating Bending; (e) Direct Axial Loading; (f) Direct Axial Loading (Necked Specimen) and (g) Diametral Loading 2.3

2.2 Stresses Induced by a Moving Wheel Load on a Pavement Element, After Brown 2.12

2.3 Graphical Representation of (a) Controlled Stress and (b) Controlled Strain Modes of Loading, After Epps and Monismith 2.13

2.4 Graphical Representation of the Differences in Fatigue Response to Various Modes of Loading 2.15

2.5 Types of Loading Waveform: (a) Sinusoidal; (b) Haversine; (c) Cyclic; (approximating a haversine) and (d) Cyclic Loading (square wave), After Said 2.16

2.6 Idealised Representation of the Failure Points for the Two Modes of Loading 2.22

3.1 Relative Stress Distributions and Element Showing Biaxial State of Stress for the Indirect Tensile Fatigue Test 3.3
3.2 Plot Demonstrating the High Compressive and Shear Stresses Developed on the Vertical Diameter of the ITFT 3.9
3.3 Plot Demonstrating the Point of Maximum Shear Stress on the Vertical Diameter of the ITFT 3.10
3.4 Schematic Demonstrating the Initial Equipment Configuration for the ITFT 3.11
3.5 Schematic Demonstrating the Present Equipment Configuration for the ITFT 3.12
3.6 Schematic Representation of the Load Pulse Applied in the ITFT 3.13
3.7 Original Rate of Data Capture on a Short Test in the ITFT 3.14
3.8 New Rate of Data Capture on a Short Test in the ITFT 3.14
3.9 New Rate of Data Capture on a Long Test in the ITFT 3.15
3.10 Typical Results from 20mm DBM Mixtures with 100pen Bitumen and Granite and Gravel Aggregate Showing Effect of Specimen Temperature During ITSM Test 3.17
3.11 Typical Results Showing the Effect of Stress Amplitude During the ITSM Test 3.18
3.12 Hypothetical Stiffness Values Showing Effect of Poisson's Ratio on the ITSM 3.18
3.13 Typical Results for Three Dense Macadams Showing the Effect of Mixture Air Void Content on the ITSM 3.19
3.14 Typical Variation in Stiffness Modulus Due to Variation in Binder Content for Two Typical HRA Mixtures 3.20
3.15 Example Graph Demonstrating the Stress Dependency of Stiffness Modulus, in the ITFT, for a 20mm DBM Material 3.22
3.16 Example Graph Demonstrating the Stress Dependency of Stiffness Modulus, in the Trapezoidal Mode of Testing, for a 20mm DBM Material 3.22

3.17 Graph Demonstrating the True Form of the Stress Dependency of Stiffness Modulus 3.23
3.18 Schematic Representation of the Trapezoidal Cantilever Test, Showing the Expected Point and mode of Failure 3.25
3.19 Schematic Representation of the Uniaxial Tension compression Test, Showing the Expected Point and mode of Failure 3.26
3.20 Schematic Representation of the Indirect Tensile Fatigue Test, Showing the Expected Point and mode of Failure 3.27
3.21 Fatigue Information for the First Contractual Use of the ITFT 3.37
3.22 Error Plot Demonstrating No Statistical Difference Between the 3 sets of Data 3.37
4.1 Typical Result for an ITFT Specimen, 28mm DBM 50 Tested at 13.5°C . 4.1
4.2 Typical Result for an ITFT Specimen, 28mm DBM 50 Tested at 20°C ... 4.2
4.3 Fatigue Characteristics for the 30/14 HRA Based on Maximum Tensile Stress (σ_{xmax}) Against Life to Failure 4.4
4.4 Fatigue Characteristics for the 20mm DBM Based on σ_{xmax} Against Life to Failure 4.4
4.5 Fatigue Characteristics for the 28mm DBM 50 Based on σ_{xmax} Against Life to Failure 4.5
4.6 Fatigue Characteristics for the 30/14 HRA SBS Modified Based on σ_{xmax} Against Life to Failure 4.5
4.7 Fatigue Characteristics for the 30/14 HRA Based on Maximum Tensile Strain (ϵ_{xmax}) Against Life to Failure 4.6
4.8 Fatigue Characteristics for the 20mm DBM Based on ϵ_{xmax} Against Life to Failure 4.6
4.9 Fatigue Characteristics for the 28mm DBM 50 Based on ϵ_{xmax} Against Life to Failure 4.7
4.10 Fatigue Characteristics for the 30/14 HRA SBS Modified Based on ϵ_{xmax} Against Life to Failure 4.7
4.11 Summary Graph Showing the relative Performance of the Four Mixtures Based on the Regression Between Both Test Methods 4.9

4.12 Comparison Plot Showing the Repeatability of the 30/14 HRA Data Set 4.12
4.13 Overall Comparison Plot Showing the Repeatability of the 30/14 HRA Data Set 4.13
4.14 Comparison Plot Showing the Repeatability of the 20mm DBM Data Set 4.13
4.15 Overall Comparison Plot Showing the Repeatability of the 20mm DBM Data Set 4.14
4.16 Comparison Plot Showing the Repeatability of the Crumb Rubber Modified Marshall Asphalt Data Set 4.15
4.17 Overall Comparison Plot Showing the Repeatability of the Crumb Rubber Modified Marshall Asphalt Data Set 4.15
4.18 First Phase of the Reproducibility Work Carried Out on the 30/14 HRA Unmodified Mixture - Strain Calculated on Regressed Stiffness Values . 4.17
4.19 First Phase of the Reproducibility Work Carried Out on the 30/14 HRA Unmodified Mixture - Strain Calculated on Averaged Stiffness Values .. 4.18
4.20 Second Phase of the Reproducibility Work Carried Out on the 30/14 HRA Unmodified Mixture - Strain Calculated on Regressed Stiffness Values 4.18
4.21 Second Phase of the Reproducibility Work Carried Out on the 30/14 HRA Unmodified Mixture - Strain Calculated on Averaged Stiffness Values 4.19
4.22 Second Phase of the Reproducibility Work Carried Out on the 40mm HDM Unmodified Mixture - Strain Calculated on Regressed Stiffness Values 4.19
4.23 Second Phase of the Reproducibility Work Carried Out on the 40mm HDM Unmodified Mixture - Strain Calculated on Averaged Stiffness Values 4.20
4.24 Statistical Significance of the 30/14 HRA Based on the Calculation of the Strain using the Averaged Stiffness Values 4.20

4.25 Statistical Significance of the 20mm DBM Based on the Calculation of the Strain using the Averaged Stiffness Values 4.21
4.26 Statistical Significance of the 40mm HDM Based on the Calculation of the Strain using the Averaged Stiffness Values 4.21
4.27 Six Data Sets, for a 20mm DBM, Demonstrating the Good Reproducibility of the ITFT 4.22
4.28 Plot Demonstrating That There is Little Statistical Difference Between The Six Sets of Data 4.23
4.29 Comparison of Tracked and Untracked Wearing Courses with an In-Service Life of 3 Years 4.24
4.30 Comparison of Tracked and Untracked Basecourses with an In-Service Life of 3 Years 4.25
4.31 Comparison of Tracked and Aged Material with Virgin Material for a 40/14 HRA Unmodified Wearing Course 4.26
4.32 Comparison of Tracked and Aged Material with Virgin Material for a 40/14 HRA SBS Modified Wearing Course 4.27
4.33 Comparison of Tracked and Aged Material with Virgin Material for a 50/20 HRA Unmodified Basecourse 4.27
4.34 Comparison of Tracked and Aged Material with Virgin Material for a 50/20 HRA SBS Modified Basecourse 4.28
4.35 Fatigue Line for the Retested 50/20 HRA Unmodified Basecourse with a Higher k_2 Value than the In-service Material Shown In Figure 4.33 . . . . . 4.28
4.36 Comparison of the ITFT with UTCT for a French 0/10mm 50pen Material 4.30
4.37 Plot showing the Residual Errors for the 0/10mm Material 4.30
4.38 Comparison of the ITFT with UTCT for a French 0/14mm 50pen Material 4.31
4.39 Plot showing the Residual Errors for the 0/14mm Material 4.31
4.40 Comparison of the ITFT with UTCT for a UK 20mm HDM Material . . . 4.32
4.41 Plot showing the Residual Errors for the 20mm HDM Material 4.32

4.42 Schematic Showing the Difference in Dissipated Energy per Cycles for the ITFT and UTCT 4.34
4.43 Comparison Between Regression Based on All the Data Points and Those Which Have a Life of Less Than 5,000 Cycles, 50/20 HRA Basecourse . 4.36
4.44 Indirect Tensile Fatigue Line for an SMA Material 4.38
4.45 Comparison of Fatigue Lines for a Typical 30/14 HRA and a SMA 4.38
4.46 Summary Plot Showing the ITFT Lines for All Materials Tested During the Research 4.41
5.1 Schematic of the Measurement System Used for the Work on Poisson's Ratio 5.5
5.2 Poisson's Ratio Against Stiffness for Various Asphaltic Concrete Mixtures - Dynamic Loading, After Alavi and Monismith 5.6
5.3 Poisson's Ratio Against Stiffness for Various Asphaltic Concrete Mixtures - Static Loading, After Navarro and Kennedy 5.6
5.4 Poisson's Ratio Against Stiffness for Various Asphaltic Concrete Mixtures - Dynamic Loading, After Navarro and Kennedy 5.7
5.5 Poisson's Ratio Against Stiffness for Various Hot Rolled Asphalt Mixtures - Dynamic Loading, After Cragg and Pell 5.7
5.6 A Typical Result from the Testing on Cylindrical Specimens in the Indirect Tensile Mode, in the NAT, Using Equation 5.10 for the Calculation of Poisson's Ratio 5.10
5.7 Poisson's Ratio Measured on a 100mm Cube of Sand-Asphalt @ 0°C ... 5.11
5.8 Poisson's Ratio Measured on a 100mm Cube of Sand-Asphalt @ 20°C .. 5.11
5.9 100mm Cube of Sand-Asphalt Retested @ 32°C Demonstrating that the Restructuring Only Happens During the First Set of Applied Loads 5.12
5.10 Summary Graph of Poisson's Ratio Against Stiffness Modulus for Cubes of Different Materials and Test conditions 5.13
5.11 Schematic of the Measurement System Used for the Validation Work on Poisson's Ratio 5.14
6.1 Schematic Showing the Test Configuration for Crack Propagation 6.2
6.2 Graph Demonstrating the Region Over Which Paris's Law Applies 6.5

6.3 Schematic Demonstrating the Five Steps in Calculating the Paris Law Constants for Use in Fracture Mechanics calculations 6.9
6.4 Schematic Showing that the True Distance of Crack Propagation is Longer than the Linear Distance Measured by Previous Research 6.11
6.5 Typical Beam Tested @ 7,500 Microstrain 6.13
6.6 Typical Beam Tested @ 8,500 Microstrain 6.13
6.7 Comparison of Different Methods of Volumetric Determination 6.16
6.8 Beam Test Result for Specimens HRA/5LL - Hot Rolled Asphalt, 50 pen Bitumen, Low Void Content and Low Binder Content 6.19
6.9 Beam Test Result for Specimens HRA/5HL - Hot Rolled Asphalt, 50 pen Bitumen, High Void Content and Low Binder Content 6.19
6.10 Beam Test Result for Specimens HRA/5HO - Hot Rolled Asphalt, 50 pen Bitumen, High Void Content and Optimum Binder Content 6.20
7.1 Rates of Crack Growth for Specimen HRA5HH3 Showing both the Linear and the True Crack Lengths 7.2
7.2 Rates of Crack Growth for Specimen HRA5HH1 Showing both the Linear and the True Crack Lengths 7.3
7.3 Rates of Crack Growth for Specimen HRA5HO2 Showing both the Linear and the True Crack Lengths 7.4
7.4 Unmodified DBM Data Showing the Power Relationship with Stiffness .. 7.7
7.5 Unmodified HRA Data Showing the Power Relationship with Stiffness .. 7.7
7.6 EVA Modified Data Showing the Power Relationship with Stiffness 7.8
7.7 SBS Modified Data Showing the Power Relationship with Stiffness 7.8
8.1 Four Examples of Standard Mixtures for Comparison Purposes 8.2
B.1 Typical ITFT Raw Data File B.3
C.1 Typical Raw Data for the Measurement of Poisson's ratio on a Cube C.7
D.1 Typical Beam Cracking Raw Data File D.4

LIST OF PLATES

6.1 Beam Cracking Apparatus 6.2

6.2 Digitised Image of Beam - Prior to Application of White Paint and Testing 6.16

6.3 Digitised Image of a Beam - After Testing 6.20

6.4 Digitised Image of a Beam in Plate 6.3 With the Crack Electronically Superimposed - Showing the Path Taken Around the Aggregate Structure 6.21

7.1 Electronically Superimposed Crack on Unpainted Beam - Specimen HRA5HH3 ..... 7.2

7.2 Electronically Superimposed Crack on Unpainted Beam - Specimen HRA5HH1 ..... 7.3

7.3 Electronically Superimposed Crack on Unpainted Beam - Specimen HRA5HO2 ..... 7.4

Appendix E Contains 47 plates of the cracks electronically superimposed on the unpainted beams ..... E1 - E15

LIST OF TABLES

2.1 Effect of Waveform Shape on Fatigue Life, After Raithby and Sterling . . 2.16

3.1 Correction Values for Use in Equation 3.9 . . . . . 3.7

3.2 General Effect of the Main Factors Affecting the ITSM 3.16

3.3 An Example of the Number of ITFT Specimens and their Volumetric Data Produced from One Roller Compacted Slab 3.29

3.4 Softening Point and penetration values for the Bitumens Used in the Main Test Programme 3.31

3.5 Test Temperatures for the Materials Based on Equivalent Bitumen Stiffness 3.32

3.6 Summary of Data for the First Contractual Use of the ITFT 3.36

4.1 Material Constants for Use in Equation 4.2 for the Four Materials Tested . 4.8

4.2 Ranking of the Four Mixtures Based Upon Both the ITFT and the Volume of Binder in the Mixture 4.11

4.3 Repeatability Results for the 30/14 HRA and 20mm DBM Mixtures 4.11

4.4 Repeatability Outside of the Data Range 4.12

4.5 Repeatability Results for the Crumb Rubber Modified Mixture 4.14

4.6 Summary Information for Each Data Set 4.23

4.7 Summary of Fatigue Equations and Correlation Coefficients for all Three Materials 4.29

4.8 Comparison of the Magnitude of Strains Found in the Two Test Methods 4.33

4.9 comparison of the Variations in Strain, Predicted Using the Two Different Methods Against the Overall Result 4.33

4.10 Comparison of Data Obtained From Short Life Tests With That Obtained From Long Life Tests 4.35

4.11 Summary Data for the SMA Cores 4.37

4.12 Summary Data for All the Standard Materials Tested During the Project Using the ITFT 4.40
5.1 Values for Poisson's Ratio at Various Temperatures, as Recommended by TRL 5.8
5.2 Poisson's Ratio for the Aluminium Cube 5.14
5.3 Poisson's Ratio for the Aluminium Core 5.15
6.1 Geometries and Volumetrics of the Specimens Used for the Pilot Test Programme 6.15
8.1 Key Parameters for Use in Equation 8.10 . . . . . 8.7
8.2 Comparison of Fatigue Lives Based Upon Three Different Methods of Analysis 8.10

Appendix B Contains all the ITFT data in 39 tables (B1 - B39) . . . . . B1 - B28
Appendix C Contains all the Poisson's ratio data in 4 tables (C1 - C4) . . . . C1 - C7
Appendix D Contains all the crack propagation data in 9 tables (D1 - D9) D1 - D10

INTRODUCTION

1.1 A Brief History of U.K. Roads

Historically, modern day pavements in the U.K., and predominantly throughout the world, have been constructed to service a particular need without very much consideration of the future demands which may be placed upon them due to financial constraints. However, the Romans and early engineers did not face these problems and were able to build long lasting expensive roads.

The Romans built roads in straight lines in order to move troops as quickly, and with the minimum of difficulty, as was possible. The roads were engineered structures consisting of a compacted soil foundation surfaced with small aggregates which were often bound with a natural cement. A layer of larger aggregate fill was then placed, before interlocked stones slabs were laid to provide the finished surface. The structures typically had retaining walls either side to prevent slippage and were properly drained by a cambered surface with ditches running either side of the road to remove the excess water (1).

By the 16th Century the network of roads left by the Romans in England had deteriorated until they were no more than cart tracks. It was then recognised that the highways were an important and necessary commodity. Thus, the position of "Surveyor of Highways" (2) was created in 1555 with statutory duties, and this eventually led to a county toll system to fund the upkeep of busy routes. This in turn became the "Turnpike trust" (3) set up in 1706 and a slow improvement in road quality began to take place. However, the construction and rehabilitation of the road network was a hit-and-miss affair as the skills and engineering principles employed by the Romans had long since been lost.

In the mid 18th Century two independent Scottish engineers John Loudon McAdam (1756 - 1836) and Thomas Telford (1757 - 1834), who built the Caledonian canal and the Menai Straits suspension bridge, plus numerous roads {*c.* 1000 miles in Scotland} and road

bridges, began the resurrection of pavement construction based upon sound engineering principles. They developed two different methods of construction (Figure 1.1), both with advantages and disadvantages, but both understood the need for good drainage, well compacted layered construction, cleanliness and the need for an impervious surface. Telford constructed his roads with little regard to construction costs using very thick layers in order to ensure a long life, whereas M^{c}Adam built roads which were relatively thin, believing that provided the surface was impervious the foundation was of less importance. These methods continued for many years and still form the backbone of today's construction practises, and the Macadam grading described in Section 1.3 is still based on M^{c}Adam's early work.

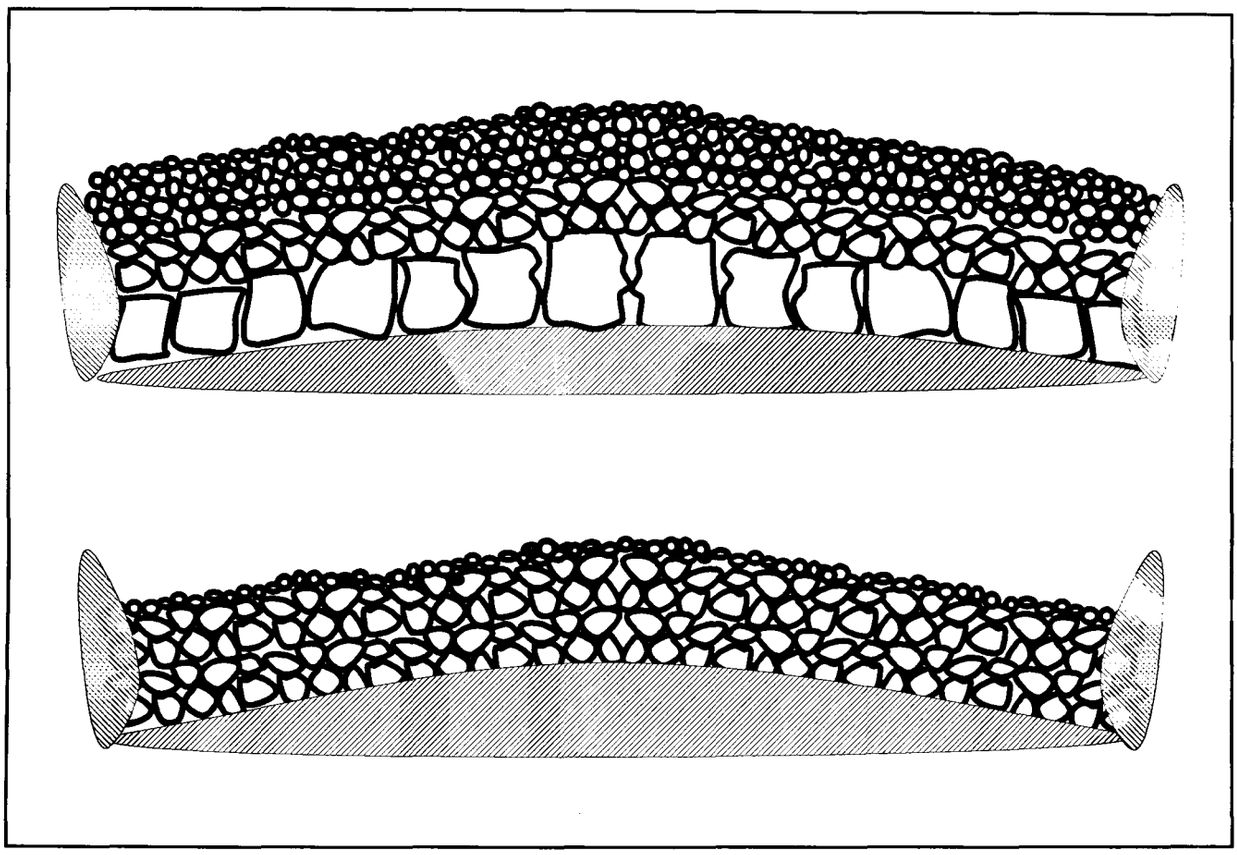


Figure 1.1 - Schematic Demonstrating the Different Construction Practises of Telford (top) and M^{c}Adam (bottom).

The next major step forward came with the recognition that heavy vehicles did more damage than light cars. City streets were constructed with a 'Macadam' strip down either side of the road to carry the lighter faster traffic and 'heavy stone setts' in the centre of the 'Macadam' strips to carry the heavier traffic (5). A road fund licence was also introduced

in 1910 (6) to help finance the country's road infrastructure. Gradual development took place from these early designs until the second world war when the military required pavements and materials which could support very heavy traffic loadings and once again it was 'a need' which drove the industry towards new technological achievements. Due to the shortage of cement (2), which was needed for buildings, the industry began to supply large tonnages of 'Tarmacadam' which was considered an acceptable alternative. From this need driven development came the first flexible designs and the first indications of the way today's pavement structures would develop.

Although by the early post second world war era it was understood that fundamental engineering properties of the road were required to properly design a pavement it was clear that little or no such information was available and obtaining it would be a time consuming and difficult task. This led to the adoption of a purely empirical, though more systematic, approach based upon observed performance of full scale road experiments and a major step was taken in the USA by the introduction of the Californian Bearing Ratio (CBR) test in the late 1940's.

In the period between the 1950's and the 1970's over 400 trial sections were laid on U.K. roads by the then Road Research Laboratory (RRL) which became the Transport and Road Research laboratory (TRRL) and is known today as the Transport Research Laboratory (TRL). These sections, along with over 900 full scale sections which were laid in the United States in the AASHO (American Association of State Highway Officials) Road Test (7), formed the basis of the empirical design methods which were in use, as Road Note 29 (8, 9), until 1970.

In 1970 the first step towards semi-analytical pavement design was taken, in the third edition of Road Note 29 (10), when the traffic loading was expressed in terms of equivalent standard axles. This was a concept that did not assume that all vehicle loadings did the same amount of damage, as had been the case previously . The axle weight of the vehicle is taken and converted to a number of standard 80kN axles using the following equation.

$$EF_w = \left(\frac{w}{80}\right)^4 \qquad (1.1)$$

Where :

EF_w	=	Equivalence Factor
w	=	Axle Load (kN)
80	=	80 kN is the standard axle load (40 kN wheel load)

Equation 1 highlights the fact that heavy axle weights do proportionally far more damage than lighter ones.

i.e. If the axle weight is doubled the damage is increased sixteen times, or one 160kN axle loading is equivalent to 16 standard 80kN axle loadings.

During the next decade the trial sections continued to be monitored and a semi-analytical pavement design method was developed to allow the design of pavements to withstand in excess of 150 million standard axles (msa) over a 20 year period, which is one criterion used in the design of today's motorways and some of the major trunk roads, and was based on the previous 30 years of knowledge. This method was published in TRRL report LR1132 in 1984 (11) and was adopted into practice in 1987 as HD14/87 entitled "Structural Design of New Road Pavements" (12), the design and construction of roads for the UK is presently covered by the Department of Transport's design manual for Roads and Bridges (13).

The developments in design methodology described previously have all been brought about by the huge growth in traffic levels and have been 'needs led'. Traffic growth has always been much greater than predicted and with the development of new materials whose properties cannot be obtained using empirical methods, the need to predict the remaining lives of pavements and the design of new pavements to withstand heavier traffic loadings with new axle and suspension configurations requires the use of an analytical method as the traditional empirical ones cannot cope.

1.2 Analytical Pavement Design

The use of such an analytical (mechanistic) method for pavement design will yield, for any particular set of end-product mechanical properties, the required pavement structure and life to failure, with the philosophy being that the structure should be treated in the same manner as any other civil engineering structure. The essential requirements may be summarised as follows:

- Specify the loading conditions,
- Estimate the size of components,
- Consider the material available,
- Carry out a structural analysis using fundamental theoretical principles,
- Compare critical stresses, strains or deflection with calculated allowable values and
- Make adjustments to materials or geometry until a satisfactory design is achieved taking into consideration the economic feasibility of the result.

There are two modes of structural failure which the designer seeks to avoid during the design life of the pavement; cracking and rutting. The concept of design life is particularly important for pavements, since they do not fail suddenly (other than in very rare instances of large thermal or ground movements, which it is not economically feasible to account for at the design stage) but gradually deteriorate over a long period. This is essentially a fatigue phenomenon, in the sense that the deterioration, which is caused by the stresses and strains in the structure, results from both the magnitude and the number of load applications that the pavement experiences.

Cracking, or **fatigue**, of the asphalt layer arises from repeated tensile strains, the maximum value of which, according to structural analysis, due to traffic loading is found at the bottom of the bituminous layer. The crack, once initiated, propagates upwards causing gradual weakening of the structure. This can be minimised by a suitable design procedure based on the mechanistic properties of the structure.

The development of a rut arises from the accumulation of permanent strain throughout the structure. This can also be minimised by a suitable design procedure and by good compaction of all the layers. The accumulation of permanent strain in the foundation can also be reduced by keeping the vertical strain in the subgrade below a certain critical level and although this is a semi-empirical method it has been found to be a very useful criterion. This is achieved by ensuring that the layers above the subgrade have a high enough stiffness (load spreading ability) to distribute the stresses and strains developed in the entire structure over a wider area.

The design problem, then, is to so proportion the pavement structure that, for the chosen materials, the critical levels of strain will not be exceeded in the design life. To achieve this, the designer needs to know the mechanical properties of his materials and be able to analyse the structure. These matters are interdependent, since analysis requires a knowledge of material characteristics and, with present levels of technology, it is relatively simple to obtain this information. Upon reviewing the following major methods:

- The Nottingham Design Method (14),
- The Shell Pavement Design Manual (15),
- NAASRA Pavement Design (16),
- AASHTO Guide for Design of Pavement Structures (17),
- MS-1 - Thickness Design (18),
- Road Note 29 (10) and
- Road Note 31 (19)

it became evident that all have certain similarities. The methods generally use or are based upon a certain amount of fundamental structural analysis and employ individual material properties to ascertain the thickness of the layers. However, all of the methods do not use fundamental methods for determining the actual material properties. For example, the Shell Pavement Design manual uses a fundamentally based method for assessing the resistance to permanent deformation, but uses methods for stiffness and fatigue that assume that there are only two levels of performance for these parameters,

normal and high, which is acceptable when assessing mixtures within the bounds of the data set from which the lines were developed but for other mixtures (porous asphalt, stone mastic asphalt etc.) or when polymer modified binders are used the method is no longer fundamentally sound. All the methods evaluated use empirical relationships for one or more of the mechanical properties and they all use empirical methods for assessing the resistance to fatigue cracking for some if not all mixtures.

When designing a pavement it is important to consider not only the thickness of the layers and the type of material to be used in the layer but also the type of pavement construction of which there are two basic forms:

- Rigid - The main structural layer is a concrete slab which also serves as the running surface and,
- Flexible - The structural layers comprise bituminous materials and the running surface is a specialised bituminous material chosen for its surface characteristics (Skid resistance, noise, glare, spray etc.) in addition to its structural properties.

There are also combinations of rigid and flexible pavements, termed composite pavements, but the remainder of this thesis will concentrate solely on flexible construction and bituminous materials.

1.3 Bituminous Materials

Bituminous materials have been in known use since 3000 B.C. (20), when bitumen mastics were used in Mesopotamia as waterproofing for reservoirs. The material used then was a naturally occurring asphalt (such as Trinidad Lake Asphalt, TLA) which is a combination of bitumen, which today is a specially produced heavy derivative of crude oil refinement, and fine natural mineral matter, and it was in this natural form that sole use was made until the 18th century. It was during this period that Telford and McAdam began to construct roads using techniques and materials familiar to users today. However, they made extensive use of tar, a dark brown or black viscous liquid obtained

from distillation of wood, coal and similar substances which was available in suitably large quantities at that time, rather than bitumen as the binder in the mixture. The use of tars has gradually reduced over the years due to far less production, health concerns over the carcinogenic nature of the material and because of the superior properties exhibited by bituminous binders.

Rolled asphalt began to be produced in the middle of the 19th century as a man made imitation of naturally occurring asphalts. The first specifications for asphalts appeared in 1933 (21, 22) and continued to evolve as B.S. 594 from 1935 to the present format of today (23). Widespread use of bituminous macadam for road construction began in the early 1900's. The mixtures used were coated single-sized macadams laid cold by hand. The need for a more graded mixture was gradually realised although the fines content did not rise above 15% for many years. The first specification for macadams was issued in the early 1940's and by the 1960's dense coated macadams had been introduced for the main load bearing layers of the road.

This development of bituminous materials has lead to the two generic mixture types:

- Asphalts
- Macadams

The difference between the two is ostensibly the quantity and particle size distribution of the coarse aggregate. Asphalts mainly consist of a fine aggregate and bitumen matrix with differing amounts of coarse aggregate, generally single sized, distributed throughout the mixture. This type of mixture is then referred to as gap-graded. Macadams, however, are referred to as continuously graded and are made up of approximately equal amounts of each individual aggregate size (based on M^{c}Adam's early work). This results in an aggregate skeleton where there is stone on stone contact throughout the mixture. Figure 1.2 shows examples of the two generic types of grading. Rolled asphalts use the dense mortar of sand, bitumen and filler (fine material which has a particle size less than 75μm) to provide the structural performance of the layer (resistance to permanent deformation and load spreading ability), as opposed to macadams which utilise their interlocked

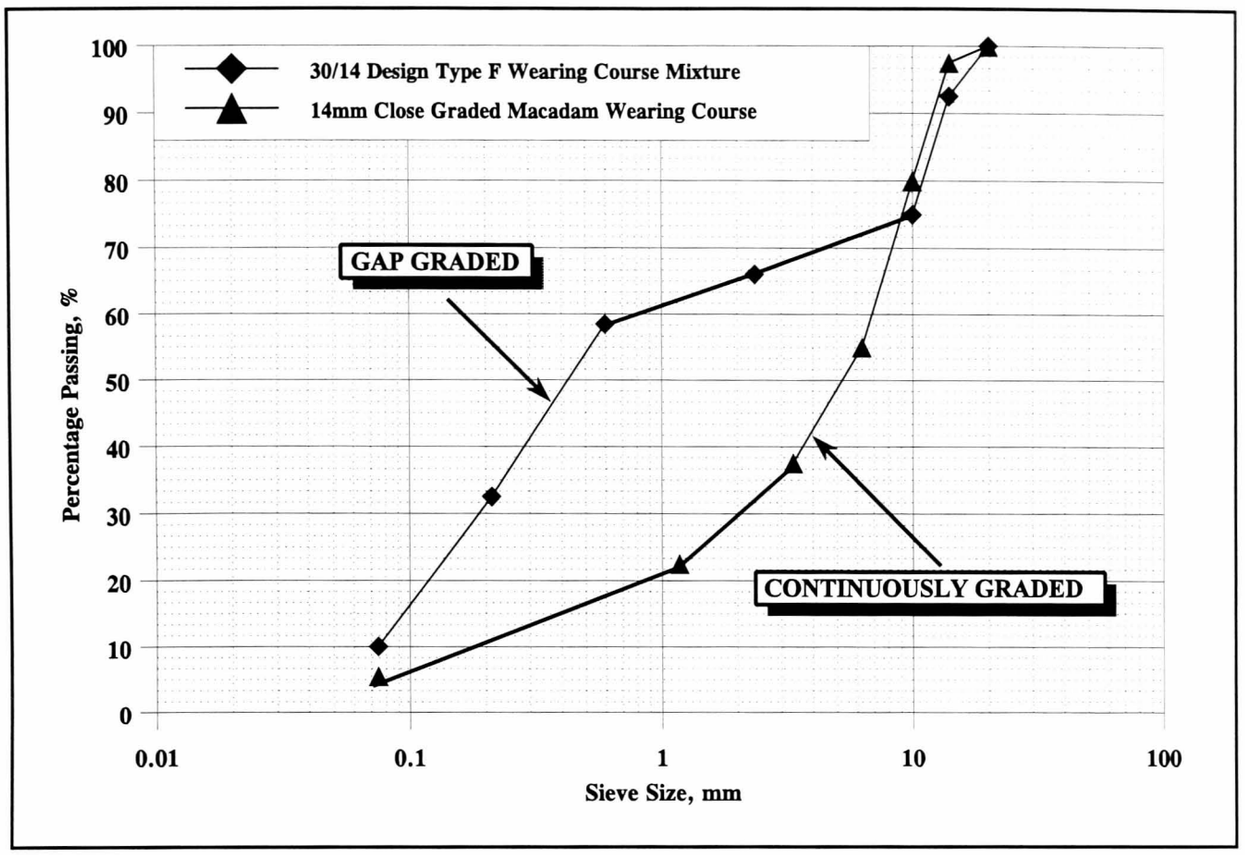


Figure 1.2 - Comparison of Gap Graded (23) and Continuously Graded Mixtures (24).

aggregate skeleton to provide these' properties. All types of bituminous material use the bitumen to resist fatigue cracking as this is caused by tensile strains generated in the pavement and the only constituent of a bituminous mixture which has a tensile capacity is the bitumen. Various works, described in the next chapter, have shown that the higher the volume of bitumen in a mixture the better its resistance to fatigue cracking.

Macadams generally provide better resistance to permanent deformation than asphalts and can be stiffer, if a consideration of the grade and type of bitumen used in the mixture is taken into account.

Asphalts have a greater quantity of fine material than macadams and, therefore, the total surface area of the mixture is higher leading to an increased demand for binder and, hence as bitumen is the most expensive constituent asphalts cost more to produce. However, the increased binder content and, hence, binder volume give asphalts a better resistance to fatigue cracking. This also makes them less permeable to both air and water, further

increasing their durability over macadams. Durability of a bituminous paving mixture has been defined as:

> "The ability of the materials comprising the mixture to resist the effects of water, ageing and temperature variation, in the context of a given amount of traffic loading, without significant deterioration for an extended period"

by Scholz in his doctoral thesis (25) along with a full description of the distress mechanisms affected by durability and their causes. Asphalts are generally more workable than macadams due to their higher binder contents.

1.3.1 Asphalt Mixture Types

Mastic Asphalt

This is an impervious material with a very high fines content and, therefore, a high binder content, of the order of 17% by mass of the total mixture, due to the large surface area of the fine material. The material is very expensive due to the high binder content and is only used for specialist applications, such as waterproofing bridge decks. The specifications for these materials are B.S. 1446 and B.S. 1447 (26, 27).

Hot Rolled Asphalt (HRA)

This is the typical form of the asphalt material used in the U.K.. It consists of a sand/filler/bitumen matrix with varying quantities of coarse aggregate generally 'floating' in the matrix, although at the very high coarse aggregate contents a skeleton will be formed. Figure 1.3 shows a typical grading and structure for this type of material. The designation for HRA is in the form of two numbers, the first number refers to the nominal percentage of coarse aggregate in the mixture and the second number refers to the maximum nominal aggregate size in millimetres. The range of mixture types vary from a 0/3 sand sheet wearing course to a 60/40 roadbase material. However, the most common material used in the U.K. is a 30/14 HRA wearing course with pre-coated chippings rolled into the surface to provide skid resistance, this typically has a binder content of between 6 and 8%, by mass of the total mixture, dependent upon the exact

grading and mechanical properties required. The specification for these materials is B.S. 594 (23).

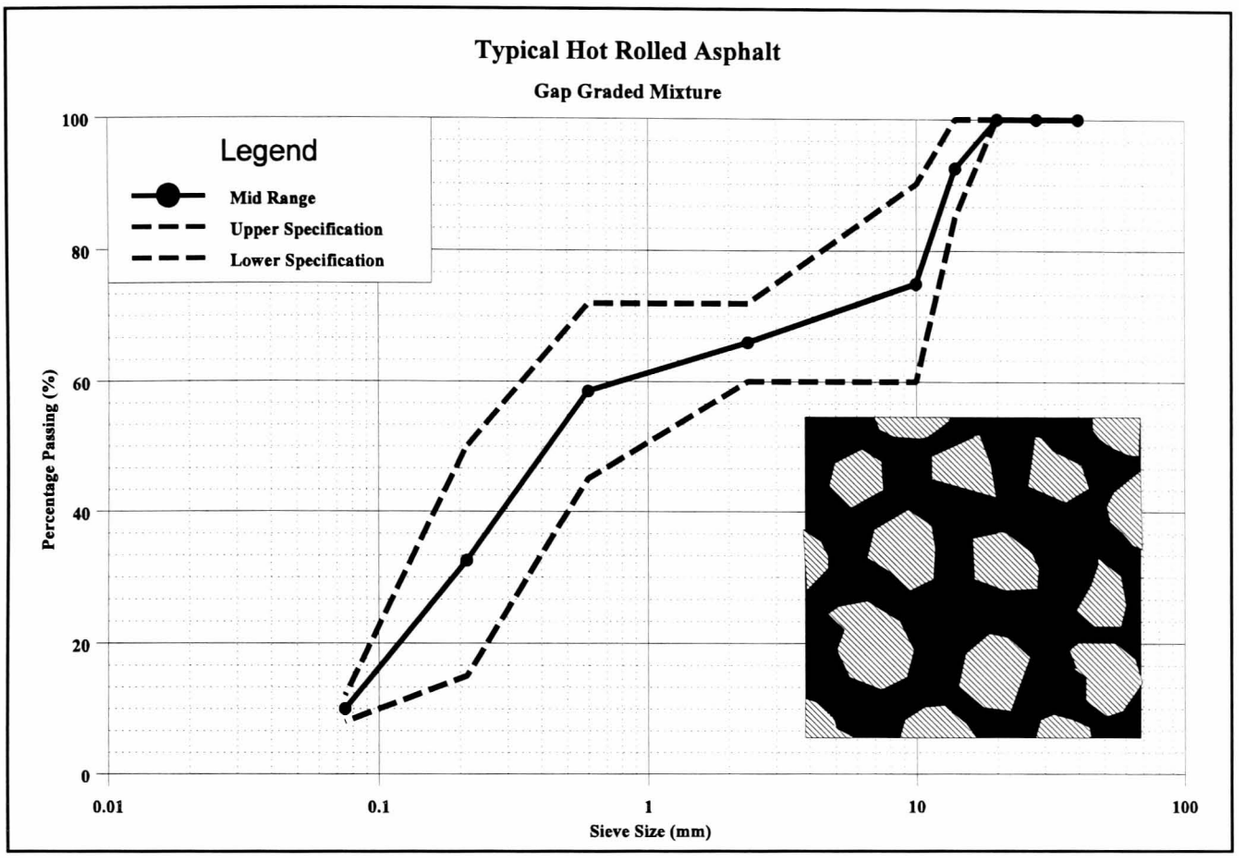


Figure 1.3 - 30/14 Hot Rolled Asphalt.

Stone Mastic Asphalt (SMA)

SMA is a material, designed, originally in Germany and Scandinavia, to resist studded tyre wear, which utilises the best aspects of both asphalts and macadams. It is, in effect, a very high stone content asphalt and uses the addition of fibres to help keep the binder content at a comparable level to traditional asphalts. This mixture type also has good skid resistance once the excess of surface binder has worn away, provided aggregates with a suitable surface texture are used. Figure 1.4 shows a typical grading and structure for this material. There is no British Standard for this material but a design method has been published by Liljedahl (28).

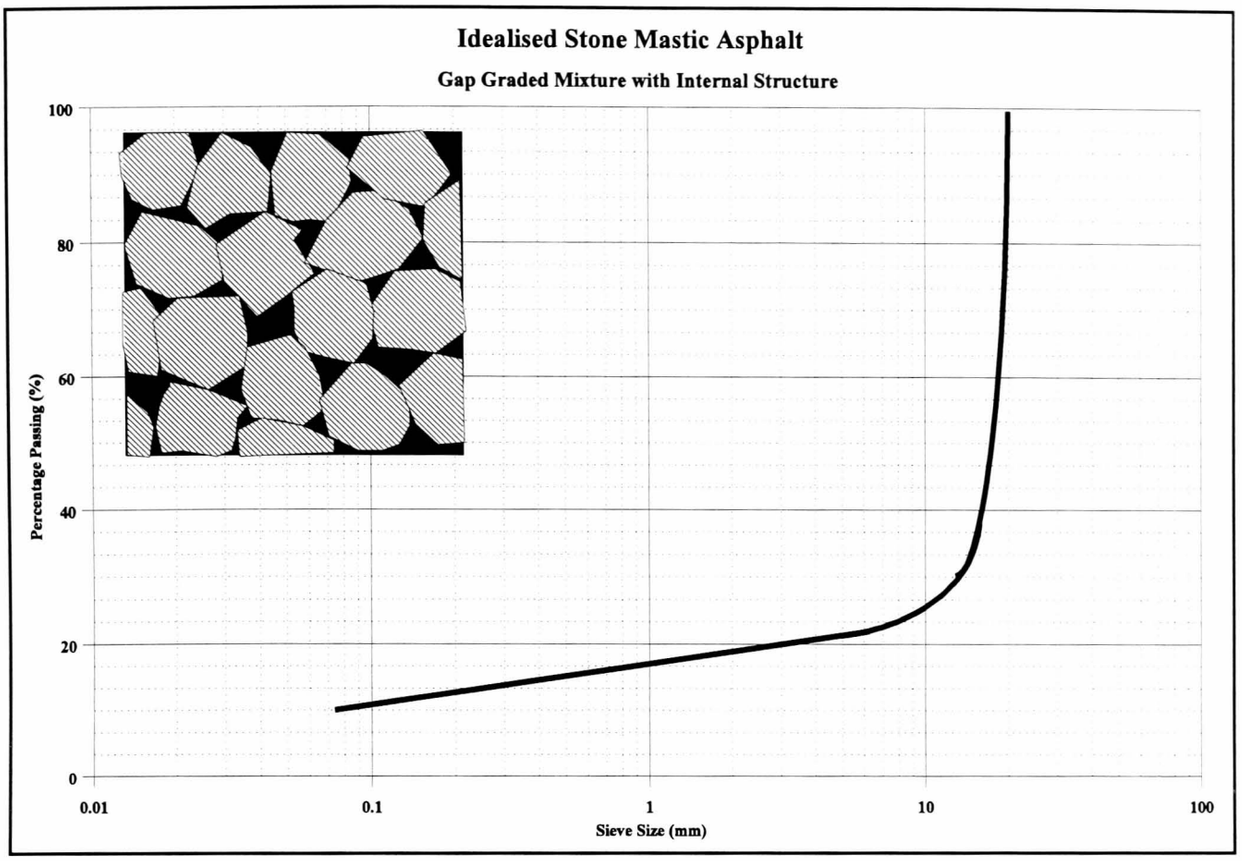


Figure 1.4 - Idealised Stone Mastic Asphalt.

1.3.2 Macadam Mixture Types

Macadams

These are continuously graded mixtures which gain their properties by the use of high quality stone, forming good aggregate skeletons. There are many types of macadam ranging from 3mm fine graded wearing course to 40mm Heavy Duty Macadam. The differences between the mixtures types are arrived at by varying the maximum nominal size of the aggregate, the bitumen grade and the filler content. To put this in perspective with HRA materials a 20mm Dense Bitumen Macadam will have a binder content by mass of total mixture of 4.7%. Figure 1.5 shows a typical grading and structure for this material. The specification for these materials is B.S. 4987 (24).

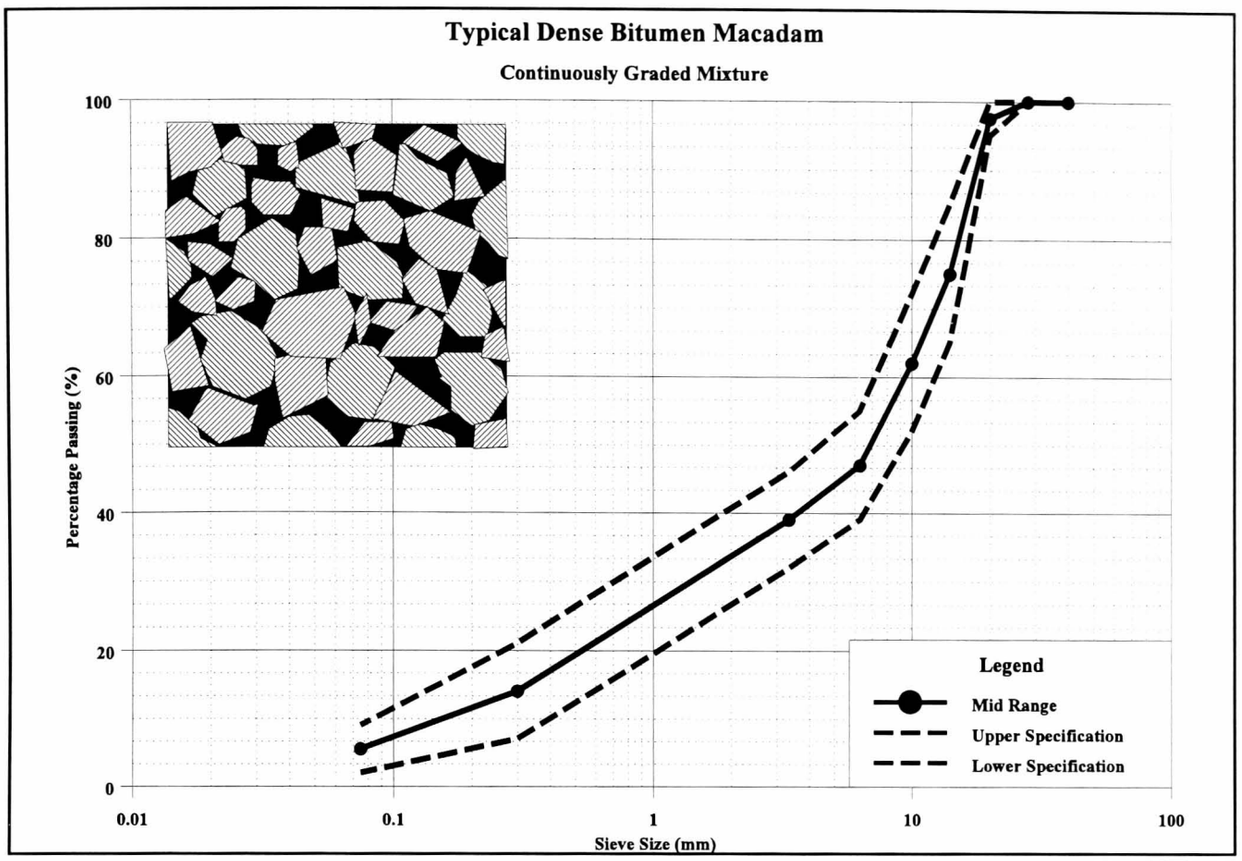


Figure 1.5 - Typical 20mm Dense Bitumen Macadam Demonstrating the Continuous Grading.

Porous Asphalt

Although the name implies that this material is an asphalt it was originally termed pervious macadam and is a free draining material which gains its' properties by achieving a good aggregate interlock, although it only consists of single-sized aggregate coated in a thick bitumen/filler/fibre mastic. It is now being used extensively in Europe as a wearing course and has been shown to reduce spray, glare, noise and surface ponding while still achieving a satisfactory performance with regard to permanent deformation. Figure 1.6 shows a typical grading and structure for this material. The British Specification for this material is B.S. 4987 (24).

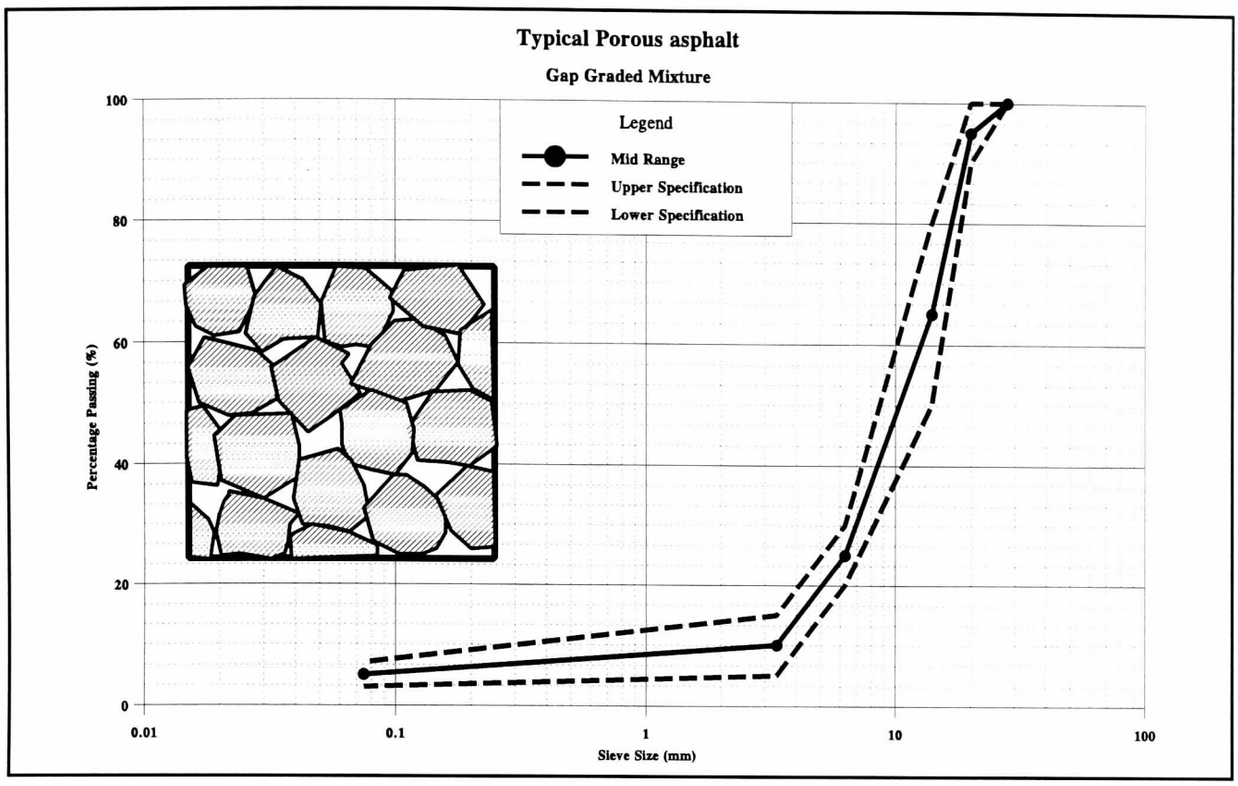


Figure 1.6 - Typical 20mm Porous Asphalt Showing the Aggregate Skeleton Without a Bitumen/Sand/Filler Matrix.

Asphaltic Concrete

This is a material extensively used throughout Europe and the United States which is very similar to a macadam in that it is continuously graded, but even denser. It is included here for completeness to show the full range of continuously graded materials. Figure 1.7 shows a typical grading and structure for this material.

Summary

The two generic mixture types, described in detail here, demonstrate that there are materials with very different properties available for use by the design engineer. Hence, pavements need to be designed rather than specified and that certain areas and/or layers should be chosen with specific properties in mind. For example where heavy vehicles are travelling at low speed materials with a high resistance to permanent deformation, such as Heavy Duty Macadam, should be used due to the aggregate skeleton and the lower binder content. However in an area where extensive fatigue cracking is predicted an asphalt would be better employed than a macadam due to the high binder volume of an asphalt which resists the tensile strains.

It should be noted that the mixtures and specifications, apart from asphaltic concrete detailed in this section are all recipe or empirical and that asphaltic concretes are 'designed' using the Marshall method (29). None of the mixtures are 'designed' using tests which relate to fundamental mechanical properties which can be used in analytical pavement design calculations.

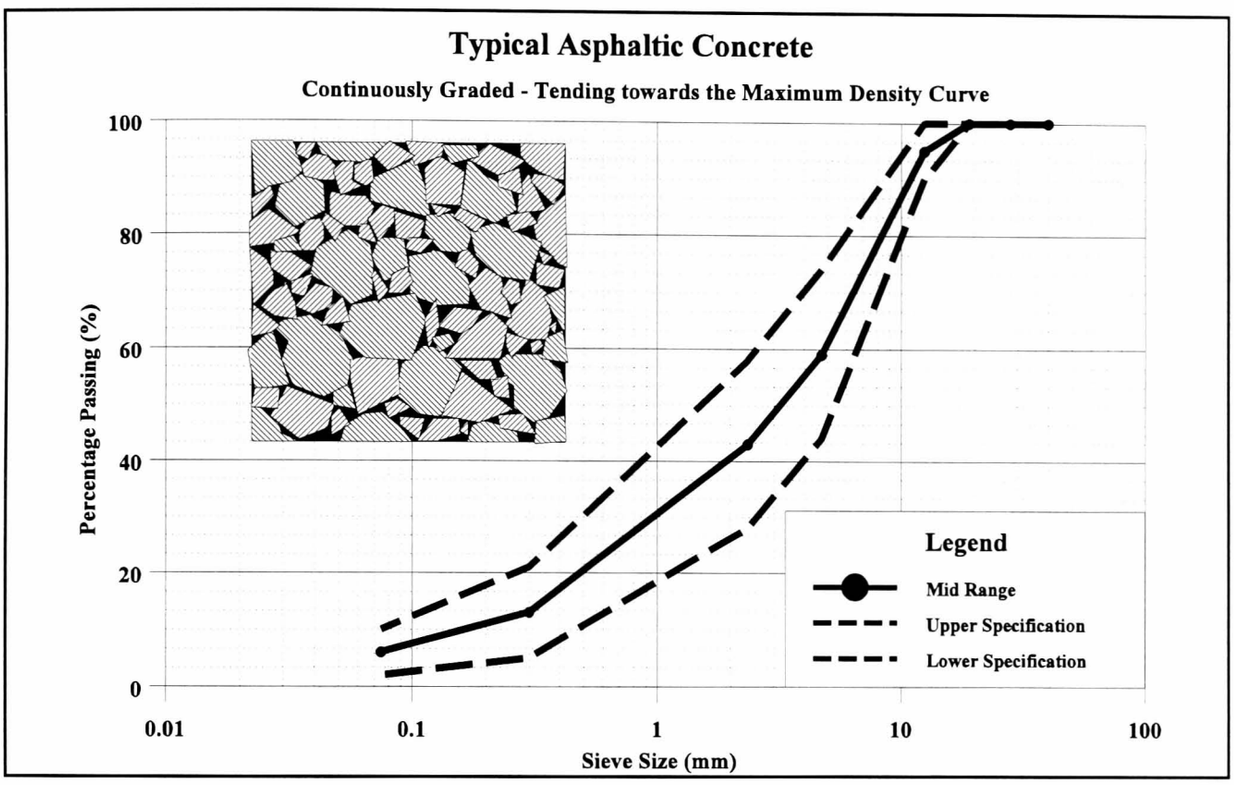


Figure 1.7 - Typical 20mm Asphaltic Concrete.

1.4 Material Properties

There are three fundamental properties which are of concern to the design engineer:

- Stiffness modulus,
- Resistance to Permanent Deformation and
- Fatigue Cracking Characteristics.

These parameters need to be measured and it would be desirable to have simple practical methods for doing this on a routine basis. To this end a suite of tests has been developed at the University of Nottingham using the Nottingham Asphalt Tester (NAT), a simple closed-loop computer controlled pneumatic testing system, allowing an assessment of each of the above properties.

1.4.1 Stiffness

The elastic stiffness in a pavement is a measure of a materials ability to spread the traffic loading over an area. The higher the elastic stiffness of the pavement and, hence, the individual layers the wider the area which reduces the level of strain experienced lower down in the pavement structure, dependent upon both the temperature and speed of loading.

This parameter is generally evaluated using a uniaxial stress / strain relationship, Equation 1.2, and although this is a measure of the elastic stiffness and bituminous materials behave in a visco-elastic manner the method has been found suitable provided that a number of boundary conditions are applied.

$$E = \frac{\sigma}{\epsilon} \qquad (1.2)$$

Where :

E = Elastic Stiffness

σ = Applied Stress

ϵ = Resultant Strain

The method of stiffness testing employed throughout this work is that of the Indirect Tensile Stiffness Modulus (ITSM) test as given in the British Standard Draft for Development 213 (30). A detailed description of the test and factors which affect it are given in Chapter 3.

1.4.2 Permanent Deformation

Permanent deformation or rutting is the accumulation of tiny irrecoverable strains in a material under repeated loading which eventually cause a measurable rut to be developed. These small strains are due to the visco-elastic response of bituminous materials to dynamic loading (Figure 1.8) and they accumulate over millions of applications of traffic loading to form a large deformation. A schematic of this is shown in Figure 1.9.

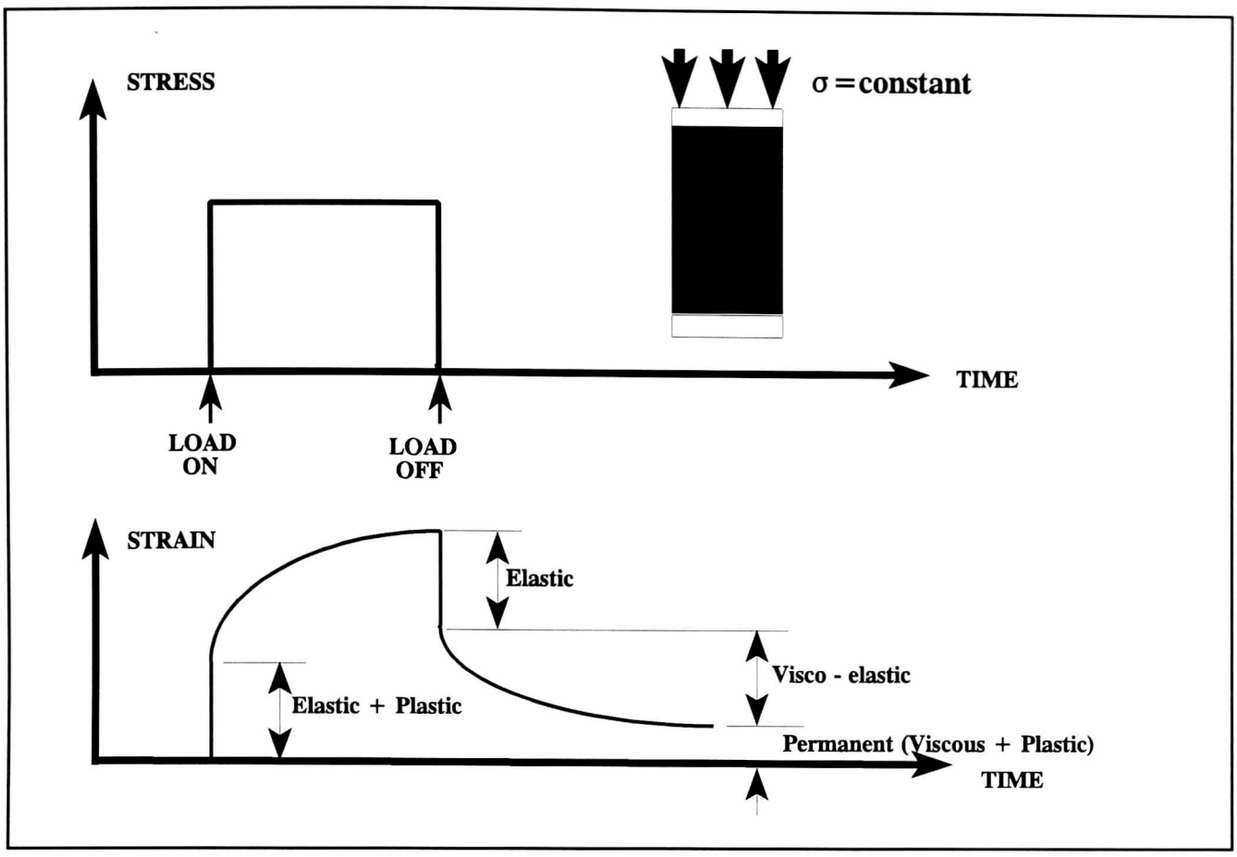


Figure 1.8 - Generalised Strain Response to an Applied Stress Pulse, After Perl, Uzan and Sides (31).

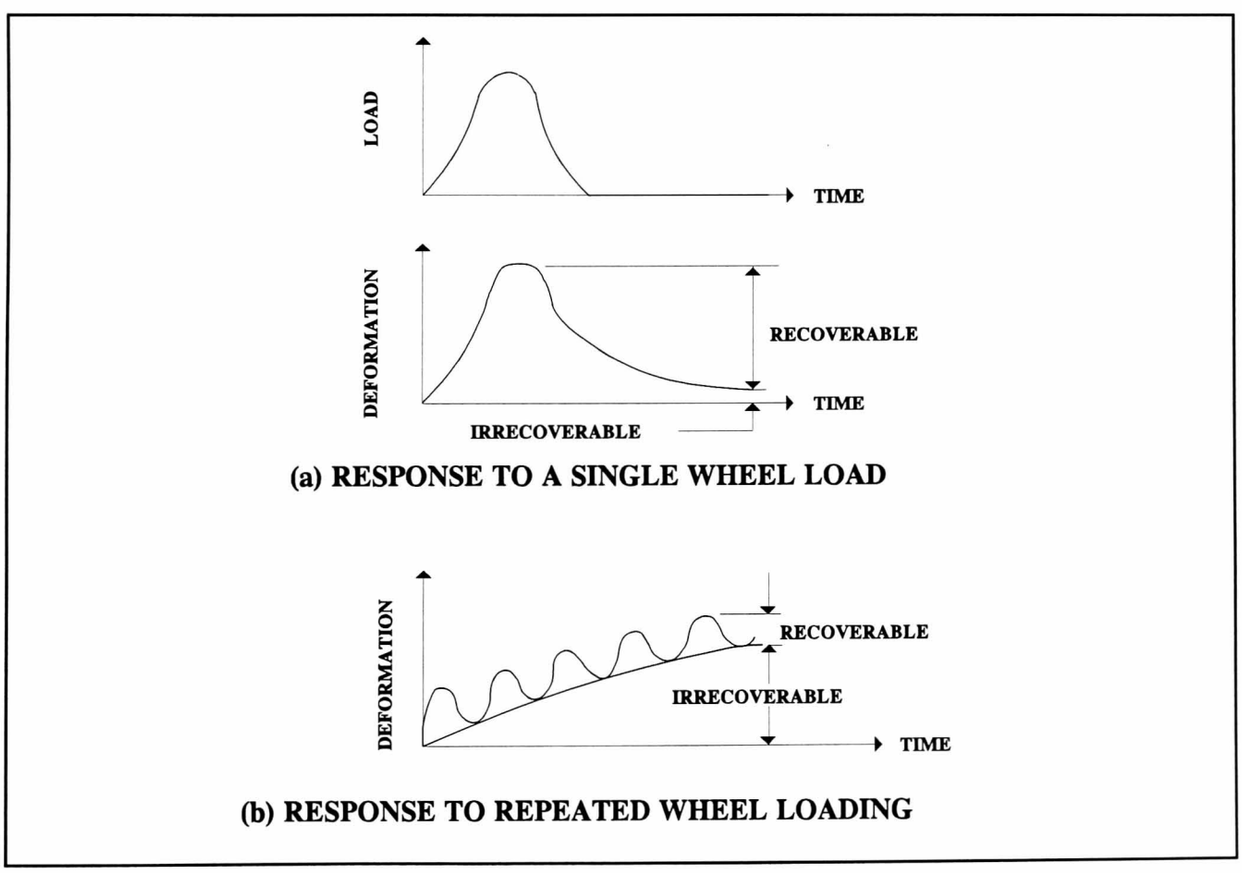


Figure 1.9 - Visco-elastic Response to Millions of Wheel Loadings.

Detailed information can be obtained from a number of sources on permanent deformation, the most recent of which is a doctoral thesis by Gibb (32). Further information is not provided here as it is outside the bounds of this work.

1.4.3 Fatigue Cracking

Fatigue cracking consists of two phases crack initiation and crack propagation. Crack initiation is generally described as the coalescence of micro-cracks to form a macro crack under the repeated application of tensile strains. Crack propagation is the growth of the macro crack through the material under further application of tensile strains. There are many complicated tests which can measure the life to crack initiation but no test which can, at present, reliably measure crack propagation, and, as described earlier, analytical methods, which are the way forward, require this information.

It must be stated at this point that the fatigue properties of a bituminous mixture cannot be taken in isolation and that the stiffness must also be considered as it is this which determines the magnitude of the tensile strain experienced by the material. This then determines the life to crack initiation of the material. It is also shown in this thesis that crack propagation is dependent upon the stiffness of the material.

Over the last 30 years there has been much research into the area of fatigue but very little has been translated into practice. This is considered to be due to both the complexity and, therefore, cost of testing and the difficulty in applying the results of the element testing to the response of the pavement. Thus it was considered important that a simple, quick cost effective method of determining an indication of the fatigue characteristics of a bituminous mixture be developed to help 'pave the gap' between research and practice.

The work described in this thesis then develops and demonstrates the theme that a simplified test method can reliably be used to ascertain the life to crack initiation and it also shows a novel method for assessing crack propagation giving an initial indication into the way in which both methods could be used in analytical methods for design purposes.

1.5 References

1. Margery, I.D., "Roman roads in Britain," John Baker, London, 1987.
2. Earle, J.B.F., "Black top - A history of the British flexible roads industry," Basil Blackwell, Oxford, Asphalt and Coated Macadam Association (ACMA), 1974.
3. Anon, "Collins Concise Encyclopedia," Book Club Associates, Wm. Collins Sons & Co. Ltd., 1978.
4. Anon, "Bituminous mixes and flexible pavements - An introduction," British Aggregate Construction Materials Industries (BACMI), 1992.
5. Reader, W.J., "MACADAM The McAdam Family and the Turnpike Roads 1798 - 1861," Heinemann, London, 1980.
6. Hill, C.P., "British Economic and Social History 1800 - 1964," Arnold, London, 1970.
7. Anon, "The AASHO road test, Report 7, Summary report," Special Report 61G, Highway Research Board, 1962.
8. Department of the Environment and Road Research Laboratory, "Road Note 29 - A guide to the structural design of pavements for new roads," HMSO, 1960.
9. Department of the Environment and Road Research Laboratory, "Road Note 29 - A guide to the structural design of pavements for new roads - Second edition," HMSO, 1965.
10. Department of the Environment and Road Research Laboratory, "Road Note 29 - A guide to the structural design of pavements for new roads - Third edition," HMSO, 1970.
11. Transport and Road Research Laboratory, "The structural design of bituminous roads," Laboratory Report 1132, 1984.
12. Department of Transport, "Structural design of new road pavements," Departmental Standard, HD 14/87, 1987.
13. Department of Transport, "Design Manual for Roads and Bridges. Volume 7: Pavement Design and Maintenance," Her Majesty's Stationary Office, London, 1994 with Amendments at August 1995.

14. Brown, S.F. and Brunton, J.M., "An introduction to the analytical design of bituminous pavements - 3rd edition," University of Nottingham, Department of Civil Engineering, U.K., 1992.

15. Anon, "Shell pavement design manual - Asphalt pavements and overlays for road traffic," Shell, 1978.

16. Anon, "Pavement design; A guide to the structural design of road pavements," National Association of Australian State Road authorities (NAASRA), 1987.

17. Anon, "AASHTO guide for design of pavement structures," Volume 1, American Association of State Highway and Transport Officials (AASHTO), 1986.

18. Anon, "Thickness design - Asphalt pavements for highways and streets," The Asphalt Institute, Manual Series N° 1 (MS - 1), September 1981.

19. Transport Research Laboratory and Overseas Development Administration, "A guide to the structural design of bitumen surfaced roads in tropical and sub-tropical countries - Overseas road note 31," Crown Copyright, 1993.

20. Whiteoak, C.D., "The Shell bitumen handbook," Shell Bitumen U.K., 1990.

21. British Standards Institution, "Single Coat Asphalt," B.S. 510, 1933.

22. British Standards Institution, "Two Coat Asphalt," B.S. 511, 1933.

23. British Standards Institution, "Hot Rolled Asphalt for Roads and Other Paved Areas," B.S. 594 : Part 1, 1992.

24. British Standards Institution, "Coated Macadams for Roads and Other Paved Areas," B.S. 4987 : Part 1, 1993.

25. Scholz, T.V., "Durability of Bituminous Paving Mixtures," PhD Thesis, University of Nottingham, Department of Civil Engineering, October 1995.

26. British Standards Institution, "Mastic Asphalt (Natural Rock Asphalt Fine Aggregate) for Roads and Footways," B.S. 1446, July 1973.

27. British Standards Institution, "Mastic Asphalt (Limestone Fine Aggregate) for Roads , Footways and Pavings in Building," B.S. 1447, 1988.

28. Liljedahl, B., "Mix Design for Heavy Duty Asphalt Pavements," Asphalt Review, Volume 11, Number 3, September 1992.

29. Anon, "Mix Design Methods for Asphaltic Concrete and Other Hot-Mix Types," Manual Series N° 2 (MS-2), The Asphalt Institute, Lexington, Kentucky, 1988.

30. British Standards Institution, "Method for the Determination of the Indirect Tensile Stiffness Modulus of Bituminous Materials," Draft for Development 213, 1993.

31. Perl, M., Uzan, J. and Sides, A., "Visco-Elasto-Plastic Constitutive Law for a Bituminous Mixture Under Repeated Loading," Transport Research record (TRR) 911, pp 20-27, 1983.

32. Gibb, J.M., "Evaluation of Resistance to Permanent Deformation in the Design of Bituminous Paving Mixtures," PhD Thesis, University of Nottingham, Department of Civil Engineering, January 1996.

BACKGROUND TO FATIGUE OF BITUMINOUS MIXTURES

2.1 Introduction

Traditionally fatigue has been defined as:

> "The phenomenon of fracture under repeated or fluctuating stress having a maximum value generally less than the tensile strength of the material."

This definition (1) has been applied to pavements by assuming that the application of wheel loads is the only mechanism which can create these repeated stresses, and therefore strains. The magnitude of the tensile strain is dependent on the stiffness modulus and the nature of the pavement. Theoretical analysis and field studies have indicated that tensile strains are of the order 30 - 200 microstrain under a standard axle load at the bottom of the main structural layer in a typical pavement construction (2). Therefore, under these conditions and applying the above definition, the possibility of fatigue cracking exists.

Recent research (3) has indicated, that in the U.K., fatigue cracking in full-depth bituminous pavements, as defined above, i.e. cracking initiating at the bottom of the layer and induced by vehicle loading, rarely occurs. However, cracking of U.K. roads does occur and, hence, a new definition, incorporating all possible methods of crack development, needs to be put forward. This proposed definition is:

> "Fatigue in bituminous pavements is the phenomenon of cracking. It consists of two main phases, crack initiation and crack propagation, and is caused by tensile strains generated in the pavement by not only traffic loading but also temperature variations and construction practices."

The pavement structure is subject to cyclic variations in temperature which cause it to expand and contract thereby inducing tensile strains in the material. The temperature

variations and gradients in a pavement can also cause differential movement between layers and this can also lead to the generation of tensile strains in the pavement. The construction practices referred to in the new definition are dominated by roller cracks in the surface of the materials generally caused by compaction when the material is too cold. A second construction practice (U.K. only) which may lead to fatigue failure is to roll coated chippings (single sized high quality aggregate coated with a thick film of bitumen) into the surface of a HRA surface course and it is considered, by the author, that these may be crack initiation sites.

Under this new definition, therefore, it is necessary to evaluate both the life to crack initiation and life for crack propagation in order to obtain an indicative picture of the fatigue performance of a bituminous mixture.

The information given in the rest if this chapter is intended not as a comprehensive literature review on fatigue, as this can be found elsewhere (4, 5, 6, 7) and would warrant a document in its own right, but as an overview of methods of evaluation, their uses and the parameters which affect fatigue.

2.2 Test Methods for Fatigue

Extensive fatigue testing has been carried out since the early fifties and during this time a number of different test configurations have emerged. It is possible to classify the commonly used ones into categories dependent upon the mode of loading as follows:

1. *Simple flexure*

   Centre point beam flexure (three point bending) (8)

   Four point flexure (9)

   Rotating cantilever beam flexure (10)

   Two point beam flexure (trapezoidal cantilever) (11)

2. *Direct Axial Loading*

   Cylindrical specimens in tension and compression (10)

Necked cylindrical specimens in tension and compression (12)

3. *Diametral Loading* (13)

Figure 2.1 gives a schematic representation of the tests which have had the most extensive use. In the Figure the arrows indicate the direction of the applied loading which induce the tensile stresses and strains and, hence, cause fatigue failure.

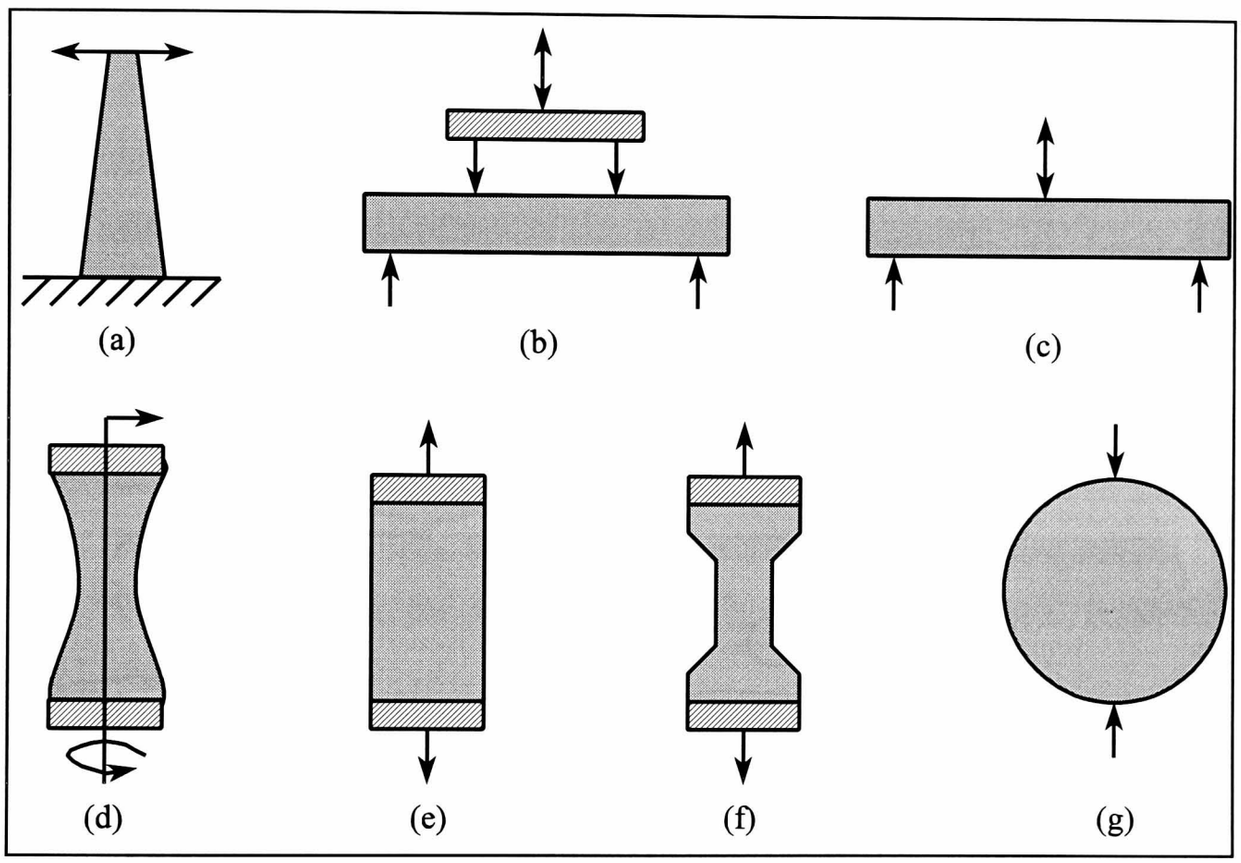


Figure 2.1 - Schematic Demonstrating the Main Forms of Fatigue Test: (a) Two Point Bending; (b) Four Point Bending; (c) Centre Point Bending; (d) Rotating Bending; (e) Direct Axial Loading; (f) Direct Axial Loading (Necked Specimen) and (g) Diametral Loading.

The advantages and disadvantages of each category have been discussed by Judycki (4) and are included here, along with the Author's views, for ease of comparing the different methods.

Simple Flexure

Advantages

1. The methods are well known, widespread in use and readily understood.
2. The measured, fundamental properties can be used for both mixture evaluation and pavement design.
3. The results can be used directly (with an appropriate shift factor) in the structural design of pavements to estimate the propensity for cracking.
4. Results of stress controlled testing (Section 2.3.2) can be used for the design of thick asphalt pavements whereas results of strain controlled testing (Section 2.3.2) can be used for the design of thin asphalt pavements.
5. In four point bending, failure of the specimen is initiated in a region of relatively uniform stress which helps to reduce the coefficient of variation of the test results, therefore, requiring fewer specimens.

Disadvantages

1. Validation of laboratory results by comparison with in-situ pavements is difficult due to the requirement for a shift factor.
2. The methods are costly, time consuming and require specialised equipment.
3. Unlike that within the pavement structure, the state of stress is essentially uniaxial.
4. In centre point loading initiation of failure in a region of relatively uniform tensile stress is not possible.
5. The centre point loading method is not suitable for fatigue tests on material with a stiffness modulus less than 3,000MPa.
6. In centre point loading the clamping effect adversely influences the accuracy of the method, which itself is generally poor.
7. The simple flexure tests do not provide adequate data for the structural design of pavements of intermediate thickness asphalt layers (between 150 and 50mm). For such pavements additional adjustment of the fatigue data is necessary as these intermediate layers work at an intermediate mode of loading (between stress and strain control).

These advantages and disadvantages for the simple flexure test are generally correct. However, it is the authors view that advantage 5 is not statistically proven and, hence, it is really a supposition rather than a fact and from the author's experience the four point bending test requires around the same number of specimens as third point loading.

Disadvantage 1 is not really a disadvantage for simple flexure tests alone but is in fact a disadvantage of all fatigue tests and is in fact the most difficult of all the disadvantages of any of the tests to overcome, as validation with in-situ pavements is almost impossible to achieve with any level of confidence.

Disadvantage 2 is true but it is, perhaps, unfair to state that simple flexure tests require specialised equipment as, in fact, all the tests require specialised equipment. However, with the advent of cheap, 'off the shelf' pneumatic equipment now widely available it is likely that the servo-hydraulic, or electro-magnetic, equipment required for simple flexure tests will become more and more specialised as time progresses.

Disadvantage 5 requires clarification as it is not immediately obvious why mixtures with a stiffness modulus less than 3,000MPa are unsuitable for simple flexure tests. It is the author's view that this is because mixtures with a low stiffness modulus will creep under their self weight and, hence, tensile strains will be imposed on the specimens in addition to those caused by the repetitive loading. This may lead to wide scatter in the results and, hence, less confidence in the fatigue lines which are generated.

The clamping effect referred to in disadvantage 6 requires some additional comment here as clamping induces stresses around the point of contact which it is very difficult to take into account in the analysis of the specimen. If these clamping stresses become too high, due to over tightening of the clamps, then with the stresses superimposed by the loading of the specimen it is possible for failure to be initiated in these areas, particularly as the high level of stress lowers the stiffness modulus of the mixture (see Chapter 3) and, hence, increases the magnitude of the tensile strain which will cause the specimen to fail prematurely. These unknowns can, therefore, lead to low confidence in the result .

Disadvantage 7 is not really a disadvantage with simple flexure tests but is a problem of interpreting the result correctly in the subsequent pavement analysis and this is true for all the test methods described herein.

Direct Axial Loading

Advantages

1. When compared to flexural tests these are simpler, less costly and testing time is generally shorter.
2. Tensile stresses and strains can be easily determined and/or measured.
3. Specimens may be circular or rectangular in cross section.
4. The 'pure' state of stress/strain with no shearing simplifies the interpretation of the results.

Disadvantage

1. The test does not well duplicate the condition of stress and strain in the field.

Advantage 1 is only in part correct as the glueing of end-caps onto the specimen and the requirement for precise alignment mean that the test is probably just as complicated as simple flexure tests which certainly are not as heavily influenced by their position in relation to applied load.

Advantage 3 is not really an advantage as the specimens are required to be sawn or cast into very precise geometries and the test is heavily influenced by the surface conditions. Therefore, the fact that two geometries may be used is an advantage but their manufacture is really a disadvantage of the test.

Diametral Loading

Advantages

1. The test is relatively simple to conduct.
2. The equipment is applicable for other test methods (stiffness and indirect tensile strength under static loading).
3. Field cores may be tested.

4. The biaxial state of stress is considered to better represent the stresses occurring in-situ than the uniaxial state of stress does.
5. Failure is initiated in an area of relatively uniform tensile stress and is not seriously affected by surface conditions.
6. The coefficient of variation of test results is low compared to other test methods, therefore, requiring fewer specimens.

Disadvantages

1. It is impossible to vary the ratio of the tensile and compressive stresses at the centre of the specimen to duplicate the stresses occurring in-situ.
2. The stress concentrations and distributions at the points of load application are very different compared to those occurring in-situ.
3. The stress reversal which occurs in-situ cannot be achieved with this method.
4. During testing permanent deformation occurs which is usually prohibited in flexural tests.
5. The fatigue life determined from this test has been found to differ significantly from that determined from other methods.

Advantage 2 is not really an advantage specific to the diametral mode of testing as measurements of stiffness modulus and static failure tests can be carried out in the other configurations previously described.

Although it is considered that the biaxial state of stress better represents field conditions this is a questionable statement as in reality there is a complex triaxial state of stress which cannot be modelled any better by a biaxial state of stress than by a uniaxial one. Also the magnitude of the stresses and strains in the diametral test are not generally measured but are calculated from elastic theory whereas in the other test method the strain at least can easily be measured.

Advantage 5 only holds true for certain conditions of test as at elevated temperature shear or compressive failure can occur as opposed to tensile failure (Chapter 3). However, the lack of sensitivity to surface conditions is certainly an advantage over other methods.

Advantage 6 was found, in this research, to be true and makes the test commercially desirable.

Disadvantage 5 states that other researchers found the diametral mode of testing to give results which differed significantly from other methods, however the object of this research was to find a method which gave an **indication** of the fatigue performance and, therefore, this was not considered by the author to be a real disadvantage. This research also found that under certain conditions of test that this disadvantage was not true.

In addition to these methods, which tend to look principally at the life to crack initiation, there has been a limited amount of testing carried out, using specially designed tests, to assess the resistance of a bituminous mixture to crack propagation. These tests can be categorised into two groups:

1. *Supported Flexure*
   Supported beam (14)
   Supported disc (15)
   Supported slab (16)

2. *Fracture Mechanics*
   Notched beams (17, 18, 19)

The advantages and disadvantages are again reproduced from Judycki (4).

Supported Flexure

Advantages

1. Better simulation of field conditions is possible.
2. The method enables testing of intermediate modes of loading (between stress and strain controlled).
3. The problem of sagging at higher temperatures due to specimen weight is eliminated.

4. The scatter of results is less than with other methods as the support of the specimens reduces the effect of minor imperfections in the specimen.

Disadvantages

1. The state of stress is predominantly uniaxial.
2. The test is far more time consuming than any other fatigue test.
3. Compared to simple flexure, test equipment is more expensive and complicated.

Although advantage 4 does indicate that the support helps to reduce the effect of minor imperfections the statement is not entirely true as the specimen will still fail at its weakest point. Therefore, attention to the surface must be paid or stress concentrations around the imperfections will still occur causing premature failure.

Disadavantage 2 is true but the length of test can be reduced by increasing the magnitude of the applied stress, provided that it is acceptable to do so. Therefore, this statement should be qualified by adding that the overall time of test for a range of specimens is longer than for other test methods.

Fracture Mechanics

Advantages

1. The test provides the possibility of analysing the crack propagation of asphaltic layers over cracked bases (reflective cracking).
2. The testing time is short compared with other methods.
3. The theory of the test is well established and has been applied successfully to other engineering materials.

Disadvantages

1. The test provides information on stable crack growth but does not explain crack initiation or unstable crack growth.
2. At higher temperatures, due to visco-elastic behaviour of the bituminous mixture, the cracking mechanism is more complex than that described by Paris's law (Section 6.2).

3. Validation of this method requires considerable amounts of data which at present are unavailable.
4. The field stress conditions are not adequately duplicated in current tests as the compressive and shearing stresses are neglected.

The first disadvantage only really holds true when considering linear elastic fracture mechanics. It has been shown that, by using visco-elastic fracture mechanics, the onset of damage, coalescence of micro cracks to form a macro crack and crack propagation can be described relatively well and a more detailed discussion of this is given in Section 6.2.

The validation of this method does require a large amount of data but, in reality, no more than is necessary for the validation of any other method and, hence, disadvantage 3 is not entirely valid.

Disadvantage 4 is a statement which also holds true for all the other methods previously described and, hence, is not specific to fracture mechanics.

The final type of test which must be considered is that which is capable of examining both crack initiation and crack propagation and these are generally wheel tracking tests of various magnitudes (20, 21). The advantages and disadvantages are summarised below (4).

Wheel Tracking Tests

Advantages

1. Better simulation of field conditions than any other test.
2. Both crack initiation and propagation can be monitored.
3. Special pavement structures can be tested (e.g. grid reinforced pavements) (22).

Disadvantages

1. The tests are extremely expensive, time consuming and require specialised equipment.

2. The scatter in the test results is large compared to other test methods.

A comparison of the different test methods and their results is difficult but a team of leading researchers at the University of California, Berkeley established a rating system, for life to crack initiation tests, during the Strategic Highway Research Program (23). The following criteria were applied to each of the tests:

1. Simulation of field conditions,
2. Application of test results,
3. Simplicity and
4. Field correlation.

According to their evaluation categories of test were ranked in the following order:

1. Simple Flexure Tests
2. Diametral Loading
3. Dissipated Energy Method (described later)
4. Fracture Mechanics Test.

Although this is one method of ranking test methods a consideration of whether the test method is fundamental should have been carried out as only after gaining fundamental knowledge can simplification be tolerated. Hence, diametral loading should be at the bottom of the above list even though it has much to recommend it.

One of the objectives of this research was the development of a simple and commercially viable fatigue test, as at present, in the U.K., there is no specified method for measuring the fatigue characteristics of a bituminous paving mixture. The diametral loading, or Indirect Tensile Fatigue Test (ITFT), has been evaluated because of this and was chosen primarily because it used cylindrical specimens and was able to make use of the simple pneumatic loading systems available in most laboratories throughout the U.K. and the

rest of the world. The details of the testing, results and conclusions of this work are presented in later chapters.

2.3 Factors Affecting Fatigue

This section deals with the factors which have been shown to affect fatigue: mode of loading; loading pattern; rest periods and mixture variables.

2.3.1 Stresses Induced in a Pavement

In order to have a representative loading condition in a fatigue test it is necessary to look at how the loading is applied to a pavement structure. Figure 2.2 shows how the stresses developed by a moving wheel apply to an element in the pavement and how they change with time.

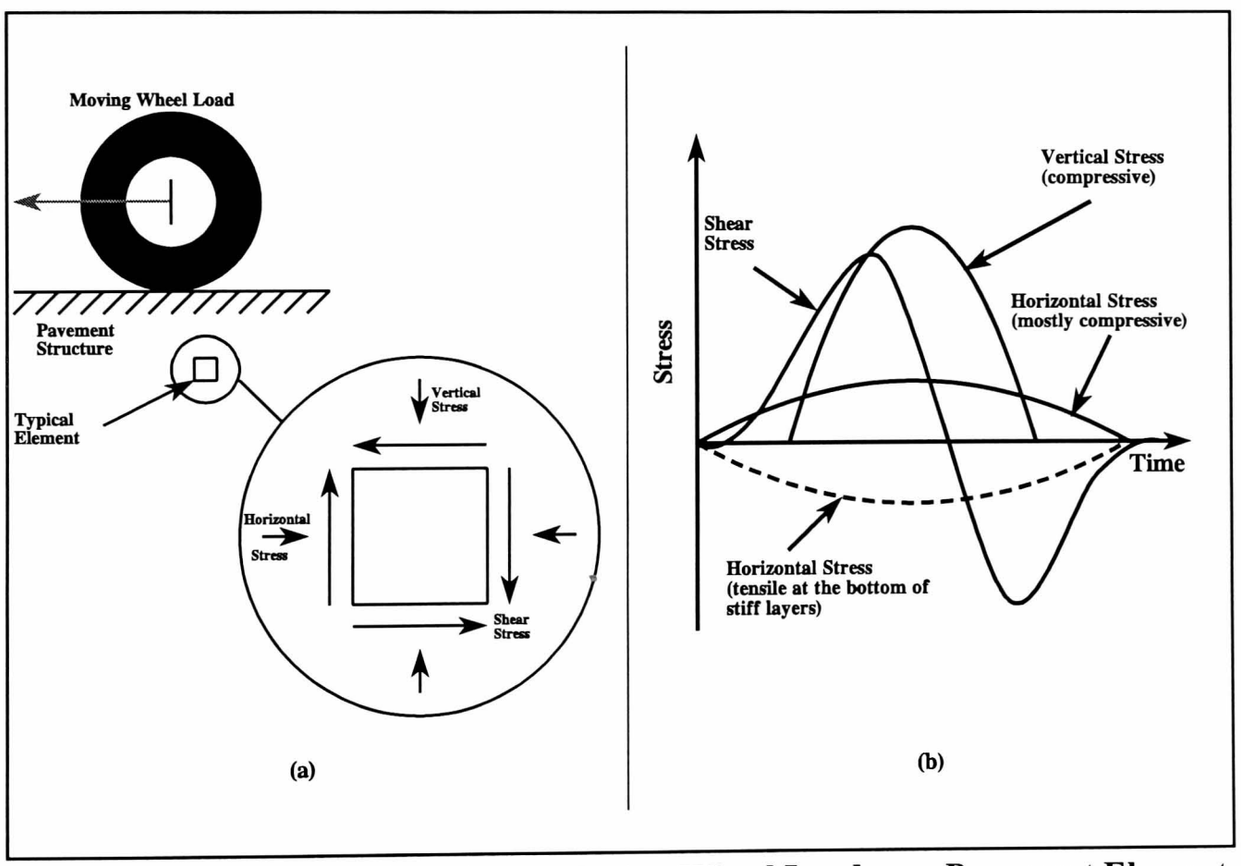


Figure 2.2 - Stresses Induced by a Moving Wheel Load on a Pavement Element, After Brown (24).

The time of loading is dependent upon vehicle speed, depth below the pavement surface and wheel, axle and suspension configuration (25). At a velocity of 60 km/h and depth

of 150mm, for example, the time of loading will be approximately 0.015s and as bituminous materials are visco-elastic their properties are time dependent which will have an effect on the magnitude of the tensile strains developed in the structure and, hence, the fatigue life.

2.3.2 Mode of Loading

There are two main modes of loading which can be applied in a fatigue test:

- Stress controlled - The amplitude of the applied load is held constant during the test.
- Strain controlled - The amplitude of the applied deformation is held constant.

Strictly speaking it is the load or displacement which is controlled and the stress and strain calculated from them. However, as controlled stress and strain are commonly used terms they will be employed through the rest of this thesis.

Figure 2.3 presents a graphical interpretation of the fatigue behaviour of bituminous

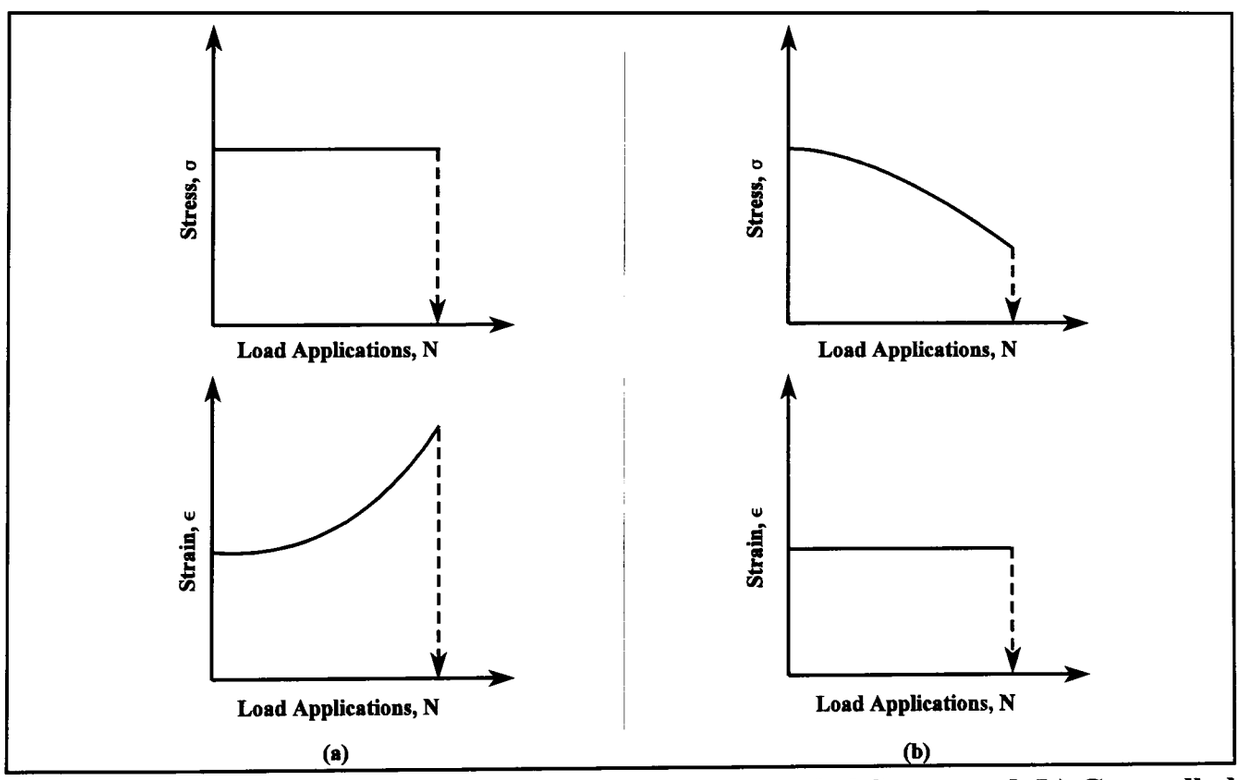


Figure 2.3 - Graphical Representation of (a) Controlled Stress and (b) Controlled Strain Modes of Loading, After Epps and Monismith (26).

mixtures under the two different modes of loading. In the controlled strain mode of loading, the strain is held constant and the stress gradually decreases as the specimen is damaged, thus, requiring less stress to produce the same strain. In the controlled stress mode of loading, the stress is held constant and the strain gradually increases as the specimen is damaged until failure.

The results from stress and strain controlled testing are different for the same bituminous mixture. This difference in behaviour has been explained in terms of the mechanism of failure, by Brown (24), as follows: The failure is initiated by the formation of cracks at discrete points of high stress concentration and during part of the test cracks propagate through the material until fracture occurs. The propagation phase depends on the stress intensity at the crack tip so that in a stress controlled test crack propagation is very rapid. In a strain controlled test, however, the stress gradually decreases after initiation as the stiffness of the material is effectively decreased. Therefore, strain controlled tests can include long periods of crack propagation.

It is important to reiterate that it is possible in a pavement to get a mode of loading in between controlled stress and controlled strain which will give an intermediate fatigue line. This is presented graphically in Figure 2.4.

Brown (24) has presented the following physical explanation of the different modes of loading in a pavement structure. The pavement as a whole system is subjected to a stress controlled loading. Those layers which have considerable structural significance (thick and stiff) will also be stress controlled. However, thin surfacings are essentially 'moved' by the lower structural layers which results in a strain controlled situation. This description was given credence by work done earlier by Monismith and Salam (27) who analysed pavement structures using multilayer elastic theory and found that:

- The strain controlled mode of loading is characteristic for thin asphalt pavements (thickness of asphalt layers less than 50mm),
- The stress controlled mode of loading is characteristic for thick asphalt pavements (thickness of asphalt layers greater than 150mm) and

- For the remaining ranges of thicknesses some intermediate mode of loading is appropriate.

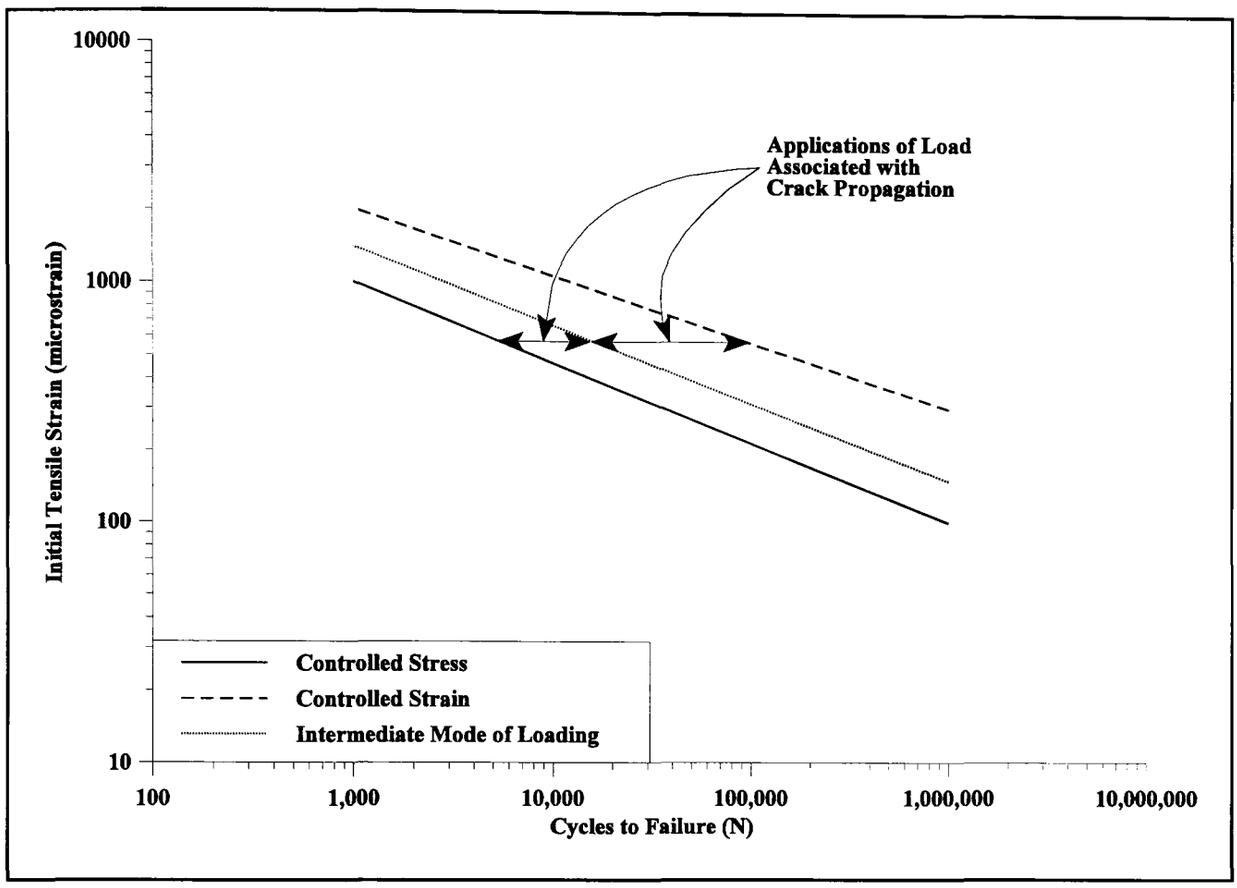


Figure 2.4 - Graphical Representation of the Differences in Fatigue Response to Various Modes of Loading.

Considering this information leads to the conclusion that, for the main trunk road network in the U.K., a controlled stress mode of loading is appropriate as the thickness of the bituminous material is normally in excess of 225mm.

2.3.3 Loading Waveform

It has been reported that the loading waveform affects the fatigue life of a bituminous material (28, 29) and the phenomenon has been explained by the energy put into the system per loading cycle. It would appear that for the same stress amplitude the fatigue life is reduced if greater energy is imposed on the tested specimen per cycle. It has been suggested that the energy is proportional to the area occupied by a load waveform in a stress (or strain) against time coordinate system (28). Table 2.1 gives the results found by Raithby and Sterling (28) and Figure 2.5 shows the main forms of loading waveform.

Table 2.1 - Effect of Waveform Shape on Fatigue Life, After Raithby and Sterling (28).

Waveform	Temperature (°C)	Stress Amplitude MN/m^2	Initial Strain	Fatigue Life	Relative Lives
Square	25	± 0.33	1.7×10^{-4}	24,690	0.42
Sinusoidal			1.2×10^{-4}	58,950	1.00
Triangular			0.67×10^{-4}	85,570	1.45

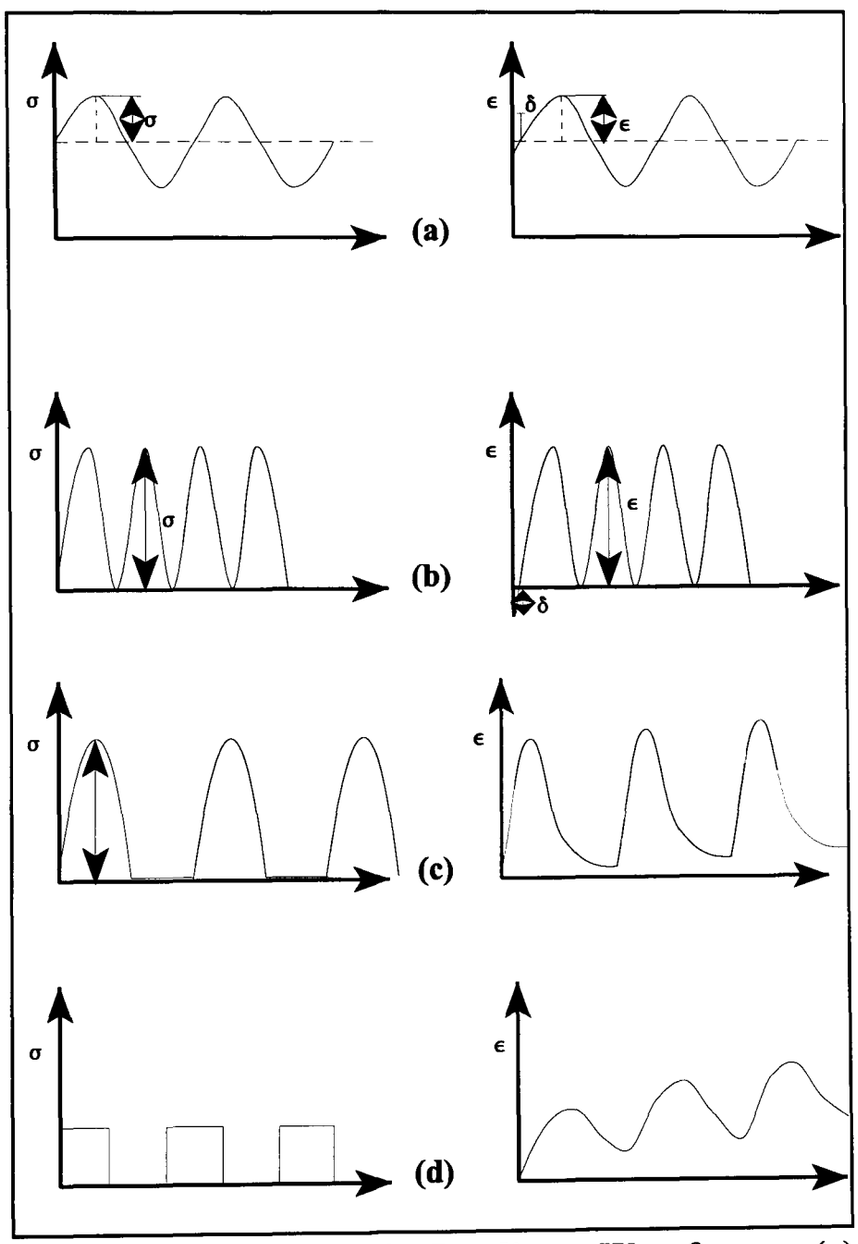


Figure 2.5 - Types of Loading Waveform: (a) Sinusoidal; (b) Haversine; (c) Cyclic Loading (approximating a haversine) and (d) Cyclic Loading (square wave), after Said (30).

Loading frequency and duration have a significant effect on fatigue life. Decreasing the duration of the load pulse (increasing the rest period), while holding the frequency constant, increases the fatigue life (increase in stiffness). Increasing the frequency of the load pulse increases the fatigue life.

It would appear from the literature that the loading waveform should approximate that which is experienced in the field, as it has a very important effect (Table 2.1). Therefore, some form of cyclic loading should be used. Figure 2.2 would also seem to indicate that a haversine is the closest waveform to that experienced in the field and, thus, a waveform of the sort shown in (c) of Figure 2.5 should be used.

2.3.4 Rest Periods

A rest period is the time between consecutive application of wheel loads and are important as they allow time for cracks to heal and stresses and strains to relax due to the viscous flow of the bitumen. Rest periods are different for different roads and for different times of the day as they are dependent upon the volume of traffic.

A number of researchers (8, 28, 31, 32, 33, 34) have investigated the effect of rest periods on the fatigue response of a bituminous paving mixture. The general conclusion is that the inclusion of a rest period gives an increase in fatigue life of between 5 and 25 times dependent upon the ratio of the loading duration to the rest period.

A second effect, shown by these researchers, is that of healing which occurs if specimens are stored for extended periods of time between applications of load. The stored specimens appear able to rejuvenate their properties and the beneficial effect is greatest at high temperatures, long storage times and high bitumen contents. The use of low viscosity binders also increases the effect of healing. These factors would seem to indicate that healing is a function of the viscous flow of the bitumen.

Rest periods and healing are able to occur on even the most heavily trafficked roads due to vehicular spacing and when the road is not subjected to frequent traffic loading (night

time etc.). Therefore, these effects should be incorporated into the fatigue data for analytical pavement design. Brunton (35), for example uses a value of 20, for the effects of rest periods.

2.3.5 Mixture Variables

Much work has been carried out in this area but probably the most definitive piece was by Cooper and Pell (36) in the early seventies. As indicated earlier this is not an extensive review and the aim of work is not to generate further information in this area. Therefore, consideration will only be given to those variables which have a primary effect on the crack initiation response of a bituminous paving mixture:

- Mixture Stiffness,
- Bitumen Content,
- Bitumen Properties,
- Air Voids,
- Aggregate and
- Filler

These volumetric parameters are described in detail in the Asphalt Institutes Manual on Mix design Methods for Asphaltic Concrete and Other Hot-Mix Types (37).

Mixture Stiffness

Mixture stiffness can be affected by the temperature, speed of loading, level of compaction and type of bitumen, with the first two having the most marked effect, and is considered to be the most important factor affecting the fatigue life of a pavement.

In the stress controlled mode of loading, mixtures with a high stiffness exhibit an increase in fatigue life, conversely in the strain controlled mode of loading there is a decrease in fatigue life. However in the controlled stress mode if the results are presented in terms of initial tensile strain against the number of load applications the fatigue relationship is much less dependent upon stiffness (26, 38, 39). Due to this it is accepted, by some researchers, that mixtures of greater stiffness should be used in thick bituminous layers

which are subject to stress control and mixtures of lower stiffness should be used in thin bituminous layers which are subject to strain control. However, this takes no account of the effect stiffness has on either the crack propagation rate or healing and if the relationships, for crack propagation, developed in this thesis are correct then low stiffness pavements will have a longer service life than high stiffness ones.

Bitumen Content

Bitumen content affects the fatigue response in the following manner:

- The increase of the bitumen content, within a practical range, will increase the fatigue resistance of a mixture.
- For the longest fatigue life the volume of bitumen should be as high as possible, but limited according to permanent deformation requirements (40).
- For a given mixture there is an optimum bitumen content for fatigue and this is higher than that for the best resistance to permanent deformation.

Bitumen Properties

The most important properties of a bitumen, for fatigue, are stiffness and thermal susceptibility. These are normally expressed (41) in terms of stiffness modulus, penetration, viscosity, softening point and penetration index. As described earlier the fatigue response is dependent upon the mode of loading and the stiffness of the mixture, therefore, when testing in the stress controlled mode a stiffer bitumen provides a longer life whereas the converse is true for the strain controlled mode of loading. This has been verified experimentally for both cases: strain controlled, Epps and Monismith (26) and stress controlled, Cooper and Pell (36). Brown *et al* (42, 43), based on the early work at the University of Nottingham, recommends the use of hard bitumens (50pen) for thick bituminous base layers and a bitumen content of 4% in comparison to conventional base material which is made from 3.5% of 100pen bitumen. According to the analytical calculations this will give a considerable increase in fatigue life or allow a reduction in thickness, for a typical design situation, resulting in a considerable cost saving.

Void Content

The influence of void content, or compaction level, has been evaluated by many researchers (4) the results of which indicate that the lower the volume of air voids the higher the resultant fatigue life. However there is a compromise between fatigue and permanent deformation as if the air voids are reduced too much they will become over filled with bitumen, pushing the aggregates apart, and the mixture will rut very quickly (40). It has also been suggested that other properties of the voids are important (26):

- Shape
- Degree of interconnection
- Size

Although, at present no data has been found which quantify the effects.

Aggregate

Dukatz (44) presented a qualitative analysis of the effects of aggregate properties on the fatigue performance of a mixture:

- Dominant effect - Durability, toughness and hardness
- Major effect - Shape, morphology, gradation and strength
- Medium effect - Absorption, specific gravity, composition, solubility slaking
- Some effect - Surface charge
- Minor effect - Surface texture

It should be restated that these are qualitative conclusions and have not been backed up with experimental or field findings.

The effect of grading, if changed within standard limits, appears to have little effect (36) and other researchers (45) have found that the maximum nominal aggregate size is not very significant for fatigue resistance.

However, from the research presented in this report it would appear that the shape of the aggregate will play a major role in the crack propagation phase with flaky aggregate

oriented normally to the applied load giving slower rates of crack propagation than nominally spherical aggregate.

Filler

The effect of filler on the fatigue resistance of a mixture can be summarised as follows (36, 46, 47):

- An increase in the filler content improves the resistance to fatigue of a mixture, especially in the controlled stress mode of testing.
- Changes in filler content have less effect on fatigue than changes in the bitumen content.
- If the filler content is reduced below a certain limit (mixture dependent) the fatigue resistance falls sharply.
- The filler properties, particularly the quantity of filler, affect the fatigue properties of a mixture

2.4 Fatigue Relationships

In order to assess the fatigue relationship for a bituminous material it is necessary to define the failure of the test specimen in a consistent way. For the controlled stress mode of loading this is relatively easy as the specimen has a relatively short crack propagation period and, hence, the failure point of the test is when the specimen has completely failed (Figure 2.6). However, with the strain controlled mode of loading the failure point is not as well defined, due to the large amount of crack propagation included in the test and, therefore, an arbitrary definition of failure has to be made. This point of failure is then normally defined as a reduction of the initial stiffness of 50% (20, 45, 48) or in practical terms a halving of the stress required to achieve the constant strain (Figure 2.6). Having defined the point of failure for the test the interpretation of the result now must be considered. There are two main ways of expressing the results:

- Log stress against log load applications
- Log strain against log load applications

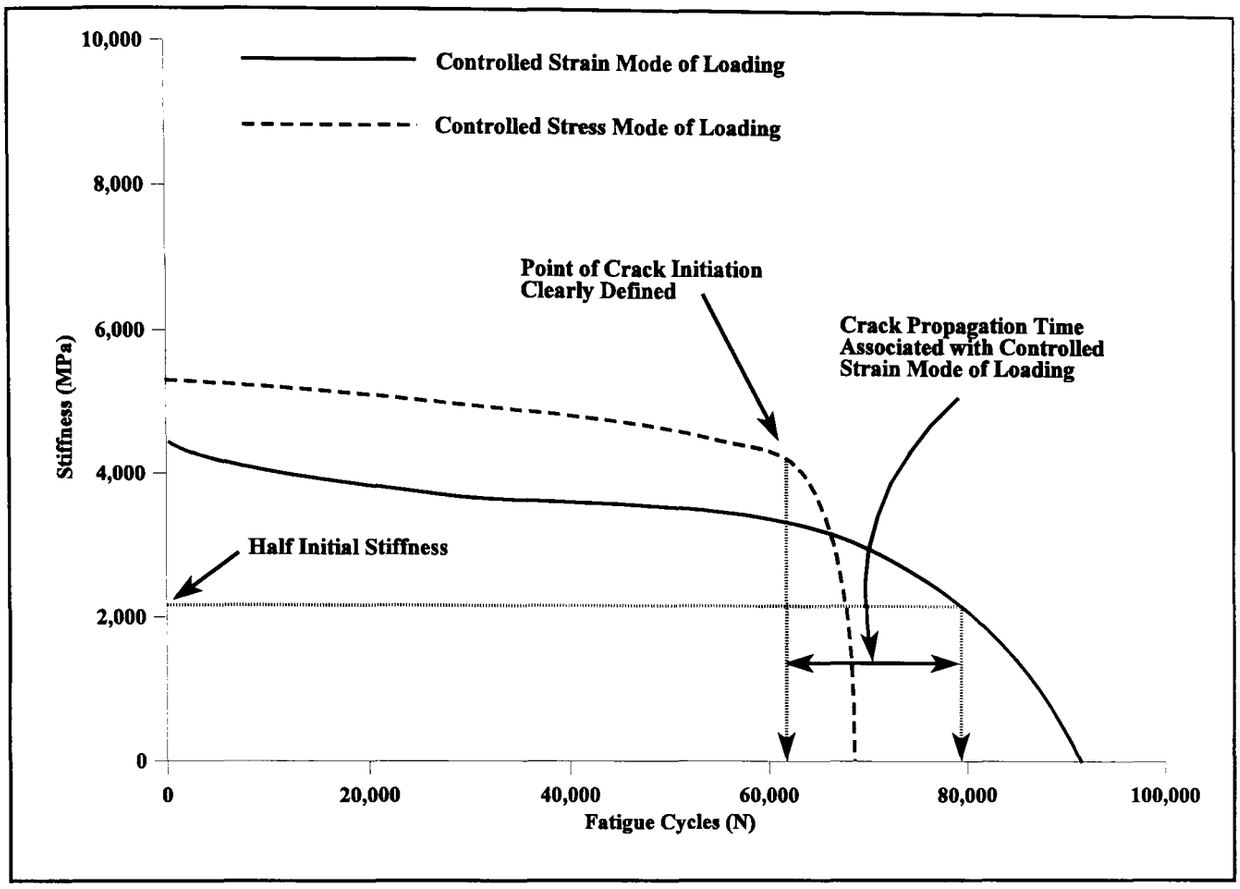


Figure 2.6 - Idealised Representation of the Failure Points for the Two Modes of Loading.

For the strain controlled test the results are normally presented in the latter manner which generates an equation of the form shown in equation 2.1.

$$N_f = A\left(\frac{1}{\epsilon}\right)^b \qquad (2.1)$$

For the stress controlled test the intuitive way to present the results is using the log stress against log load applications which generates an equation of the form shown in equation 2.2.

$$N_f = C\left(\frac{1}{\sigma}\right)^d \qquad (2.2)$$

Where:

N_f = Number of load applications to failure,

ϵ, σ = Tensile strain or stress repeatedly applied and

A, b, C, d = Material coefficients.

However, it has been demonstrated by Pell (38) that the tensile strain is the important parameter for fatigue cracking and, hence, the results from the controlled stress mode of loading are generally presented in a form similar to that shown in Equation 2.1 but with different material coefficients as shown in equation 2.3.

$$N_f = K_1 \left(\frac{1}{\epsilon_i} \right)^{K_2} \qquad \textbf{(2.3)}$$

Where:

N_f = Number of load applications to failure at a particular level of initial strain,

ϵ_i = Initial tensile strain and

K_1, K_2 = Material Coefficients.

Thus, it would appear important that, when developing a suitable test method for assessing the fatigue life to crack initiation, a reliable method of measuring, or calculating, the initial strain be generated.

It has been considered by Van Dijk *et al* (20, 32, 49) that the differences in the fatigue life of a bituminous mixture determined in stress and strain control can be explained by the dissipated energy concept. This is the amount of energy which is lost from the system, due to fatigue damage, per cycle summed for the entire life of the specimen. Van Dijk stated that for a given mixture the relationship between the dissipated energy and the number of load repetitions to fatigue is valid, independent of the testing method and temperature. This work has been progressed by Himeno (50) who developed the dissipated energy concept for three dimensional stress conditions and applied it to the failure of an asphaltic layer in pavement and by Rowe (11) who has recently shown that dissipated energy can be used to accurately predict the life to crack initiation. The author considers this method to have promise but, for the development of a practical test, it was considered pertinent to use the initial strain criterion. This was due to the fact that the measurement of dissipated energy, for a diametral test, is relatively complicated and not in keeping with the theme of a simple and commercially viable fatigue test method.

2.5 Use of Fatigue Relationships

The analytical methods presented in the first Chapter all require an input for the fatigue characteristics of the different bituminous layers. This being said all the methods use empirical nomographs or constitutive relationships which are only really applicable to the range of mixtures used to develop them. One example is the relationship developed by Cooper and Pell (36) which is used in the Nottingham Analytical Design Method (51), this can be presented as either a nomograph or as a constitutive equation. The equation is given here for ease of reference:

$$\log N_{100} = 4.13 \log V_B + 6.95 SP_i - 11.13 \qquad \textbf{(2.4)}$$

Where:

N_{100} = Number of load applications to failure at an initial strain, ϵ, of 100 microstrain,

V_B = Volume of bitumen in the mixture, % and

SP_i = Initial softening point of the bitumen, °C.

This method uses the concept that there is a focus in the log initial strain against log number of load applications domain through which all fatigue lines pass. Bonnaure *et al* (47) criticise this method of prediction as it takes no account of temperature, the equation is only appropriate for tests carried out under the controlled stress mode of loading and the concept of focal point is debatable due to the scatter of results. This being said the equation was developed further at the University of Nottingham (51) and has been used successfully in the form shown in equation 2.5 provided that it is not used at temperatures in excess of 30°C.

$$\log \epsilon_t = \frac{14.39 \log V_B + 24.2 \log SP_i - k - \log N}{5.13 \log V_B + 8.63 \log sp_i - 15.8} \qquad \textbf{(2.5)}$$

Where:

ϵ_t = Tensile strain at the bottom of the asphalt layer, microstrain,

N = Millions of standard axles,

V_B, SP_i = As in equation 2.4,

k = 46.06 for life to failure and

k = 46.82 for life to critical condition.

Therefore, if the magnitude of the tensile strain is calculated, using an appropriate analytical method (51), then the number of standard axles to the critical or failure condition can be calculated. Critical condition is defined here as a 10mm rut or the first appearance of cracking in the wheel path. Failure is defined as a 20mm rut or extensive cracking in the wheel path.

The other methods mentioned in the first Chapter are not recounted here but all use some form of constitutive relationship. However, none of the methods give the same answer when used on a standard mixture and for this reason the author felt it imperative that a simple and quick method for **measuring** the fatigue life be developed.

2.6 Summary

From the information presented in the first chapter it can be seen that there is a need for analytical pavement design techniques which in turn need input parameters based on fundamental mechanical properties. The parameter which is important, as far as this work is concerned, is fatigue.

This Chapter has described the large number of tests, test parameters, material variables, data interpretation and methods of using the fatigue relationships developed and has given an indication of the difficulties associated with each. It is the author's belief that there is a real need for a simple, cheap and quick test for measuring the fatigue properties of bituminous paving mixtures. The work reported in the rest of this thesis then concentrates on the development of such a simplified test, the development of a method for measuring the crack propagation of a bituminous mixture and the effects certain mixture variables have on crack propagation. A method is also proposed for combining all this information in a practical manner for use in analytical pavement design.

2.7 References

1 Pell, P.S., "Fatigue of Bituminous Materials in Flexible Pavements," Journal of the Institute of Highways Engineers, pp 17-23, August 1971.

2 Kingham, I.R., "Failure Criteria Developed from AASHO Road Test Data," Highway Research Board, Special Report 140, Proceedings of a Symposium on Structural Design of Asphalt Concrete Pavements to Prevent Fatigue Cracking, pp 183-196, 1973.

3 Wu, F., "Assessment of Residual Life of Bituminous Layers for the Design of Pavement Strengthening," PhD. Thesis, Council for National Academic Awards, London, March 1992.

4. Judycki, J. "Fatigue of Asphalt Mixes," University of Oulu, Publications of Road and Transport Laboratory, Oulu, Finland, 1991.

5. Anon, "Fatigue Characterisation of Asphalt Mixes: Literature Review," Project F 1(a), Australian Asphalt Pavement Association (AAPA), July 1993.

6. Anon, "Fatigue Characterisation of Asphalt Mixes: Dissipated Energy Concept," Project F 1(b), Australian Asphalt Pavement Association (AAPA), July 1993.

7. Tayebali, A.A., Deacon, J.A., Coplantz, J.S., Harvey, J.T. and Monismith, C.L., "Fatigue Response of Asphalt-Aggregate Mixtures, Part 1-Test Method Selection," Strategic Highway Research Program (SHRP), SHRP Project A-003A, Institute of Transportation Studies, University of California, Berkeley, November 1992.

8. Bonnaure, F.P., Huibers A.H.J.J., Boonders A., "A Laboratory Investigation on the Fatigue Characteristics of Bituminous Mixes," Proceedings of Association of Asphalt Paving Technologists (AAPT), Volume 51, pp 104-126, 1982.

9. Monismith, C.L., Epps, J.A. and Finn, F.N., "Improved Asphalt Mix Design," Proceedings of Association of Asphalt Paving Technologists (AAPT), Volume 54, pp 347-390, 1985.

10. Pell, P.S. and Cooper, K.E., "The Effect of Testing and Mix Variables on the Fatigue Performance of Bituminous Paving Mixtures," Proceedings of Association of Asphalt Paving Technologists (AAPT), Volume 44, pp 1-37, 1975.

11. Rowe, G.M., "Performance of Asphalt Mixtures in the Trapezoidal Fatigue Test," Proceedings of the Association of Asphalt Paving Technologists (AAPT), Volume 62, pp 344-384, 1993.

12. Eckmann, B., "Exxon Research in Pavement Design 'Moebius' Software; A case Study Reduction of Creep Through Polymer Modification," Proceedings of the Association of Asphalt Paving Technologists (AAPT), Volume 58, pp 337-361, 1989.

13. Kennedy, T.W., "Characterization of Asphalt Pavement Materials Using the Indirect Tensile Test," Proceedings of the Association of Asphalt Paving Technologists (AAPT), Volume 46, pp 132-150, 1977.

14. Majidzadeh, K., Kauffmann, E.M. and Saraf, C.L., "Analysis of Paving Mixtures from the Fracture Mechanics Viewpoint," American Society of testing and Materials (ASTM) Special Publication 508, Fatigue of Compacted Bituminous Aggregate Mixtures, ASTM, Philadelphia, pp 67-84, 1971.

15. Hugo, F. and Kennedy, T.W., "Surface Cracking of Asphalt Mixtures in Southern Africa," Proceedings of the Association of Asphalt Paving Technologists (AAPT), Volume 54, pp 454-501, 1985.

16. Yuce, R. and Monismith, C.L., "Prediction of Load Associated Cracking in Pavement Slabs from Laboratory Determined Fatigue Data," Proceedings of the Association of Asphalt Paving Technologists (AAPT), Volume 43, pp 332-349, 1974.

17. Majidzadeh, K. and Karakouzian, M., "Practical Method for Evaluating Fracture Toughness of Pavement Materials," Transport Research Record (TRR) 695, pp 15-20, 1985.

18. Salam, Y.M. and Monismith, C.L., "Fracture Characteristics of Asphalt Concrete," Proceedings of the Association of Asphalt Paving Technologists (AAPT), Volume 41, pp 215-255, 1972.

19. Jacobs, M.M.J., "Crack Growth in Asphaltic Mixes," PhD. Thesis, Delft University of Technology, Netherlands, 1995.

20. Van Dijk, W., "Practical Fatigue Characterisation of Bituminous Mixes," Proceedings of the Association of Asphalt Paving Technologists (AAPT), Volume 44, pp 38-74, 1975.

21. Brown, S.F. and Bell, C.A., "The Prediction of Permanent Deformation in Asphalt Pavements," Proceedings of the Association of Asphalt Paving Technologists (AAPT), Volume 48, pp 439-474, 1979.

22. Caltabiano, M.A., "Reflection Cracking in Asphalt Overlays," M.Phil Thesis, University of Nottingham, Department of Civil Engineering, March 1990.

23. Rao Tangella, S.C.S., Craus, J., Deacon, J.A. and Monismith, C.L., "Summary Report on Fatigue Response of Asphalt Aggregate Mixtures," Strategic Highway Research Program, Project A-003-A, TM-UCB-A-003-A-89-3, Institute of Transportation Studies, University of California Berkeley, California, February 1990.

24. Brown, S.F., "Material Characterisation for Analytical Pavement Design," Developments in Highway Pavement Engineering -1, Applied Science Publishers, London, pp 42-92, 1978.

25. Collop, A.C. and Cebon, D., "A Theoretical Analysis of Fatigue Cracking in Flexible Pavements," Proceedings of Institution of Mechanical Engineers, Volume 209, pp 345-361, 1995.

26. Epps, J.A. and Monismith, C.L., "Fatigue of Asphalt Concrete Mixes - Summary of Existing Information," American Society of testing and Materials (ASTM) Special Publication 508, Fatigue of Compacted Bituminous Aggregate Mixtures, ASTM, Philadelphia, pp 19-45, 1971.

27. Monismith, C.L. and Salam, Y.M., "Distress Characteristics of Asphalt Concrete mixes," Proceedings of the Association of Asphalt Paving Technologists (AAPT), Volume 42, pp 320-349, 1979.

28. Raithby, K.D. and Sterling, A.B., "Laboratory Fatigue Tests on Rolled Asphalt and Their Relation to Traffic Loading," Roads and Road Construction, № 596 - 597, pp 219-223, 1972.

29. Irwin. L.H., "Use of Fracture Energy as a Fatigue Failure Criterion," Proceedings of the Association of Asphalt Paving Technologists (AAPT), Volume 46, pp 41-63, 1977.

30. Said, S.F., "Tensile and Fatigue Properties of Bituminous Mixtures Using the Indirect Tensile Method," Bulletin 1982: 2, Department of Highway Engineering, Royal Institute of Technology, Stockholm, Sweden, 1988.

31. Raithby, K.D. and Sterling, A.B., "The Effect of Rest Periods on the Fatigue Performance of a Hot-Rolled Asphalt Under Repeated Loading," Association of Asphalt Paving Technologists (AAPT), Volume 39, pp 134-152, 1970.

32. Van Dijk, W. and Visser, W., "The Energy Approach to Fatigue for Pavement design," Association of Asphalt Paving Technologists (AAPT), Volume 46, pp 1-41, 1977.

33. Francken, L., "Fatigue Performance of a Bituminous Road Mix Under Realistic Test Conditions," Transport Research Record, No 712, pp 30-37.

34. Francken, L. and Clauwert, C., "Characterisation of Structural Assessment of Bound Materials for Flexible Road Structures," 6th International Conference on Structural Design of Asphalt Pavements (ISAP), Ann Arbor, pp 130-144, 1987.

35. Brunton, J.M., "Developments in the Analytical Design of Asphalt Pavements Using Computers," PhD Thesis, University of Nottingham, Department of Civil Engineering, May 1983.

36. Cooper, K.E. and Pell, P.S., "The Effect of Mix Variables on the Fatigue Strength of Bituminous Materials," TRRL Laboratory Report 633, Crowthorne, Berkshire, 1974.

37. Anon, "Mix Design Methods for Asphaltic Concrete and Other Hot-Mix Types," Manual Series No 2 (MS-2), The Asphalt Institute, Lexington, Kentucky, 1988.

38. Pell, P.S., "Characterisation of Fatigue Behaviour," Highway Research Board, Special Report 140, Proceedings of a Symposium on Structural Design of Asphalt Concrete Pavements to Prevent Fatigue Cracking, pp 49-64, 1973.

39. Brown, S.F., Gibb, J.M., Read, J.M., Scholz, T.V. and Cooper, K.E., "Design and Testing of Bituminous Mixtures," SERC/DoT LINK Scheme First Final Report, Department of Civil Engineering, University of Nottingham, January 1995.

40. Gibb, J.M., "Evaluation of Resistance to Permanent Deformation in the Design of Bituminous Paving Mixtures," PhD Thesis, University of Nottingham, Department of Civil Engineering, January 1996.

41. Whiteoak, C.D., "The Shell bitumen handbook," Shell Bitumen U.K., 1990.

42. Brown, S.F., Brunton, J.M. and Pell, P.S., "The Development and Implementation of Analytical Pavement Design for British Conditions," 5th International Conference on Structural Design of Asphalt Pavements (ISAP), Delft, pp 3-16, 1982.

43. Brown, S.F., "Effect of Mix Properties on Structural Design - A Review," Association of Asphalt Paving Technologists (AAPT), Volume 57, pp 245-261, 1988.

44. Dukatz, E.L., "Aggregate Properties Related to Pavement Performance," Association of Asphalt Paving Technologists (AAPT), Volume 58, pp 492-502, 1989.

45. Moutier, F., Duan, T.H. and Chauvin, J.J., "The Effects of Formulation Parameters on the Mechanical Behaviour of Mixes," Association of Asphalt Paving Technologists (AAPT), Volume 57, pp 213-242, 1988.

46. Barksdale, R.D., "Practical Application of Fatigue and Rutting Tests on Bituminous Base Mixes," Association of Asphalt Paving Technologists (AAPT), Volume 47, pp 115-159, 1978.

47. Bolk, N.J.N, Van der Heide, J.P.J. and Van Zantvliet, M.C., "Basic Research into the Effect of Filler on the Mechanical Properties of Dense Asphaltic Concrete," Association of Asphalt Paving Technologists (AAPT), Volume 51, pp 398-448, 1982.

48. Bonnaure, F., Gravois, A. and Udron, J., "A New Method for Predicting the Fatigue Life of Bituminous Mixes," Association of Asphalt Paving Technologists (AAPT), Volume 49, pp 499-528, 1980.

49. Van Dijk, W., Moreaud, H., Quediville, A. and Uge, P., "The Fatigue of Bitumen and Bituminous Mixes," 3th International Conference on Structural Design of Asphalt Pavements (ISAP), London, Volume 1, pp 354-366, 1972.

50. Himeno, K., Watanabe, T., and Maruyama, T., "Estimation of Fatigue Life of Asphalt Pavements," 6th International Conference on Structural Design of Asphalt Pavements (ISAP), Ann Arbor, pp 272-288, 1987.

51. Brown, S.F. and Brunton, J.M., "An introduction to the analytical design of bituminous pavements - 3rd edition," University of Nottingham, Department of Civil Engineering, U.K., 1992.

INDIRECT TENSILE FATIGUE

3.1 Introduction

The ITFT was a particularly attractive candidate fatigue test due to its simplicity, relative to alternative methods, and because it used cylindrical specimens, which can be easily manufactured in the laboratory or cored straight from the pavement. The work carried out by Kennedy *et al* (1) in the early to mid seventies was of particular interest as this had included a full evaluation of the performance of the ITFT compared with other test methods. This work indicated some problems which, at that time, could not be resolved, e.g. the ITFT exhibited far shorter lives to failure, on the basis of log stress against log life, than any other commonly used fatigue test method.

Generally fatigue testing (Chapter 2) has been carried out using either:

1) A bending beam (four point, Figure 2.1), where repeated loading is applied to the centre of a beam which is supported at both ends. This generates tensile strains at the bottom of the beam causing it to fail after a certain number of load applications.

2) A trapezoidal cantilever (two point, Figure 2.1), where the wider base of the trapezium is clamped rigidly and then repeated loading is applied to the top of the trapezium. This generates tensile strains along the outer fibres on the edge of the trapezium causing it to fail after a certain number of load applications.

It was shown, during the SHRP A003-A project, that these two methods can give equivalent results (2) and it was hoped that by comparing the candidate simplified test method against one of these methods (trapezoidal cantilever) that it could be validated as a fatigue test.

The Strategic Highway Research Program (SHRP) in the United States also included an evaluation of the ITFT and a comparison of it with the trapezoidal cantilever and four point bending beam tests. The conclusions drawn from this work are detailed below (3).

Summary of the ITFT v Simple Flexure As Reported by SHRP A003-A

ADVANTAGES

- The test is simple.
- Design of mixtures and pavements for fatigue is possible in principle, using the ITFT response together with field correlations.
- The equipment is applicable for other tests, for example, stiffness.
- Failure is initiated in a region of relatively uniform tensile stress.
- A biaxial state of stress exists in the ITFT, possibly of a type better representing field conditions than is found in simple flexure tests.
- Tests can be performed on field cores in addition to laboratory briquettes.
- The ITFT appears able to discriminate between mixtures containing different binders based upon both stiffness and cycles to failure.
- The reliability (repeatability) of the ITFT for cycles to failure is far better than either trapezoidal or beam flexure.

DISADVANTAGES

- Although a biaxial stress state exists at the centre of the specimen, it is impossible to vary the ratio of the vertical and horizontal components and, hence, to replicate the stress state at critical locations within the pavement.
- The method significantly underestimates fatigue life if the principal tensile stress is used as the damage determinant.
- The absence of stress reversal and the accumulation of permanent deformation is of great concern.
- The reliability of the ITFT for measuring stiffness is not as good as that of either the trapezoidal or beam flexure tests.

From these advantages, disadvantages and the various stress analyses, detailed fully in the next section, it was decided to concentrate the research on validation of the ITFT.

3.2 Analysis of the ITFT

In the ITFT mode of fatigue testing pavement materials, a repeated line loading (generally controlled stress) is applied along the vertical diameter of a cylindrical specimen as shown in Figure 3.1.

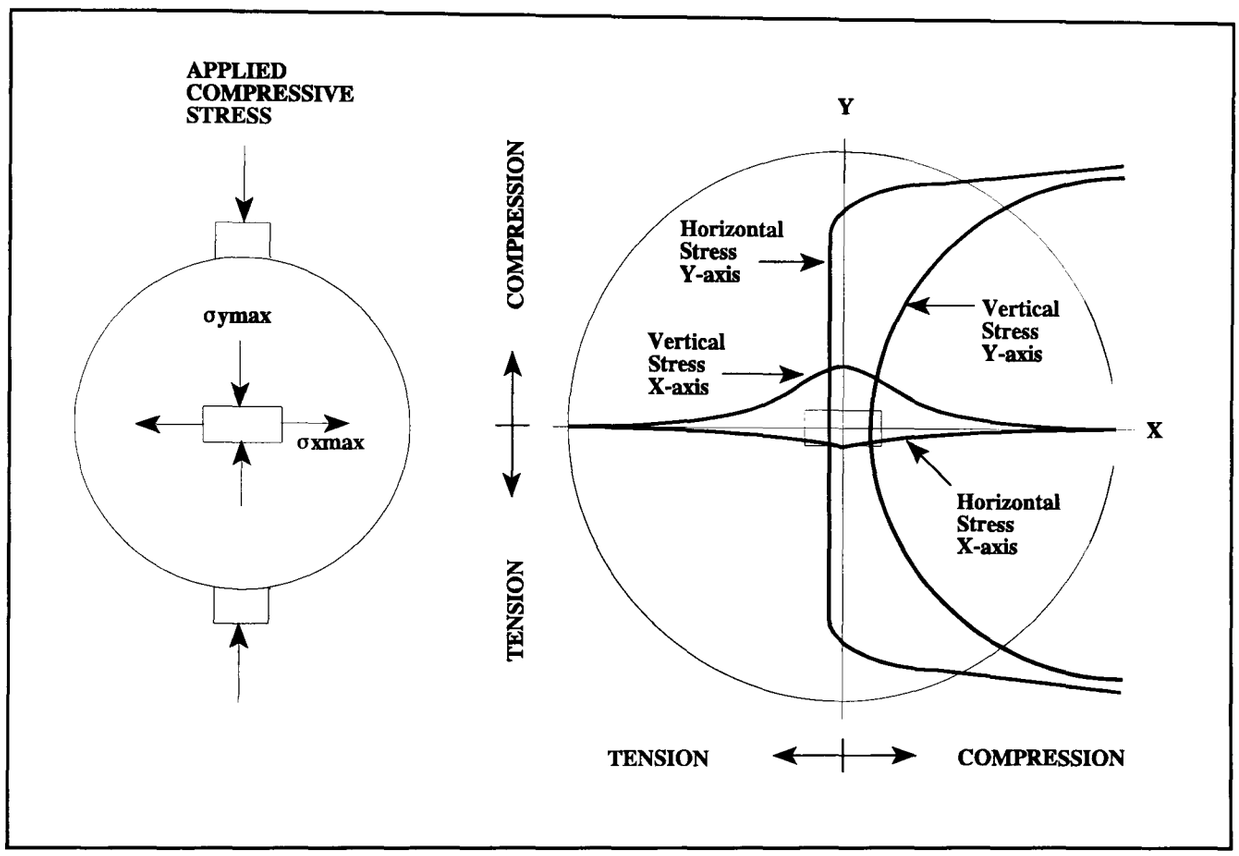


Figure 3.1 - Relative Stress Distributions and Element Showing Biaxial State of Stress for the Indirect Tensile Fatigue Test.

This vertical loading produces both a vertical compressive stress and a horizontal tensile stress on the diameters of the specimen. The magnitudes of the stresses vary along the diameters as shown in Figure 3.1 but are at a maximum in the centre of the specimen. The situation, as depicted in Figure 3.1, enables the calculation of the maximum strain at the centre of the specimen but depends on a number of assumptions, namely:

- The specimen is subjected to plane stress conditions ($\sigma_z = 0$).
- The material behaves in a linear elastic manner.

- The material is homogenous.
- The material behaves in an isotropic manner.
- Poisson's ratio (υ) for the material is known.
- The force (P) is applied as a line loading.

When all of these conditions are met, or assumed, then the stress conditions in the specimen are given by the closed form solution of the theory of elasticity, which has been derived by various authorities in the field of stress analysis (4, 5, 6, 7). These theories all show that when the width of the loading strip is less than or equal to 10% of the diameter of the specimen and the distance of the element of material from the centre is very small then:

$$\sigma_{xmax} = \frac{2\,P}{\pi\,d\,t} \tag{3.1}$$

and

$$\sigma_{ymax} = -\frac{6\,P}{\pi\,d\,t} \tag{3.2}$$

where:

σ_{xmax} = Maximum horizontal tensile stress at the centre of the specimen,

σ_{ymax} = Maximum vertical compressive stress at the centre of the specimen,

P = Applied vertical force,

d = Diameter of the specimen and

t = Thickness of the specimen.

As the analysis of the ITFT, for calculation of the strain, is concerned with an element of material at the centre of the specimen Equations (3.1) and (3.2) hold true.

By simple linear elastic stress analysis (Hooke's Law):

$$\epsilon_{xmax} = \frac{\sigma_{xmax}}{S_m} - \frac{\upsilon\ \sigma_{ymax}}{S_m} \tag{3.3}$$

where:

ϵ_{xmax} = Maximum initial horizontal tensile strain at the centre of the specimen,

υ = Poisson's ratio, full details of this are given in Chapter 5, and

S_m = Stiffness modulus of the specimen.

Substituting Equations (3.1) and (3.2) into Equation (3.3) gives:

$$\epsilon_{xmax} = \frac{2\ P}{\pi\ d\ t\ S_m} + \frac{\upsilon\ 6\ P}{\pi\ d\ t\ S_m} \tag{3.4}$$

Substituting Equation (3.1) into Equation (3.4) gives:

$$\epsilon_{xmax} = \frac{\sigma_{xmax}}{S_m}\ (1 + 3\upsilon) \tag{3.5}$$

Equation (3.5) is used for the calculation of the maximum tensile strain (ϵ_{xmax}) at the centre of the specimen in this thesis. However, it was considered possible to further refine the calculation to incorporate the effects of specimen bulging. This effect has been studied by Roque and Buttlar (8) who have presented a 3-dimensional finite element modelled analysis of the system. Their paper reports that for a specimen geometry such as that used for the ITFT (d≈100mm, t≈40mm) the specimen bulges when a load is applied to it and as such the two dimensional, plane stress condition does not apply. To account for this, a 3-dimensional analysis was carried out which gave the following equations:

$$\sigma_{xcorr} = \frac{2\ P}{\pi\ d\ t} \times C_{\sigma xCTR} \tag{3.6}$$

$$\sigma_{ycorr} = -\frac{6\,P}{\pi\,d\,t} \times C_{\sigma yCTR} \qquad (3.7)$$

where:

σ_{xcorr} = Corrected σ_{xmax} to account for $\sigma_z \neq 0$,

σ_{ycorr} = Corrected σ_{ymax} to account for $\sigma_z \neq 0$,

$C_{\sigma xCTR}$ = Correction factor applied to the horizontal point stress occurring at the centre of the specimen, as predicted by the 2 dimensional plane stress solution, to account for 3 dimensional effects (bulging) and

$C_{\sigma yCTR}$ = Correction factor applied to the vertical point stress occurring at the centre of the specimen, as predicted by the 2 dimensional plane stress solution, to account for 3 dimensional effects (bulging).

Therefore using Hooke's Law:

$$\epsilon_{xcorr} = \frac{\sigma_{xcorr}}{S_m} - \frac{\upsilon\,\sigma_{ycorr}}{S_m} \qquad (3.8)$$

Evaluating Equation (3.8) in the same manner as Equation (3.4) yields:

$$\epsilon_{xcorr} = \frac{\sigma_{xmax}}{S_m} \times (C_{\sigma xCTR} + (3\ \upsilon\ C_{\sigma yCTR})) \qquad (3.9)$$

where:

ϵ_{xcorr} = Corrected maximum initial horizontal tensile strain at the centre of the specimen.

The correction factors for use in Equation (3.9) are given in Table 3.1 (taken from Roque and Buttlar, 8), these should allow a more accurate calculation of the actual horizontal tensile strain at the centre of the specimen. This method has been compared against linear elastic analysis for the calculation of Poisson's ratio, described fully in Chapter 5

of this thesis. The correction was found to make only a negligible difference to the result and it was, therefore, decided to use Equation (3.5) for the calculation of ϵ_{xmax}.

Table 3.1 - Correction Values for Use in Equation (3.9).

		THICKNESS TO DIAMETER RATIO (t/d)				
	υ	0.167	0.333	0.500	0.625	0.750
$C_{\sigma xCTR}$	0.20	0.9471	0.9733	1.0251	1.0696	0.7500
	0.35	0.9561	1.0007	1.0871	1.1682	1.2321
	0.45	0.9597	1.0087	1.1213	1.2307	1.3171
$C_{\sigma yCTR}$	0.20	-0.9648	-0.9754	-0.9743	-0.9693	-0.9611
	0.35	-0.9732	-0.9888	-0.9844	-0.9710	-0.9538
	0.45	-0.9788	-0.9971	-0.9864	-0.9646	-0.9395

All of the analyses of the ITFT reported thus far have been aimed toward the calculation of the maximum tensile strain at the centre of the specimen assuming that this is the only failure mode. However, it can be shown that under certain conditions of test (high compressive stress and/or high temperature) that either compressive or shear failure can occur. Equations 3.10 and 3.11 describe the principle stresses along the vertical diameter of the ITFT, after Timoshenko (4).

$$\sigma_{\theta y} = + \frac{2P}{\pi} \times \left[\frac{\left[\left(1 - \frac{r^2}{R^2} \right) \times \sin (2\alpha) \right]}{\left[1 - \left(\frac{2r^2}{R^2} \times \cos (2\alpha) \right) + \left(\frac{r^4}{R^4} \right) \right]} - \tan^{-1} \left(\frac{\left[1 + \left(\frac{r^2}{R^2} \right) \right]}{\left[1 - \left(\frac{r^2}{R^2} \right) \right]} \times \tan (\alpha) \right) \right] \qquad \textbf{(3.10)}$$

$$\sigma_{ry} = - \frac{2P}{\pi} \times \left[\frac{\left[\left(1 - \frac{r^2}{R^2} \right) \times \sin (2\alpha) \right]}{\left[1 - \left(\frac{2r^2}{R^2} \times \cos (2\alpha) \right) + \left(\frac{r^4}{R^4} \right) \right]} + \tan^{-1} \left(\frac{\left[1 + \left(\frac{r^2}{R^2} \right) \right]}{\left[1 - \left(\frac{r^2}{R^2} \right) \right]} \times \tan (\alpha) \right) \right] \qquad \textbf{(3.11)}$$

Where:

$\sigma_{\theta y}$	=	Tangential normal stress at a point on the vertical diameter
σ_{ry}	=	Radial normal stress at a point on the vertical diameter
P	=	Applied load (2kN used for the calculations herein)
r	=	Radial distance at a point from the origin
R	=	Radius of the circular element (50mm)
2α	=	Angle at the origin subtended by the loaded section of the rim (14.36°)

Figure 3.2 shows these equations graphically represented with Mohr's circles developed from them. This demonstrates that large shear stresses can be developed on the vertical axis of the specimen. Figure 3.2 also shows that just below the loading strips high compressive stresses are generated.

Figure 3.3 plots the difference between the principle stresses developed on the vertical diameter against the position at which they occur. This shows that the point of maximum shear stress occurs at one eighth of the radius below the point of load application at 45° to the applied load.

This information then demonstrates that under certain conditions of test (high temperature, high compressive stress) that localised shear or compressive failure may result before tensile failure occurs. This, in the case of shear failure, will be manifested by a wedge of material being pushed through the specimen from the top loading platen. However, the author's experience was that, under the recommended conditions of test (120ms, 20°C), tensile failure occurred first in all cases. This was clearly visible by cracks appearing at the centre of the specimen and propagating out towards the loading platens. It is true to say, however, that once the tensile failure had occurred shear failure also occurred with a wedge of material being driven toward the crack at the centre of the specimen.

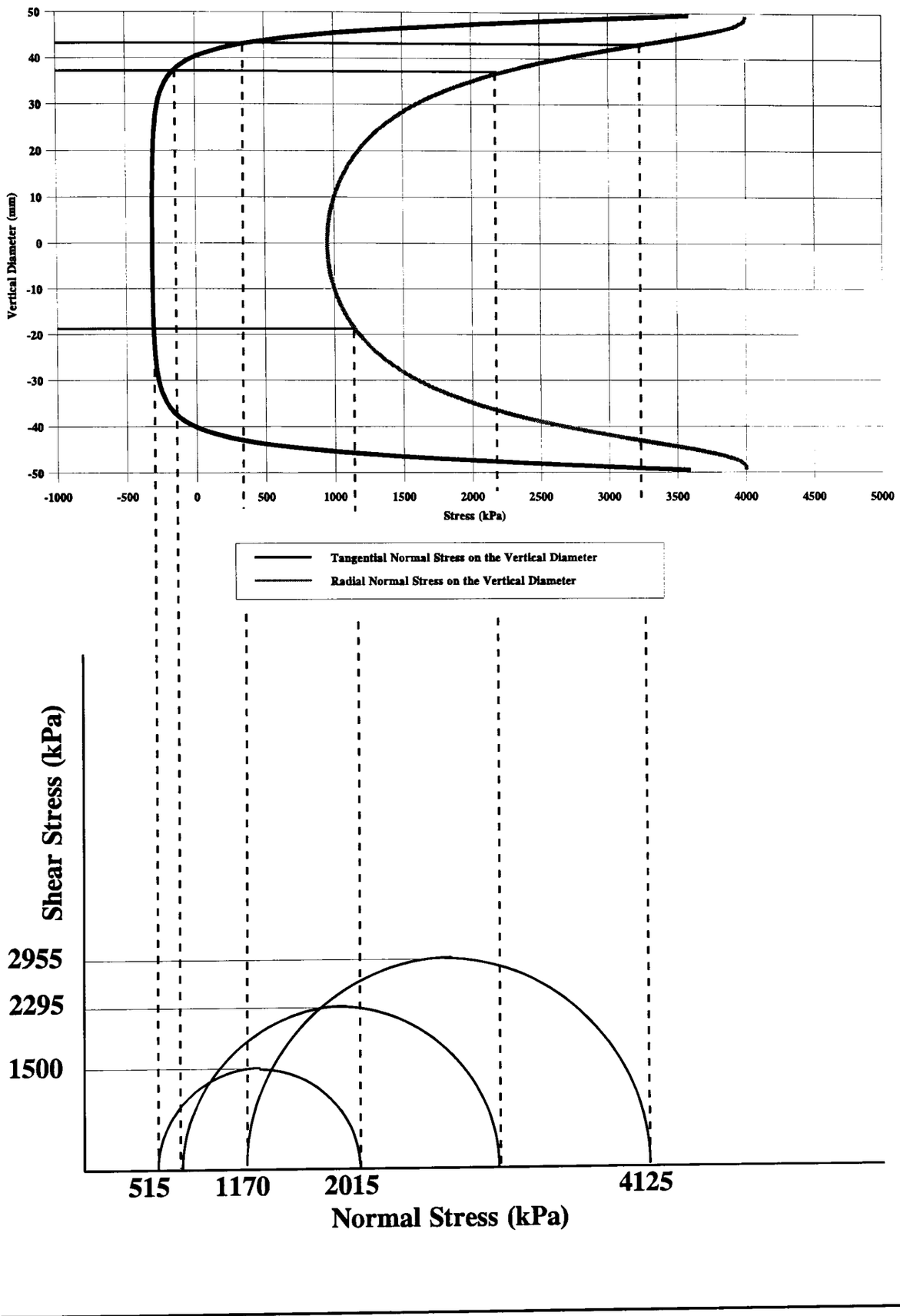


Figure 3.2 - Plot Demonstrating the High Compressive and Shear Stresses Developed on the Vertical Diameter of the ITFT.

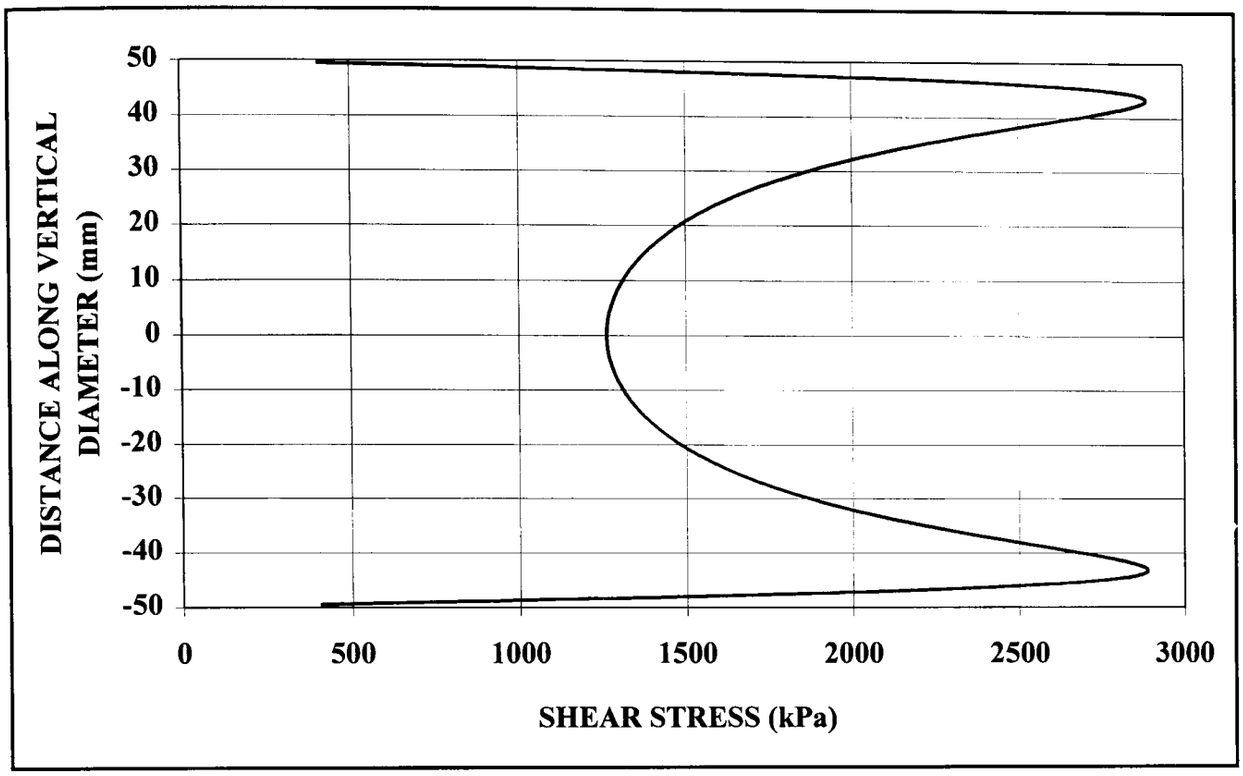


Figure 3.3 - Plot Demonstrating the Point of Maximum Shear Stress on the Vertical Diameter of the ITFT.

3.3 Equipment Development

The information given here details the development of the ITFT hardware and software which took place during the research described in this thesis.

3.3.1 Hardware Development

The initial hardware utilised for the ITFT was essentially the same as that used for the Indirect Tensile Stiffness Modulus (ITSM) test which is described fully, including the appropriate Figures, in the British Standard Draft for Development 213 (9). The main differences were that no frame was used to mount Linear Variable Differential Transformers (LVDT's) horizontally as it was considered that the possibility of violent fracture of the specimens might damage the LVDT's. The vertical deformation was monitored using LVDT's of the type described in the British Standard Draft for Development 185 (10) which had a measurement range of 10mm. A schematic of the apparatus configuration in its' initial state, at the start of the research, is included as Figure 3.4.

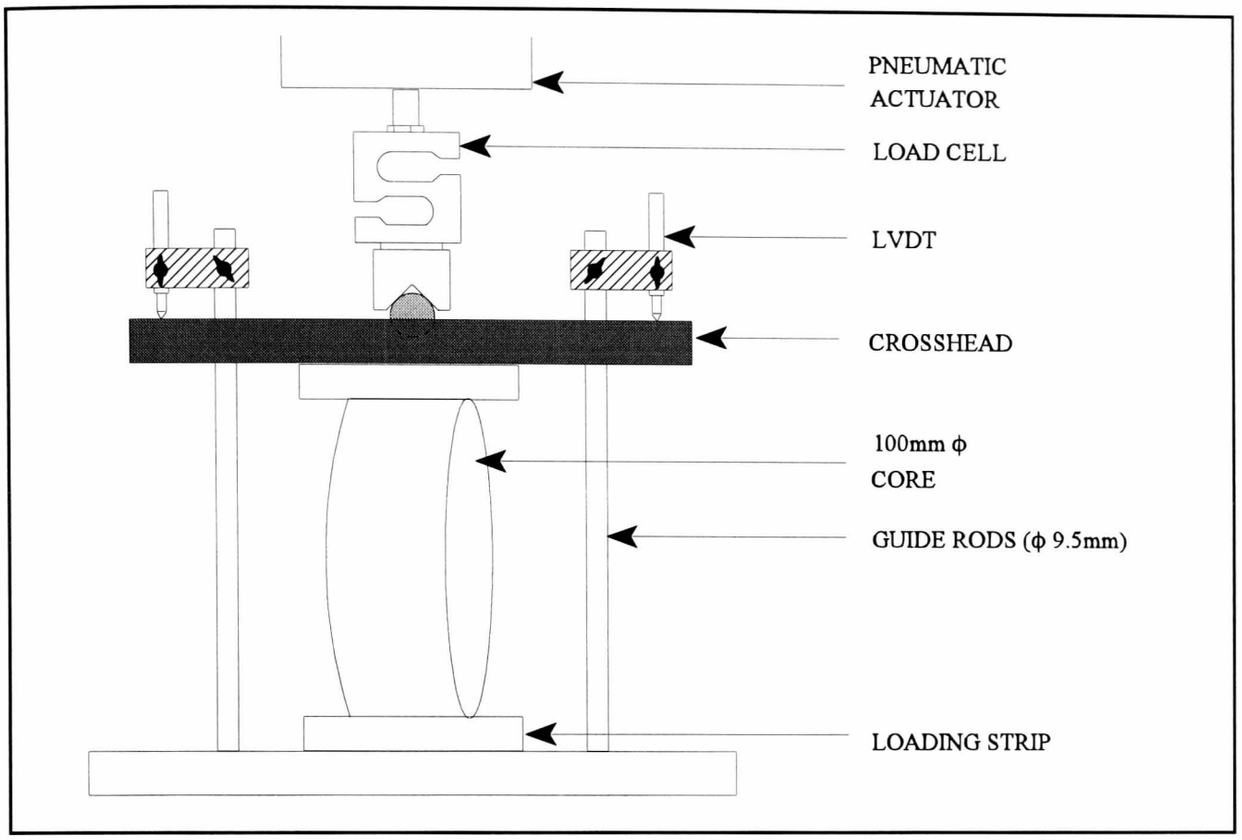


Figure 3.4 - Schematic Demonstrating the Initial Equipment Configuration for the ITFT.

After the first series of specimens had been tested (main test programme described later in this Chapter), it became evident that the indirect tensile sub-frame crosshead did not always remain horizontal as the test progressed. This was leading to premature specimen failure and, therefore, the ITFT was giving lower lives to failure than expected. To combat this problem, a crosshead fitted with linear bearings was manufactured. The linear bearings, that were available and appropriate to fulfill this purpose, had an internal diameter of 12.7mm and the original silver steel upright guide rods had a diameter of 9.5mm. It was, therefore, necessary to manufacture new uprights with the appropriate dimensions.

Testing then continued for an extended period without any problems, requiring hardware modification, until the testing of a very stiff mixture at a relatively low temperature (DBM50, 13.5°C). This resulted in an extremely violent failure which caused the rigid load cell cable entry to shear off. To prevent this occurring, and to protect the loading strips from damage, vertical stops were added which limited the maximum drop of the crosshead, at failure, to 3mm. In addition a cable tie was used to connect the flexible

cable of the load cell to the load cell itself so that the brittle connection was not subject to shear forces. These two modifications prevented the problem recurring and an up-to-date schematic is shown in Figure 3.5. This is the configuration which is now commercially available from Cooper Research Technology Limited and ELE Limited.

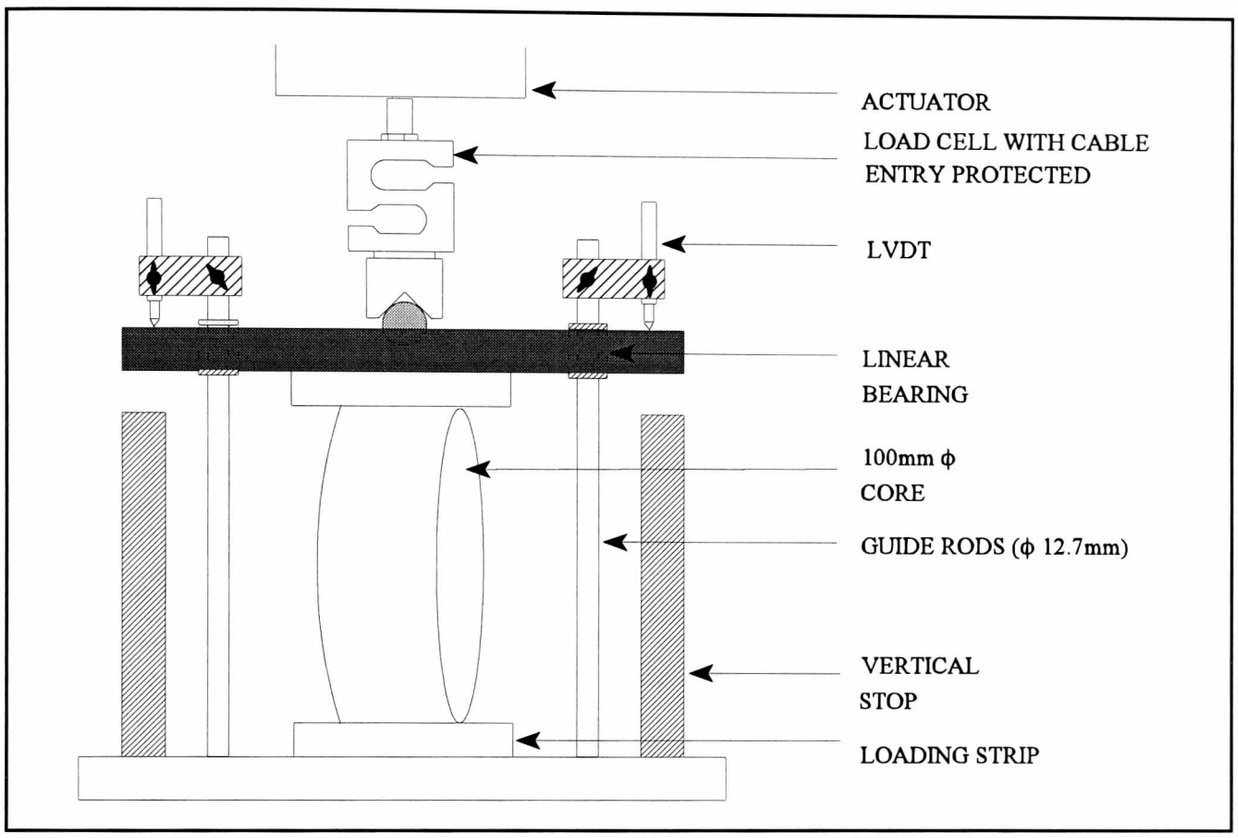


Figure 3.5 - Schematic Demonstrating the Present Equipment Configuration for the ITFT.

3.3.2 Software Development

The original software, developed at the University of Nottingham, was written to apply a cyclic controlled stress pulse (as shown in Figure 2.5c) to a specimen until a target vertical deformation (generally 9mm) was achieved. The first software revision was necessary due to the need to demonstrate the reproducibility of the test. Three different laboratories were given the apparatus and the software and it became evident that, due to the performance of the different computers, the frequency of the load pulse application varied from 11 pulses per minute to 65 pulses per minute. To overcome this problem the software was revised so that the frequency of the loading pulse was controlled by the software to be 40 pulses per minute (Figure 3.6). In order to ensure that this rate of loading was achieved a minimum performance of the controlling computer was specified

for all further use of the test. These two criteria ensured that all participating laboratories tested at a frequency of 0.67Hz.

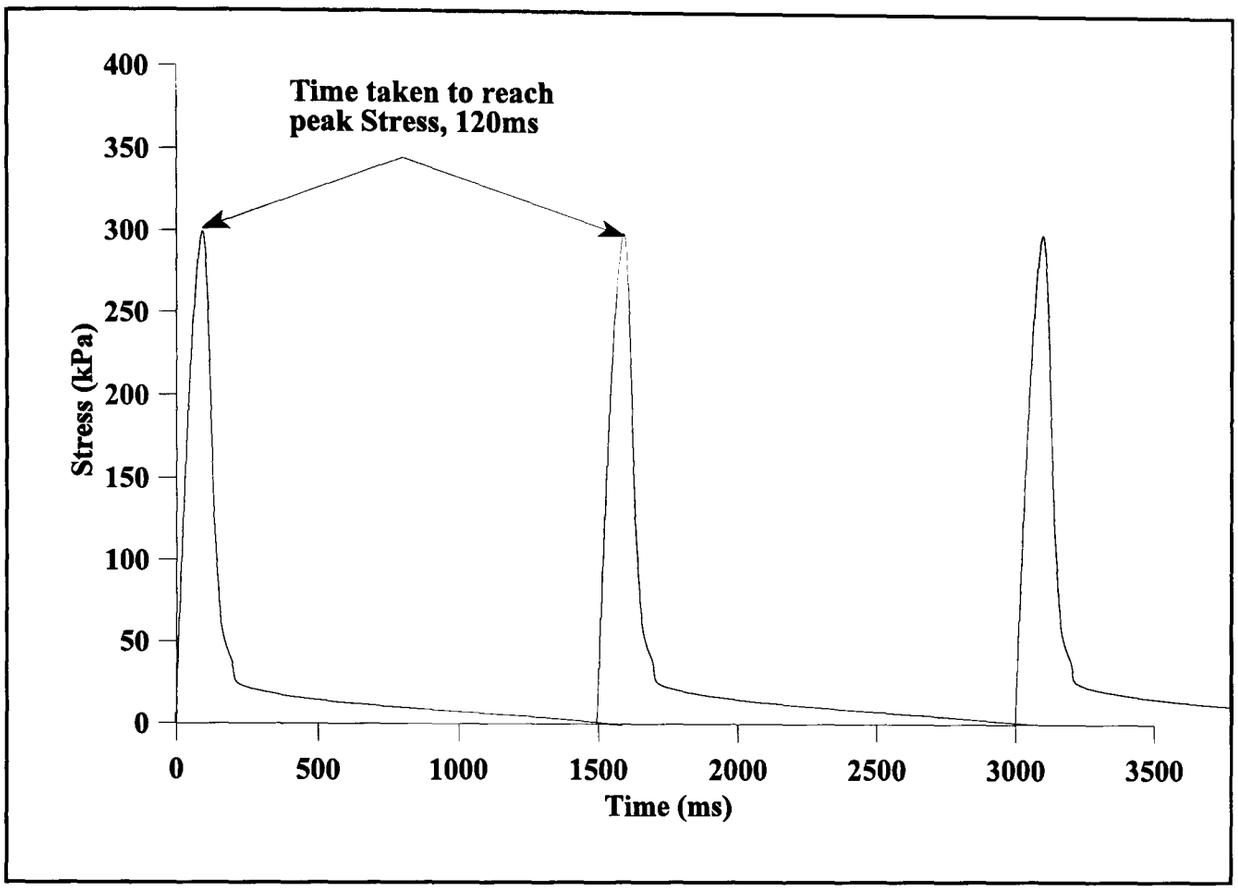


Figure 3.6 - Schematic Representation of the Load Pulse Applied in the ITFT.

The second major revision to the software was to enable the capture of a larger quantity of data. Prior to this revision the software captured data on a logarithmic basis to 1,000 pulses and then at 1,000 pulse intervals. Although this was satisfactory for tests where the life to failure was greater than 25,000 cycles, it was inadequate for tests which had a life to failure of less than 1,000 cycles (Figure 3.7). Therefore, this revision retained the old rate of data capture and in addition captured data at every 0.05mm of vertical deformation (Figure 3.8), thereby, giving up to 180 extra data points if the maximum vertical deformation was set at 9mm. This also ensured that in the very short life to failure tests (less than 200 load applications) the data was captured at every load pulse. This revision was deemed necessary due to the potential method of ascertaining the point of crack initiation (N_1), where the number of cycles (N) divided by the transient vertical deformation (V_d) is plotted against the number of cycles (N). This method, based on dissipated energy concepts, assumes that stiffness is inversely proportional to the

transient vertical deformation. This method of defining N_1 using stiffness change is fully detailed by Rowe (11).

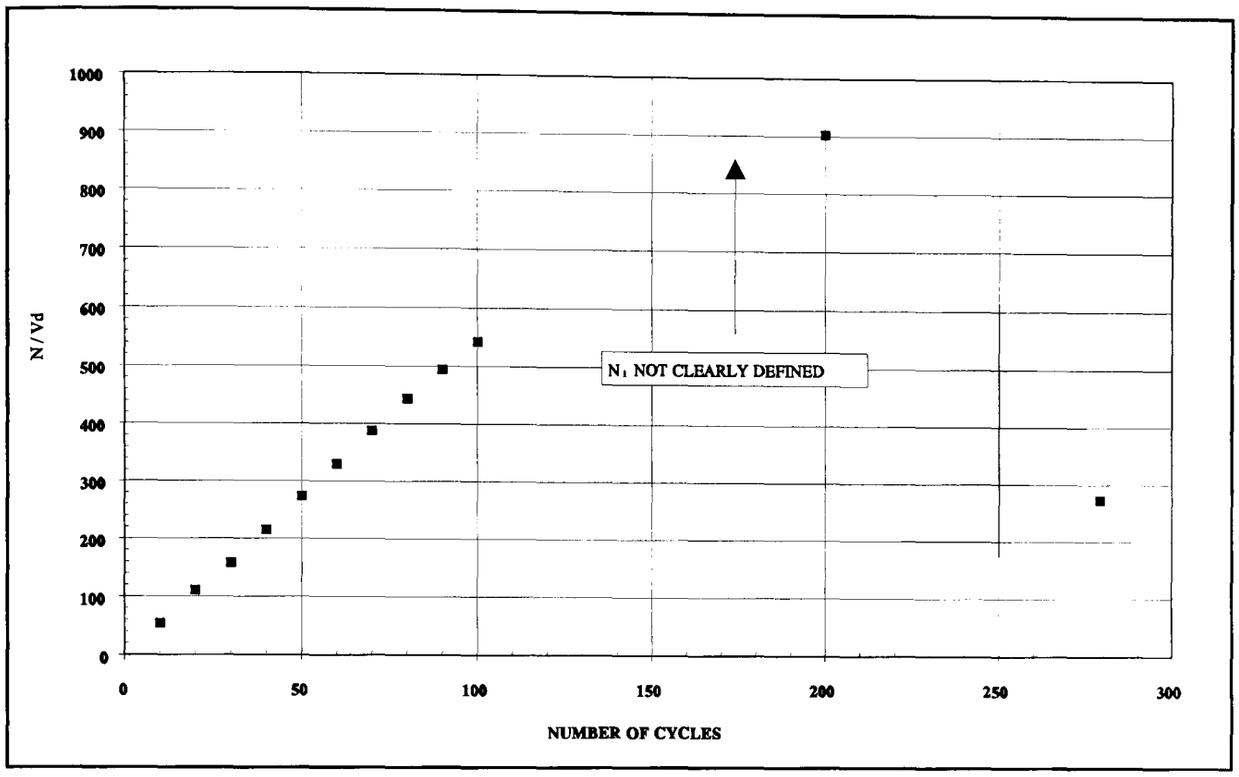


Figure 3.7 - Original Rate of Data Capture on a Short Test in the ITFT.

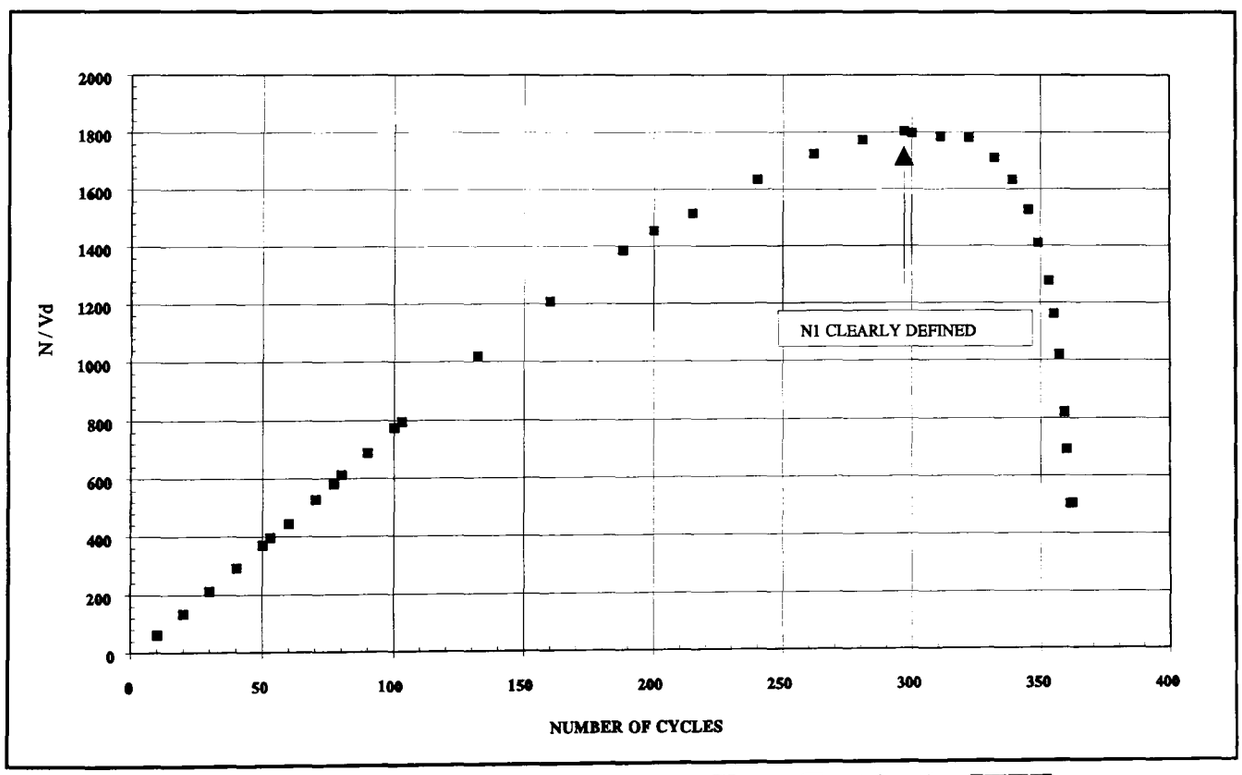


Figure 3.8 - New Rate of Data Capture on a Short Test in the ITFT.

Three examples of results plotted using this technique are shown in Figures 3.7, 3.8 and 3.9. They demonstrate how the new method of data capture has helped to clearly define the curve and the point N_1.

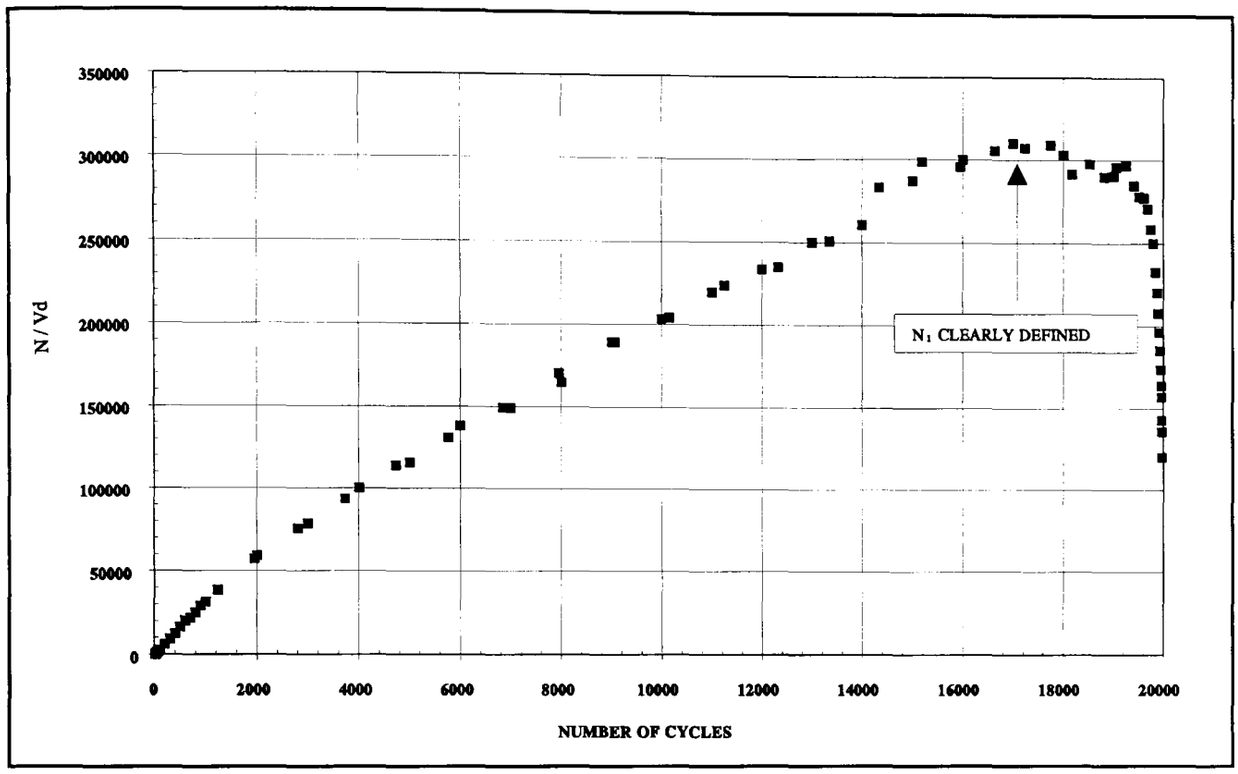


Figure 3.9 - New Rate of Data Capture on a Long Test in the ITFT.

3.4 Stiffness Modulus

The initial stiffness modulus (S_m) of all specimens is required, prior to fatigue testing, in order to calculate ϵ_{xmax} from Equation (3.5). To obtain this value, the Indirect Tensile Stiffness Modulus (ITSM) test was used as described in the British Standard Draft for Development 213 (9).

Due to the visco-elastic nature of bituminous materials, the temperature susceptible nature of bitumens and the characteristics of the ITSM test there are a number of factors which affect the stiffness of bituminous materials and these are detailed in Table 3.2. Of the factors listed, the temperature of the test specimen is, by far, the most important in that small deviations can result in significant variations in the stiffness modulus as illustrated in Figure 3.10. The stiffness modulus is less sensitive to loading frequency,

particularly in the frequency range commonly associated with typical traffic loading (0.1 to 10Hz) and at low temperatures (12).

Table 3.2 - General Effect of the Main Factors Affecting the ITSM.

Factor	General Effect on ITSM
Specimen temperature during test	High temperature ➜ low stiffness modulus Low temperature ➜ high stiffness modulus
Loading frequency	Low frequency ➜ low stiffness modulus High frequency ➜ high stiffness modulus
Stress amplitude	High stress ➜ low stiffness modulus Low stress ➜ high stiffness modulus
Poisson's ratio (assumed)	Low value ➜ low stiffness modulus High value ➜ high stiffness modulus
Bitumen grade (for a particular mixture type)	High penetration bitumen ➜ low stiffness modulus Low penetration bitumen ➜ high stiffness modulus
Bitumen content (for a particular mixture type)	Highest stiffness modulus is generally achieved at or very near the optimum binder content for compacted aggregate density (BS 598, 13)
Bitumen modifiers	Use of modified bitumen in mixtures can significantly increase or reduce the stiffness modulus of the mixture and the magnitude of the effect greatly depends on the type of modifier. It should be noted, however, that modifiers are generally used to improve characteristics of the mixture other than its stiffness modulus.
Void content (for a particular mixture type)	High air voids ➜ low stiffness modulus Low air voids ➜ high stiffness modulus (for some mixtures very low air voids can result in a reduction in stiffness modulus)
Aggregate type and gradation	Materials made with crushed rock tend to have higher stiffness than those made with gravels. For continuously graded materials the larger the aggregate the higher the stiffness. For all mixtures the higher the quantity of coarse aggregate the higher the stiffness (14).

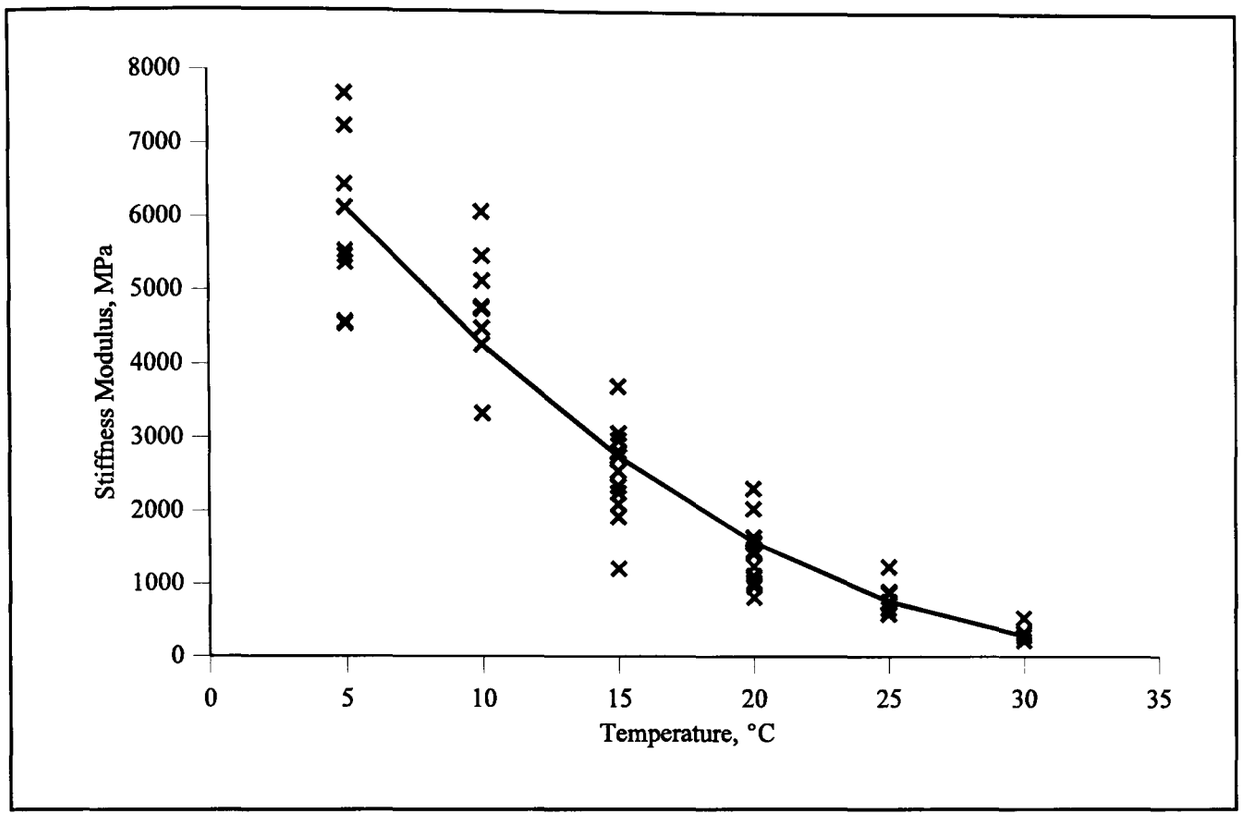


Figure 3.10 - Typical Results from 20mm DBM Mixtures with 100pen Bitumen and Granite and Gravel Aggregate Showing Effect of Specimen Temperature During ITSM Test.

Typical variations in stiffness modulus arising from different stress amplitudes applied during ITSM testing are illustrated in Figure 3.11. The data from tests on a 30/14 HRA wearing course mixture indicates that moderate to low variations in stiffness modulus result from tests conducted under relatively large differences in stress amplitude. The differences in stiffness modulus amongst the various lines are due to variations in void content.

Figure 3.12 shows the variation in stiffness modulus for a range of assumed Poisson's ratios with all other variables being held constant. The plot indicates that Poisson's ratio has a significant effect on the stiffness modulus, being of the same order as the stress dependency of the modulus. Although it would seem logical to assume different Poisson's ratios for different conditions (e.g., mixtures types, bitumen types, temperatures, etc.), previously there was insufficient information to make specific recommendations for appropriate values. The influence Poisson's ratio has on modulus cannot be ignored and Chapter 5 provides further details regarding Poisson's ratio and suggests that a value of 0.35 is reasonable and can be used for all testing conditions.

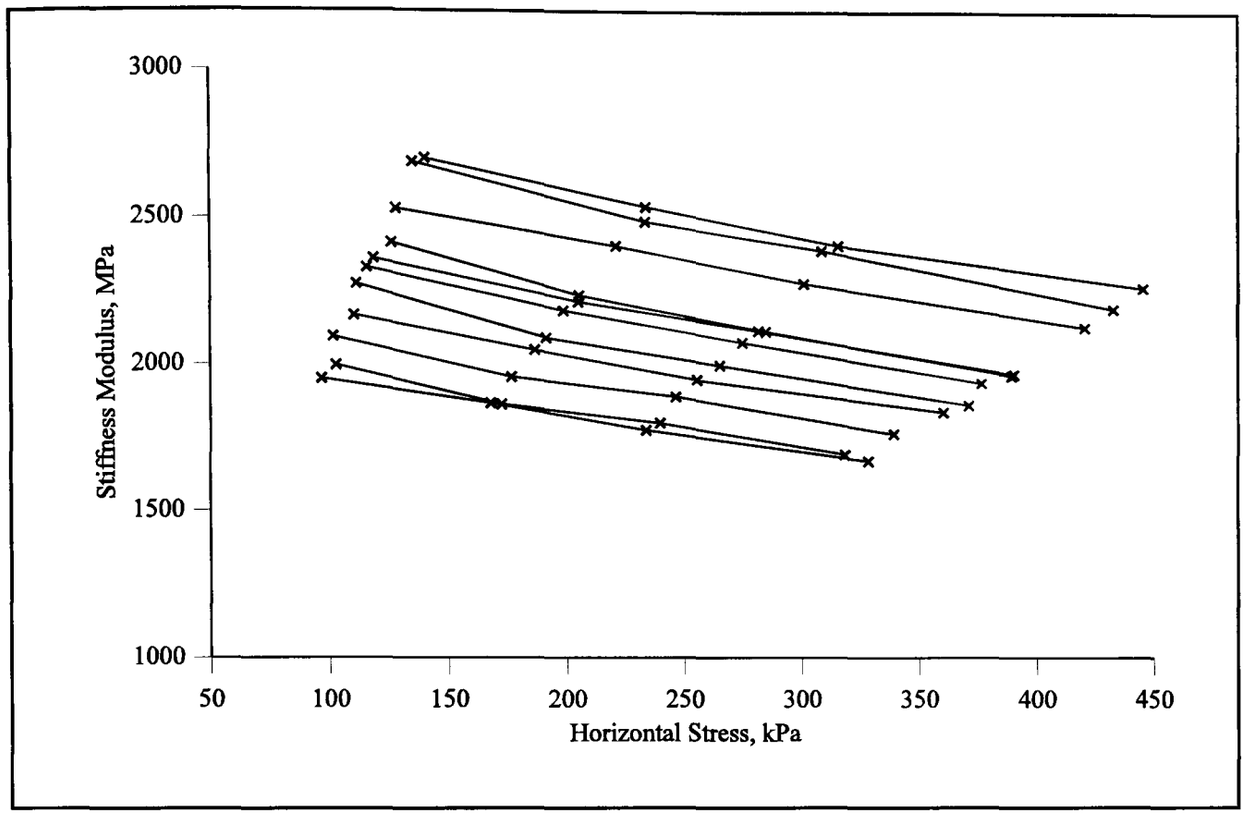


Figure 3.11 - Typical Results Showing the Effect of Stress Amplitude During the ITSM Test.

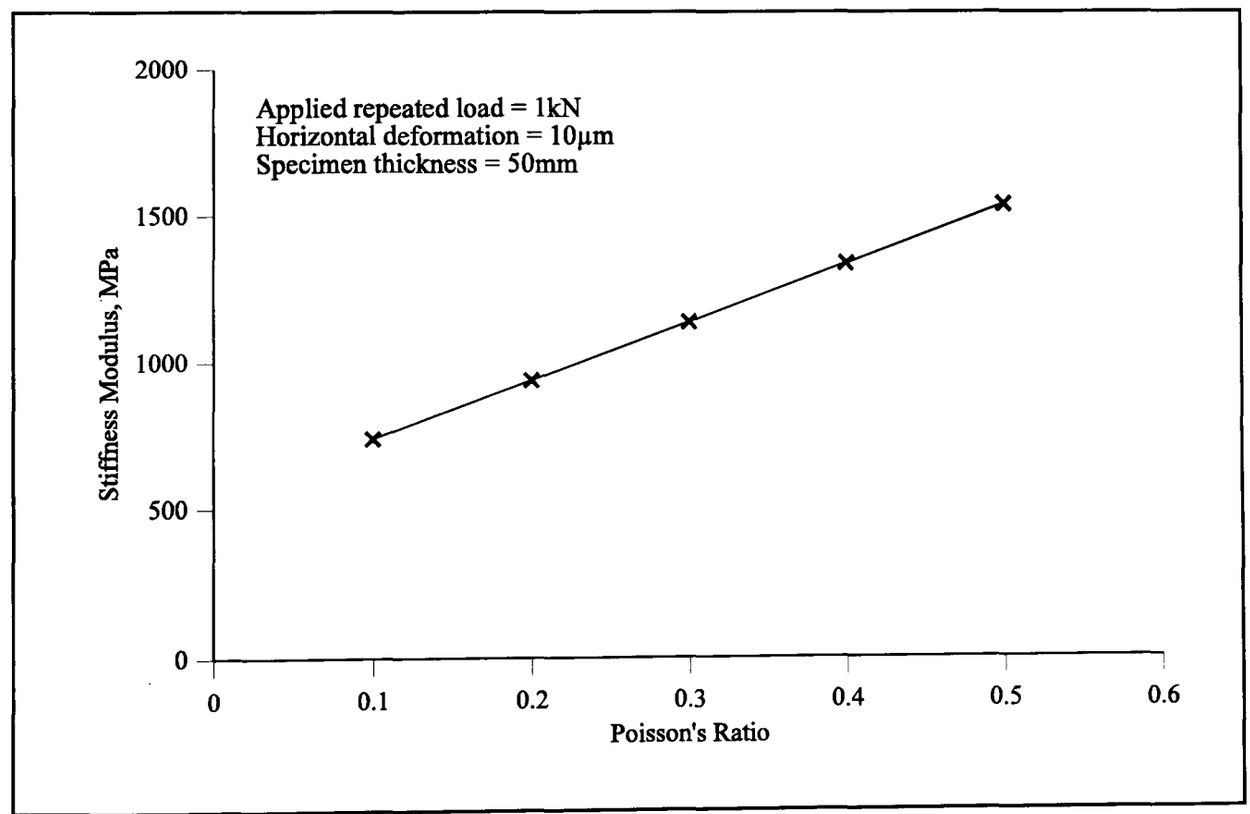


Figure 3.12 - Hypothetical Stiffness Values Showing Effect of Poisson's Ratio on the ITSM.

A variation in the void content of a particular mixture results in a variation in stiffness modulus. Figure 3.13 shows typical ITSM test results for three dense macadams which indicate that the stiffness modulus decreases as the air void content increases.

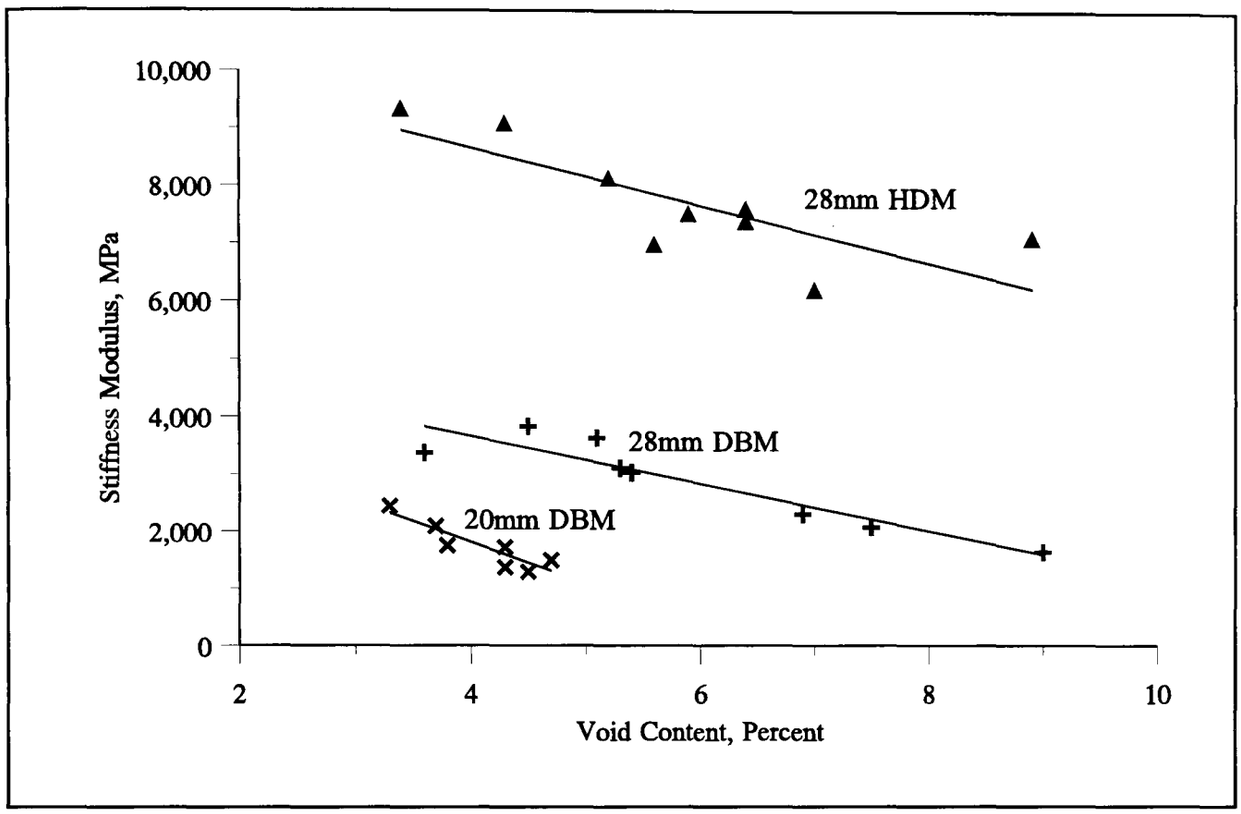


Figure 3.13 - Typical Results for Three Dense Macadams Showing the Effect of Mixture Air Void Content on the ITSM.

The effect of bitumen content on the stiffness modulus of typical 30/14 HRA mixtures is shown in Figure 3.14. The data indicates that the maximum stiffness modulus occurs very near to the binder content corresponding to the maximum compacted aggregate density.

Indirect tension testing has several advantages over other methods (e.g., direct tension and/or compression or bending beam) to determine the stiffness of bituminous materials. The principal advantages include:

1) The test is relatively simple, quick to conduct (i.e., user-friendly) and effectively non-destructive when testing conditions ensure essentially elastic response.
2) Tests are conducted on moulded specimens or cores eliminating difficult specimen manufacture.

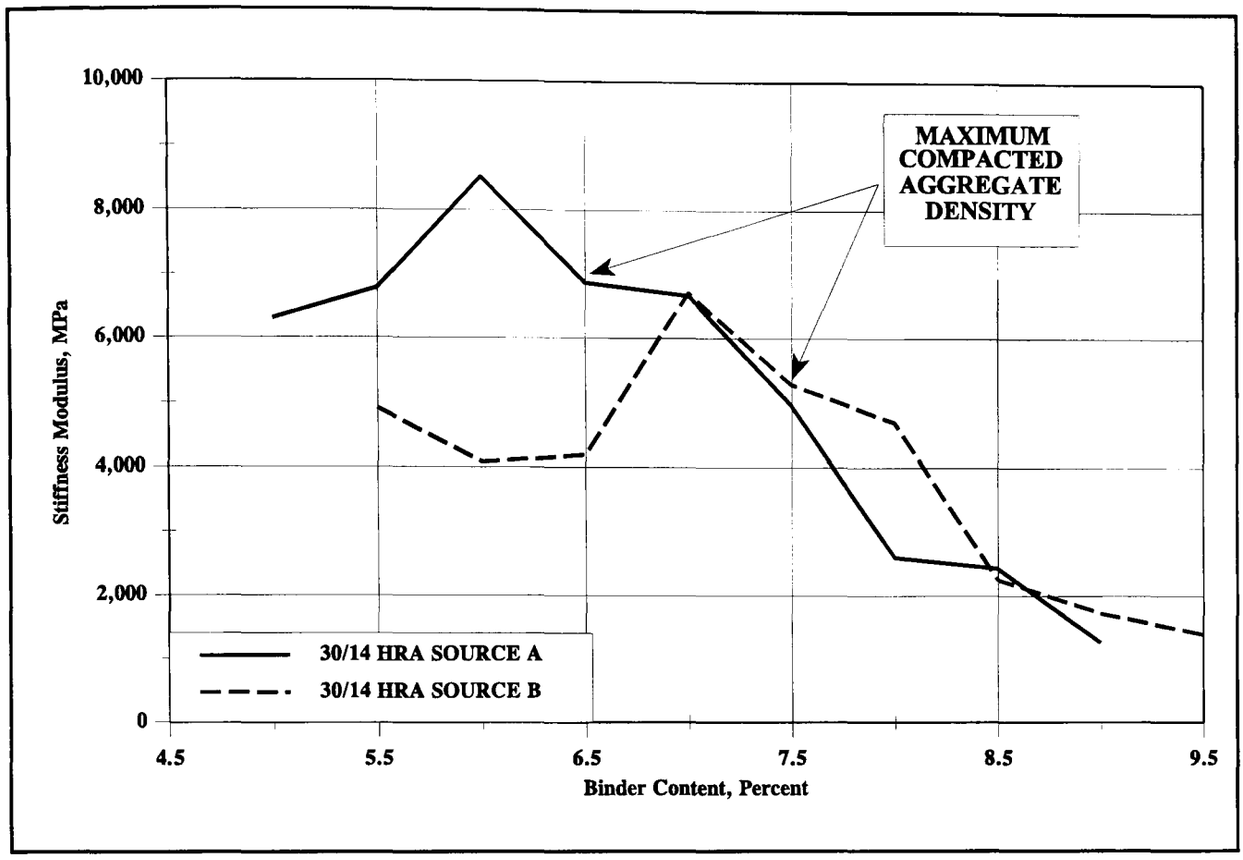


Figure 3.14 - Typical Variation in Stiffness Modulus Due to Variation in Binder Content for Two Typical HRA Mixtures.

3) Tests can be conducted on "thin" specimens thereby allowing cores from surfacing layers, typically 50mm thick, to be tested.
4) A biaxial state of stress exists in the specimen during the test which may better represent field conditions than the stress conditions found in flexure tests.
5) The test can be effectively used for the purposes of comparing mixture variables such as constituent materials and volumetric proportions as well as changes due to the effects of ageing and water damage.
6) The test can, in principle, be used for the design of bituminous mixtures.
7) The equipment used for the test is relatively inexpensive and can be used for other types of tests such as fatigue (ITFT) and permanent deformation (Repeated Load Axial Test or static creep, 10).

The principal disadvantages of indirect tension testing of bituminous mixtures, relative to other methods, include:

1) The method relies on theoretical analysis using elastic theory. Consequently, tests need to be carried out in such a way as to make this assumption reasonable e.g., moderate temperatures and reasonably fast loading times, when the material response is essentially elastic.
2) Although Poisson's ratio is necessary for the determination of the stiffness modulus in indirect tension testing, it cannot be accurately determined in such tests and must be assumed. For this reason, indirect tension tests may be less reliable than direct tension/ compression or flexural tests.
3) The absence of stress reversal during testing allows the accumulation of plastic (permanent) deformation, particularly at high test temperatures.
4) The stiffness modulus cannot be accurately measured at relatively high temperatures (e.g., 40°C) owing to the large permanent deformations which occur during testing at such temperatures.

The test conditions (temperature, rise-time and stress level) for the ITSM test need to be identical to those used for the subsequent fatigue test. Unfortunately, the ITSM used was a controlled horizontal tensile strain test from which the applied stress was calculated, which meant that the actual applied stress was not the same as that applied during the ITFT. To overcome this problem, the strain level was incremented and the stiffness and stress at each strain level recorded. Sample results are given in Figure 3.15 which show that the higher the applied stress (or strain) level, the lower the resulting stiffness modulus. Due to this stress dependent nature of stiffness modulus, a least squares linear regression was used in order to calculate the stiffness modulus at the chosen level of stress application in the ITFT.

The phenomenon of stress related stiffness modulus has been reported before by Cragg *et al* (15) and more recently by Heinicke *et al* (16) and to ascertain whether this was a genuine material effect or caused by the mode of testing, the results from trapezoidal cantilever testing are shown in Figure 3.16 which shows the same trend. Thus, the effect appears to be a genuine one reflecting real material behaviour. Because of this data, the majority of the testing detailed in this report has used the method of testing at different

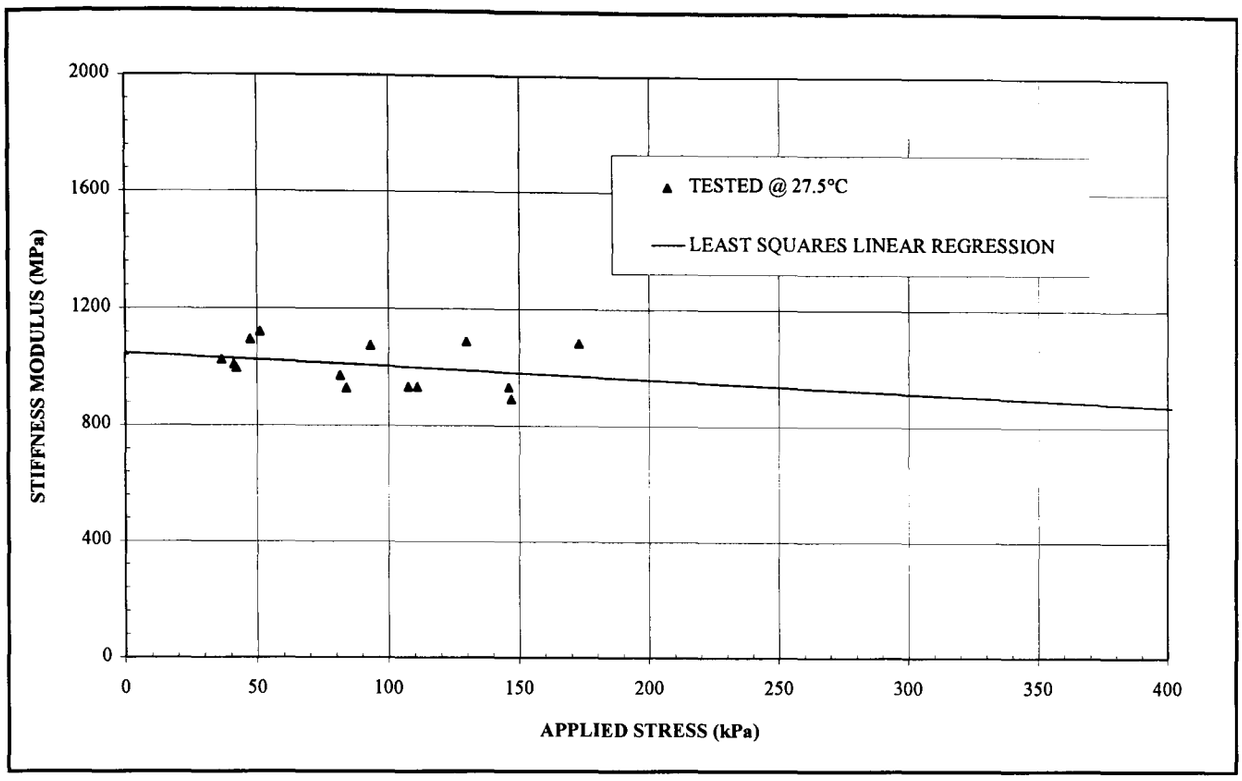


Figure 3.15 - Example Graph Demonstrating the Stress Dependency of Stiffness Modulus, in the ITFT, for a 20mm DBM Material.

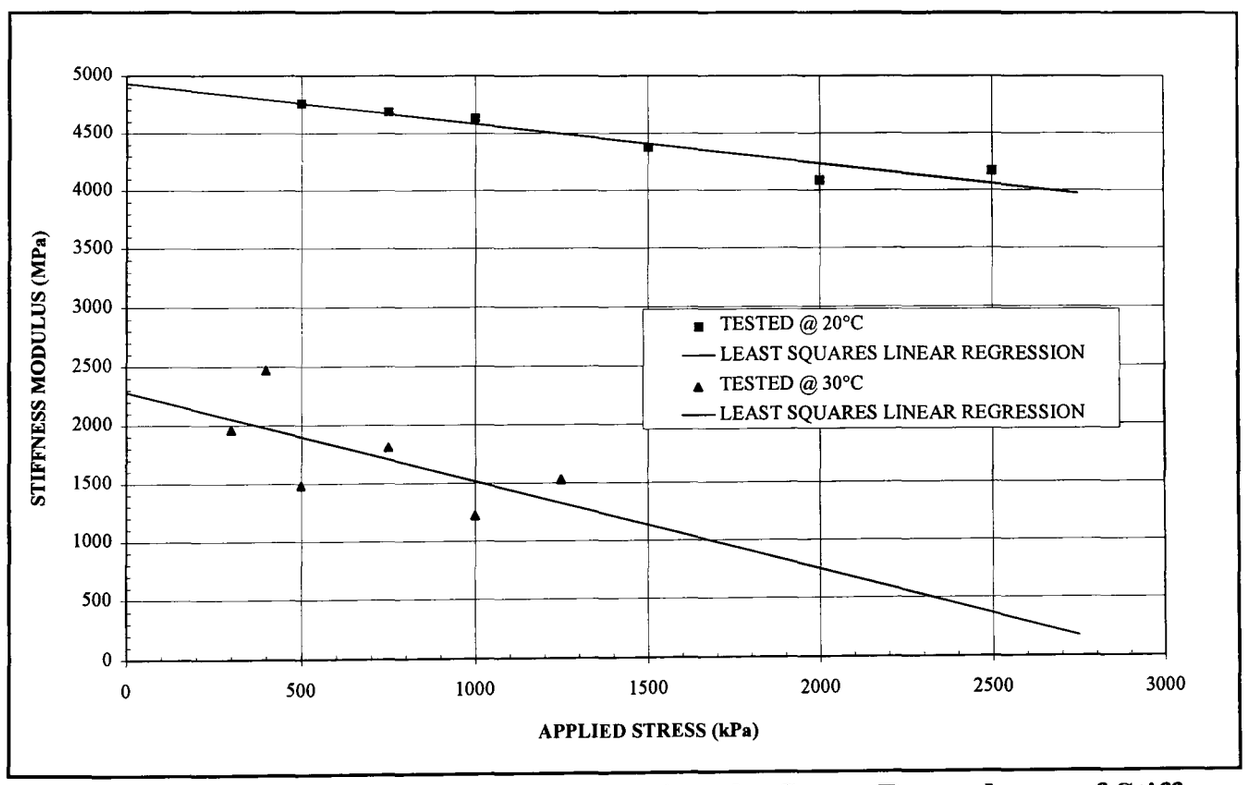


Figure 3.16 - Example Graph Demonstrating the Stress Dependency of Stiffness Modulus, in the Trapezoidal Mode of Testing, for a 20mm DBM Material.

strain levels and then a least squares linear regression to calculate the stiffness modulus at the ITFT stress level. However, during the main reproducibility test programme, described in Section 3.8, it became apparent that the true form of the stress against stiffness curve was as shown in Figure 3.17. This was mainly manifested in spurious

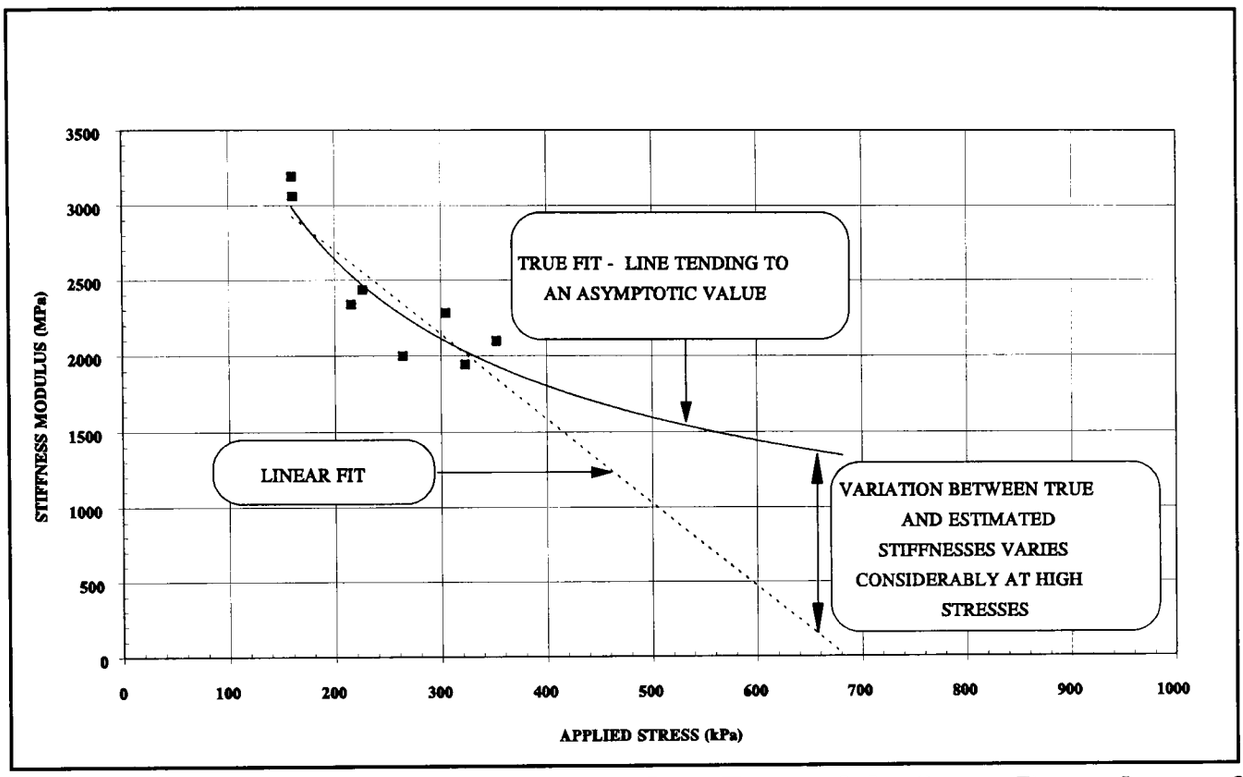


Figure 3.17 - Graph Demonstrating the True Form of the Stress Dependency of Stiffness Modulus.

outliers which could not be accounted for within the normal scatter found in the results from the ITFT.

The possibility of large errors occurring in the high stress region of testing was of great concern as it is in this region that the majority of testing in the ITFT is carried out. To overcome this problem, a two stage solution was adopted:

(i) The ITSM testing was carried out as described previously (increments of strain) but instead of a least squares linear regression being used, the results were averaged. The effect of this procedure can be seen in Chapter 4. This averaged value of stiffness modulus was then used in Equation (3.5).

(ii) The adoption of a controlled stress version of the ITSM test. This then allowed a single measurement of stiffness modulus to be obtained at the correct stress level for use in Equation (3.5) for ϵ_{xmax}.

The latter solution was not in place until after the completion of this research and, therefore, all the results presented here used the averaging method described in the first solution.

3.5 Fatigue Test Methods

The research described in this thesis used three different types of fatigue testing:

- Trapezoidal cantilever (2 point bending - simple flexure),
- Necked uniaxial tension compression (direct axial loading) and
- Indirect Tensile Fatigue Testing (diametral fatigue).

The first two methods were used to validate the ITFT with various mixture types.

3.5.1 Trapezoidal cantilever

The geometry of the trapeziums used had a top width of 40mm, base width of 120mm with a depth of 40mm and a height of 350mm. This was chosen to ensure that the maximum bending moment occurred in the middle third of the height, along the outer fibre. The speed of loading was 20Hz with temperatures ranging from 20 to 30°C and the waveform chosen was sinusoidal. The test could be used in either the controlled stress or controlled strain mode of loading, but for this research all the testing was carried out in controlled stress. This was due to decision to use this mode of control for the ITFT. The failure point of the test was defined as a 90% reduction in the stiffness and this in every case caused the specimen to fracture. A number of specimens fractured outside of the middle third of the beam, generally at one of the ends. It was the author's opinion that this was due to the stress concentrations which were induced when gluing the end plates to the specimens, as epoxy resins shrink when curing, this was shown to be the case by Rowe (11) using finite element analysis. When this occurred the specimen was discarded and another one tested in its place. Figure 3.18 shows how the specimens

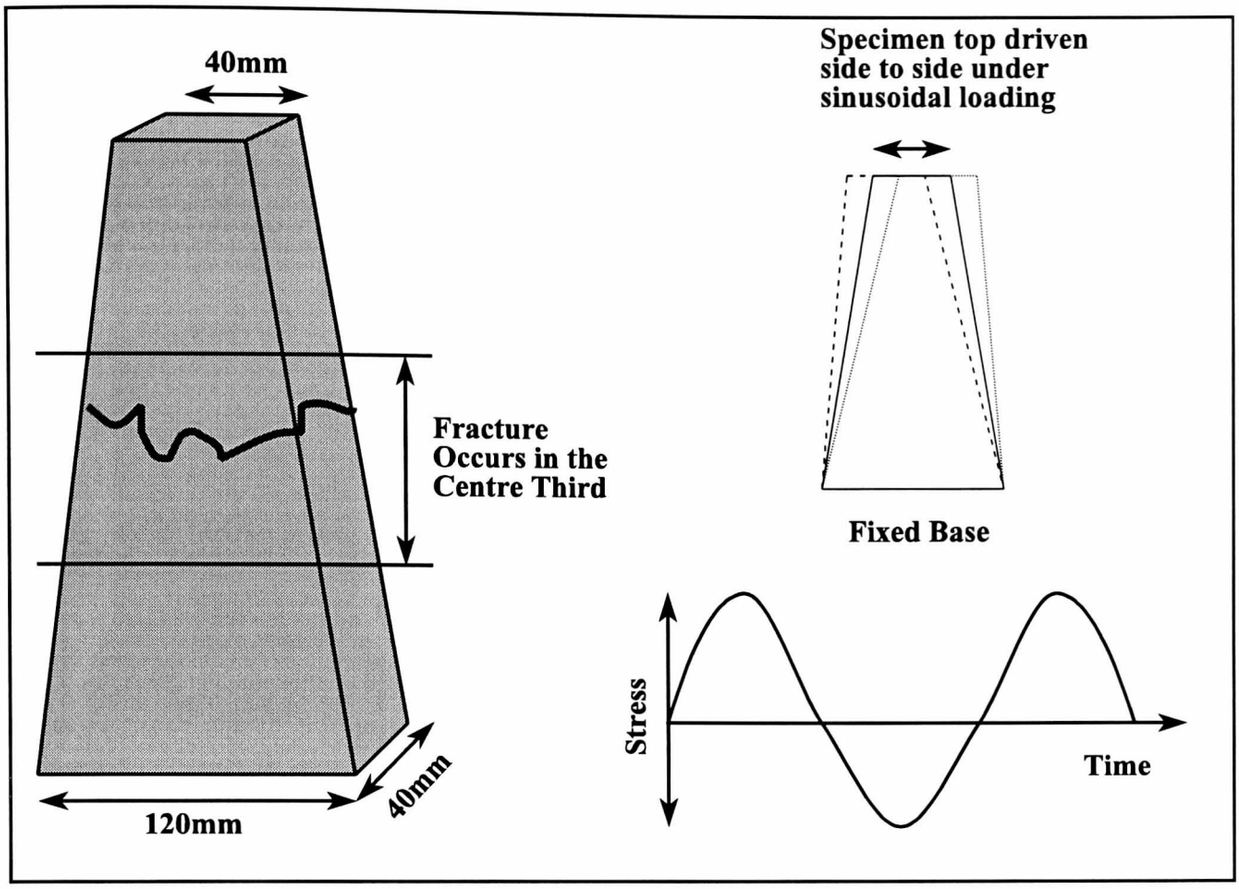


Figure 3.18 - Schematic Representation of the Trapezoidal Cantilever Test, Showing the Expected Point and Mode of Failure.

were loaded and how they failed. A more detailed description is given by Rowe (11) who used the same apparatus for much of his work into the definition of the point of crack initiation using the concept of dissipated energy.

3.5.2 Uniaxial Tension - Compression

The uniaxial tension compression testing was carried out, under the instruction of the author, at Esso's laboratories in Mont St. Aignan (MSA) in France. The cylindrical specimens were 100mm in diameter and 200mm in length. A neck was machined in the specimens which gave an effective diameter of 90mm and avoided the problems of failure at the end caps which was an obvious problem with the trapezoidal tests. The testing was carried out using a sinusoidal waveform with a test frequency of 10Hz. The test temperature for all samples was 10°C. Figure 3.19 shows how the specimens were loaded and how they failed. A more detailed description is given by Eckmann (17) who used the same apparatus for development of the 'Moebius' software (analytical pavement design).

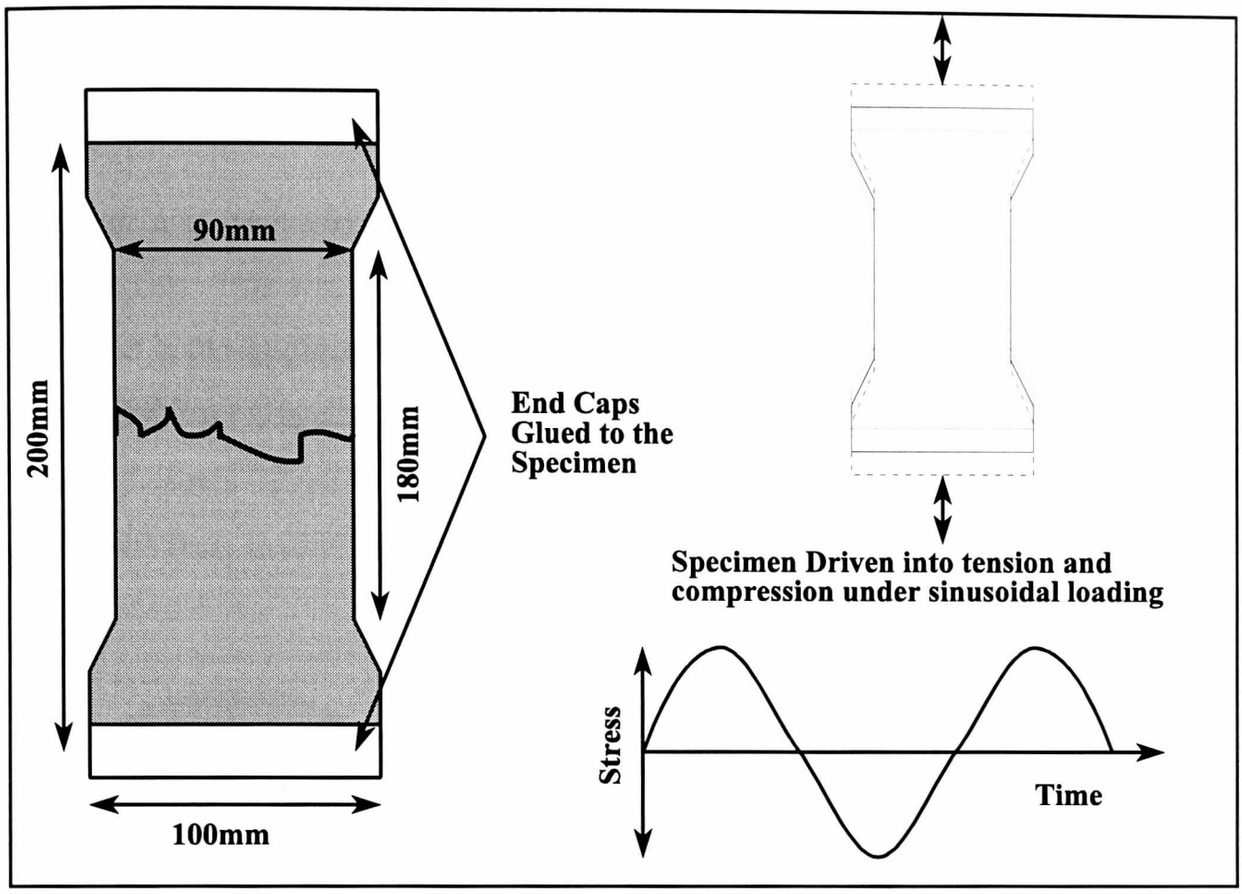


Figure 3.19 - Schematic Representation of the Uniaxial Tension Compression Test, Showing the Expected Point and Mode of Failure.

3.5.3 Indirect Tensile Fatigue Testing

This testing was carried out in the Nottingham Asphalt Tester, a simple pneumatic apparatus (18). A cyclic load pulse was applied to the specimen with the time to the peak of the load pulse being 120ms. It has been shown by comparative testing (19) that this is equivalent to a beam bending frequency of approximately 1Hz, which is approximately the same as the theoretical calculation gives, equation 3.12:

$$t = \frac{1}{2\ \pi\ f} \Rightarrow f = \frac{1}{2\ \pi\ t} \qquad \textbf{(3.12)}$$

Where:

t = Time (s) and

f = Frequency.

Substituting the loading time of 120ms (0.12s) into the equation gives a test frequency of 1.3Hz.

The specimen geometry selected for all the ITFT testing was 100mm in diameter by 40mm thick. This was chosen to ensure that a reasonably high tensile stress could be generated in the specimen to facilitate quick failure. By using equation 3.1 it can be seen that a 4 kN load generates a stress of greater than 600 kPa . A stress of this magnitude typically causes failure in less than 500 load applications. Figure 3.20 shows how the specimens were loaded and how they failed.

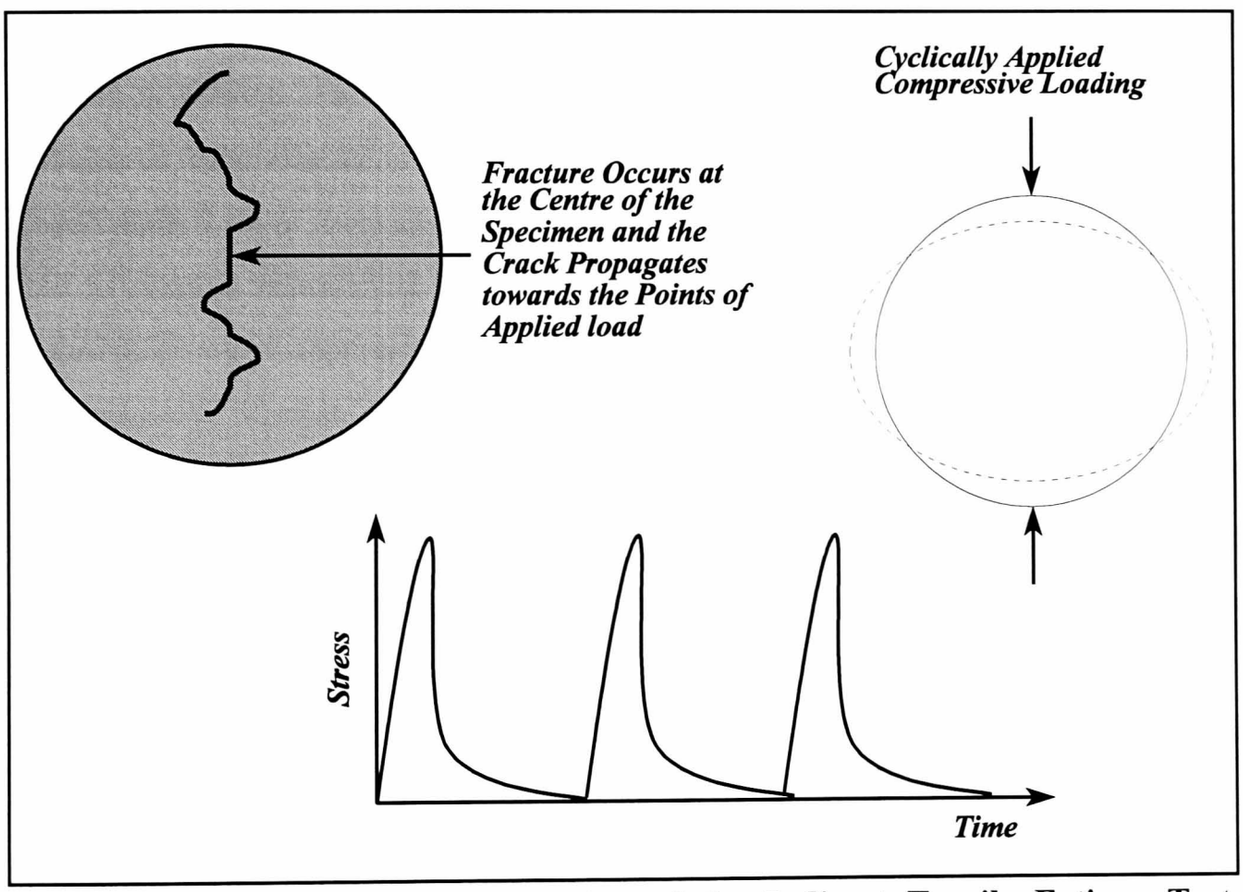


Figure 3.20 - Schematic Representation of the Indirect Tensile Fatigue Test, Showing the Expected Point and Mode of Failure.

3.6 ITFT Protocols

As the one of the goals of this research was to develop a simplified and commercially viable fatigue test, protocols for the use of the ITFT were drafted, by the author, as the ITFT evolved. To date, there have been four versions of the protocol:

"Method for the Determination of the Fatigue Characteristics of a Bituminous Mixture Using the Indirect Tensile Fatigue Test "

These were versions 1.0, 2.0a, 3.0 and British Standard Draft for Development ABF (20). Version 1.0 was written in the form of a report rather than a Standard and did not have sufficient detail for the user. This version also made no mention of the stress dependency of stiffness modulus and only required the operator to carry out the ITSM test in accordance with the British Standard Draft for Development 213 (9). Version 2.0a was written in the form of a Standard with as many technical details and tolerance limits included as was practicable at the time. It also addressed the problem of the stress dependency of stiffness modulus in the manner described in section 3.4. The method required by Version 2.0a was to test for stiffness at four strain levels each repeated on an axis normal to the original test, thus producing eight test results. These results were then plotted in the form of stress against stiffness modulus and a least squares linear regression used to obtain a relationship between these parameters. It became apparent that this methodology was inappropriate (Figure 3.17) and that a further revision to the protocol was necessary. Version 3.0 required that controlled stress ITSM testing be used where possible, thus, enabling the operator to carry out one test as described in the British Standard Draft for Development 213 to obtain the stiffness modulus of the specimen at the ITFT stress level. If controlled stress testing was not available, then testing was to be carried out as described above (Version 2.0a) but the stiffness modulus results were to be averaged rather than using the linear regression approach. There were also a number of other corrections made in Version 3.0 of the protocol, which were raised by the commercial laboratories which now use the test.

Just prior to writing this thesis the author was requested, by the British Standards Institution, to write the protocol in the form of a full British Standard. This has now been written and has been released as a public document. A copy of the Draft for Development is included in Appendix A.

3.7 Main Test Programme

This test programme was designed to compare the fatigue performance of four different mixtures in both the ITFT and the trapezoidal cantilever test. The four mixtures were as follows:

- 30/14 Hot Rolled Asphalt (HRA) - 50 pen bitumen.
- 20mm Dense Bitumen Macadam (DBM) - 100 pen bitumen.
- 28mm Dense Bitumen Macadam - 50 pen bitumen.
- 30/14 Hot Rolled Asphalt[Note 1] - Cariphalte DM - Styrene Butadiene Styrene (SBS) modifier.

Note 1 This mixture was identical to the first 30/14 mixture but with the straight-run 50 pen bitumen replaced, by the same quantity, of Cariphalte DM.

In order to carry out the comparisons, slabs of material (404 × 280 × 127mm) were produced with the roller compactor in accordance with " The Protocol for Manufacture and Storage " (Appendix A). This produced exceptionally repeatable specimens in terms of volumetric composition, an example of which is shown in Table 3.3. The volumetric data for all the specimens used in ITFT work are included in Appendix B. All volumetric calculations are based on the methodology and equations given in MS-2 (21).

Table 3.3 - An Example of the Number of ITFT Specimens and their Volumetric Data Produced from One Roller Compacted Slab.

Specimen N°	Diameter (mm)	Thickness (mm)	Bulk Specific Gravity	Maximum Specific Gravity	Voids in Mineral Aggregate (%)	Air Voids (%)	Volume of Bitumen (%)
4/1/C	99	39	2.304	2.391	21.1	3.6	17.5
4/2/C	99	40	2.302	2.391	21.1	3.7	17.4
4/3/C	99	40	2.313	2.391	20.8	3.3	17.5
4/4/C	99	40	2.313	2.391	20.7	3.2	17.5
4/5/C	99	40	2.31	2.391	20.9	3.4	17.5
4/6/C	99	40	2.319	2.391	20.6	3.0	17.6
4/7/C	99	38	2.316	2.391	20.6	3.1	17.5
4/8/C	99	38	2.318	2.391	20.6	3.0	17.6
4/9/C	99	40	2.319	2.391	20.6	3.0	17.6

Each test specimen was measured with digital vernier callipers (accurate to 0.01mm) in accordance with the protocol and then the specific gravity measured by weighing in air, and then, in water after sealing with self adhesive aluminium foil. The specific gravity of the foil (1.650) is accounted for in Equation 3.11.

$$G_{mb} = \frac{M_{au}}{M_{ac} - M_{wc} - \left(\frac{M_{ac} - M_{au}}{S_{gf}} \right)} \qquad \textbf{(3.11)}$$

where:

G_{mb} = Bulk specific gravity of the mixture,

M_{au} = Mass of the specimen in air uncoated (kg),

M_{ac} = Mass of the specimen in air coated with aluminium foil (kg),

M_{wc} = Mass of the specimen in water coated in aluminium foil (kg) and

S_{gf} = Specific gravity of the aluminium foil.

The maximum mixture specific gravity (G_{mm}) was measured in accordance with the relevant British Standard Draft for Development (22) developed at the University of Nottingham after the Rice method (23). From this volumetric data, a calculation of Air Voids (V_v, %), Voids in the Mineral Aggregate (VMA, %) and the Binder content by Volume (V_B, %) was carried out.

From each slab, a number of trapezoidal specimens and cores were cut for testing in the trapezoidal fatigue apparatus and the ITFT apparatus respectively. The test conditions for the two methods of testing were ascertained by making the trapezoidal tests the standards and then selecting the ITFT conditions so that the bitumen stiffnesses were equal. This equivalency was obtained by utilising Van der Poel's nomograph (24), which required the Softening Point and Penetration of the bitumen (Table 3.4).

Table 3.4 - Softening Point and Penetration Values for the Bitumens Used in the Main Test Programme.

	Softening Point (°C)	Penetration (dmm)
50 pen used in 30/14 HRA	54.5	49.5
100 pen used in 20mm DBM	44.5	102
50 pen used in 28mm DBM 50	53.5	57
50 pen SBS modified used in 30/14[Note 1]	84	87

Note 1 Although Van der Poel's Nomograph does not apply to polymer modified bitumens it was used here to provide an estimate of the required value in lieu of any better method.

For the 30/14 HRA and the 20mm DBM, two sets of test temperatures were used to ascertain whether the two test methods were truly equivalent. The 30/14 HRA modified with SBS was tested at one temperature in order to reduce the testing time and number of specimens. The 28mm DBM 50 was manufactured on-site in the large portable mould (4m × 1m × 0.3m), in order to ascertain if site prepared specimens gave different results to laboratory prepared ones, and consequently trapezoidal specimens were more difficult to manufacture. A metre square block of material was cut from the slab using a pneumatic hammer and the block was then sawn into suitable sizes, for a table top diamond tipped saw, using a special floor saw. As the number of resulting trapezoidal specimens was small, only one test temperature was used for the 28mm DBM 50.

The test conditions for the ITFT to give equivalent bitumen stiffnesses are detailed in Table 3.5.

On average, six trapezoidal specimens and twelve ITFT specimens were tested for each material and test temperature. Because the method for calculating the maximum tensile strain (ϵ_{xmax}) for the ITFT requires that the stiffness modulus is known, each specimen was initially tested for its indirect tensile stiffness modulus as described in Section 3.6. All fatigue testing in the ITFT was carried out in accordance with the protocol (The Method for the Determination of the Fatigue Characteristics of a Bituminous Mixture Using the Indirect Tensile Fatigue Test) with the failure criterion set at 9mm of vertical

deformation, ensuring complete failure of all mixtures. The failure criterion for the trapezoidal test was a reduction in initial stiffness of 90%, this, as in the ITFT failure criterion, ensured complete failure of the specimens.

Table 3.5 - Test Temperatures for the Materials Based on Equivalent Bitumen Stiffness.

Test Mode	Material	Temperature (°C)	Equivalent Loading Times (s)[Note 1]	Bitumen Stiffness (MPa)
Trapezoidal	30/14 HRA	20.0	0.05	38.1
		30.0	0.05	8.5
	20mm DBM	20.0	0.05	13.6
		30.0	0.05	1.9
	28mm DBM 50	20.0	0.05	31.7
	30/14 HRA - SBS	20.0	0.05	17.4
ITFT	30/14 HRA	13.5	0.12	38.1
		25.5	0.12	8.5
	20mm DBM	16.5	0.12	13.6
		27.5	0.12	1.9
	28mm DBM 50	13.5	0.12	31.7
	30/14 HRA - SBS[Note 2]	18.0	0.12	17.4

Note 1 *It was recognised after the testing that the frequency for the ITFT was calculated incorrectly as the author assumed that, as for the trapezoidal test, the frequency was the reciprocal of the loading time. However the true frequency is as expressed in equation 3.10. As it transpired this had no effect as the temperature only affected the stiffness of the material which affected where on the fatigue line the point falls not the position of the fatigue line itself.*

Note 2 *Although the recommended test temperature for this material was 18°C it was actually tested at 20°C as the testing of the first three materials had shown that, temperature only affects the stiffness and, hence, the position the point falls on the line and not the position of the line itself. Temperature and frequency both affect the stiffness modulus and, hence the magnitude of the calculated strain. When the strain changes so does the associated life to failure and, hence, a change in either the temperature or frequency only affects the position a point falls on the fatigue line and not the position of the line itself (25).*

The results of the main test programme and the additional test programme, apart from the results of the contractual use of the ITFT which are given in section 3.8.4., are given in Chapter 4.

3.8 Additional Test Programme

Following the successful conclusion of the main test programme it was decided to further evaluate and evolve the ITFT for incorporation as a British Standard. This work involved examining the following areas:

- Repeatability
- Reproducibility
- Practical Use
- Contractual Use
- Further Validation of the test against another fatigue test (Direct axial loading)

3.8.1 Repeatability of the ITFT

This was evaluated by repeating the testing carried out on the 30/14HRA and the 20mm DBM materials described in Section 3.7. The specimens for the repeat testing were manufactured at the same time as those for the first testing and were originally intended as spare specimens in case of problems occurring with the test or test method.

3.8.2 Reproducibility of the ITFT

This was evaluated in the first instance by producing duplicate batches of the 30/14HRA material and supplying it to two laboratories (Northamptonshire County Council and Suffolk County Council) which had been appropriately equipped. This first phase of work was very encouraging and hence a second trial involving nine laboratories was carried out. The laboratories and the materials tested were as follows:

- Buckinghamshire County Council - 20mm DBM,
- Kent County Council - 20mm DBM,
- Surrey County Council - 20mm DBM,
- Mobil Oil Company - 20mm DBM,

- Norfolk County Council - 40mm HDM,
- Northamptonshire County Council - 40mm HDM,
- Shell Bitumen - 40mm HDM,
- Suffolk County Council - 40mm HDM and
- SWK Pavement Engineering - 40mm HDM.

This second trial detected the problems with stiffness described earlier and due to the poor results of the 20mm DBM a third trial was undertaken repeating the 20mm DBM. Six laboratories participated in this final trial:

- Buckinghamshire County Council,
- Kent County Council,
- Tarmac Quarry Products,
- Northamptonshire,
- Shell Bitumen and
- SWK Pavement Engineering.

3.8.3 Practical Use of the ITFT

The ITFT was used for the evaluation of asphalt mixtures in a three year old, heavily trafficked, section of a trunk road. The road surfacing consisted of a polymer modified (SBS) 50/20 HRA basecourse and a polymer modified (SBS) 40/14 HRA wearing course, both layers having sections of unmodified material built into them. Specimens of all four materials were extracted from both the edge of the carriageway and the wheel track and then tested in the ITFT. Following this work it was decided to manufacture laboratory specimens to the same original mixture designs as the site materials. The purpose of this exercise was to compare the virgin fatigue properties with those of the aged and trafficked materials in order to assess the ITFT's ability to distinguish between materials and to be able to properly rank materials according to their fatigue resistance.

3.8.4 Contractual Use of the ITFT

The ITFT, following the research reported here, has been successfully used in many recent contractual situations (26, 27, 28). The first contractual use was carried out by the

author under contract to SWK Pavement Engineering (a leading firm of UK pavement consultants) and is given here to show the ability of the ITFT.

This first contract involved an evaluation of the fatigue performance of 30 cores of HRA basecourse material. The need for the evaluation arose after compositional analysis revealed that several areas did not comply with the relevant specification with respect to the soluble binder content, corrected values being lower than the specified minimum.

Twenty cores (2 sets of 10) were removed from two areas where compositional analysis had revealed lower than specified corrected binder content. A further 10 cores were removed from an area where the binder content was within the specified limits. The ITFT was used, in accordance with the protocol, to compare the fatigue performance of the two low binder areas with the control area where the binder content was satisfactory.

The relevant data for the cores is given in Table 3.6. The ITFT was unable to distinguish between the three sets of data due to the fact that the volume of binder is between 10.0 and 10.5% for all 30 cores (FigureS 3.21 and 3.22): although the binder content by mass of the control cores was 1% higher than that of the cores from the two poor areas, the air void content was between 1 and 2% higher, thus reducing the volume of binder to the same narrow range for all 30 cores. It has previously been shown that fatigue performance on the basis of applied tensile strain is primarily influenced by binder volume and binder type (25). However, Table 3.6 shows that there is a difference between the stiffness of the control section (2215 ± 400MPa) and the other two areas (1321 ± 300MPa) which will result in lower tensile strains being generated in the control section and, hence, a marginally longer fatigue life. This conclusion however, appears to conflict with the fact that lower air voids and higher percentages of aggregate will result in higher stiffnesses and this, therefore, brings into questions the volumetric measurements which were carried out.

Table 3.6 - Summary of Data for the First Contractual Use of the ITFT.

Specimen Reference[Note 1]	Void Content (%)	Binder Volume (%)	Stiffness (Mpa)[Note 2]	Stress (kPa)	Strain (microstrain)	Cycles to Failure
1	2.3	10.1	1,010	600	1,218	107
2	3.8	10.0	1,000	550	1,128	99
3	1.9	10.1	1,142	500	898	147
4	1.3	10.2	1,108	400	740	590
5	1.5	10.2	1,112	350	645	933
6	2.1	10.1	1,297	300	474	1,120
7	1.7	10.2	1,290	625	993	92
8	1.6	10.2	1,172	250	437	2,565
9	1.3	10.2	1,409	250	364	5,033
10	1.7	10.2	1,380	175	260	25,641
11	2.0	10.1	2,021	625	634	129
12	2.1	10.1	1,073	600	1,146	131
13	1.5	10.1	934	550	1,207	107
14	0.3	10.3	1,345	500	762	218
15	1.1	10.2	1,044	450	884	400
16	0.6	10.2	1,522	125	168	80,334
17	0.6	10.2	1,500	400	547	650
18	0.7	10.2	1,495	350	480	978
19	1.6	10.1	1,577	250	325	9,387
20	0.8	10.2	1,979	425	440	959
21	3.1	10.5	2,678	625	478	224
22	3.0	10.5	2,879	600	427	248
23	2.7	10.5	2,004	550	563	247
24	3.2	10.5	2,100	500	488	356
25	2.6	10.5	2,458	450	375	703
26	2.4	10.5	1,613	235	299	11,312
27	2.6	10.5	2,094	400	392	1,976
28	4.0	10.4	2,242	350	320	1,174
29	3.1	10.5	2,308	150	133	40,451
30	3.0	10.5	1,774	250	289	6,484

Note 1 *Cores 1 to 10 had a binder content by mass of 3.8%, cores 11 to 20 had a binder content by mass of 4.2% and cores 21 to 30 had a binder content by mass of 5.2%.*

Note 2 *The stiffness testing was carried out at 20°C and using a risetime of 120ms, as required by the ITFT.*

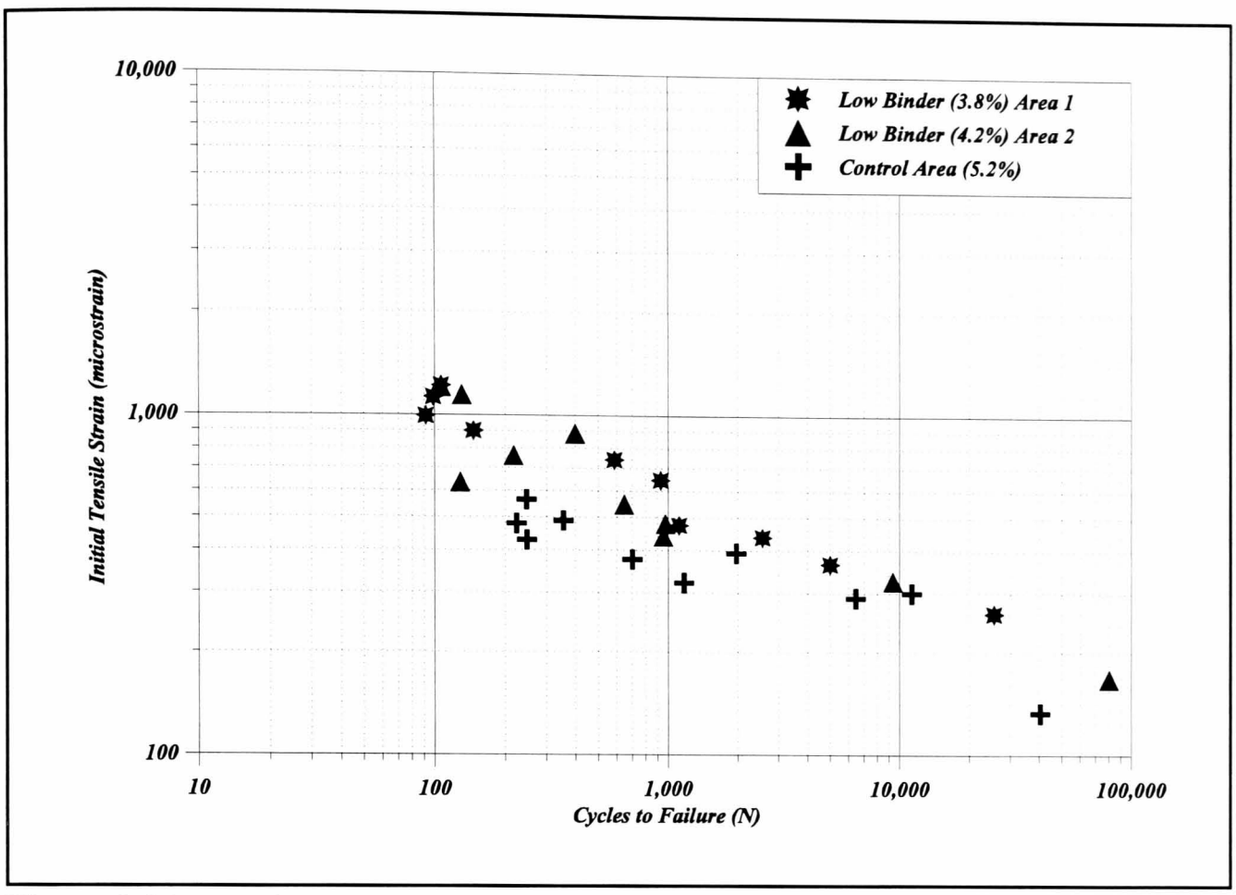


Figure 3.21 - Fatigue Information for the First Contractual Use of the ITFT.

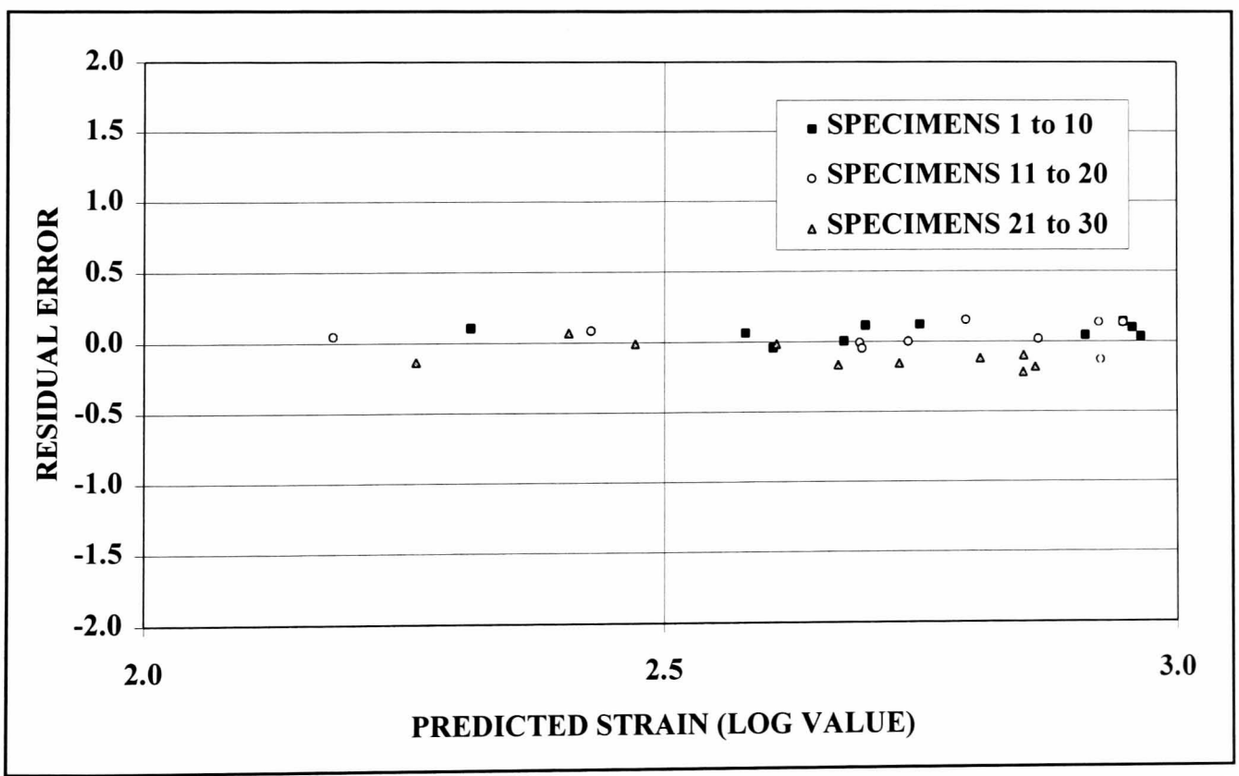


Figure 3.22 - Error Plot Demonstrating No Statistical Difference Between the 3 Sets of Data.

A number of the specimens had extremely short fatigue lives and as highlighted earlier in this Chapter it is possible, under the conditions which lead to short lives, for shear or compressive failure to occur. As these tests were carried out by SWK Pavement Engineering it was not possible for the author to determine the actual mode of failure. However, as all the points, for each of the areas, appear to fall on the same line then it would seem that the failure mode was the same for all the specimens. Whether this failure mode was shear, compressive or tensile is impossible to say categorically, however, the author's experience would indicate that it was tensile particularly for the long life specimens and, hence, for all the specimens.

The conclusions of the work were as follows:

- The ITFT was not able to discriminate between the three areas in terms of their strain-life relationships. Thus there appeared to be no significant difference between the disputed and control areas in terms of fatigue life.
- It was believed that this lack of difference was due to the fact that the volume of binder was between 10.0 and 10.5% for all 30 cores although, as explained in the text, some concern over the volumetric measurements has been raised.
- The control area had higher stiffness and, hence, lower tensile strain and the fatigue life can be expected to be marginally longer than for the disputed areas.
- It was presumed that the fatigue performance of the control area was not in dispute: as this was the case, then the fatigue performance of the disputed area should also be acceptable since its fatigue performance could not be markedly distinguished from that of the control area.

The final outcome was to leave the previously disputed material in place, thus, saving hundreds of thousands of pounds and, to date, there have been no problems with the material.

3.8.5 Further Validation of the ITFT

It was decided that a further validation of the ITFT should be carried out by comparing it against a direct axial fatigue test. The uniaxial tension compression testing was carried out, under the instruction of the author, at Esso's laboratories in Mont St Aignan (MSA) in France, where all the specimens were manufactured. Esso provided the author with 10 cores of each of 3 materials. These were a 20mm HDM (1987), a 0 to 10mm Asphaltic Concrete (1992) and a 0 to 14mm Asphaltic Concrete (1995), the numbers in brackets are the Identity codes for the three materials. The testing was completed in accordance with the protocol and the results are given in the next Chapter.

3.9 References

1. Porter, B.W. and Kennedy, T.W., "Comparison of Fatigue Test Methods for Asphalt Materials," Research Report 183-4, Project 3-9-72-183, Centre for Highway Research, University of Texas at Austin, April 1975.
2. Deacon, J.A., Tayebali, A., Coplantz J.A., Finn, F.N. and Monismith, C.L., "Fatigue Response of Asphalt-Aggregate Mixes, Part I - Test Method Selection," SHRP Project A003-A, Asphalt Research Program, Institute of Transportation Studies, University of California Berkeley, November 1992.
3. Rao Tangella, S.C.S., Craus, J., Deacon, J.A. and Monismith, C.L., "Summary Report on Fatigue Response of Asphalt Aggregate Mixtures," Strategic Highway Research Program, Project A-003-A, TM-UCB-A-003-A-89-3, Institute of Transportation Studies, University of California Berkeley, California, February 1990.
4. Timoshenko, S., "Theory of Elasticity," McGraw Hill Book Co., New York, pp 104-108, 1934.
5. Frocht, M.M., "Photoelasticity," John Wiley & Sons Inc., New York, Volume 2, pp 121-129, 1948.
6. Muskhelishvili, N.I., "Some Basic Problems of the Mathematical Theory of Elasticity," P. Noordhoff Ltd, Groningen, pp 324-328, 1953.
7. Sokolnikoff, I.S., "Mathematical Theory of Elasticity," McGraw Hill Book Co., New York, pp 280-284, 1956.

8. Roque, R. and Buttlar, W.G., "The Development of a Measurement and Analysis System to Accurately Determine Asphalt Concrete Properties Using the Indirect Tensile Mode," Proceedings of the Association of Asphalt Paving Technologists, Volume 61, pp 304-332, 1992.

9. British Standards Institution, "Method for the Determination of the Indirect Tensile Stiffness Modulus of Bituminous Materials," Draft for Development 213, 1993.

10. British Standards Institution, "Method for Assessment of Resistance to Permanent Deformation of Bitumen Aggregate Mixtures Subject to Unconfined Uniaxial Loading," Draft for Development 185, 1993.

11. Rowe, G.M., "Performance of Asphalt Mixtures in the Trapezoidal Fatigue Test," Proceedings of the Association of Asphalt Paving Technologists, Volume 62, pp 344-384, 1993.

12. Alavi, S.H. and Monismith, C.L., "Time and Temperature Dependent Properties of Asphalt Concrete Mixtures Tested as Hollow Cylinders and Subjected to Dynamic Axial and Shear Loads," Proceedings of the Association of Asphalt Paving Technologists (AAPT), Volume 63, pp , 1994.

13. British Standards Institution, "Sampling and Examination of Bituminous Mixtures for Roads and Other Paved Areas," BS 598, Part 107, 1990.

14. Kalcheff, I.V. and Tunicliff, D.G., "Effects of Crushed Stone Aggregate Size and Shape on Properties of Asphalt Concrete," Proceedings of the Association of Asphalt Paving Technologists (AAPT), Volume 51, pp 453-482, 1982.

15. Cragg, R. and Pell, P.S., "The Dynamic Stiffness of Bituminous Road Materials," Proceedings of the Association of Asphalt Paving Technologists (AAPT), Volume 40, pp 126-193, 1969.

16. Heinicke, J.J. and Vinson, T.S., "Effect of Test Condition Parameters on IRM," Journal of Transportation Engineering, Volume 114, No 2, March 1988.

17. Eckmann, B., "Exxon Research in Pavement Design 'Moebius' Software; A case Study Reduction of Creep Through Polymer Modification," Proceedings of the Association of Asphalt Paving Technologists (AAPT), Volume 58, pp 337-361, 1989.

18. Cooper, K.E. and Brown, S.F., "Development of a Simple Apparatus for the Measurement of the Mechanical Properties of Asphalt Mixes," Proceedings, Eurobitume Symposium, Madrid, 1989, *pp* 494-498.

19. Brown, S.F., Gibb, J.M., Read, J.M., Scholz, T.V. and Cooper, K.E., "Design and Testing of Bituminous Mixtures," SERC/DoT LINK Scheme First Final Report, Department of Civil Engineering, University of Nottingham, January 1995.

20. British Standards Institution, "Method for the Determination of the Fatigue Characteristics of bituminous Mixtures Using Indirect Tensile Fatigue," Draft for Development ABF, 1995.

21. Anon, "Mix Design Methods for Asphaltic Concrete and Other Hot-Mix Types," Manual Series No 2 (MS-2), The Asphalt Institute, Lexington, Kentucky, 1988.

22. British Standards Institution, "Measurement of the Maximum Density of Bituminous Paving Mixtures," Draft for Development XYZ, 1994.

23. Rice, J.M., "The Measurement of Voids in Bituminous Mixtures," Proceedings of the Association of Asphalt Paving Technologists (AAPT), Volume 21, 1952.

24. Van der Poel, C.V., " A General System Describing the Visco-elastic Properties of Bitumens and its Relation to Routine Test Data," Journal of Applied Chemistry, Volume 4, 1954.

25. Cooper, K.E. and Pell, P.S., "The Effect of Mix Variables on the Fatigue Strength of Bituminous Materials," TRRL Laboratory Report 633, Crowthorne, Berkshire, 1974.

26. Thom, N.H., "Second Bangkok International Airport: Design of Airfield Pavements," SWK (PE) Client Report, A105, November 1995.

27. Elliott, R.C., "Determination of Mechanical Properties of 'WESTMIX' SMA," SWK (PE) Client Report, B180, March 1995.

28. Elliott, R.C. and Read, J.M., "Use of Modified Binders in Marshall Asphalt Mixtures : Mixture Test Programme," SWK (PE) Client Report, P921, November 1995.

RESULTS OF THE INDIRECT TENSILE FATIGUE TESTING

4.1 Introduction

This Chapter contains all the results from the testing described in Chapter 3. It is intended that it demonstrate the validation of the ITFT by its comparison with two other fatigue test methods, the high repeatability and reproducibility of the test and the practical application of the method to existing pavements.

4.2 Initial Findings

One of the first areas of concern with the test method was that the definition of failure was unacceptable as it was given in terms of a vertical deformation. Figures 4.1 and 4.2 give typical results for an ITFT specimen and a trapezoidal specimen respectively and demonstrate that both show the same trend of having approximately 10% of the entire life to failure as a crack propagation phase.

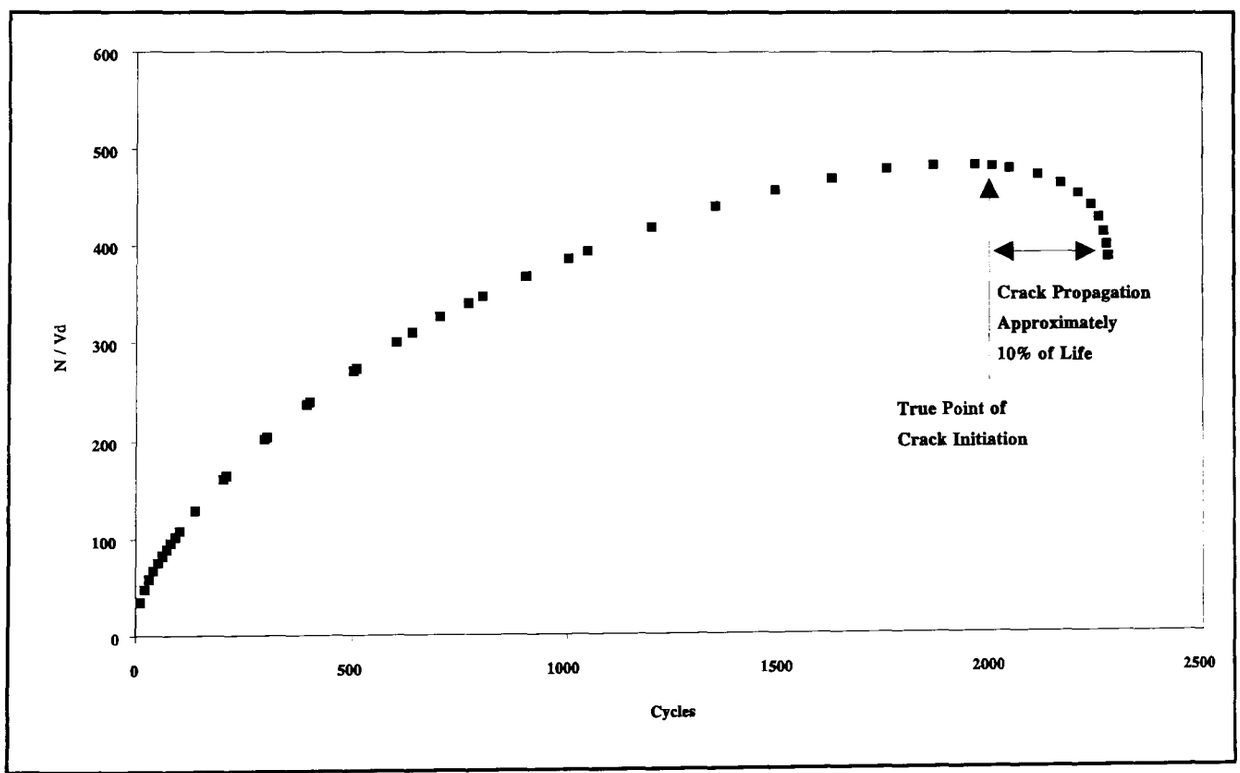


Figure 4.1 - Typical Result for an ITFT Specimen, 28mm DBM 50 Tested at 13.5°C at a Stress Level of 450kPa.

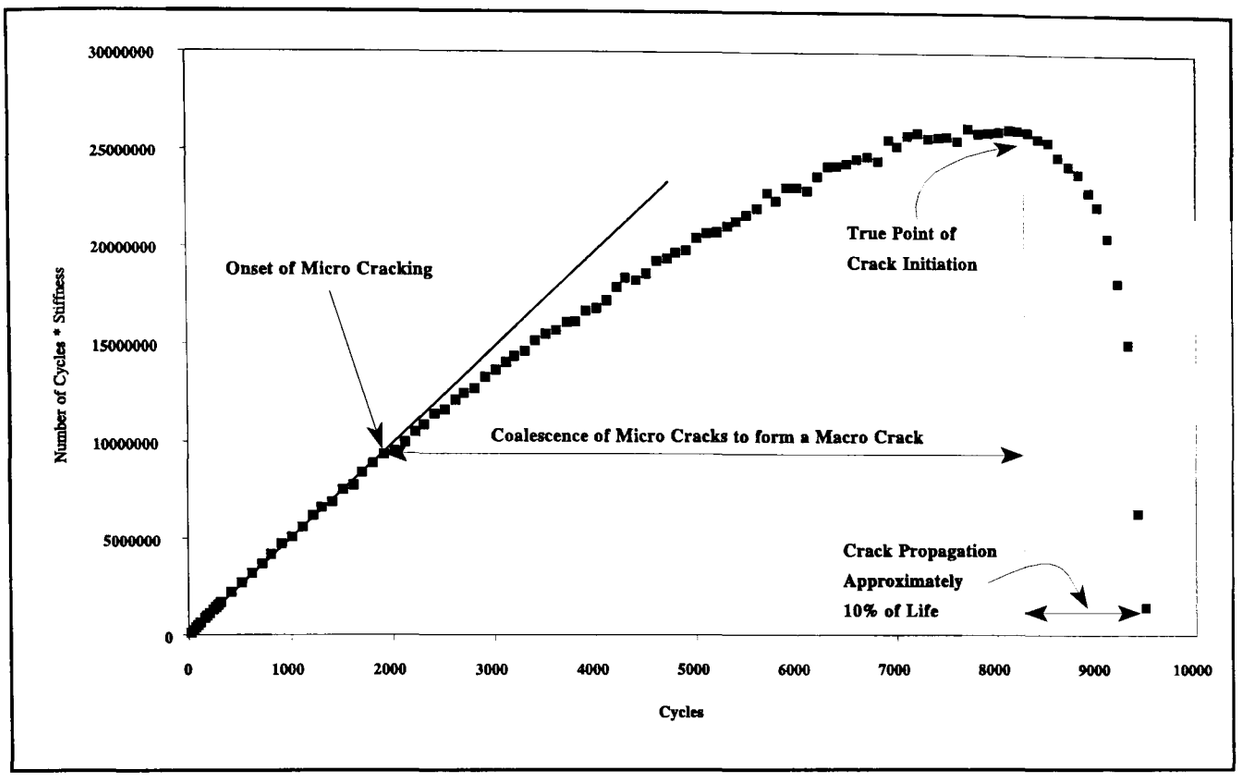


Figure 4.2 - Typical Result for a Trapezoidal Specimen, 28mm DBM 50 Tested at 20°C at a Stress Level of 1000kPa.

As the proportion of the life remained at approximately 10% for both tests regardless of the length of test or the temperature it was decided to take the number of load applications to failure as being correct. This further simplified the interpretation of the ITFT making it even more desirable than had been the case previously.

This was also found to be the case for polymer modified mixtures although they generally did not fail completely by 9mm of vertical deformation and were still capable of supporting load. This gave the first indication of the improved crack propagation properties of some polymer modified mixtures.

Figure 4.2 also demonstrates graphically the onset of damage, in the form of micro cracking and the coalescence of these micro cracks to form a macro crack which then propagates to failure. It can also be seen that the length of time for coalescence varies considerably (Figures 3.7, 3.8, 4.1 and 4.2) and it is considered that this is due to the magnitude of the applied stress. The higher the stress the quicker the onset of micro cracking and, hence, the longer, proportionally, the period of coalescence.

4.3 Results of the Main Test Programme

The initial results based upon the maximum tensile stress (σ_{xmax}) against the number of cycles to failure (N) (Figures 4.3, 4.4, 4.5 and 4.6) seemed to indicate the problems found by other researchers, in particular by Kennedy *et al* (1, 2, 3). Although this initially gave cause for concern it was considered, as described previously, that the initial tensile strain generated in the specimen was the important parameter and, therefore, it was this parameter which should be calculated and plotted against the life to failure.

On the basis of Figures 4.3 to 4.6 it can be seen that temperature plays an important role, with the fatigue lines for the same material being parallel but separated at different temperatures. When the results are presented in terms of tensile strain (Figures 4.7 to 4.10) it can be seen that the experimental data tend to form a single relationship under the range of conditions of test evaluated in this work as the temperature and frequency affect the stiffness of the specimen which only affects the magnitude of the tensile strain generated in the specimen. This being said, it can be seen that the data sets for the ITFT and the trapezoidal do not always overlap to a large extent (Figure 4.7) and this could lead to some question as to whether the data sets do actually fall on the same line. It can also be seen that some of the ITFT data sets appear to have markedly different slopes to the trapezoidal results (Figure 4.8). Although this is true it can be explained by the fact that this occurs when the testing has not been carried out over a wide enough range of tensile strains and the protocols written (Appendix A) have clauses to ensure this does not happen in practice. However, it can be seen that in the region of tensile strain which is of interest to pavement engineers, 30 to 200 microstrain, there is good agreement, for all the materials, between the two test methods even where the best fit line indicates that the trapezoidal data are not really on that line (Figure 4.9).

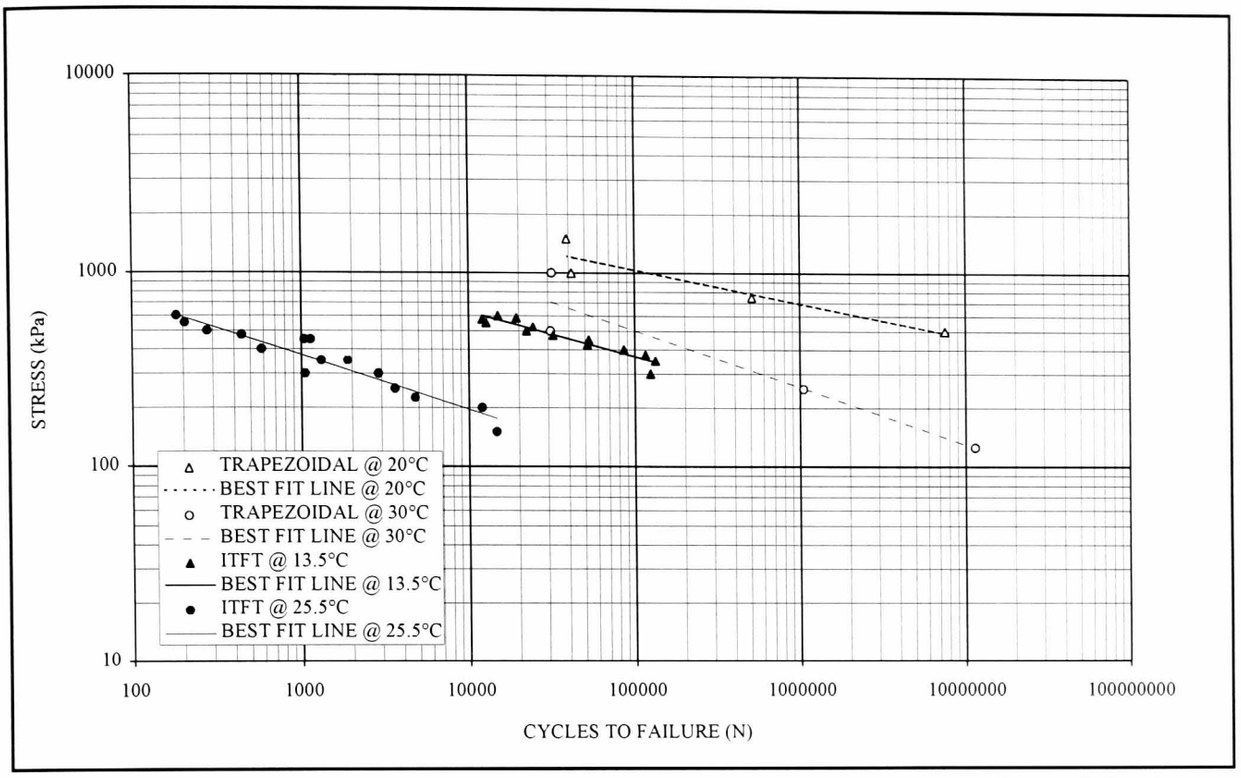


Figure 4.3 - Fatigue Characteristics for the 30/14 HRA Based on Maximum Tensile Stress (σ_{xmax}) Against Life to Failure.

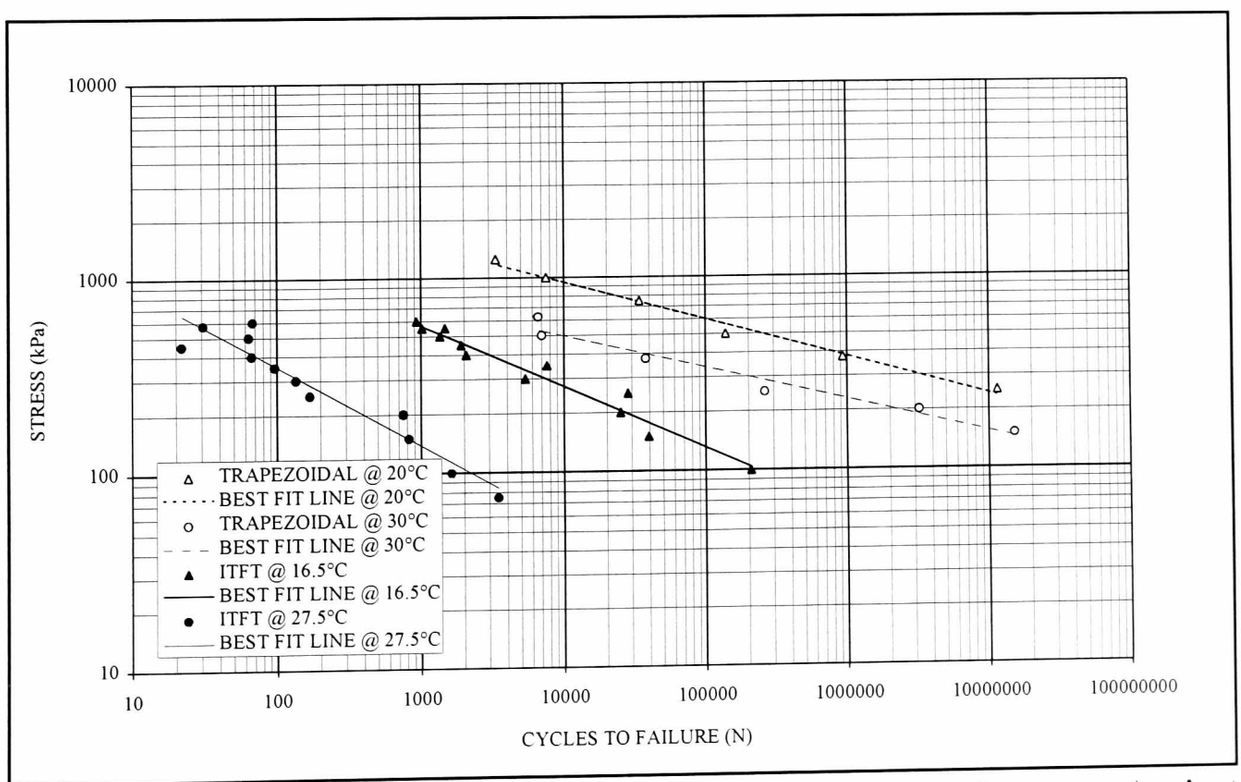


Figure 4.4 - Fatigue Characteristics for the 20mm DBM Based on σ_{xmax} Against Life to Failure.

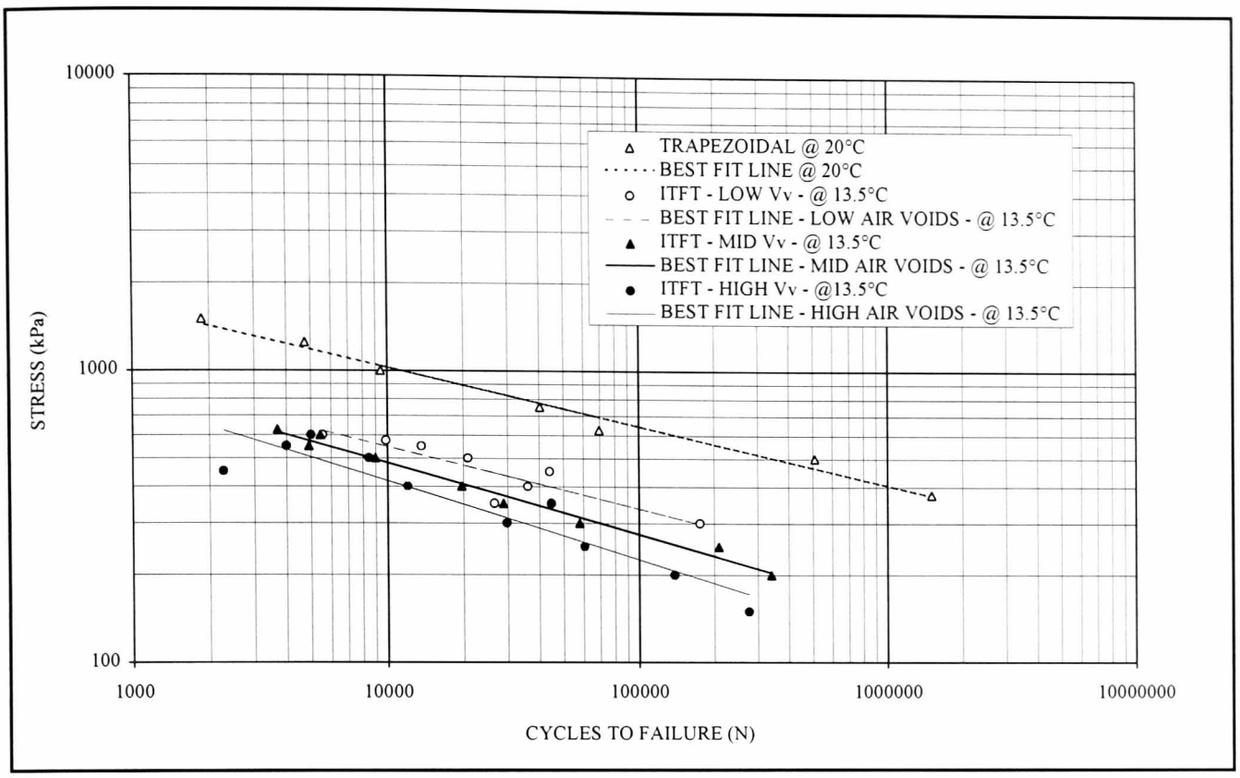


Figure 4.5 - Fatigue Characteristics for the 28mm DBM 50 Based on σ_{xmax} Against Life to Failure.

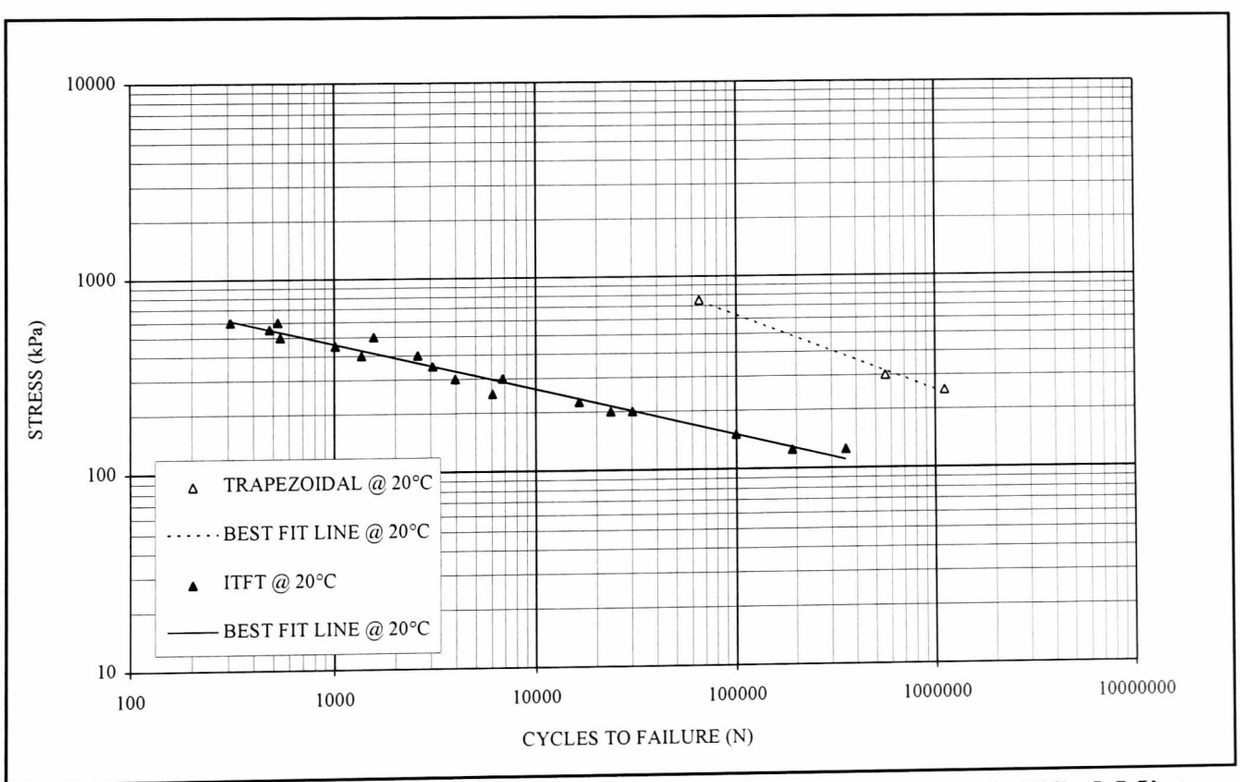


Figure 4.6 - Fatigue Characteristics for the 30/14 HRA SBS Modified Mixture Based on σ_{xmax} Against Life to Failure.

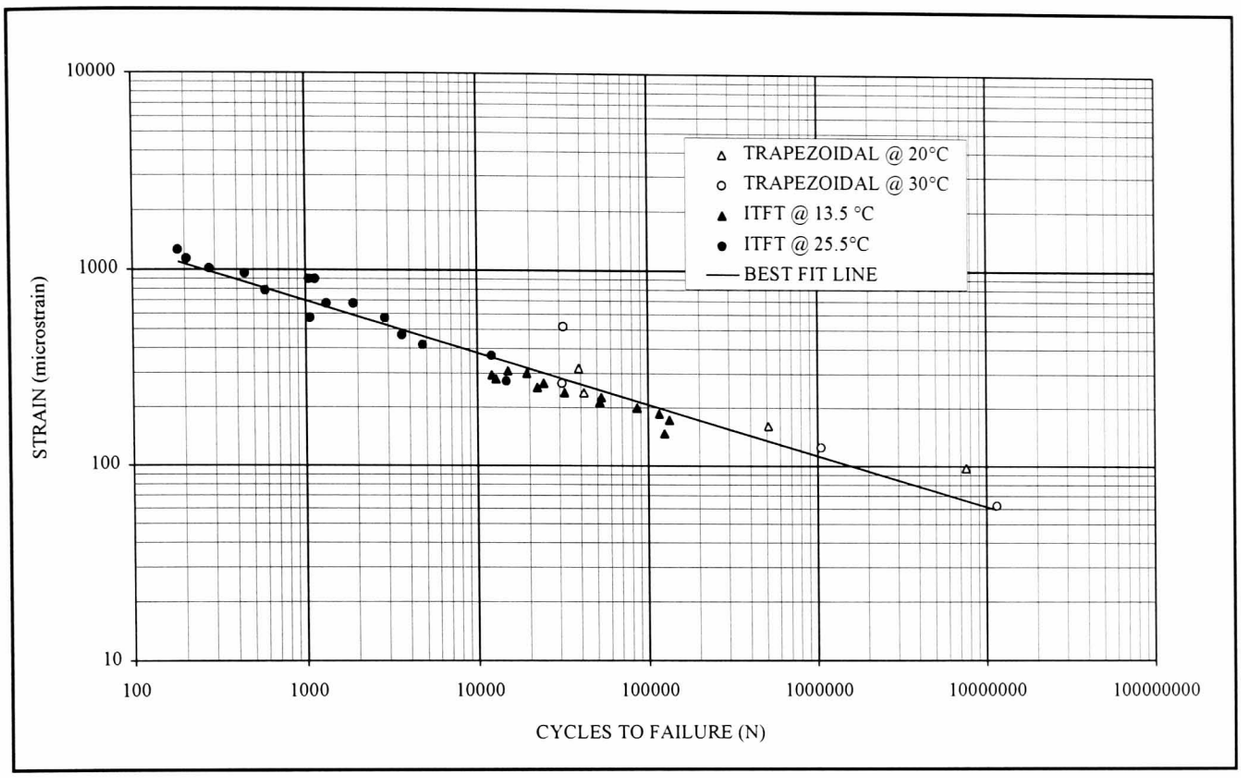


Figure 4.7 - Fatigue Characteristics for the 30/14 HRA Based on Maximum Initial Tensile Strain (ϵ_{xmax}) Against Life to Failure.

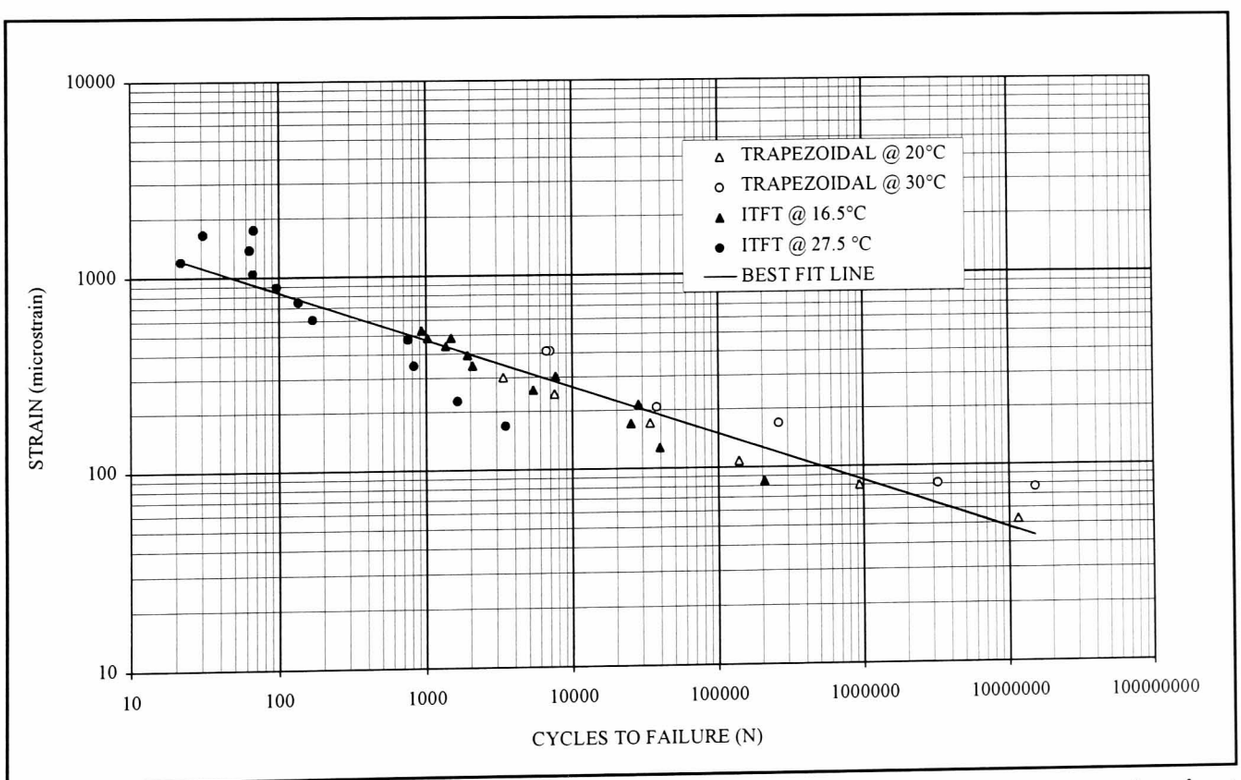


Figure 4.8 - Fatigue Characteristics for the 20mm DBM Based on ϵ_{xmax} Against Life to Failure.

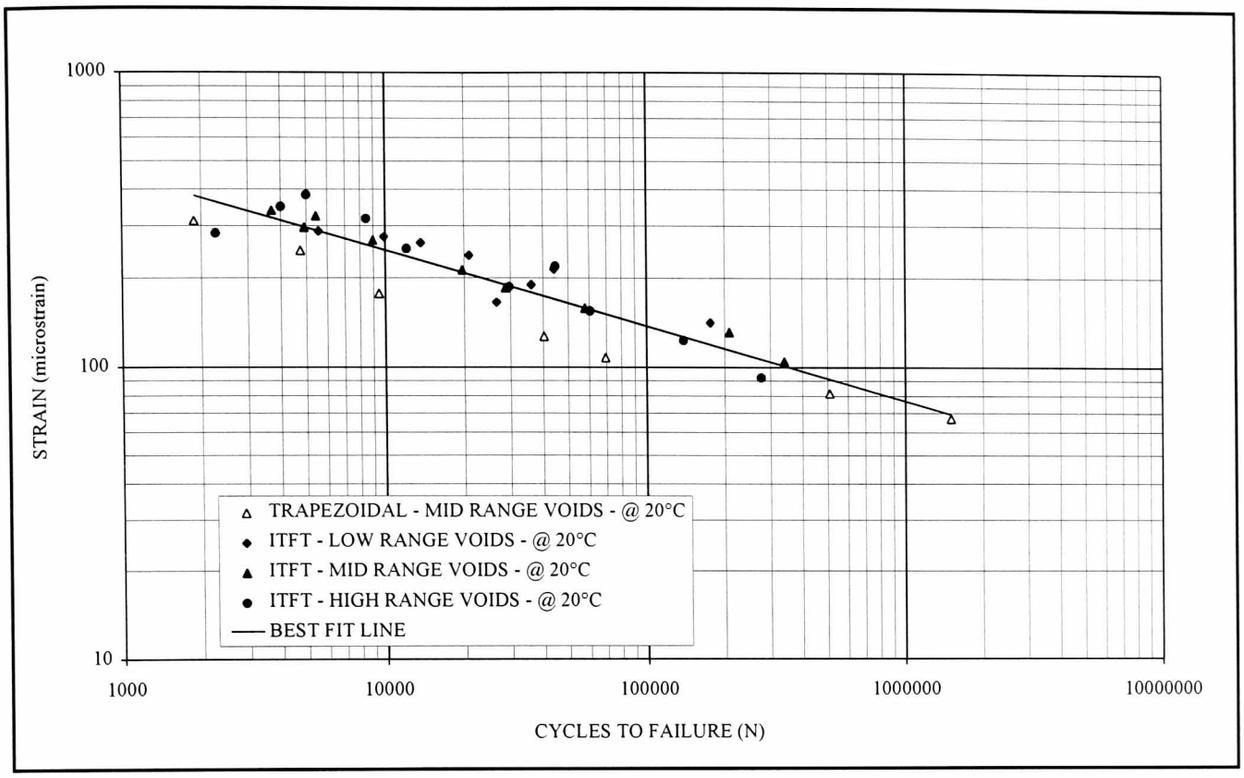


Figure 4.9 - Fatigue Characteristics for the 28mm DBM 50 Based on ϵ_{xmax} Against Life to Failure.

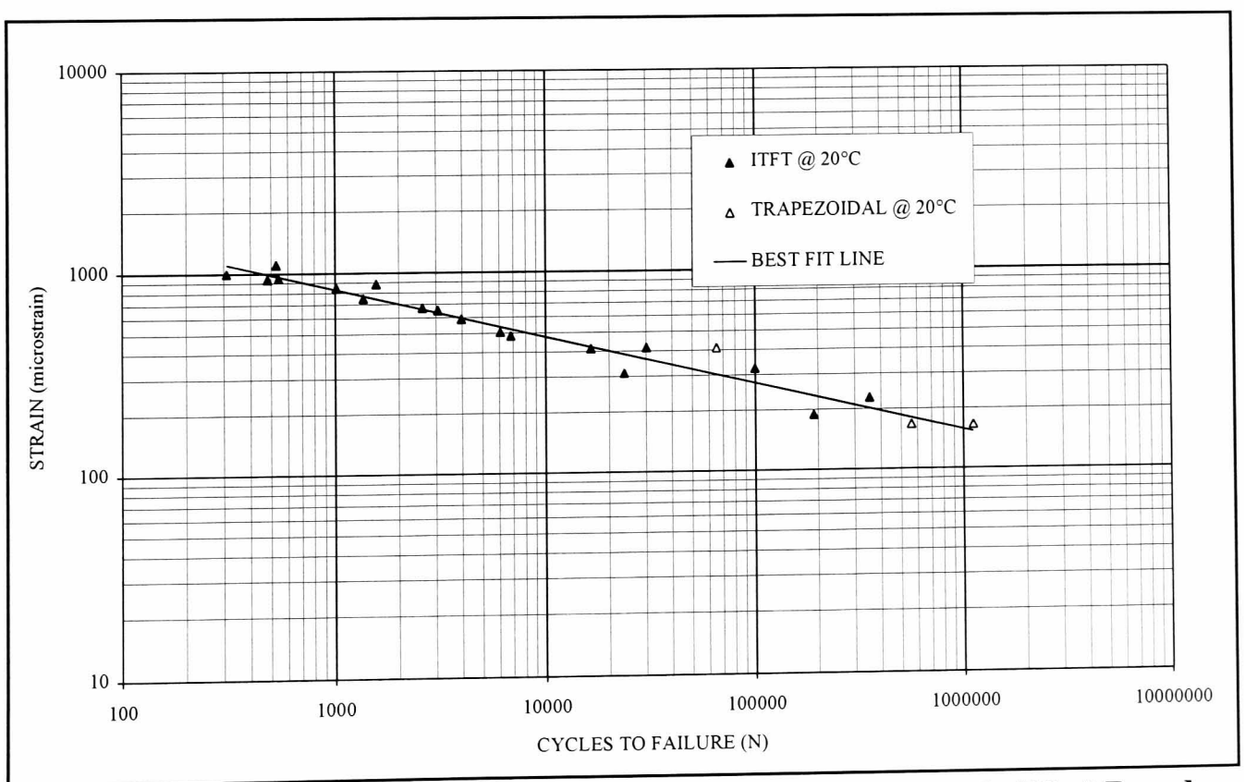


Figure 4.10 - Fatigue Characteristics for the 30/14 HRA SBS Modified Based on ϵ_{xmax} Against Life to Failure.

Equation (3.5) was used to determine tensile strain in the ITFT while, for the trapezoidal test, the following equation was appropriate.

$$\epsilon_{xmax} = \frac{\sigma_{pp}}{2 * S_m} \qquad \textbf{(4.1)}$$

Where :

ϵ_{xmax} = The maximum tensile strain on the outer fibre of the trapezium,

σ_{pp} = The maximum peak to peak stress applied to the outer fibre of the specimen and

S_m = Stiffness modulus of the specimen after 10 cycles.

The material constants of the fatigue lines, on the basis of log (strain) against log (number of cycles to failure), are reported in Table 4.1 and it can be seen, from the k_2 value, that the slopes are very similar for all four materials.

An overall summary graph is included as Figure 4.11.

Table 4.1 - Material Constants for Use in Equation (4.2) for the Four Materials Tested.

	k_1	k_2
30/14 HRA	5.926×10^{13}	-3.788
20mm DBM	6.057×10^{13}	-4.032
28mm DBM 50	2.445×10^{13}	-3.922
30/14 HRA SBS Modified	1.294×10^{15}	-4.149

The values given in Table 4.1 relate to Equation (4.2)

$$N_f = k_1 (\epsilon)^{k_2} \qquad \textbf{(4.2)}$$

where:

ϵ = Tensile strain, microstrain and

k_1, k_2 = Mixture dependent constants.

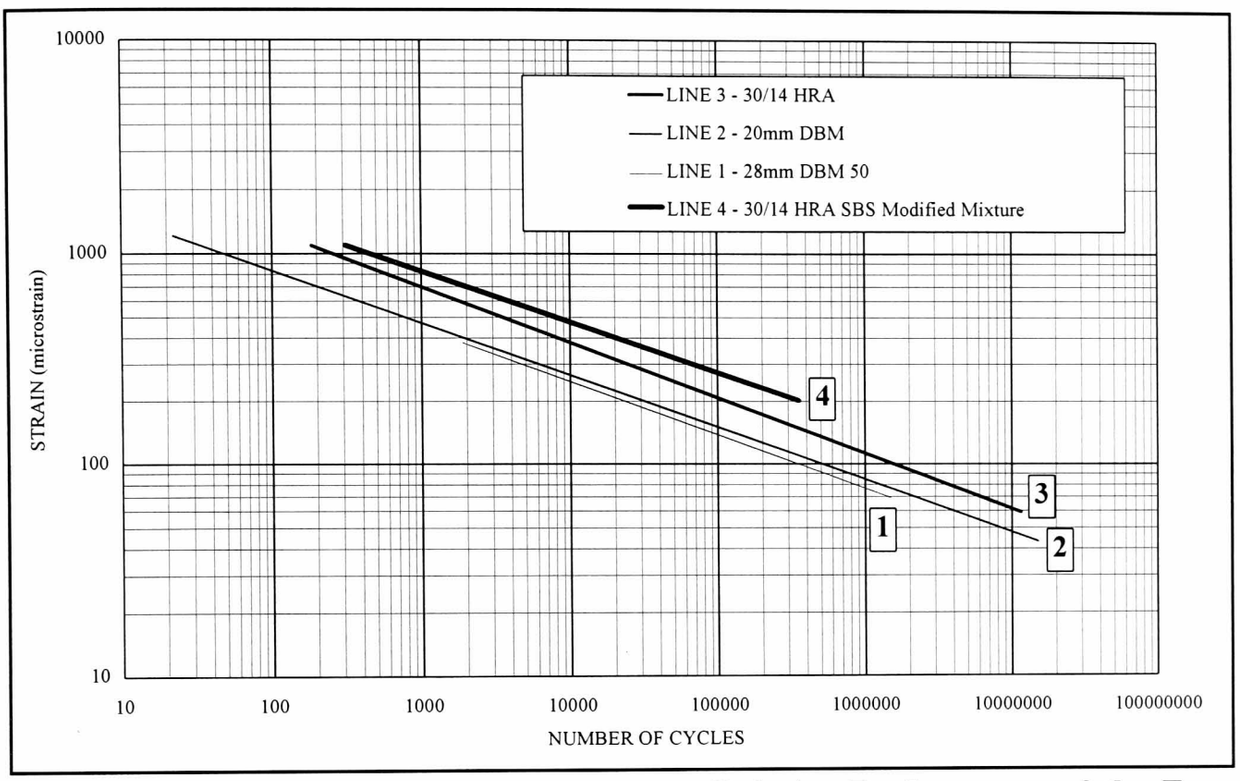


Figure 4.11 - Summary Graph Showing the Relative Performance of the Four Mixtures Based on the Regression Between Both Test Methods.

A commentary on the results given in Figures 4.3 to 4.11 is given below for each material type:

30/14 HRA — The results show good agreement between the two test methods with very little scatter and an overall correlation coefficient of 0.932.

20mm DBM — The results show good agreement between the two test methods, although with more scatter than the 30/14 HRA, the overall correlation coefficient was 0.893.

28mm DBM 50	The results show fair agreement between the two test methods, although with more scatter than the 20mm DBM, the overall correlation coefficient was 0.868.
30/14 HRA SBS Modified	The results show excellent agreement between the two test methods with very little scatter and an overall correlation coefficient of 0.952.

The ITFT results show a good correlation with the trapezoidal results in the region of tensile strain which is of interest. This is a good indication that the ITFT is an acceptable method of fatigue testing for practical design purposes although some discussion of why there is agreement is necessary. In the ITFT there is, in effect, a rest period between load applications which according to previous research, outlined in Chapter 2, will allow some significant extension of life relative to continuous cyclic loading. Therefore, it would seem unlikely that agreement between the ITFT and the trapezoidal could be expected. However, when examining the trapezoidal test, there is a compensating factor which may account for the rest period effect in the ITFT. This concerns the effect of putting the point of maximum bending moment into compression every cycle. This has the effect of closing any cracks which may have opened during the tensile phase of the loading cycle. These compensating factors lead to the conclusion that although good agreement has been found under the conditions of test used in this research, agreement under other conditions of test cannot be inferred.

It is also interesting to note that if the unmodified materials were ranked according to the volume of binder in the mixture (this has been shown in Chapter 2 to be one of the primary indicators of fatigue performance) the same ranking would be given as that shown in Figure 4.11, see Table 4.2. This ranking lends weight to the argument for the use of the ITFT with polymer modified binders, as if a constitutive relationship were used to calculate the fatigue line, then it would predict either the same or lower performance for the SBS modified HRA when compared to the unmodified HRA. This point demonstrates the need for testing of materials, particularly novel ones, as opposed to

empirical prediction techniques which cannot cope with the material developments now being made in the field of bituminous materials. These results also give confirmation of the tensile strain criterion being the appropriate one for crack initiation.

Table 4.2 - Ranking of the Four Mixtures Based Upon Both the ITFT and the Volume of Binder in the Mixture.

Mixture Type	Volume of Binder (%)	Ranking According to the ITFT	Ranking According to the Volume of Binder
30/14 HRA	17.5	30/14 HRA SBS ▼ 30/14 HRA ▼ 20mm DBM ▼ 28mm DBM 50	30/14 HRA SBS = 30/14 HRA ▼ 20mm DBM ▼ 28mm DBM 50
20mm DBM	10.6		
28mm DBM 50	8.9		
30/14 HRA SBS modified	17.5		

4.4 Repeatability of the ITFT

To ascertain if the repeatability, or "within laboratory" variability, of the ITFT was acceptable duplicate sets of specimens of the 30/14 HRA and the 20mm DBM were manufactured and tested. This provided comparative results which are shown graphically in Figures 4.12 to 4.15 and the equations of the lines are tabulated in Table 4.3.

Table 4.3 - Repeatability Results for the 30/14 HRA and 20mm DBM Mixtures.

	Equation Based on Strain	Strain at 10^6 Cycles	Variation from Overall Result (%)	Equation Based on Number of Cycles	Cycles at 100 microstrain	Variation from Overall Result (%)
30/14 HRA						
First Data Set	$\epsilon = 6236\ N^{-0.311}$	85	0	$N = 1.60 \times 10^{12}\ \epsilon^{-3.216}$	591,725	2.5
Second Data Set	$\epsilon = 6011\ N^{-0.307}$	86	1.2	$N = 2.11 \times 10^{12}\ \epsilon^{-3.261}$	634,282	4.5
Overall Result	$\epsilon = 6165\ N^{-0.310}$	85	-	$N = 1.75 \times 10^{12}\ \epsilon^{-3.230}$	606,789	-
20mm DBM						
First Data Set	$\epsilon = 4058\ N^{-0.319}$	49	2.0	$N = 2.01 \times 10^{12}\ \epsilon^{-3.132}$	109,445	3.2
Second Data Set	$\epsilon = 3783\ N^{-0.311}$	52	4.0	$N = 3.65 \times 10^{12}\ \epsilon^{-3.214}$	118,320	4.6
Overall Result	$\epsilon = 3985\ N^{-0.317}$	50	-	$N = 2.32 \times 10^{12}\ \epsilon^{-3.156}$	113,107	-

From this data it can be seen that the prediction of results using one of the sample data sets gives no more than 5% variation from the population result, provided that a prediction is made within range of the data. This is considered to be a very good result. However, if a prediction is made outside of the range of the data the variation is larger though still acceptable (Table 4.4).

Table 4.4 - Repeatability Outside of the Data Range.

	Strain at 10^8 Cycles	Variation from Overall Result	Cycles at 30 microstrain	Variation from Overall Result
30/14 First Data Set	20	0	28,424,840	4.1
30/14 Second Data Set	21	5.0	32,165,481	8.5
30/14 Overall Result	20	-	29,643,972	-
DBM First Data Set	11	8.3	4,751,735	6.0
DBM Second Data Set	12	0	5,670,111	12.2
DBM Overall Result	12	-	5,054,676	-

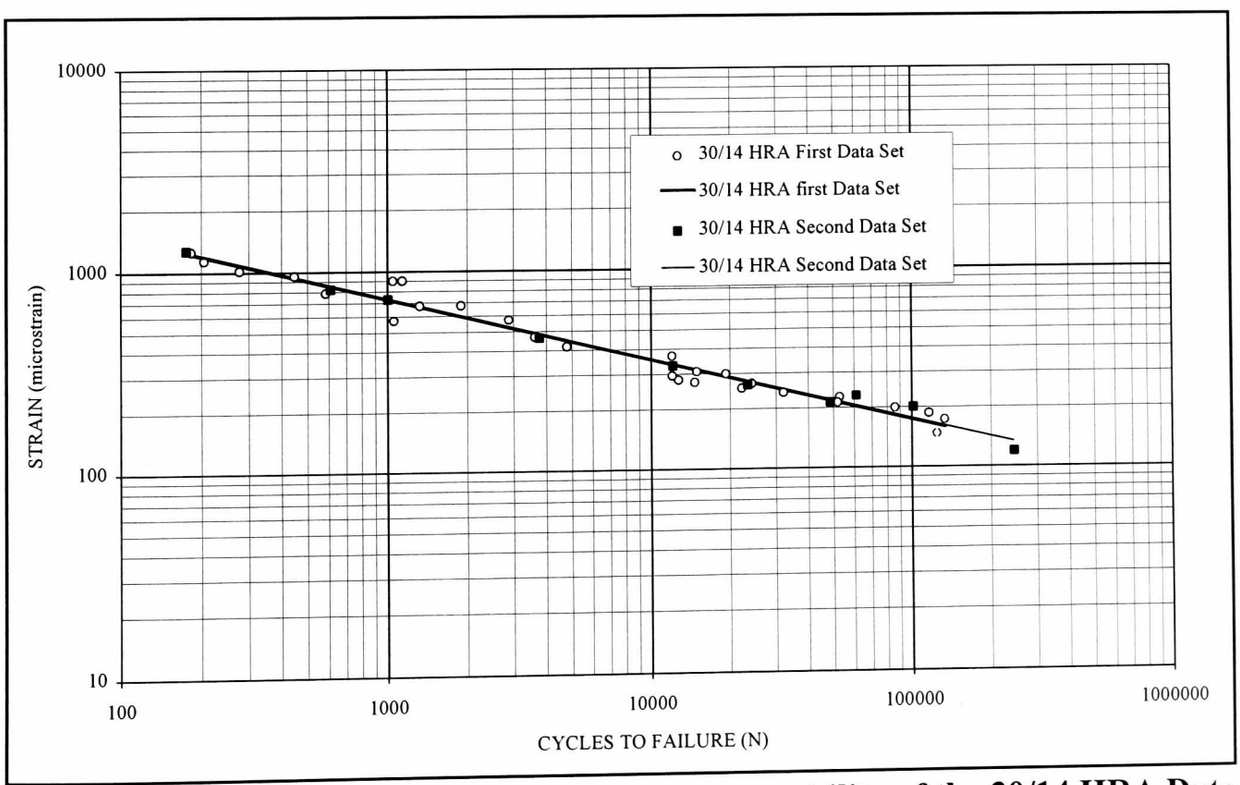


Figure 4.12 - Comparison Plot Showing the Repeatability of the 30/14 HRA Data Set.

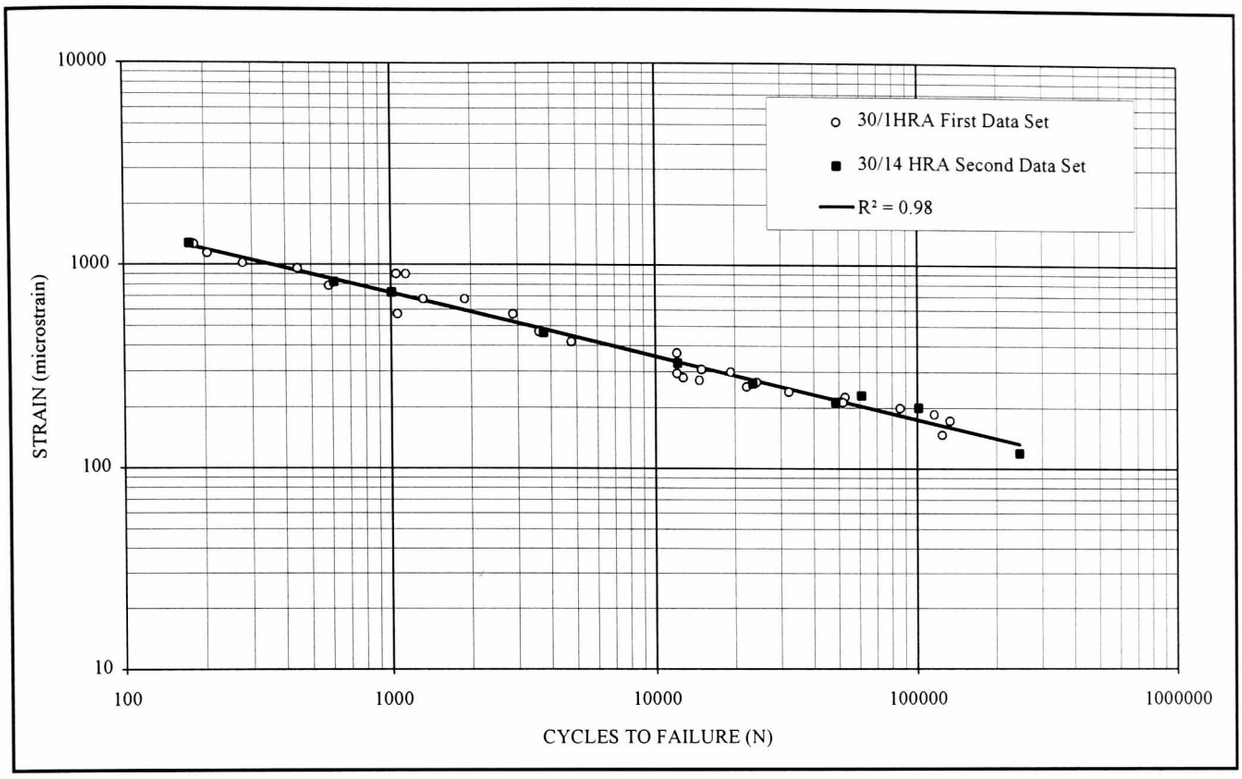


Figure 4.13 - Overall Comparison Plot Showing the Repeatability of the 30/14 HRA Data Set.

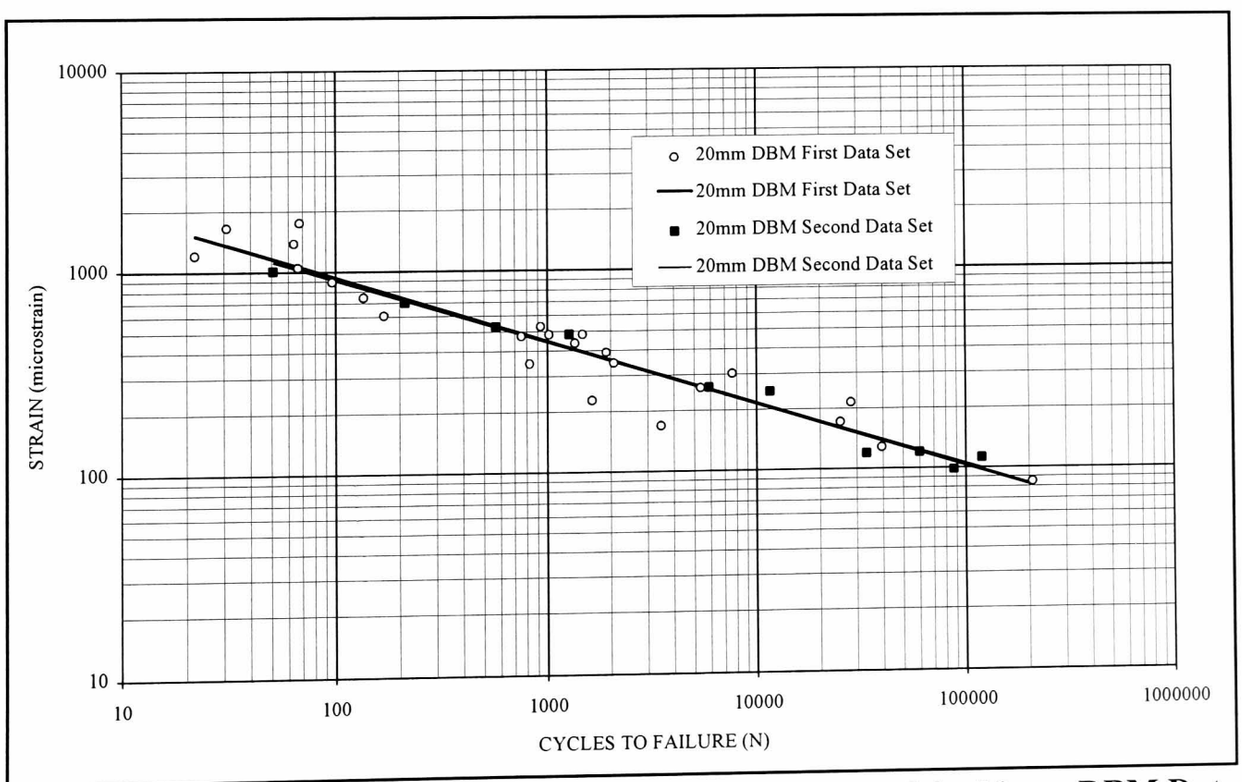


Figure 4.14 - Comparison Plot Showing the Repeatability of the 20mm DBM Data Set.

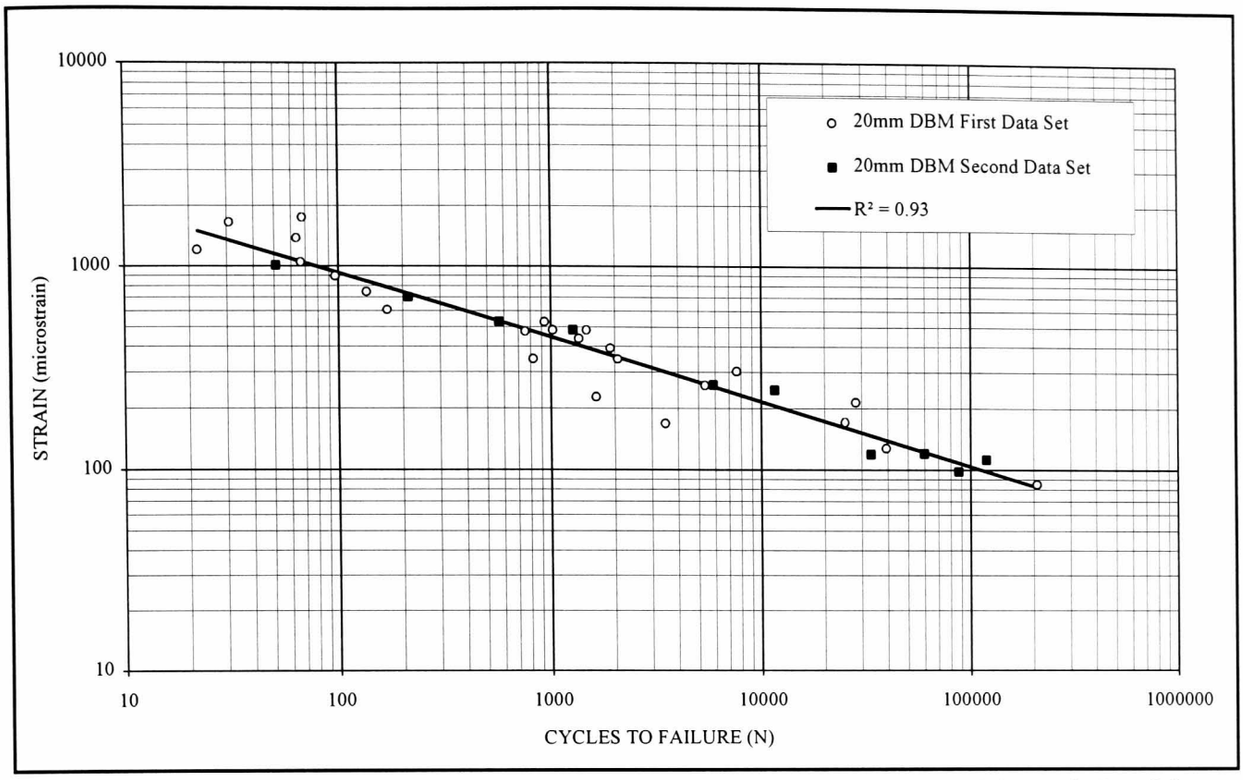


Figure 4.15 - Overall Comparison Plot Showing the Repeatability of the 20mm DBM Data Set.

Following this initial work on repeatability a contractual situation arose (4) which offered the opportunity of carrying out a further repeatability comparison on a crumb rubber modified Marshall asphalt (asphaltic concrete). The crumb rubber was of coarse particulate nature and, hence, there were concerns over segregation of this material and it not providing a good comparison. It can be seen from the following Table and two Figures that the results were not as high as those achieved with the 30/14 HRA and 20mm DBM materials but the results were still very good.

Table 4.5 - Repeatability Results for the Crumb Rubber Modified Mixture.

	Equation Based on Strain	Strain at 10^6 Cycles	Variation from Overall Result (%)	Equation Based on Number of Cycles	Cycles at 200 microstrain	Variation from Overall Result (%)
First Data Set	$\epsilon = 1121\ N^{-0.146}$	149	4.9	$N = 7.50 \times 10^{20}\ \epsilon^{-6.846}$	132,498	16.1
Second Data Set	$\epsilon = 1387\ N^{-0.167}$	138	2.8	$N = 5.77 \times 10^{18}\ \epsilon^{-5.971}$	105,130	7.9
Overall Result	$\epsilon = 1278\ N^{-0.159}$	142	-	$N = 3.22 \times 10^{19}\ \epsilon^{-6.280}$	114,130	-

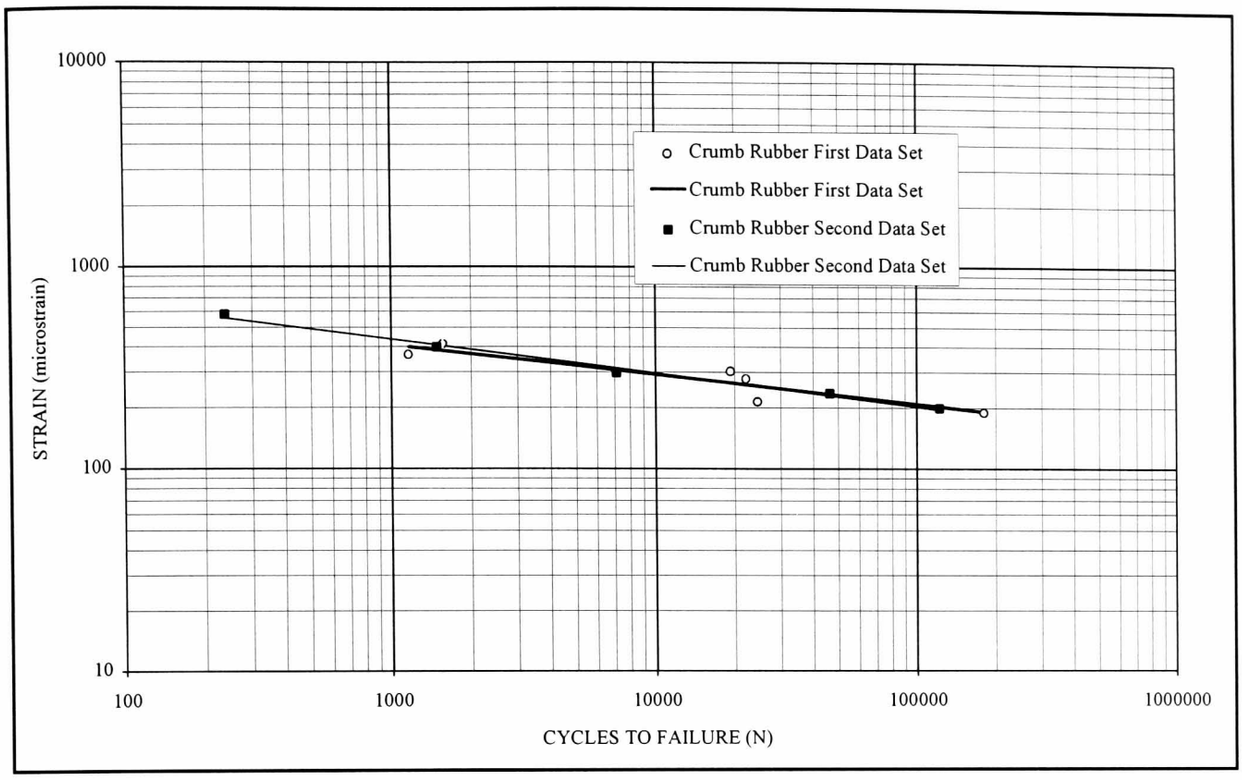


Figure 4.16 - Comparison Plot Showing the Repeatability of the Crumb Rubber Modified Marshall Asphalt Data Set.

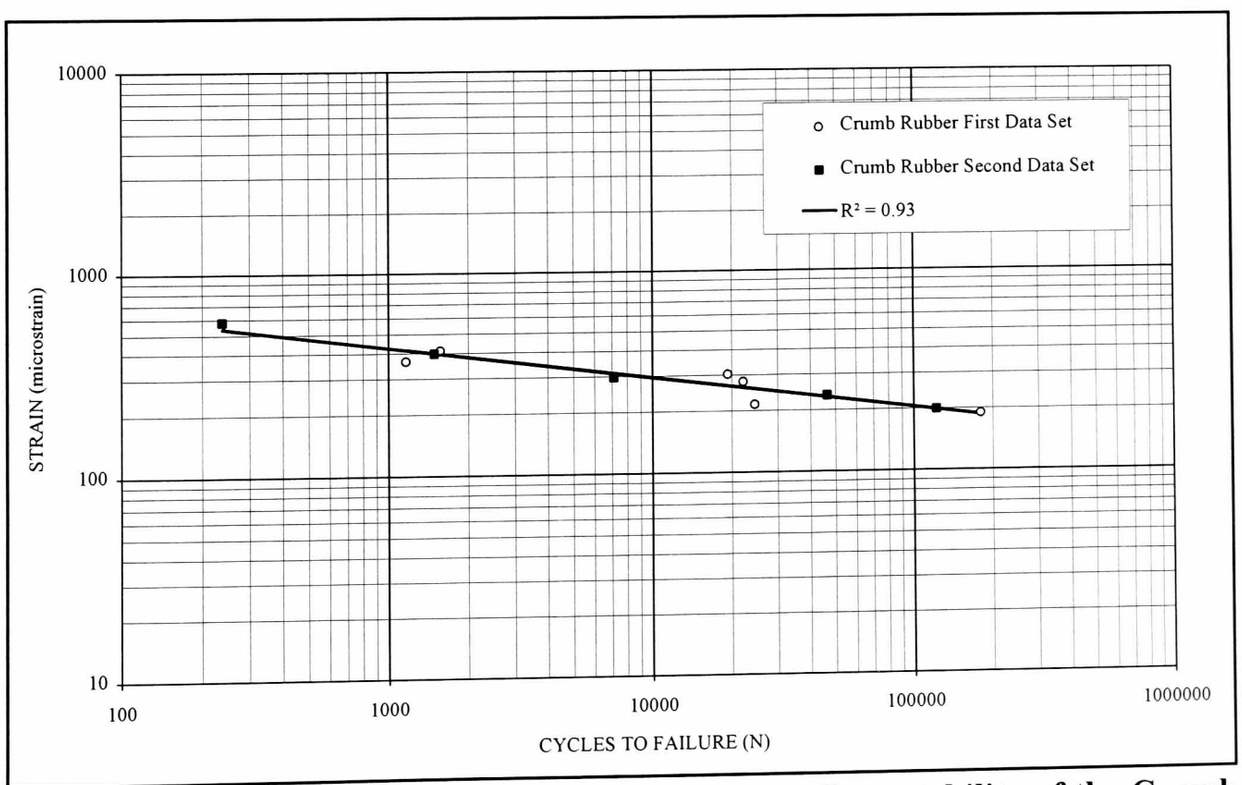


Figure 4.17 - Overall Comparison Plot Showing the Repeatability of the Crumb Rubber Modified Marshall Asphalt Data Set.

It can be seen from Table 4.5 that the second measure of variability between the data sets is based on life to 200 microstrain as opposed to 100 microstrain as was the case in the other comparisons. The reason for this is to keep the variability comparison within the range of the data set rather than extrapolating the data and getting large errors. It was considered that the reason for the poorer repeatability of the crumb rubber data set was a function of the material variability, due to segregation of the rubber and differential ageing between the two sets of specimens, and the fact that there were far fewer specimens tested than for the other two mixtures.

Based upon these three sets of repeatability results it was considered that the ITFT was suitable to be further investigated and three reproducibility (between laboratories) trials were carried out.

4.5 Reproducibility of the ITFT

This section details the three phases of the reproducibility work. The first phase involved issuing two sets of nominally identical specimens of a mixture identical to the 30/14 HRA shown in Figure 4.7 to two laboratories. This produced results which indicated that there was a difference between the results shown in Figure 4.7 and those produced by the two participating laboratories. Hence, a second phase of work was undertaken with specimens of a 40mm Heavy Duty Macadam (HDM) and a 20mm DBM. The specimens were distributed to nine participating laboratories:

Figures 4.18 to 4.23 show the results for the three materials tested (30/14 HRA, 20mm DBM and 40mm HDM) in the first two phases of the work.

The results for each material have been plotted twice. Results in the first Figure for each material use the method outlined in the protocol for the ITFT (Version 2.0a), where the stiffness and stress values were used to obtain an equation which allowed the calculation of stiffness at any stress. The second Figure is based on using the average stiffness value to calculate the maximum tensile strain. The reason for this second approach has been described in Section 3.4.

It was considered that the results from the reproducibility trials were very encouraging, based on the averaging technique. Two of the materials, the 30/14 HRA and the 40mm HDM (Figures 4.19 and 4.23) show results which are not statistically different (Figures 4.24 and 4.26), however, the 20mm DBM material (Figure 4.21) shows a high degree of scatter (Figure 4.25). The statistical significance of the data has been determined by plotting the residual error (actual strain values subtracted from the predicted strain values) against the predicted strain (Figures 4.24 to 4.26). The resulting graph allows the validity of the regression model to be ascertained and also whether any set of data is statistically different from any other set of data. Taking the error plot for the 40mm HDM, Figure 4.26 as an example, it can be seen that there is no positive or negative trend in the whole data set and that positive and negative errors occur over the entire predicted strain range. This indicates that linear regression, for the fatigue lines, is the appropriate regression model for this data set. The individual data sets also have positive and negative errors over the entire predicted strain range and do not appear to have individual trends.

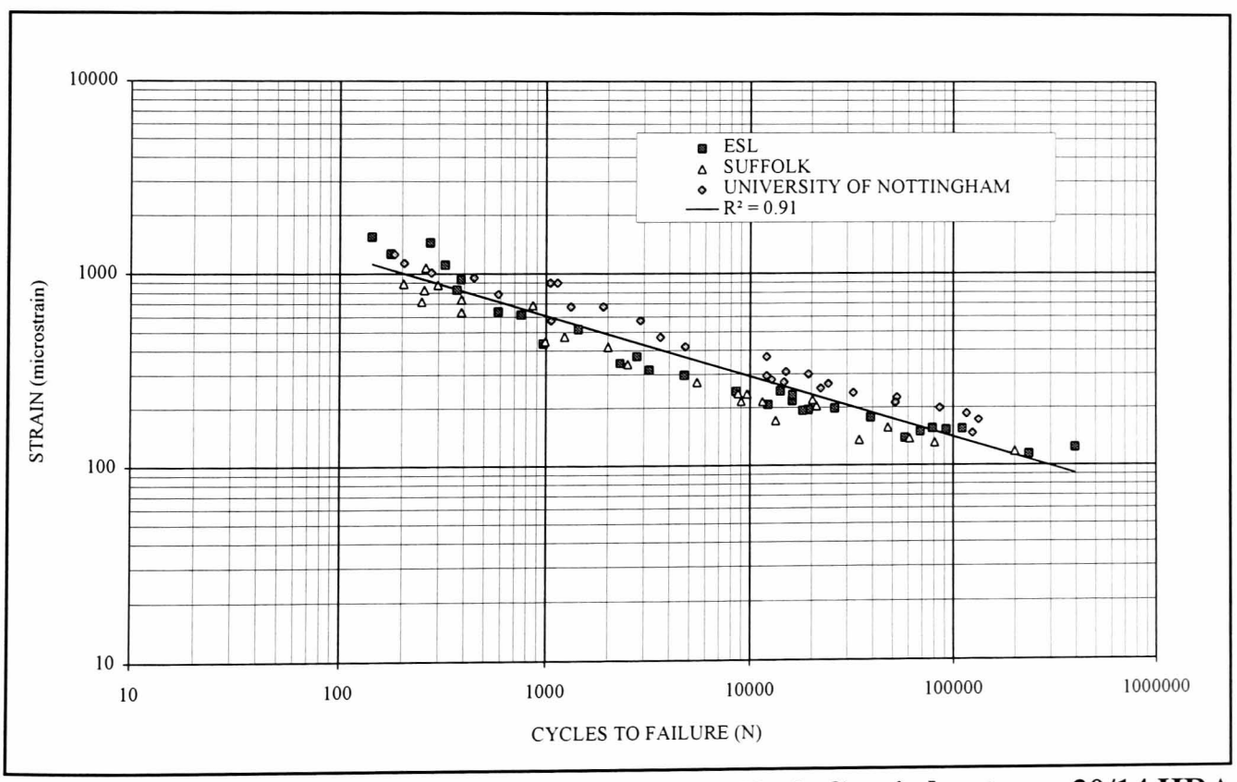


Figure 4.18 - First Phase of the Reproducibility Work Carried out on a 30/14 HRA Unmodified Mixture - Strain Calculated on Regressed Stiffness Values.

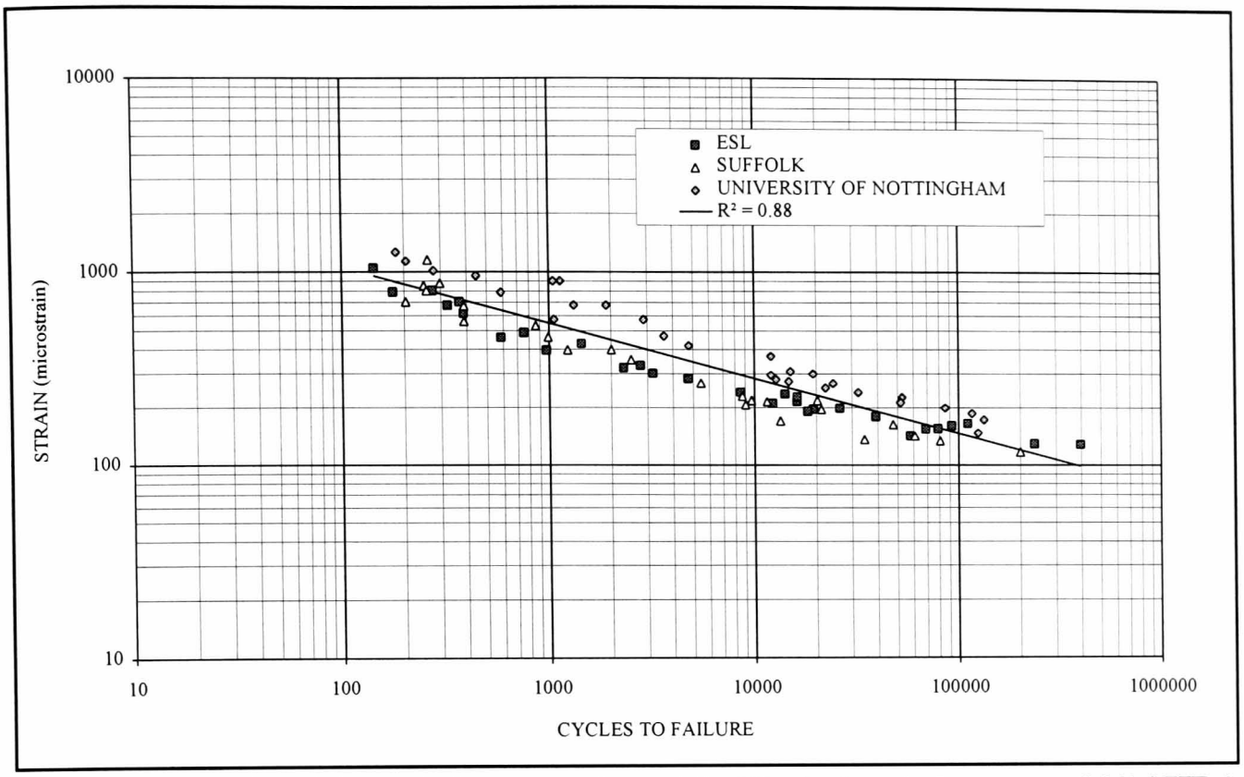


Figure 4.19 - First Phase of the Reproducibility Work Carried out on a 30/14 HRA Unmodified Mixture - Strain Calculated on Averaged Stiffness Values.

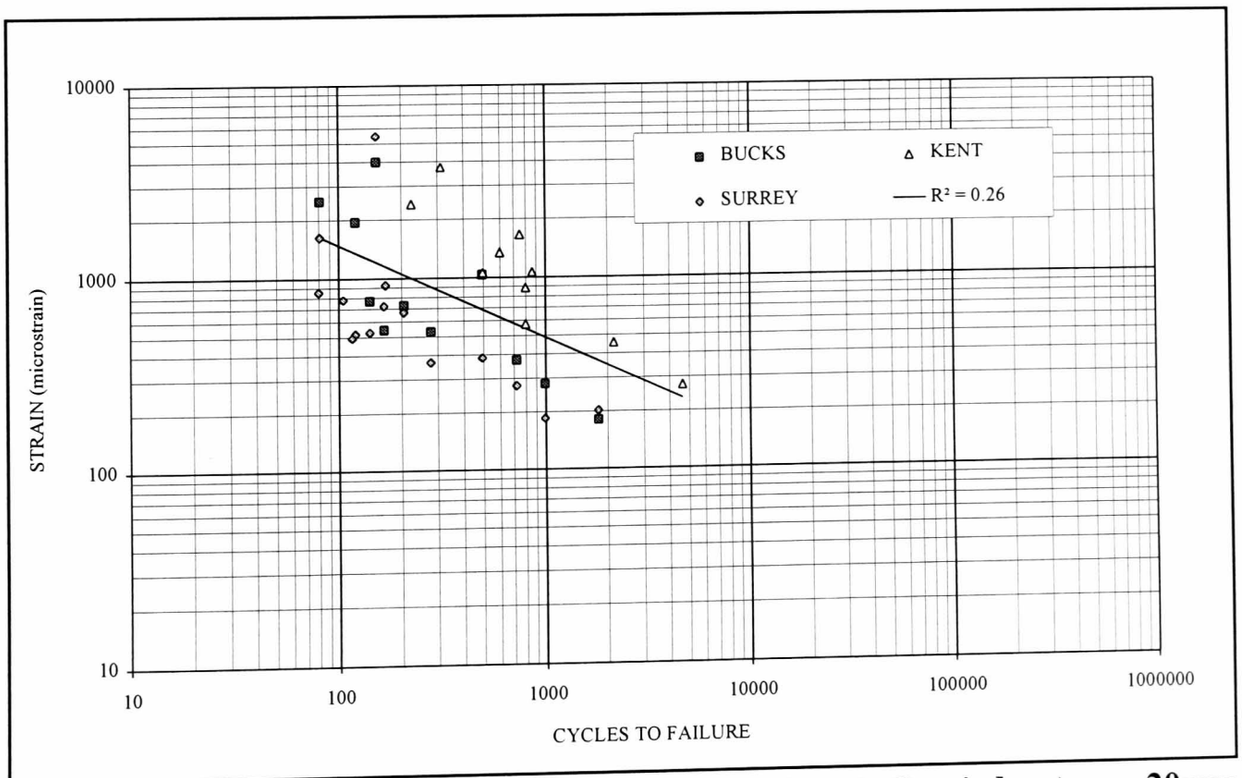


Figure 4.20 - Second Phase of the Reproducibility Work Carried out on a 20mm DBM Unmodified Mixture - Strain Calculated on Regressed Stiffness Values.

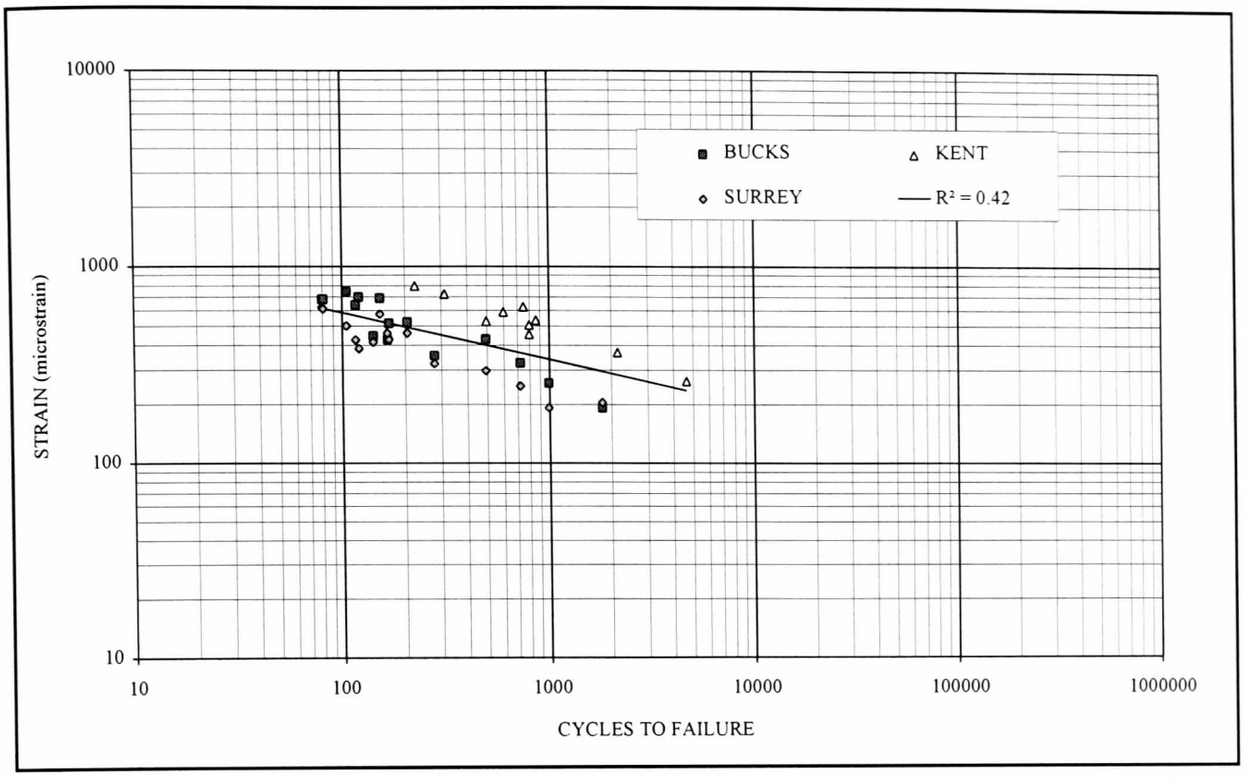


Figure 4.21 - Second Phase of the Reproducibility Work Carried out on a 20mm DBM Unmodified Mixture - Strain Calculated on Averaged Stiffness Values.

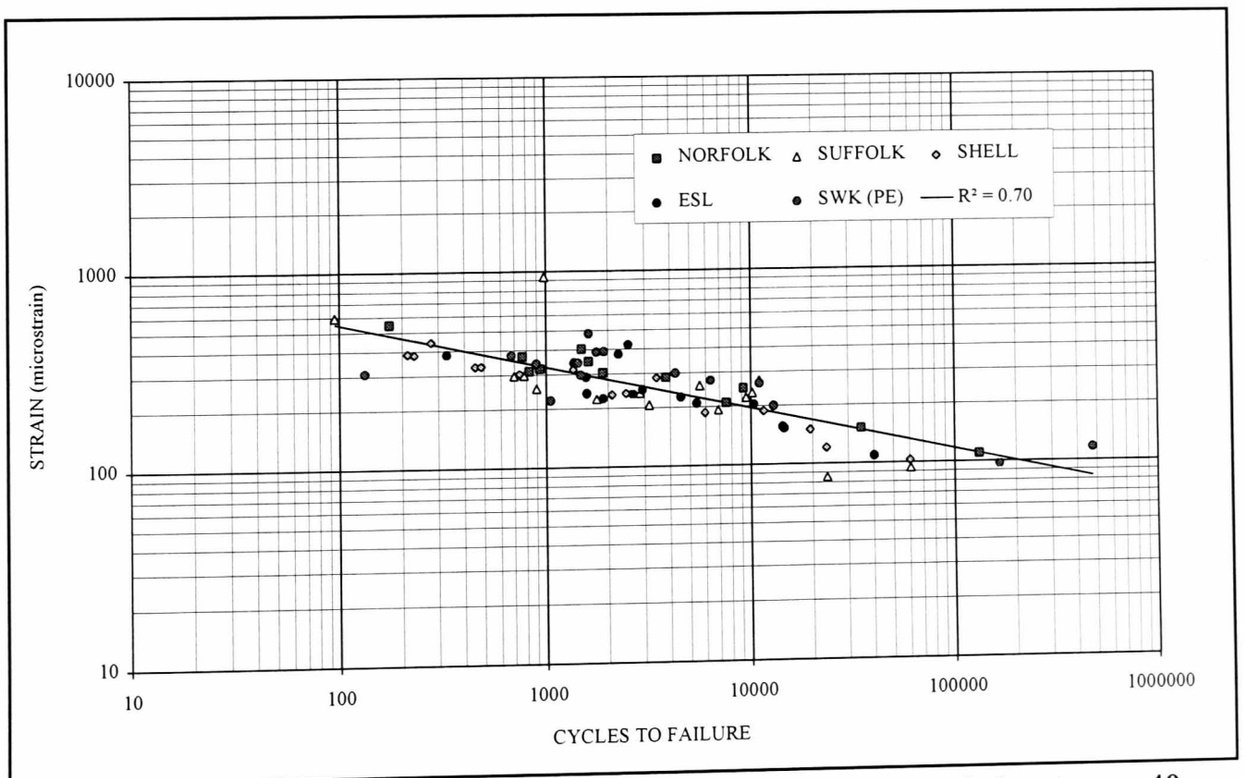


Figure 4.22 - Second Phase of the Reproducibility Work Carried out on a 40mm HDM Unmodified Mixture - Strain Calculated on Regressed Stiffness Values.

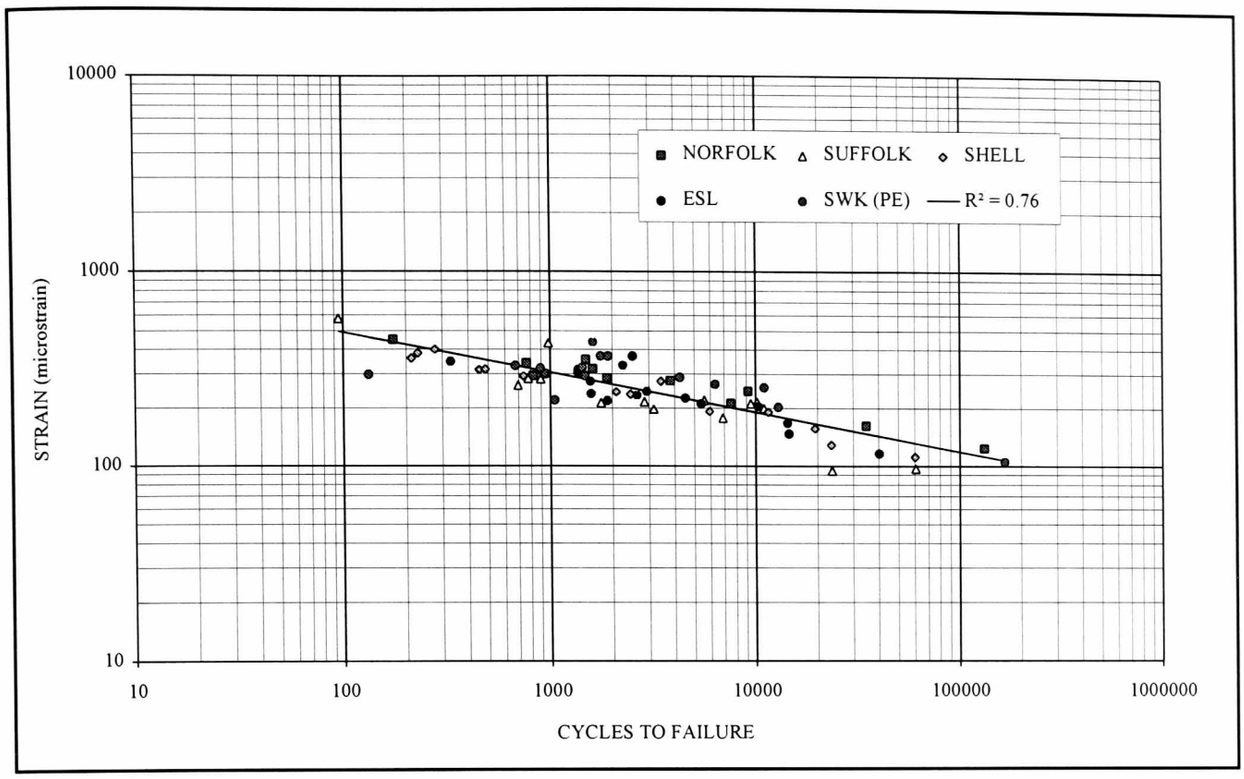


Figure 4.23 - Second Phase of the Reproducibility Work Carried out on a 40mm HDM Unmodified Mixture - Strain Calculated on Averaged Stiffness Values.

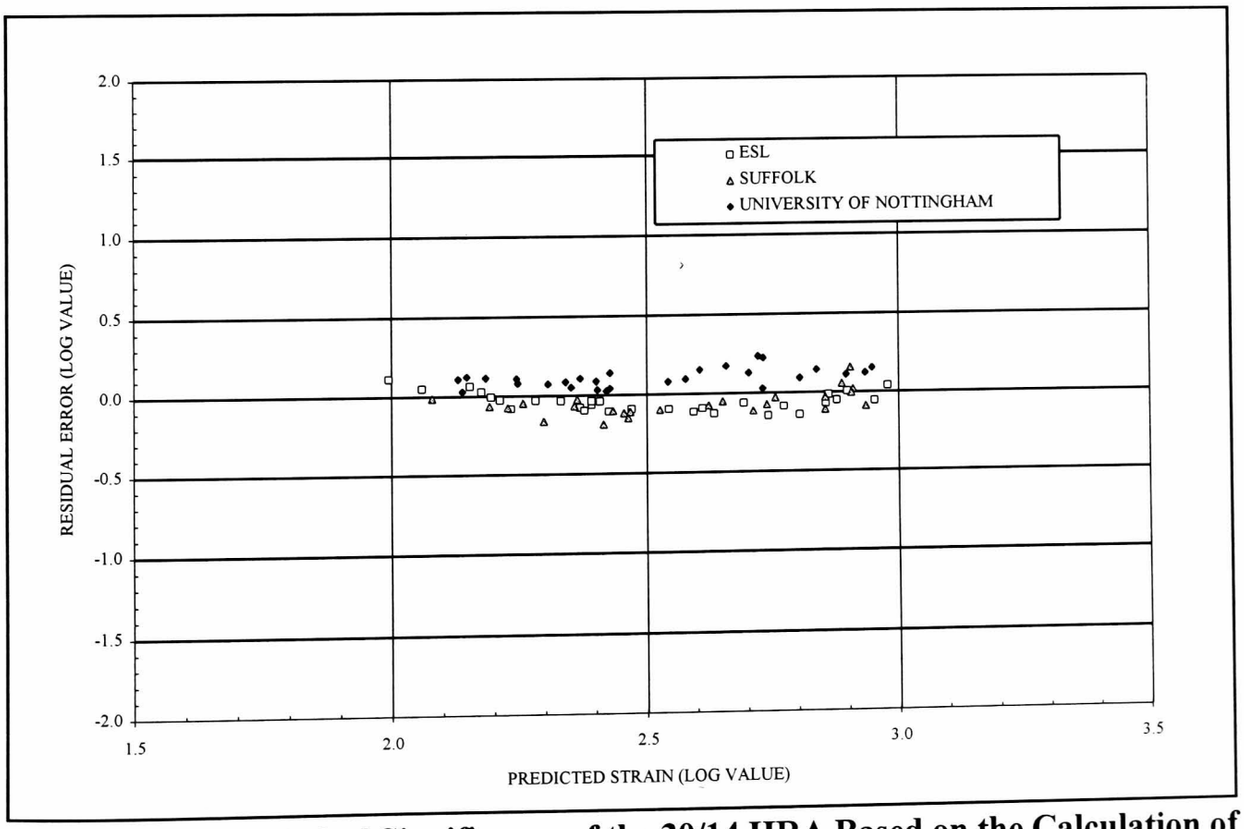


Figure 4.24 - Statistical Significance of the 30/14 HRA Based on the Calculation of the Strain Using the Averaged Stiffness Values.

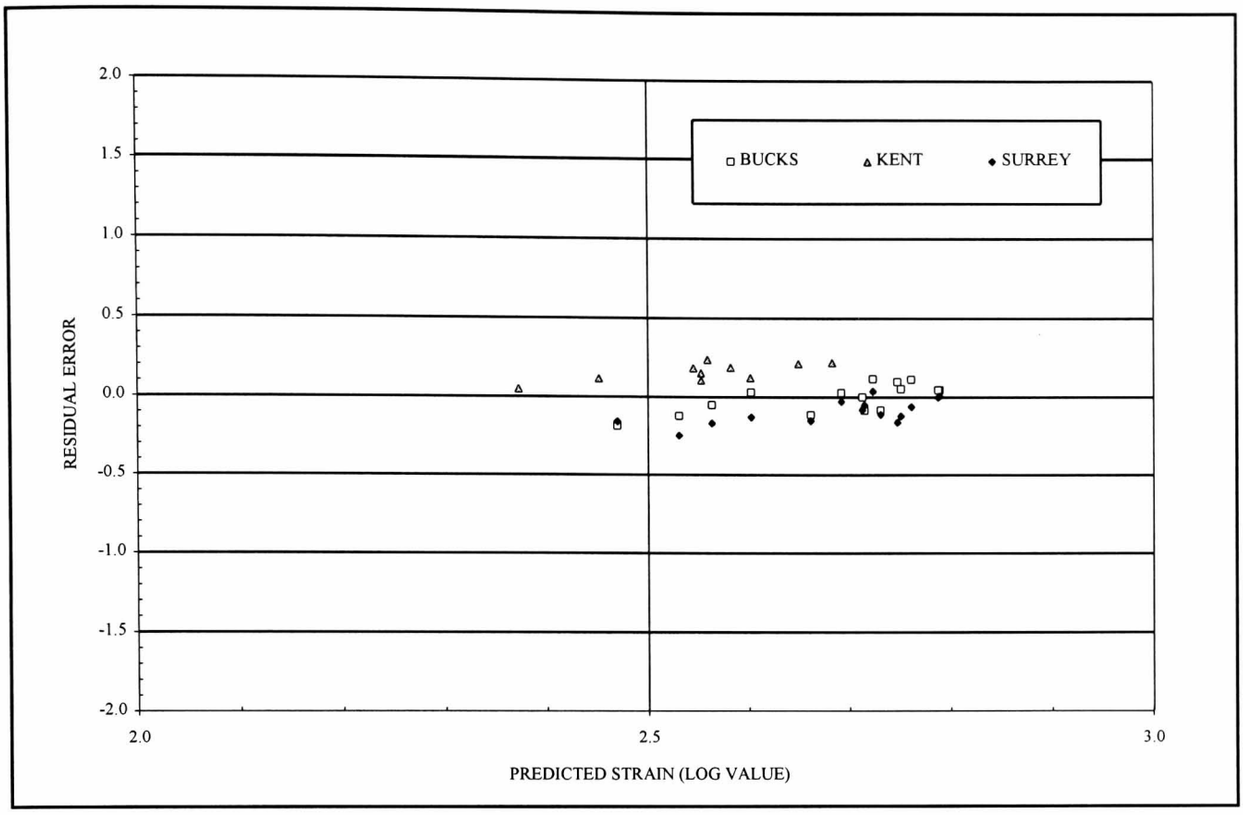


Figure 4.25 - Statistical Significance of the 20mm DBM Based on the Calculation of the Strain Using the Averaged Stiffness Values.

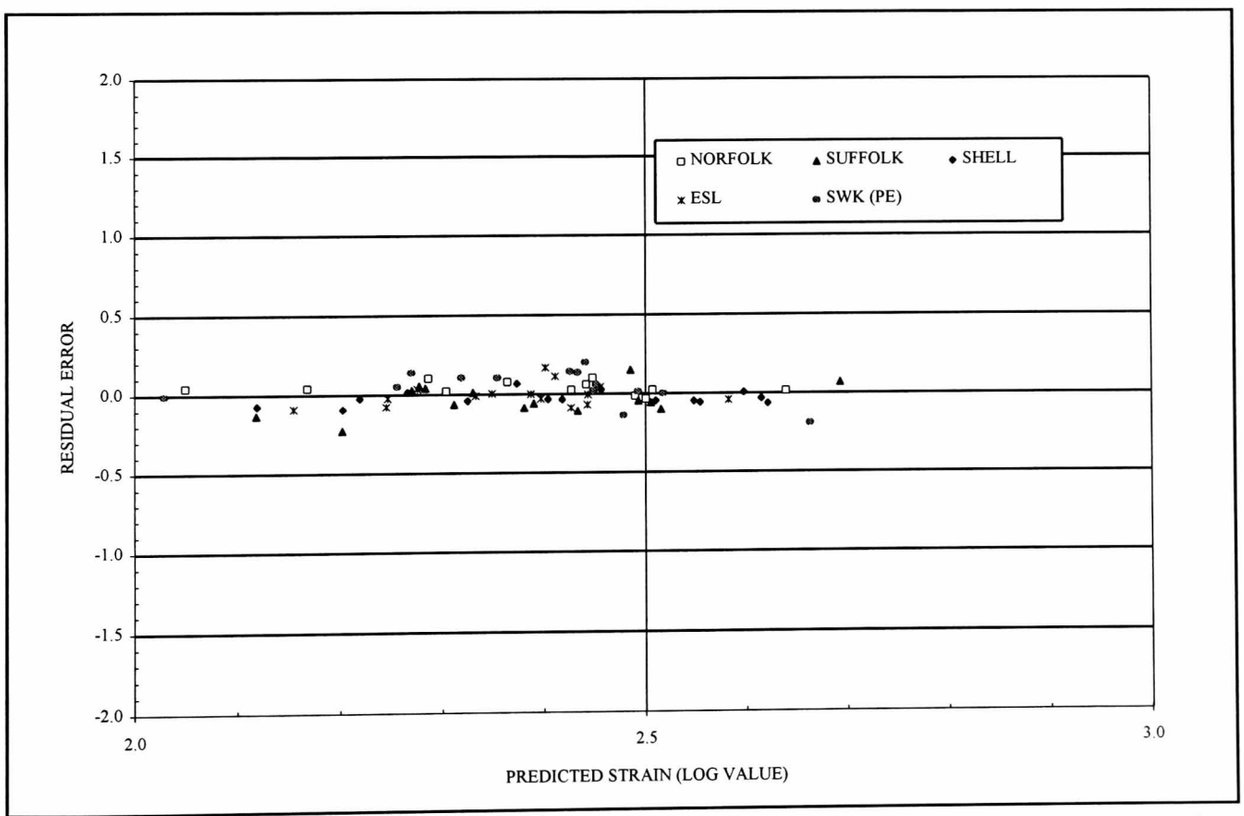


Figure 4.26 - Statistical Significance of the 40mm HDM Based on the Calculation of the Strain Using the Averaged Stiffness Values.

This implies that none of the individual data sets were statistically different from one another. Similar results are apparent for the 30/14 HRA, Figure 4.24, but it can be seen that the set of data for specimens manufactured a year earlier and tested at the University of Nottingham appears to have a different trend from the other two sets, potentially because the mixtures were marginally different. It was for this reason that the second phase of the reproducibility work was undertaken.

It is unfortunate that one of the sets of results for the 20mm DBM was unusable due to data corrupted in transit between the participant and the University of Nottingham. Although the useful data for the 20mm DBM is not as good as that for the other two materials, the trend of the line is still valid and it is possible to reliably rank the materials in order of their fatigue performance. Due to this disappointing result for the 20mm DBM a third phase of work was undertaken involving six laboratories. Figure 4.27 shows all of the data on a single plot with a linear regression. This regression demonstrates that the data fits a single line very well ($R^2 = 0.85$) and Figure 4.28 shows

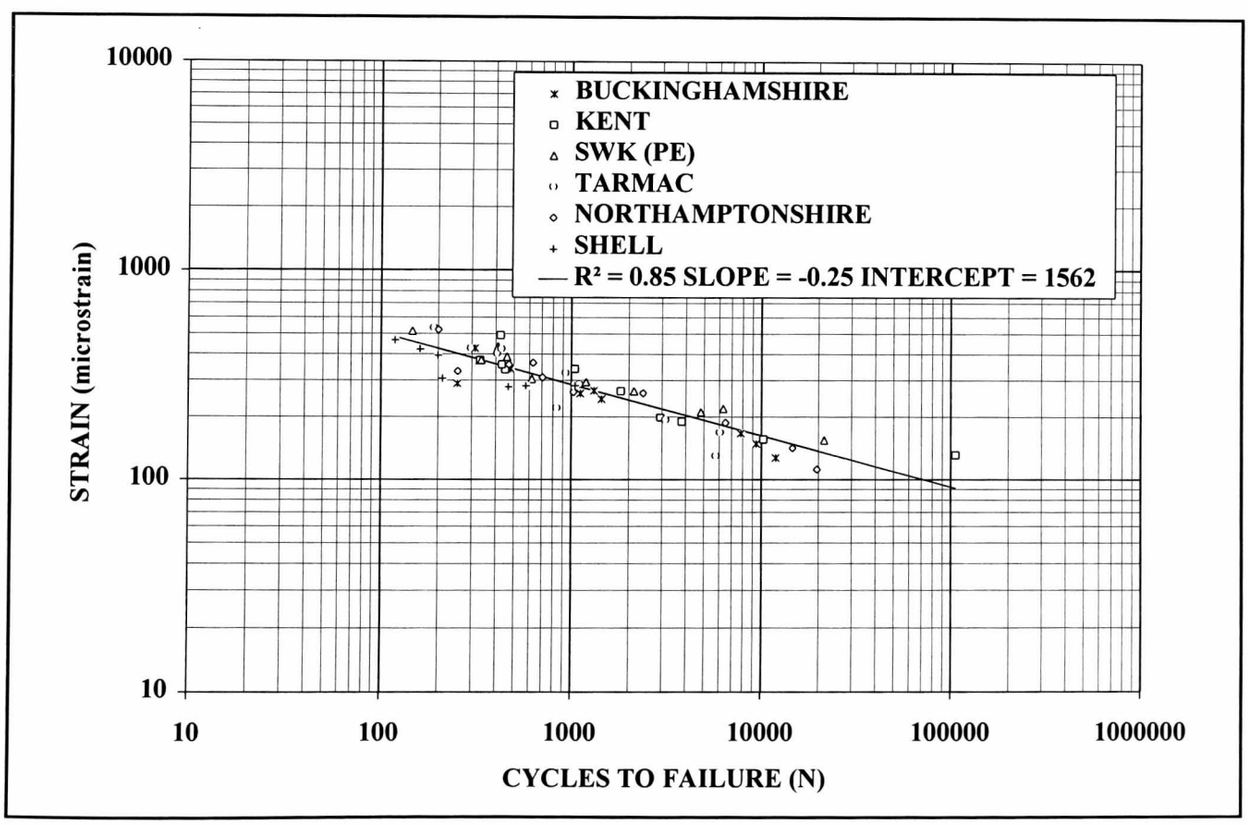


Figure 4.27 - Six Data Sets, for a 20mm DBM, Demonstrating the Good Reproducibility of the ITFT

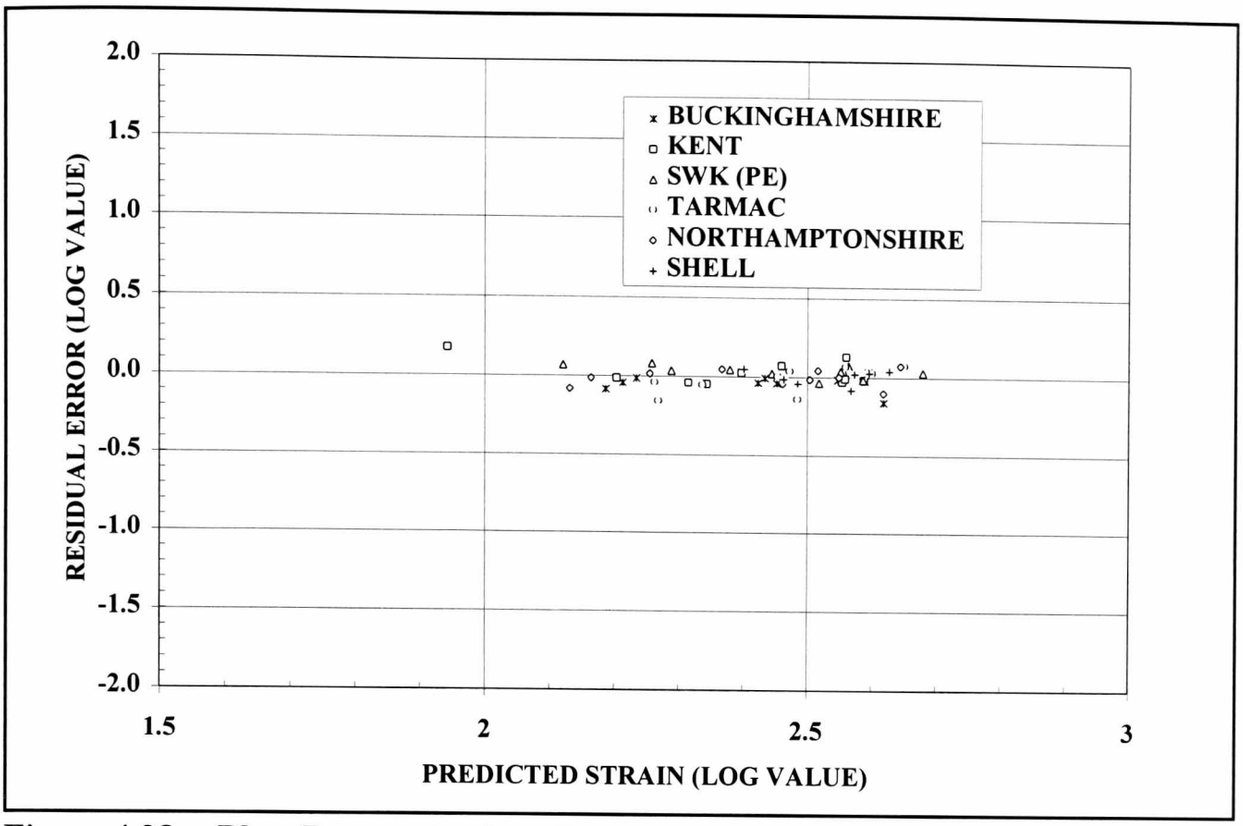


Figure 4.28 - Plot Demonstrating That There is Little Statistical Difference Between The Six Sets of Data

that no data set is statistically different from another. Table 4.6 gives summary information for each data set and the overall data set.

Table 4.6 - Summary Information for Each Data Set.

Organisation	Average Stiffness (MPa)	Equation of the line	Microstrain @ 10^4 Cycles	Variation from Overall Result (%)
Bucks	3314	$\epsilon = 1602\ N^{-0.26}$	146	6.4
Kent	3115	$\epsilon = 1386\ N^{-0.22}$	183	17.3
SWK (PE)	2731	$\epsilon = 1503\ N^{-0.23}$	181	16.0
Tarmac	2870	$\epsilon = 3522\ N^{-0.36}$	127	18.6
ESL	3161	$\epsilon = 1927\ N^{-0.27}$	160	2.6
Shell	2967	$\epsilon = 1330\ N^{-0.24}$	146	6.4
Overall	**3026**	$\epsilon = 1562\ N^{-0.25}$	**156**	-

From Table 4.6 it can be seen that the values of strain at 10^4 cycles do not vary by more than 19% for all the data sets. Therefore, this data along with that already presented

confirms the acceptable reproducibility of the ITFT. The value of 10^4 cycles is used here to avoid extrapolation of the data.

4.6 Practical Use of the ITFT

The ITFT was used for an evaluation of asphalt mixtures in a three year old, heavily trafficked, section of a trunk road. The road surfacing consisted of a polymer modified (SBS) 50/20 HRA basecourse and a 40/14 HRA wearing course, both layers having control sections of unmodified material built into them. Specimens of all four materials were extracted from both the edge of the carriageway and the wheel track and then tested in the ITFT, the results being shown in Figures 4.29 and 4.30.

These fatigue results demonstrate that the material in the wheel track was in the same condition as the material at the edge of the carriageway for all four cases. This would seem to indicate that any change in the fatigue characteristics of a material in the early life of a pavement are caused by a mechanism, possibly environmental, other than repeated loading.

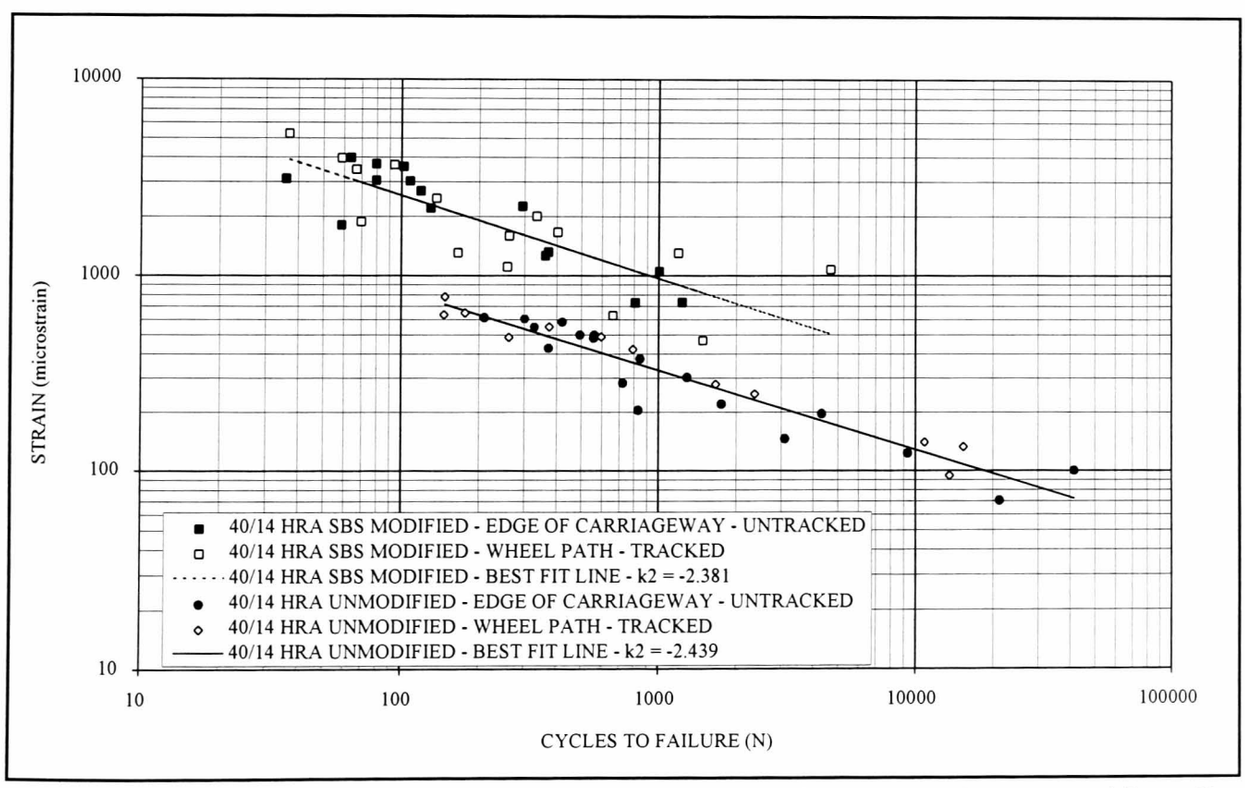


Figure 4.29 - Comparison of Tracked and Untracked Wearing Courses with an In-Service Life of 3 Years.

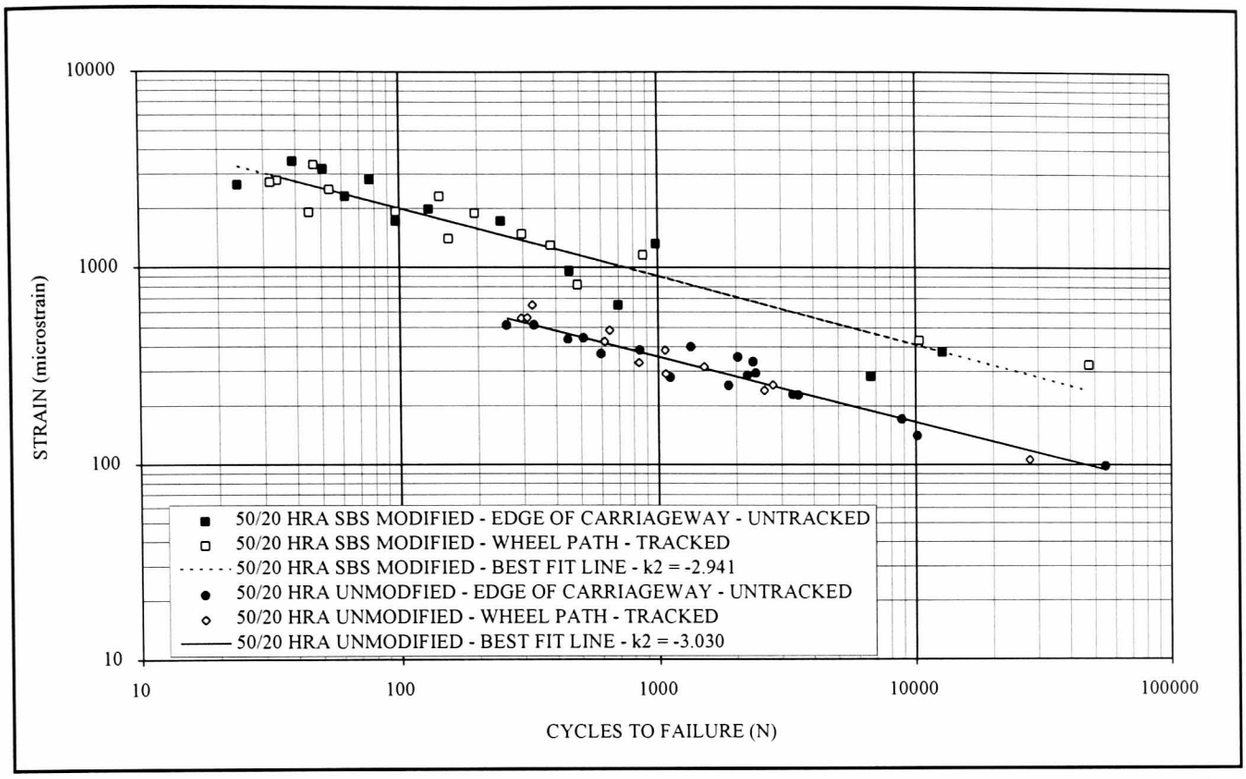


Figure 4.30 - Comparison of Tracked and Untracked Basecourses with an In-Service Life of 3 Years.

Following this introductory work, laboratory specimens were manufactured to the same original mixture designs as the material from site. The purpose of this exercise was to compare the virgin materials fatigue properties with those of the aged and trafficked materials, Figures 4.31 to 4.34 show the results.

In all but Figure 4.33, it can be seen that the k_2 value for the line is about -4.000 for the virgin materials, however, the values of the unmodified material, which had been in service for three years, were of the order of -2.500 and the values of the modified material of the same age were about -3.000, both values being lower than those found in the virgin materials. This would seem to indicate that there is a reduction in the residual life of the in-service material, at low strain levels, but that it is probably caused by environmental or construction factors as opposed to repeated traffic loading. The data in Figure 4.33 does not fall into this pattern as the results for the virgin 50/20 HRA basecourse SBS modified material are similar to those for the in-service material. In order to evaluate whether this was a genuine result, the virgin material was retested (Figure 4.35) and yielded a greater slope of -3.106. Hence the general trend of results was the same. It seems likely that environmental conditions and construction practices cause the

differences observed with site specimens which is the same conclusion drawn by Fenghe Wu (5) in a fairly extensive study on the UK trunk road network. It is also important to note that the effect seen in Figures 4.31 to 4.34 is more pronounced for the wearing course materials than for the basecourse materials. This, again, is in keeping with the idea that the change in the fatigue performance is due to environmental conditions or construction practices (rolling in of chippings to the hot rolled wearing course).

The fact that the virgin material has a higher absolute value for the slope than the in-service material is not suprising as it is exactly what would be expected from a higher viscosity bitumen. This is again in agreement with the conclusion that the difference between the virgin and in-service materials is caused by environmental effects due to an increase in viscosity of the bitumen as it ages and experiences a loss of volatiles.

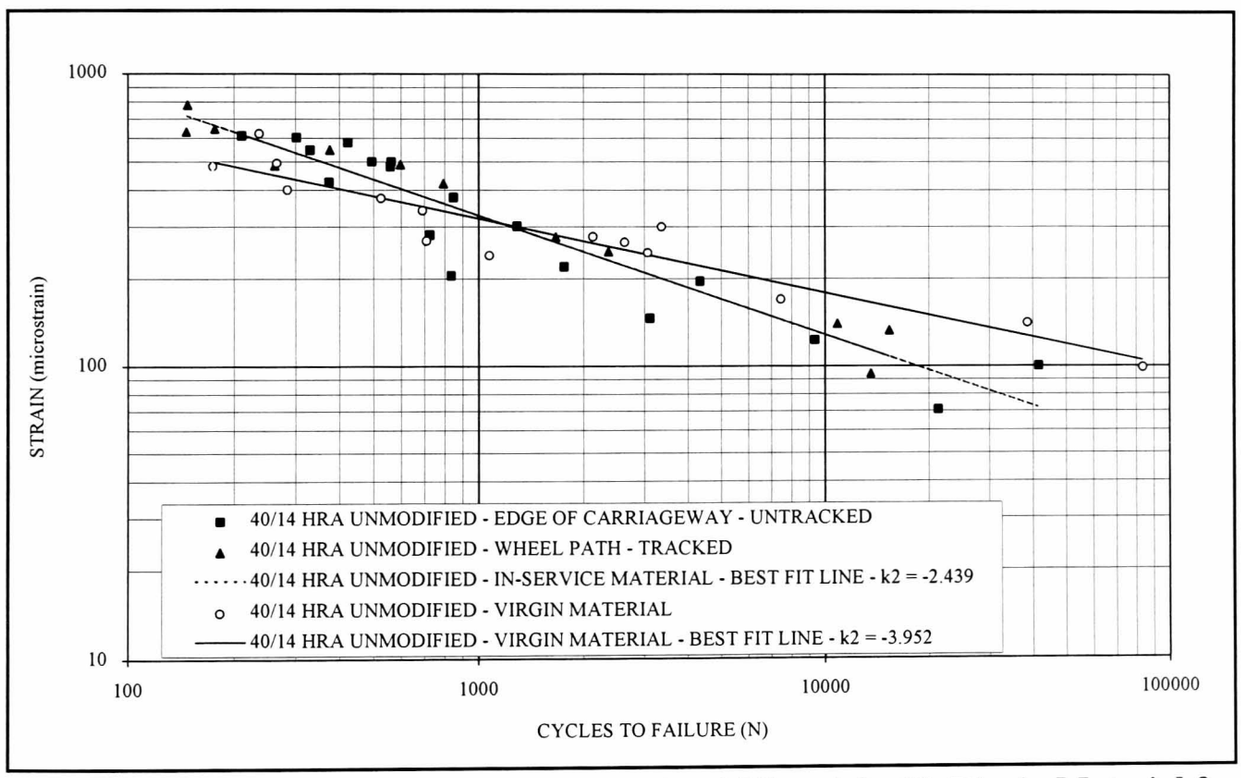


Figure 4.31 - Comparison of Tracked and Aged Material with Virgin Material for a 40/14 HRA Unmodified Wearing Course.

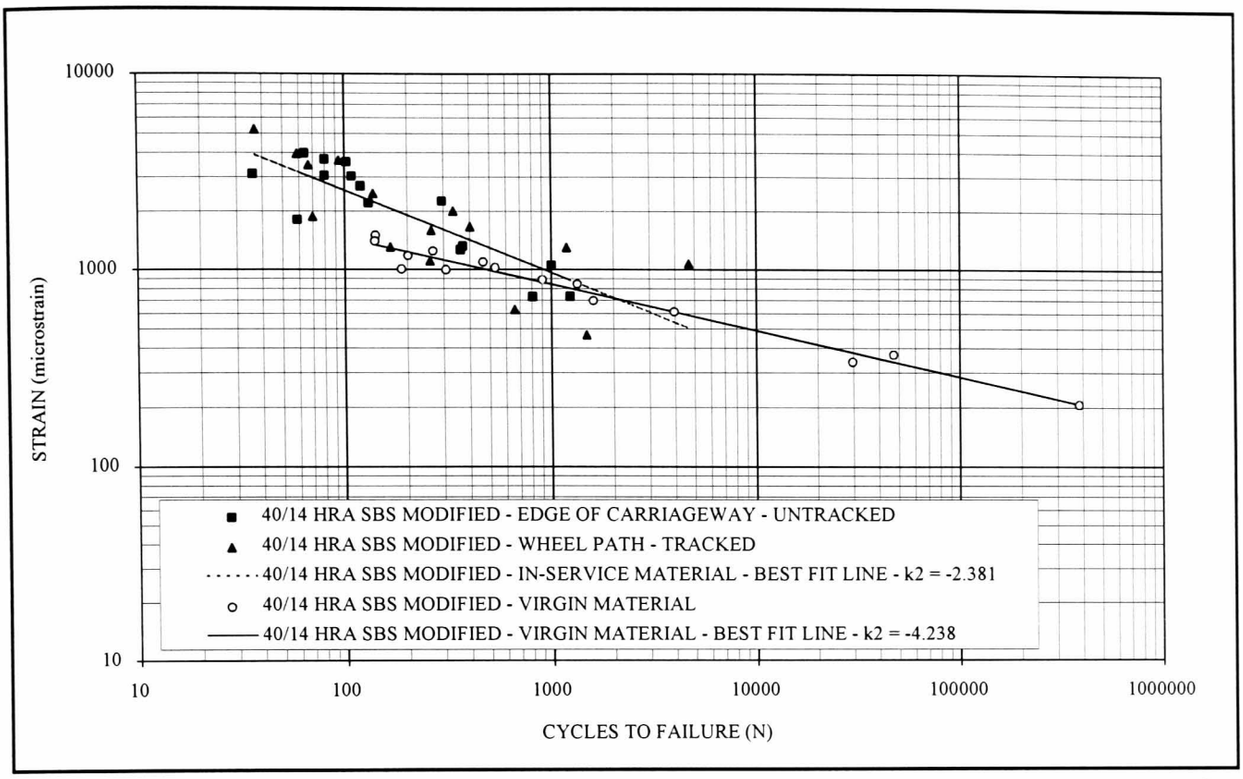


Figure 4.32 - Comparison of Tracked and Aged Material with Virgin Material for a 40/14 HRA SBS Modified Wearing Course.

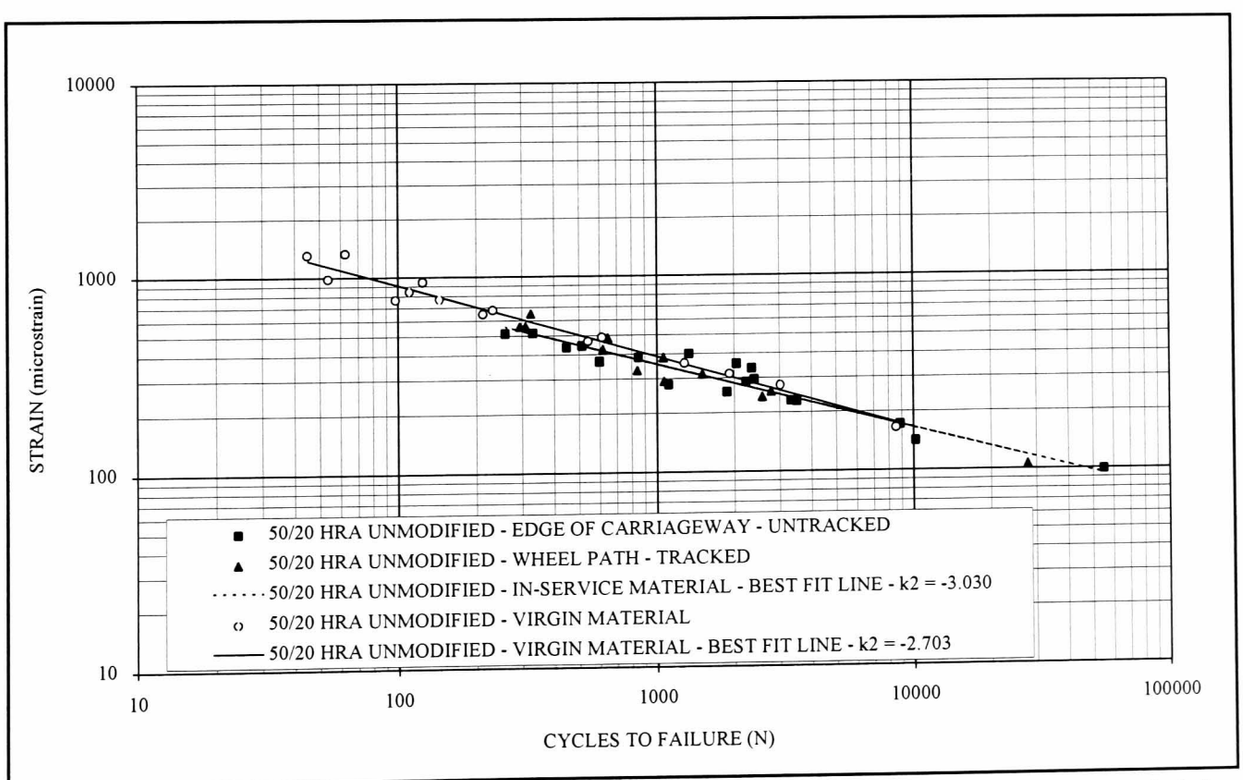


Figure 4.33 - Comparison of Tracked and Aged Material with Virgin Material for a 50/20 HRA Unmodified Basecourse.

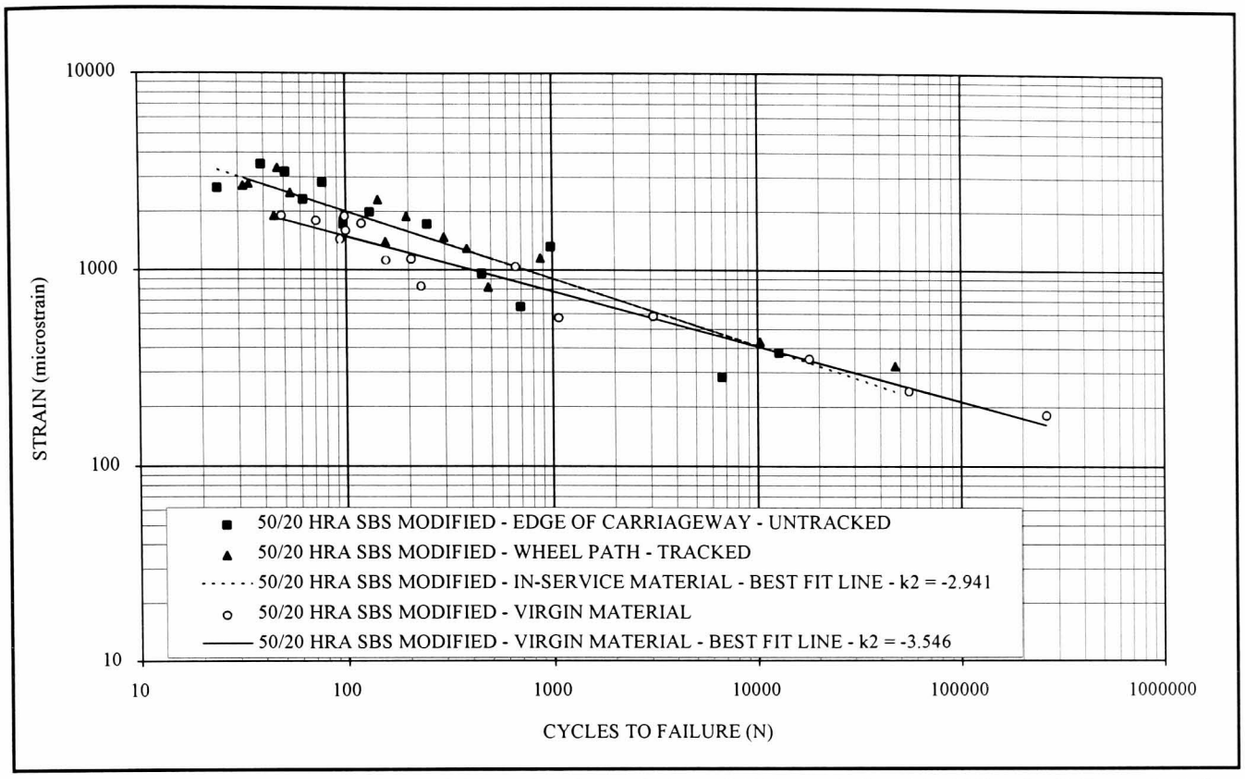


Figure 4.34 - Comparison of Tracked and Aged Material with Virgin Material for a 50/20 HRA SBS Modified Basecourse.

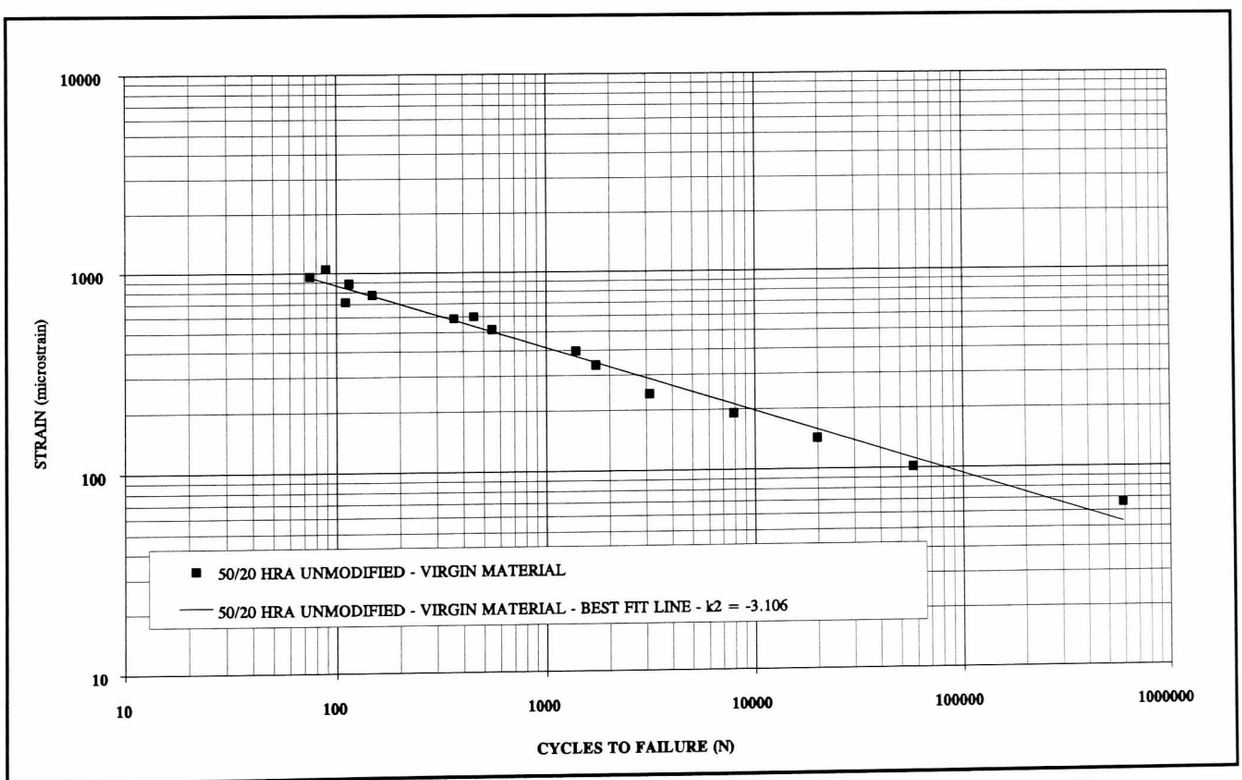


Figure 4.35 - Fatigue Line for the Retested 50/20 HRA Unmodified Basecourse with a Higher k_2 Value than the In-service Material Shown in Figure 4.33.

4.7 Further Validation of the ITFT

Esso provided the University with 10 cores of each of 3 materials. These were a 20mm HDM (1987), a 0 to 10mm Asphaltic Concrete (1992) and a 0 to 14mm Asphaltic Concrete (1995), the numbers in brackets are the Esso identity codes for the three materials. These specimens were subjected to Indirect Tensile Fatigue Testing, thus, giving two European materials which have been evaluated with the ITFT. Esso also produced necked cylindrical specimens from the same material which were tested in their uniaxial tension-compression apparatus. Comparisons of the results are shown in Figures 4.36, 4.38 and 4.40 with the error plots being shown in Figures 4.37, 4.39 and 4.41. These Figures show a good correlation between the Uniaxial Tension-Compression Test (UTCT, 10Hz, 10°C) and the ITFT (20°C, 120ms risetime). The equations of the lines are different (Table 4.7) but, within the range of strains normally found in a pavement, 30-200 microstrain (6), the agreement is good, although this requires extrapolation of the ITFT data which, as shown in Section 4.4, is not desirable. Table 4.8 gives the results of the strains found at two different lives for the two test methods.

These results give an extra confirmation that the ITFT is an acceptable fatigue test and also provide a higher level of confidence for predicting lives at in-service strain levels.

Table 4.7 - Summary of Fatigue Information for All Three Materials.

	Equation			Correlation Coefficient		
	ITFT	UTCT	BOTH	ITFT	UTCT	BOTH
0/10mm	$\varepsilon = 1362\ N^{-0.22}$	$\varepsilon = 552\ N^{-0.18}$	$\varepsilon = 1645\ N^{-0.26}$	0.96	0.97	0.95
0/14mm	$\varepsilon = 1528\ N^{-0.25}$	$\varepsilon = 509\ N^{-0.17}$	$\varepsilon = 1692\ N^{-0.26}$	0.98	0.99	0.95
20mm HDM	$\varepsilon = 1144\ N^{-0.24}$	$\varepsilon = 552\ N^{-0.19}$	$\varepsilon = 1260\ N^{-0.26}$	0.95	0.99	0.96

Table 4.7 contains summary information for the three materials including the degree of correlation within each data set and between each data set. This shows that the statistical significance of the ITFT result is as high as that for the UTCT. Tables 4.7 and 4.8 also show that a UK 20mm DBM has very similar fatigue characteristics to both a French 0/10mm mixture and a French 0/14mm mixture.

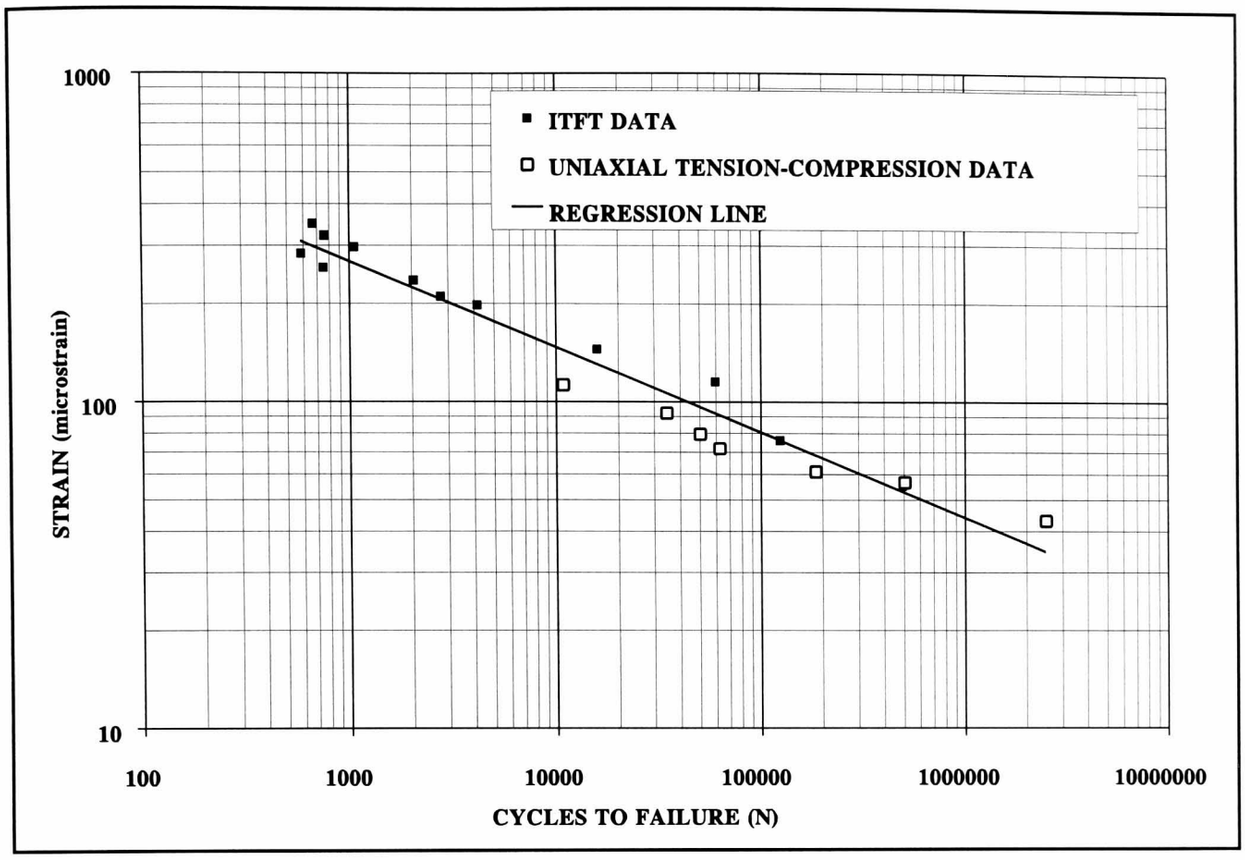


Figure 4.36 - Comparison of ITFT with UTCT for a French 0/10mm 50pen Material.

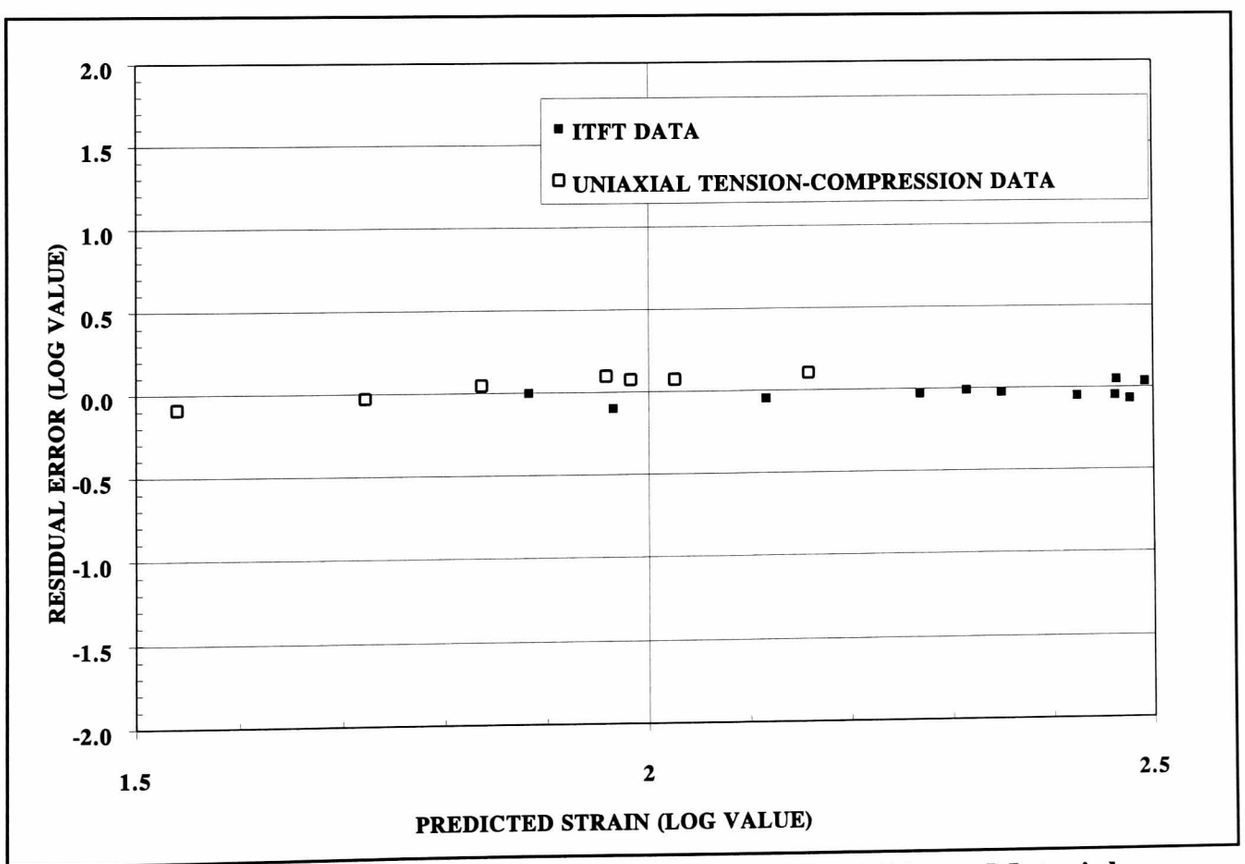


Figure 4.37 - Plot Showing the Residual Errors for the 0/10mm Material.

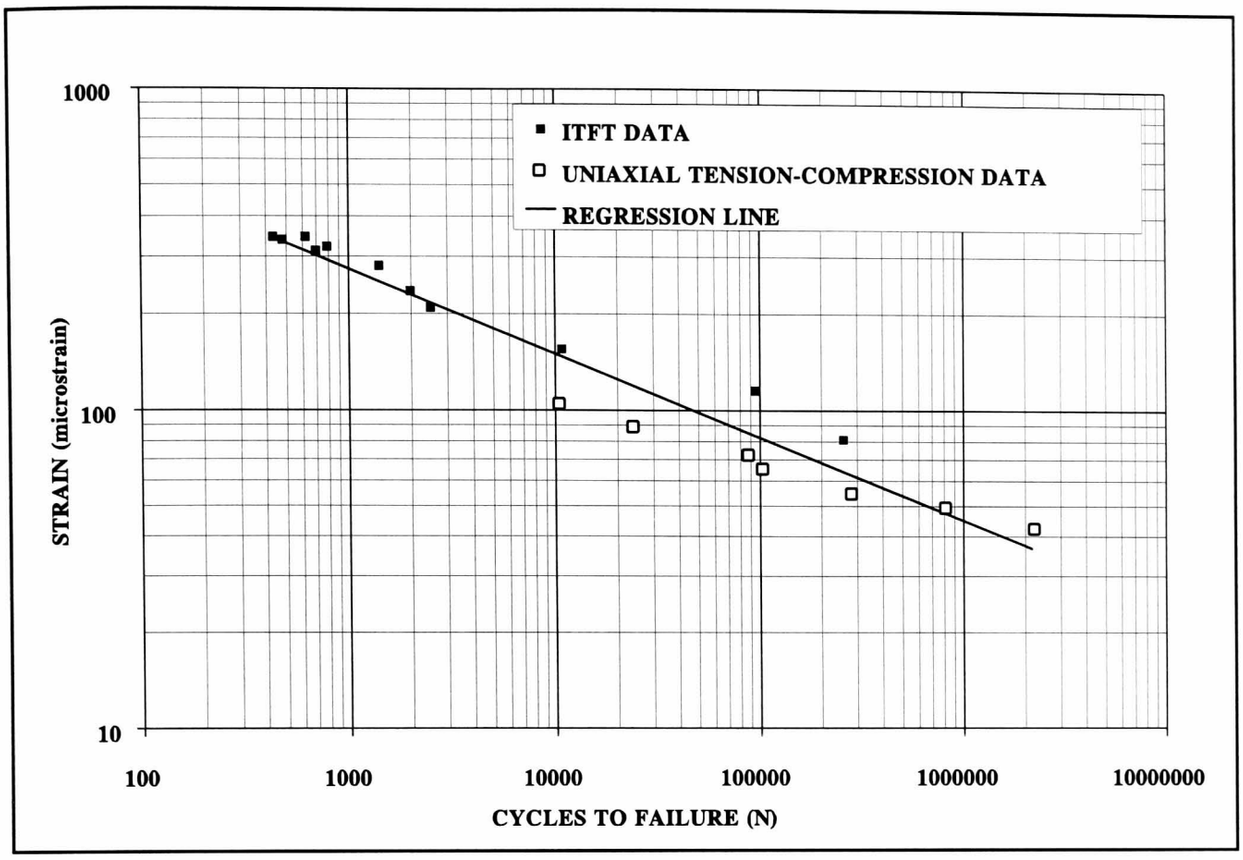


Figure 4.38 - Comparison of ITFT with UTCT for a French 0/14mm 50pen Material.

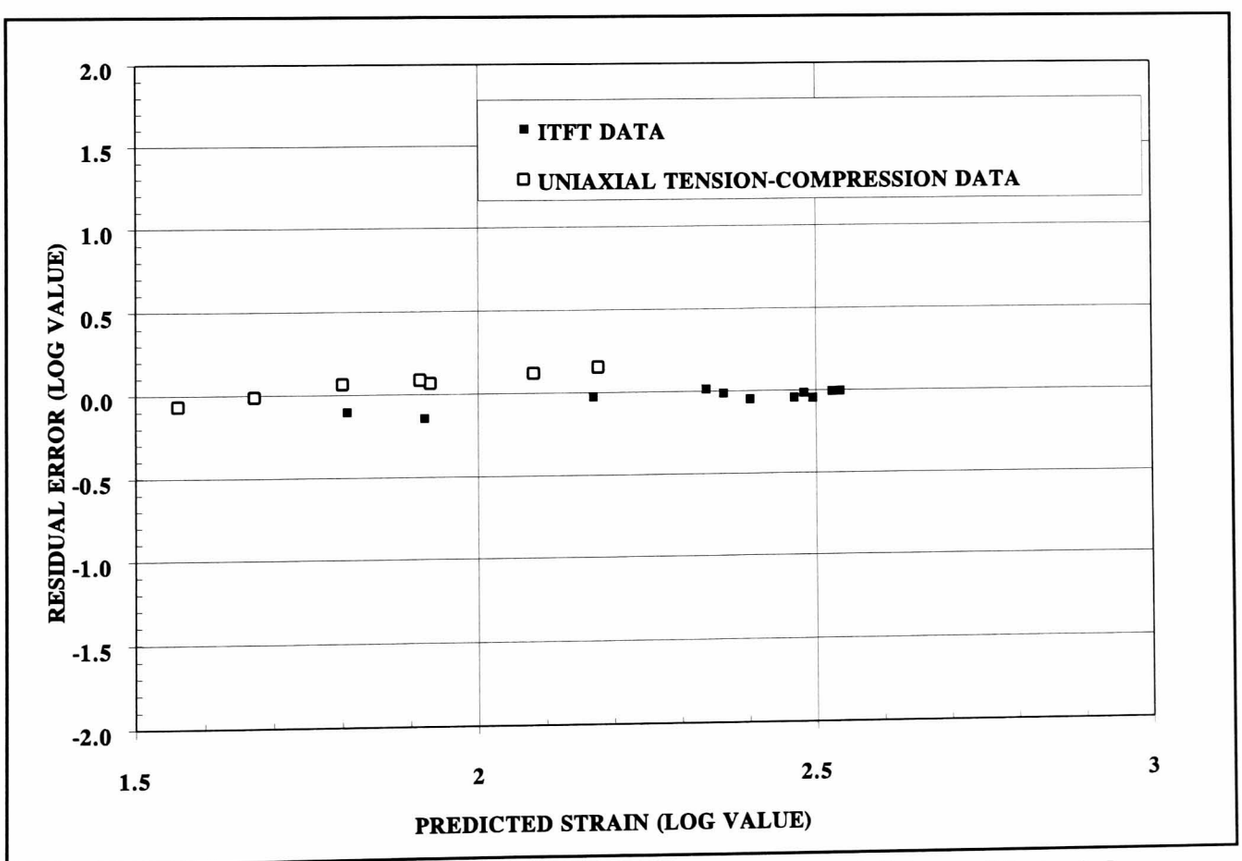


Figure 4.39 - Plot Showing the Residual Errors for the 0/14mm Material.

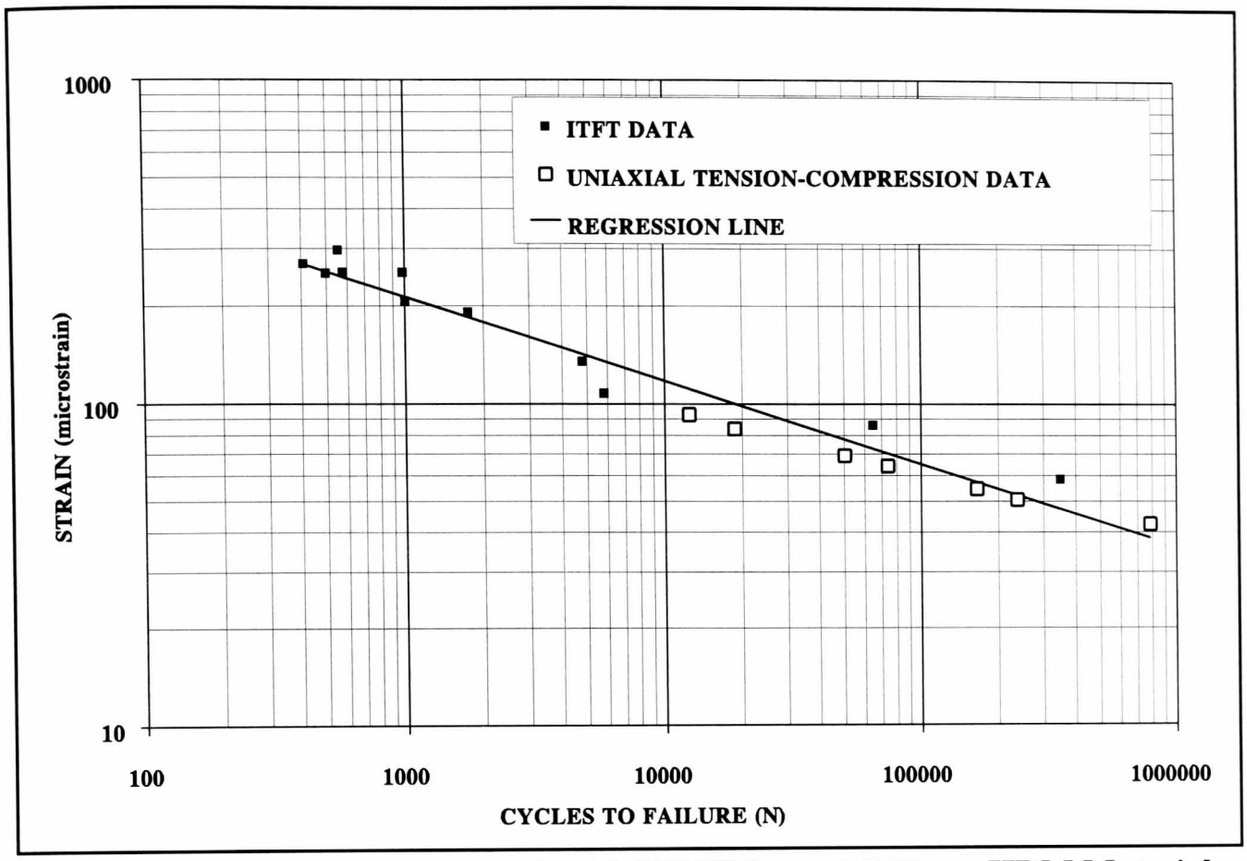


Figure 4.40 - Comparison of ITFT with UTCT for a UK 20mm HDM Material.

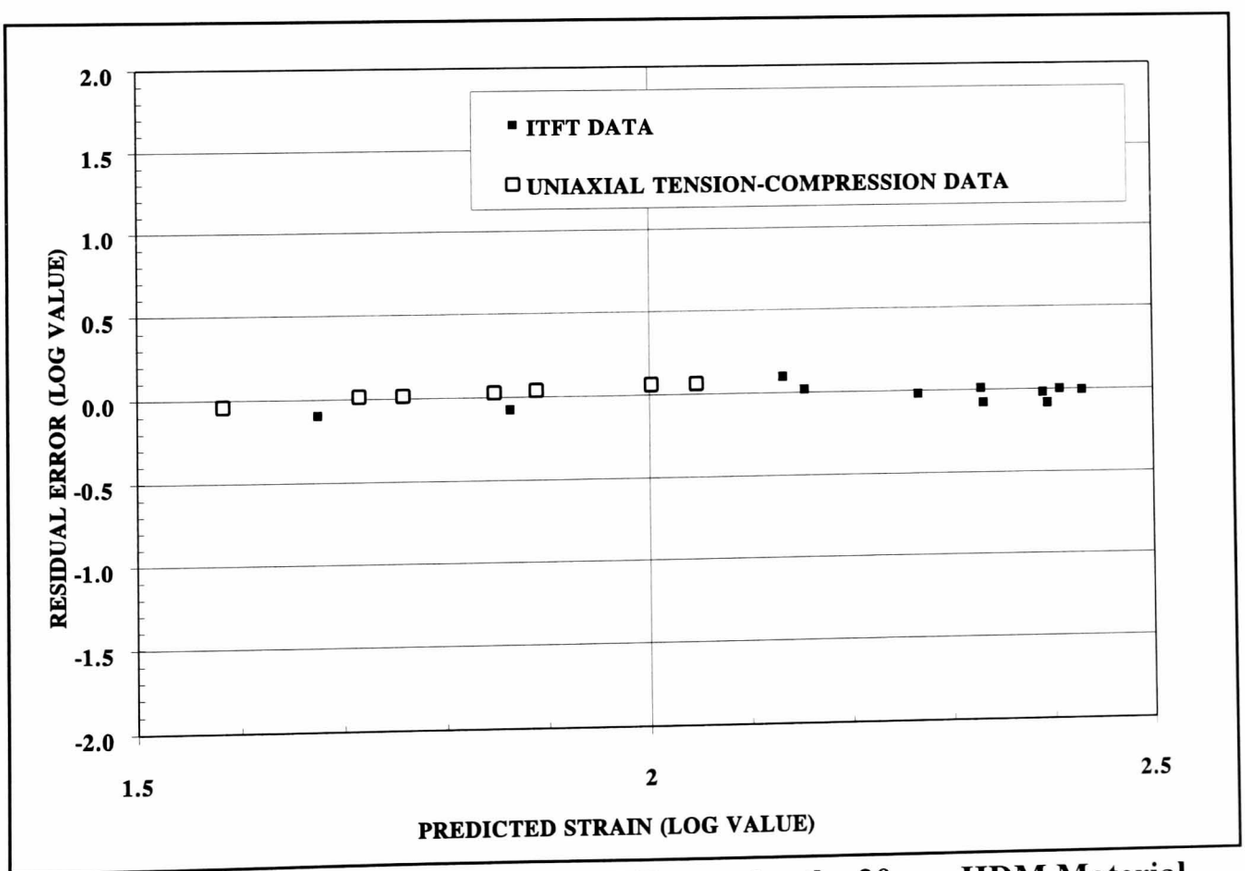


Figure 4.41 - Plot Showing the Residual Errors for the 20mm HDM Material.

Table 4.8 - Comparison of the Magnitude of Strains Found in the Two Test Methods.

	STRAIN (microstrain)								
	U.K. 20mm HDM			French 0/10mm			French 0/14mm		
Cycles	ITFT	UTCT	OVERALL	ITFT	UTCT	OVERALL	ITFT	UTCT	OVERALL
10^5	73	61	65	90	69	80	103	72	82
10^6	42	40	36	51	47	44	61	48	45

Note *The results headed overall are based upon a regression placed through both sets (ITFT and UTCT) of data.*

The variations in the data are shown in Table 4.9 where it can be seen that the largest variation is about 36% with the average variation being 15%.

Table 4.9 - Comparison of the Variations in Strain, Predicted Using the Two Different Methods against the Overall Result.

	Variation (%)			
	ITFT		UTCT	
	10^5 Cycles	10^6 Cycles	10^5 Cycles	10^6 Cycles
0/10mm	12.3	16.6	6.2	11.1
0/14mm	12.5	15.9	13.4	15.9
20mm HDM	25.6	35.6	12.2	6.7

As with the trapezoidal test there are differences in the slopes of the individual lines but in the region of interest the results agree well. However, for the same reasons as for the trapezoidal test, agreement between the UTCT and the ITFT cannot be expected based on consideration of the respective test conditions. The agreement can again be explained in terms of the compression phase of the loading cycle which is graphically demonstrated in Figure 4.42. This Figure shows that while all of the energy in the ITFT is dissipated in tension the UTCT dissipates a lot of its energy in compression helping to reverse the damage which occurs during the tension phase of the loading cycle. Therefore, as with the trapezoidal comparison, there appear to be compensating factors,

due to the continuous sinusoidal loading, which lead to the agreement between the test methods. Therefore, agreement cannot be inferred under conditions of test other than those used in this research. There may also be other factors which are difficult to quantify or even qualify which are playing a role in causing an agreement between the tests. Figure 4.42 is only a schematic as the version of the ITFT used in this research did not store the data necessary to produce hysteresis loops needed to make an actual comparison.

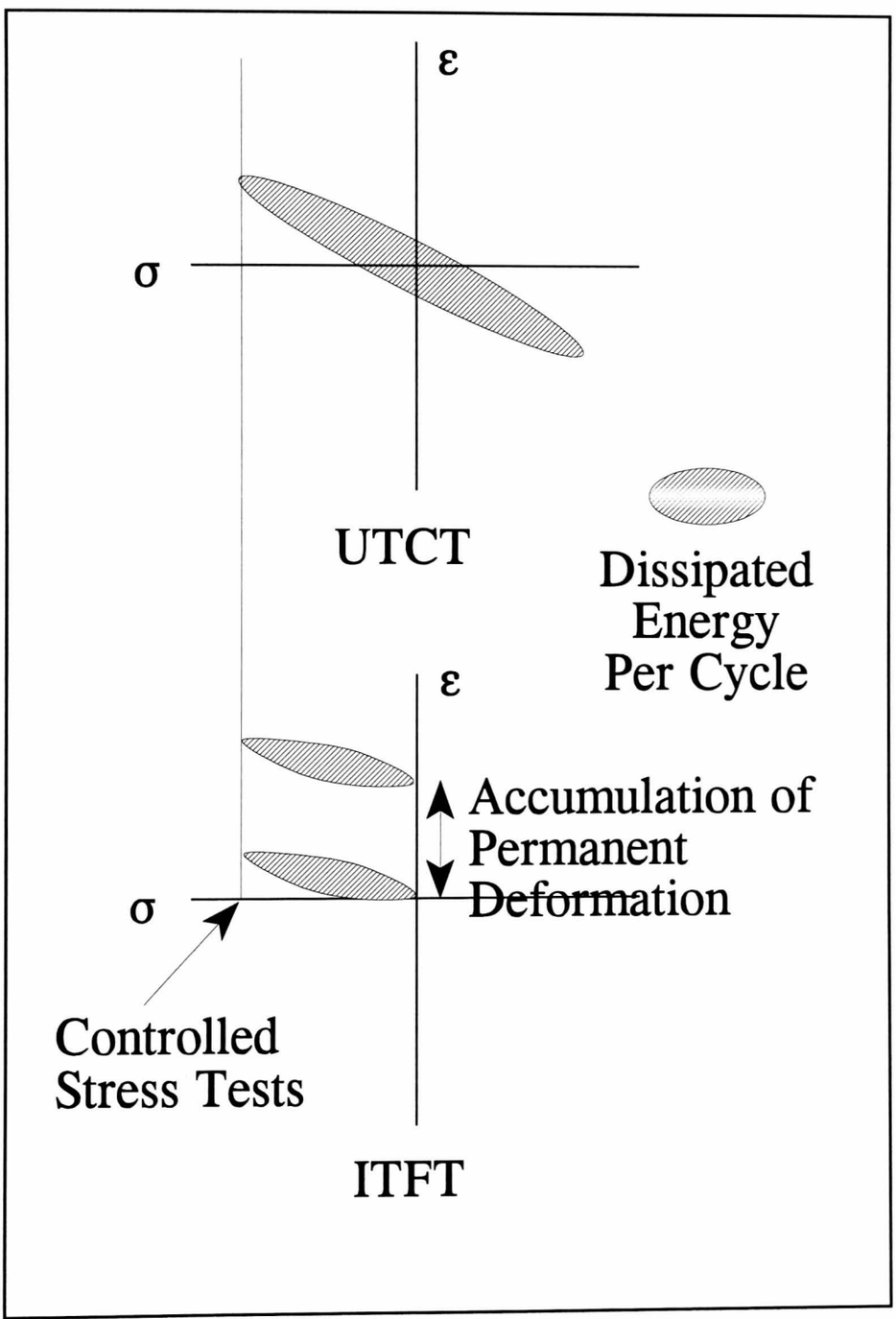


Figure 4.42 - Schematic Showing the Difference in Dissipated Energy per Cycle for the ITFT and UTCT.

4.8 Additional Results

During the course of the testing it became evident that, although desirable to test over very long time periods, it was possible to test over a relatively short range of lives and to extrapolate the data to get the fatigue relationship. This method is not recommended when trying to obtain reliable figures for use in analytical techniques or in contractual situations, but if the object of the exercise is to make a comparison between two different mixtures then this method can be useful. Figure 4.43 shows the same data as is given in Figure 4.35 for a 50/20 HRA basecourse material. This has been chosen as being typical of an ITFT relationship. Figure 4.43 also shows a regression line which has been placed through only those data points for which the life to failure was less than 5,000 cycles. The equations of the two lines are given in Table 4.10 along with other relevant data.

Table 4.10 - Comparison of Data Obtained from Short Life Tests with That Obtained From Long Life Tests.

	Equation Based on Strain	Strain at 10^6 Cycles	Variation from Overall Result (%)	Equation Based on Number of Cycles	Cycles at 200 microstrain	Variation from Overall Result (%)
Overall Data	$\epsilon = 3829\ N^{-0.322}$	45	-	$N = 1.32 \times 10^{11}\ \epsilon^{-3.104}$	81,766	-
All Points Where N<5,000	$\epsilon = 4415\ N^{-0.345}$	38	15.6	$N = 3.61 \times 10^{10}\ \epsilon^{-2.896}$	58,278	28.7

Although it can be seen that there is some variation it is no more than might be expected if the same test were repeated (Section 4.3). Therefore it would seem reasonable that testing can be carried out in a very short time period. For example the above test would have been complete in less than 3½ hours if just the testing below 5,000 cycles was carried out. The testing time can be further reduced by having less points over the same spread of life. However, it can be seen that if a line had been drawn through those data points with a life of over 2,000 cycles, a different relationship would have been developed and this highlights the need to carry out testing over as wide as range of lives as is possible. It is not, therefore, the intention to recommend that testing only at the high strain end of the fatigue curve be carried out in every case but it serves as a useful method of making a very quick check on the fatigue properties of a mixture if required.

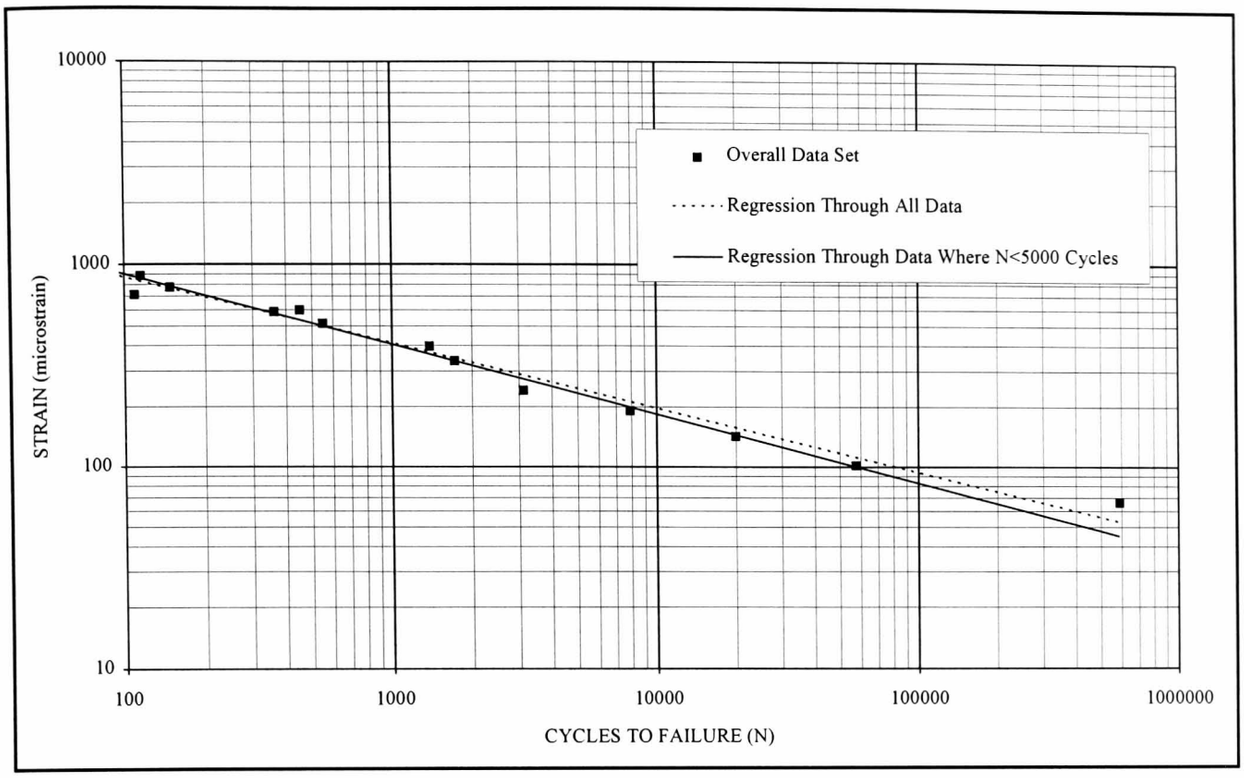


Figure 4.43 - Comparison Between Regression Based on All the Data Points and Those Which Have a Life of Less Than 5,000 Cycles, 50/20 HRA Basecourse.

During all the testing it became apparent that for the ITFT to gain widespread use and recognition that data would have to be presented on materials from outside the U.K. as well as U.K. mixtures. To this end the author was provided with some specimens of a proprietary SMA mixture, in addition to the two French mixtures described in the previous section, which used fibres to hold the bitumen in the mixture. Further information about the composition of the mixture was unavailable due to commercial sensitivity. Figure 4.44 and 4.45 present the results of the testing and Table 4.11 gives a summary of the ten cores supplied for test.

The spread of stiffness results gives a good indication of the consistency of the material and Figure 4.44 gives the fatigue result. From this it can be seen that the ITFT is a suitable test method for SMA materials due to the very high correlation coefficient (R^2 = 0.99). For comparison purposes, Figure 4.45 compares the SMA result with a typical 30/14 Hot Rolled Asphalt (HRA). This shows that the higher binder content HRA performs significantly better than the SMA with regard to crack initiation. The equations of the line for the SMA are:

$$N = 4.35\times10^{11}\ \varepsilon^{-3.354} \quad (4.3)$$

$$\varepsilon = 2950\ N^{-0.30} \quad (4.4)$$

Table 4.11 - Summary Data for the SMA Cores.

	PROPERTIES					
	Diameter (mm)	Thickness (mm)	Stiffness (MPa)	Test Stress Level (kPa)	Maximum Initial Tensile Strain (microstrain)	Cycles to Failure (N)
T 1	99	26*	-	-	-	-
T 2	99	28*	-	-	-	-
T 3	99	29*	-	-	-	-
T 4	99	40	1,872	500	548	204
T 5	99	44	1,848	400	444	417
T 6	99	43	1,807	300	340	1,677
T 7	99	42	1,819	200	225	5,403
T 8	99	36	1,697	100	121	50,901
T 9	99	37	1,666	550	677	224
T 10	99	41	2,033	50	50	771,806

* Denotes cores which were too thin to test

For the SMA, the life at 100 microstrain is 87,193 load applications and the strain at 10^6 cycles is 48 microstrain. This is of comparable performance to the three materials detailed section 4.6 but considerably poorer than a 30/14 HRA which would typically have a life at 100 microstrain of around 1.5 million load applications and a strain at 10^6 cycles of 113 microstrain. As both the SMA and the 30/14 HRA have similar stiffnesses (≈2000MPa) a similar level of tensile strain will, therefore, be generated for the same load.

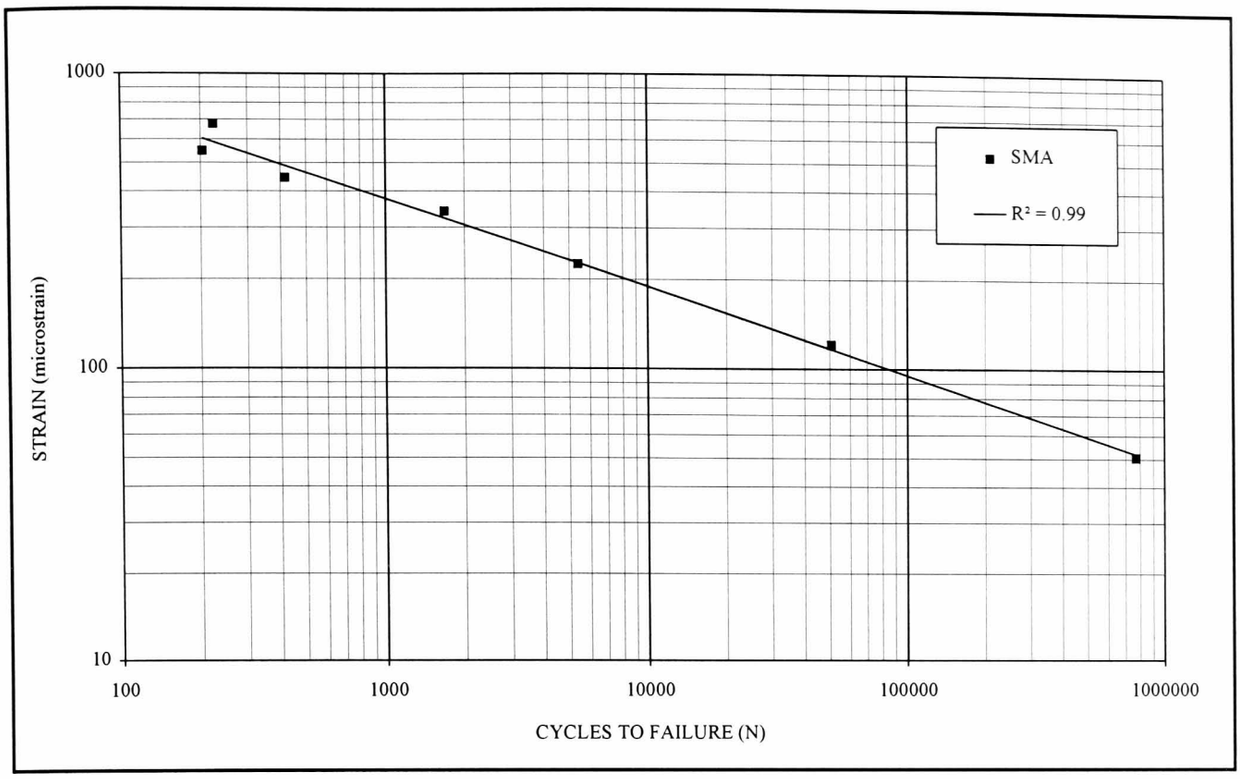


Figure 4.44 - Indirect Tensile Fatigue Line for an SMA Material.

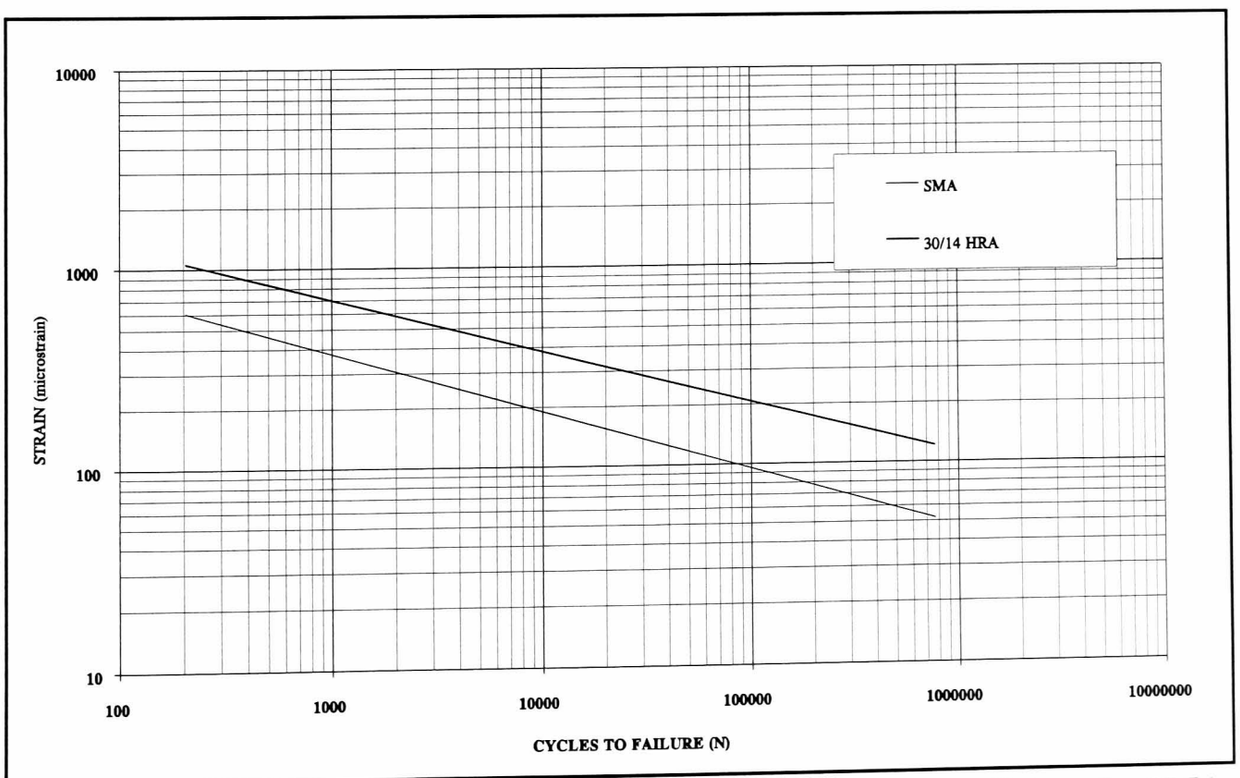


Figure 4.45 - Comparison of Fatigue Lines for a Typical 30/14 HRA and a SMA.

This indicates that SMA should not be substituted for an HRA as the surface course, without proper evaluation, as an appreciable drop in performance with regard to crack initiation may occur. SMA does, however, have other properties which make it desirable such as its resistance to permanent deformation, high durability, resistance to wear and relatively good skid resistance (7).

4.9 Summary of Results

The results presented in this Chapter demonstrate that the ITFT is an acceptable test method in comparison with other methods. It also provides the engineer with a tool which can approximate the fatigue characteristics of a bituminous paving mixture within 4 hours and determine them fully within less time than required by conventional methods. The test has been shown to be both repeatable and reproducible allowing a high degree of confidence in the results and has shown that it is capable of testing the full range of mixtures encountered in the industry. For reference purposes, Table 4.12 and Figure 4.46 present a summary of the fatigue results on the range of materials tested during the course of the research.

Table 4.12 - Summary Data for All the Standard Materials Tested During the Project Using the ITFT

MIXTURE TYPE	EQUATION FOR STRAIN	STRAIN @ 10^6 CYCLES (microstrain)	EQUATION FOR CYCLES TO FAILURE	CYCLES @ 100 microstrain
40/14 HRA SBS	$\varepsilon = 4301\ N^{-0.236}$	165	$N = 2.51\times10^{15}\ \varepsilon^{-4.238}$	8,388,296
30/14 HRA SBS	$\varepsilon = 4388\ N^{-0.241}$	157	$N = 1.30\times10^{15}\ \varepsilon^{-4.149}$	6,545,508[Note 2]
CR MA[*Note 1*]	$\varepsilon = 1278\ N^{-0.159}$	142	$N = 3.22\times10^{19}\ \varepsilon^{-6.280}$	8,868,616
30/14 HRA	$\varepsilon = 4322\ N^{-0.264}$	113	$N = 5.93\times10^{13}\ \varepsilon^{-3.788}$	1,574,181[Note 2]
50/20 HRA SBS	$\varepsilon = 5440\ N^{-0.282}$	111	$N = 1.86\times10^{13}\ \varepsilon^{-3.552}$	1,463,905
28mm DBM 50	$\varepsilon = 2595\ N^{-0.255}$	77	$N = 2.45\times10^{13}\ \varepsilon^{-3.923}$	349,274[Note 2]
40mm HDM	$\varepsilon = 1229\ N^{-0.205}$	72	$N = 1.20\times10^{15}\ \varepsilon^{-4.881}$	207,578
French 0/10mm	$\varepsilon = 1362\ N^{-0.224}$	62	$N = 9.15\times10^{13}\ \varepsilon^{-4.455}$	112,570
40/14 HRA	$\varepsilon = 1838\ N^{-0.253}$	56	$N = 7.99\times10^{12}\ \varepsilon^{-3.952}$	99,666
20mm DBM	$\varepsilon = 1562\ N^{-0.246}$	52	$N = 9.81\times10^{12}\ \varepsilon^{-4.068}$	71,725
French 0/14mm	$\varepsilon = 1528\ N^{-0.246}$	51	$N = 9.05\times10^{12}\ \varepsilon^{-4.069}$	65,864
SMA	$\varepsilon = 2950\ N^{-0.298}$	48	$N = 4.35\times10^{11}\ \varepsilon^{-3.354}$	85,210
50/20 HRA	$\varepsilon = 3824\ N^{-0.322}$	45	$N = 1.34\times10^{11}\ \varepsilon^{-3.106}$	82,244
20mm HDM	$\varepsilon = 1144\ N^{-0.239}$	42	$N = 5.99\times10^{12}\ \varepsilon^{-4.178}$	26.389

Note 1 *CR MA stands for Crumb Rubber modified Marshall Asphalt and although not actually tested during the course of this research the results are included in the section on repeatability.*

Note 2 *These equations include the data for the trapezoidal testing.*

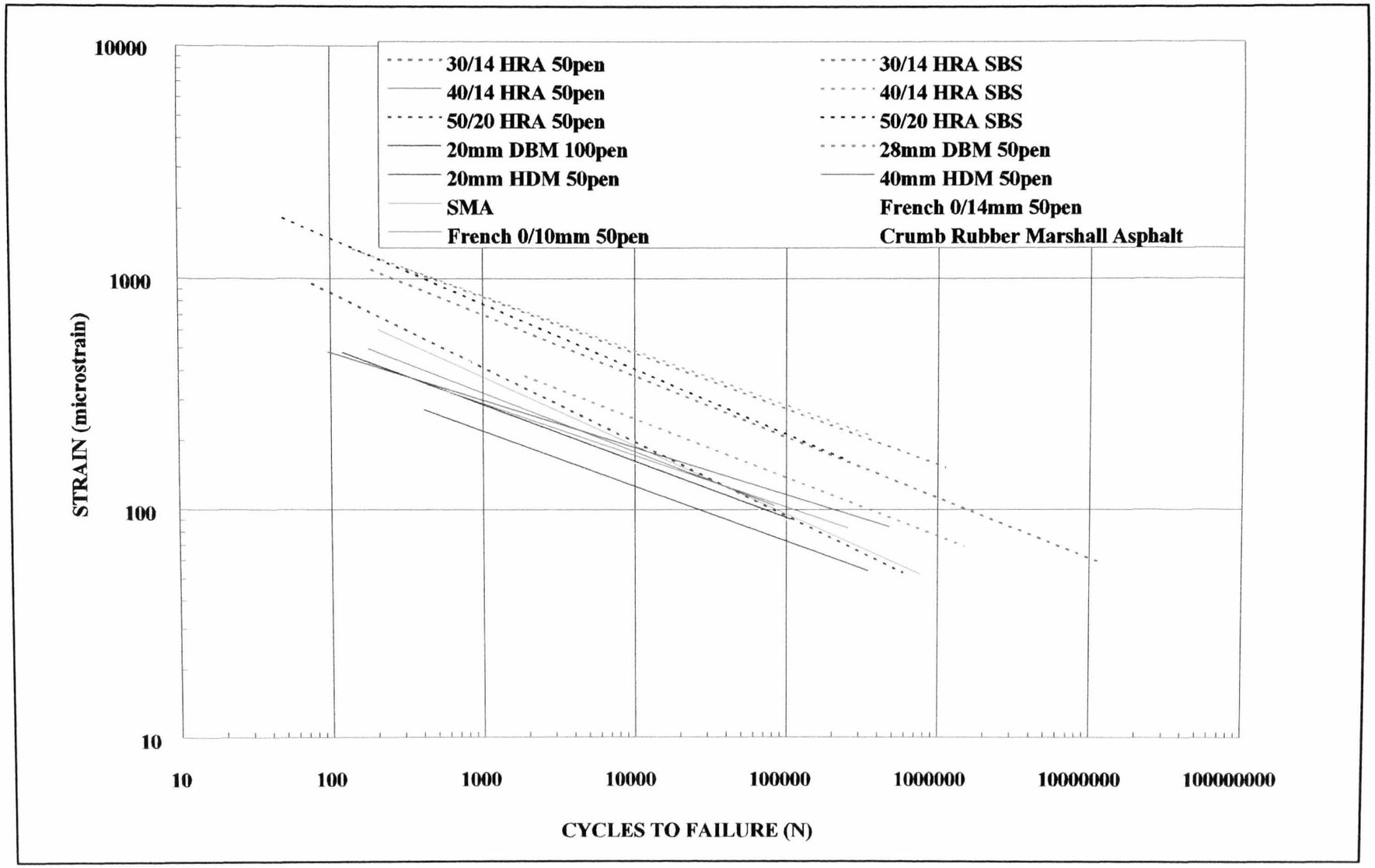


Figure 4.46 - Summary Plot Showing the ITFT Lines for All Materials Tested During the Research.

4.10 References

1. Navarro, D. and Kennedy, T.W., "Fatigue and Repeated-Load Elastic Characteristics of Inservice Asphalt-Treated Materials," Research Report 183-2, Project 3-9-72-183, Centre for Highway Research, University of Texas at Austin, January 1975.
2. Porter, B.W. and Kennedy, T.W., "Comparison of Fatigue Test Methods for Asphalt Materials," Research Report 183-4, Project 3-9-72-183, Centre for Highway Research, University of Texas at Austin, April 1975.
3. Adedimila, A.S. and Kennedy, T.W., "Repeated-Load Indirect Tensile Fatigue Characteristics of Asphalt Mixtures," Centre for Highway Research, University of Texas at Austin, December 1975.
4. Elliott, R.C. and Read, J.M., "Use of Modified Binders in Marshall Asphalt Mixtures : Mixture Test Programme," SWK (PE) Client Report, P921, November 1995.
5. Wu, F., "Assessment of Residual Life of Bituminous Layers for the Design of Pavement Strengthening," PhD. Thesis, Council for National Academic Awards, London, March 1992.
6. Kingham, I.R., "Failure Criteria Developed from AASHO Road Test Data," Highway Research Board, Special Report 140, Proceedings of a Symposium on Structural Design of Asphalt Concrete Pavements to Prevent Fatigue Cracking, pp 183-196, 1973.
7. Liljedahl, B., "Mix Design for Heavy Duty Asphalt Pavements," Asphalt Review, Volume 11, Number 3, September 1992.

POISSON'S RATIO

5.1 Introduction

The work on the Indirect Tensile Fatigue Test has highlighted the need to know Poisson's ratio for bituminous materials as the calculation of the maximum tensile strain at the centre of the specimen (ϵ_{xmax}) is dependent upon it. Equation 5.1 shows that as well as Poisson's ratio the stiffness modulus of the material is also required and in the indirect tensile mode of testing this too requires a knowledge of Poisson's ratio, Equation 5.2.

$$\epsilon_{xmax} = \frac{\sigma_{xmax}}{S_m} \times (1 + 3\upsilon) \qquad \textbf{(5.1)}$$

$$S_m = \frac{P}{\delta \times t} \times (0.27 + \upsilon) \qquad \textbf{(5.2)}$$

Where:

ϵ_{xmax}	=	Maximum tensile strain at the centre of the specimen,
σ_{xmax}	=	Maximum tensile stress at the centre of the specimen,
S_m	=	Stiffness modulus of the material,
υ	=	Poisson's ratio,
P	=	Compressive force applied to the specimen,
δ	=	Transient horizontal deformation and
t	=	Thickness of the specimen.

The horizontal tensile strain generated at the centre of an indirect tensile test specimen may be calculated from:

$$\epsilon_{xmax} = \frac{1}{S_m} (\sigma_{xmax} - \upsilon\sigma_{ymax}) \qquad \textbf{(5.3)}$$

where:

σ_{ymax} = Compressive Stress Generated on the Vertical Diameter.

The vertical compressive strain generated at the centre of the specimen may be calculated from:

$$- \epsilon_{ymax} = \frac{-1}{S_m} (\sigma_{ymax} - \upsilon\sigma_{xmax}) \qquad \textbf{(5.4)}$$

where:

$-\epsilon_{ymax}$ = Compressive strain generated at the centre of the specimen

The following equation may be obtained by equating the stiffnesses for Equations 5.3 and 5.4.

$$\left[\frac{\sigma_{xmax} - \upsilon\sigma_{ymax}}{\epsilon_{xmax}}\right] = \left[\frac{\sigma_{ymax} - \upsilon\sigma_{xmax}}{-\epsilon_{ymax}}\right] \qquad \textbf{(5.5)}$$

At the centre of the specimen the following equation applies which has been described in Chapter 3 (Equations 3.1 and 3.2).

$$\sigma_{ymax} = -3\sigma_{xmax} \qquad \textbf{(5.6)}$$

Substituting equation (5.6) into equation (5.5) and rearranging gives:

$$\upsilon = -\frac{\left[\left(-3\frac{\epsilon_{xmax}}{-\epsilon_{ymax}}\right) - 1\right]}{\left[3 + \frac{\epsilon_{xmax}}{-\epsilon_{ymax}}\right]} \qquad \textbf{(5.7)}$$

This derivation for the calculation of Poisson's ratio is based upon two dimensional ($\sigma_z = 0$) plane stress conditions. However, Roque and Buttlar (1), as described previously, carried out a three dimensional finite element analysis of the system and produced a very complex equation to calculate Poisson's ratio. Some interpolation between their data sets has been necessitated by the use of a specimen with a geometry of 100mm diameter and 40mm thickness. The interpolation means that $C_{\sigma xCTR}$ and $C_{\sigma yCTR}$ are defined by equations as opposed to being values taken from Table 3.1 of this report. The equation is:

$$\upsilon = \frac{\left(\frac{2P}{\pi dt} * C_{\sigma_{xCTR}}\right) - \left(\frac{\left(\left(\frac{H_M}{GL}\right) * \left(1.01 - 0.12\upsilon - 0.05\left(\frac{t}{t_{STD}}\right) * 1.07\right)\right)}{\left(\left(\frac{Y_M}{GL}\right) * (0.994 - 0.128\upsilon) * 0.98\right)}\right) * \left(\frac{6P}{\pi dt} * C_{\sigma_{yCTR}}\right)}{\left(\frac{6P}{\pi dt} * C_{\sigma_{yCTR}}\right) - \left(\frac{\left(\left(\frac{H_M}{GL}\right) * \left(1.01 - 0.12\upsilon - 0.05\left(\frac{t}{t_{STD}}\right) * 1.07\right)\right)}{\left(\left(\frac{Y_M}{GL}\right) * (0.994 - 0.128\upsilon) * 0.98\right)}\right) * \left(\frac{2P}{\pi dt} * C_{\sigma_{xCTR}}\right)} \quad \textbf{(5.8)}$$

Where:

H_m = Measured horizontal deformation (mm),

Y_m = Measured vertical deformation (mm),

GL = Gauge length (mm),

t = Measured specimen thickness (mm),

t_{STD} = Standard specimen thickness = 0.625 * specimen diameter (mm),

P = Total load applied to the specimen (kN),

d = Measured specimen diameter (mm),

$C_{\sigma xCTR}$ = Correction factor applied to the horizontal point stress occurring at the centre of the specimen's face as predicted by 2-D plane stress solution to account for 3-D effects,

$C_{\sigma yCTR}$ = Correction factor applied to the vertical point stress occurring at the centre of the specimen's face as predicted by 2-D plane stress solution to account for 3-D effects,

$C_{\sigma xCTR}$ = $(0.235396 \times n) + 0.951234$ and

$C_{\sigma yCTR}$ = $(-0.07211 \times n) - 0.96089$.

This equation can only be solved using an iterative procedure to gain convergence between an assumed and calculated value. This iterative procedure has been built into a computer program and the values produced compared against values calculated from Equation 5.7 to ascertain the effects of bulging in the indirect tensile mode of testing. All the results, three examples of which are shown below, were gained from the testing system described in the following pages. It should be noted that all the analyses are based upon point strains at the centre of the specimen which are the maximum values. However the experimental measurements were obtained over a gauge length of 25mm and, therefore, the measured results will be always be marginally lower than the actual ones (Figure 3.1).

Case 1 - Specimen H7 tested at 20°C with a risetime of 120ms.

Vertical Deformation	=	414μm		
Horizontal Deformation	=	165μm		
Two dimensional Analysis (Equation 5.7)			υ =	0.646
Three dimensional Analysis (Equation 5.8)			υ =	0.648

Case 2 - Specimen H12 tested at 20°C with a risetime of 120ms.

Vertical Deformation	=	446μm		
Horizontal Deformation	=	175μm		
Two dimensional Analysis (Equation 5.7)			υ =	0.643
Three dimensional Analysis (Equation 5.8)			υ =	0.648

Case 1 - PVC Specimen tested at 20°C with a risetime of 120ms.

Vertical Deformation	=	419μm		
Horizontal Deformation	=	40μm		
Two dimensional Analysis (Equation 5.7)			υ =	0.415
Three dimensional Analysis (Equation 5.8)			υ =	0.419

Although only 3 comparisons are given here all the mixtures and test conditions were compared and it was found that the three dimensional finite element analysis only affected the third decimal place and it was, therefore, considered reasonable to use the simple two dimensional model (Equation 5.7) for the calculation of Poisson's ratio.

The measurement system which was used to generate all the data described in this Chapter is shown in Figure 5.1. The miniature LVDT's shown here on a cube of material, can be applied equally as well to a cylindrical specimen. The LVDT's and the aluminium locating pips were extremely lightweight and should not have had a noticeable effect on the performance of the material to which they are attached.

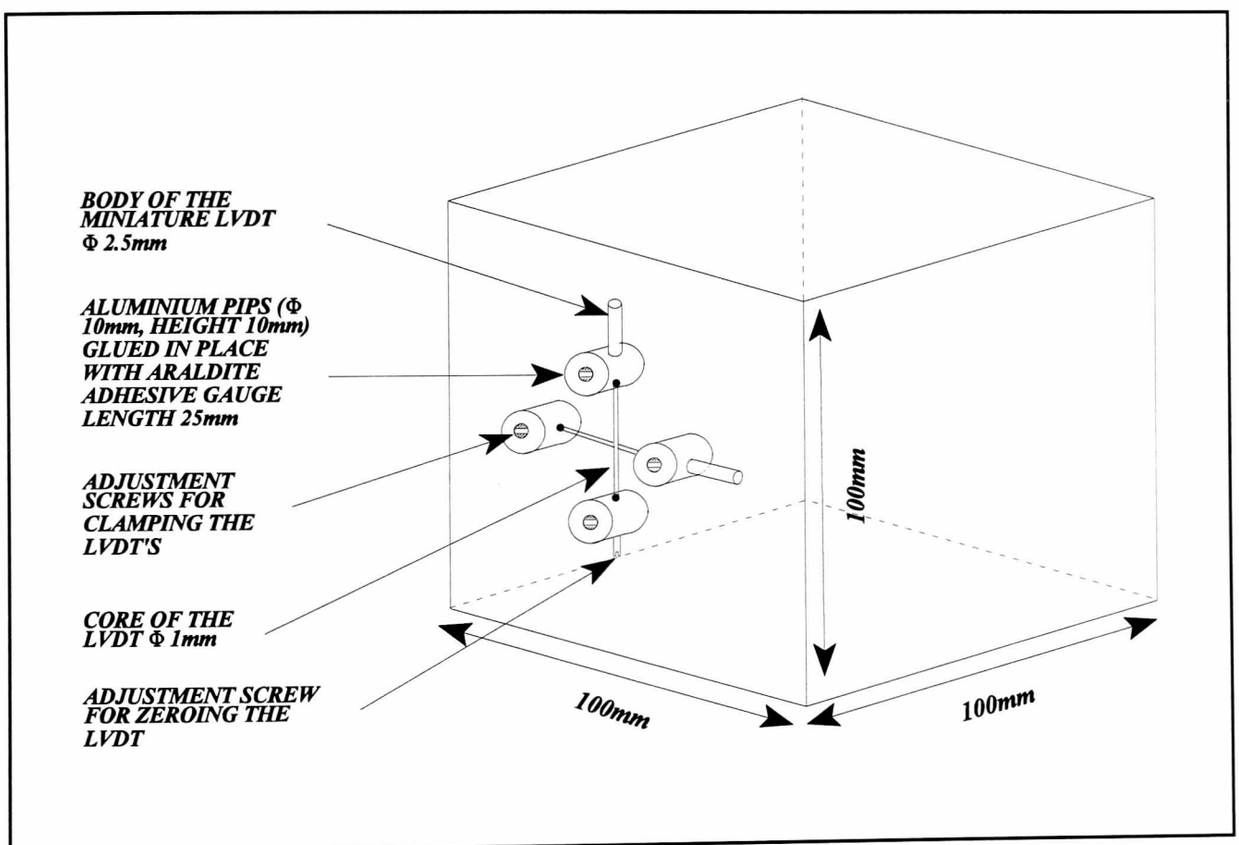


Figure 5.1 - Schematic of the Measurement System Used for the Work on Poisson's Ratio.

Little previous work has been carried out to ascertain values for Poisson's ratio but some relevant data is shown in Figures 5.2 to 5.5. The graphs are all plotted in the form of Poisson's ratio against stiffness to give comparative results.

From these Figures it is evident that representative results for Poisson's ratio are difficult to obtain and that the graphs display a lot of scatter. However, it can be seen that Poisson's ratio for bituminous materials has generally been found to lie somewhere in the range 0.10 to 0.45.

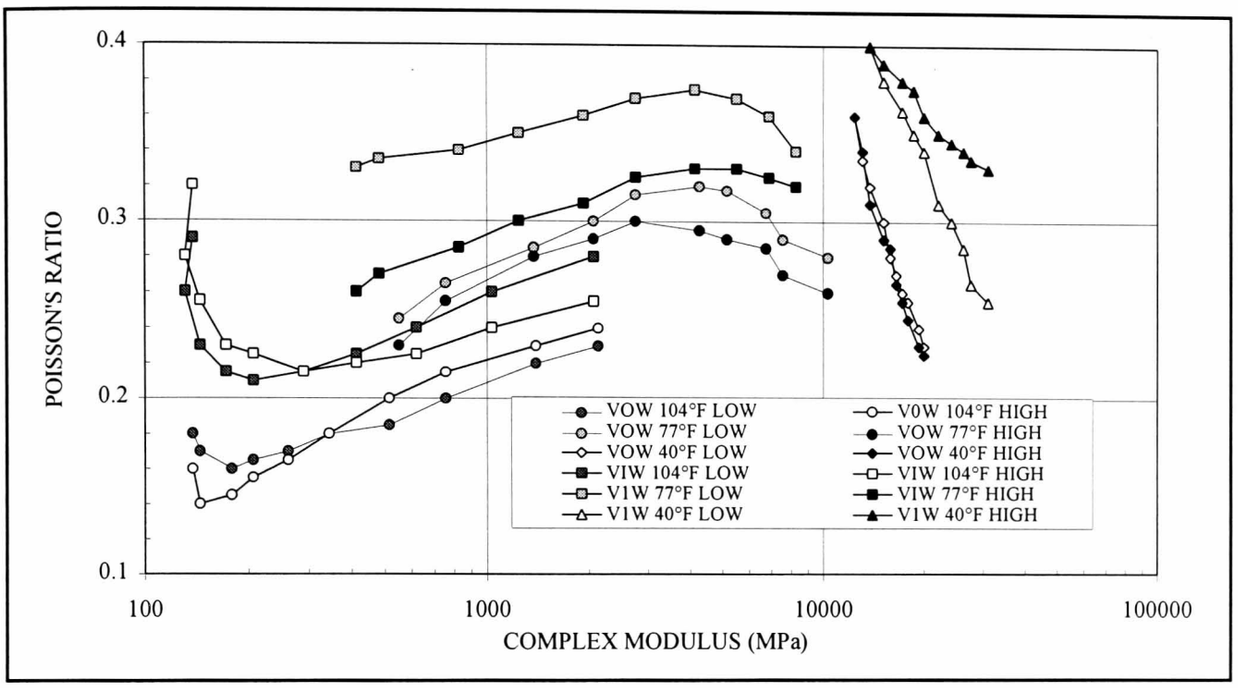


Figure 5.2 - Poisson's Ratio Against Stiffness for Various Asphaltic Concrete Mixtures - Dynamic Loading, After Alavi and Monismith (2).

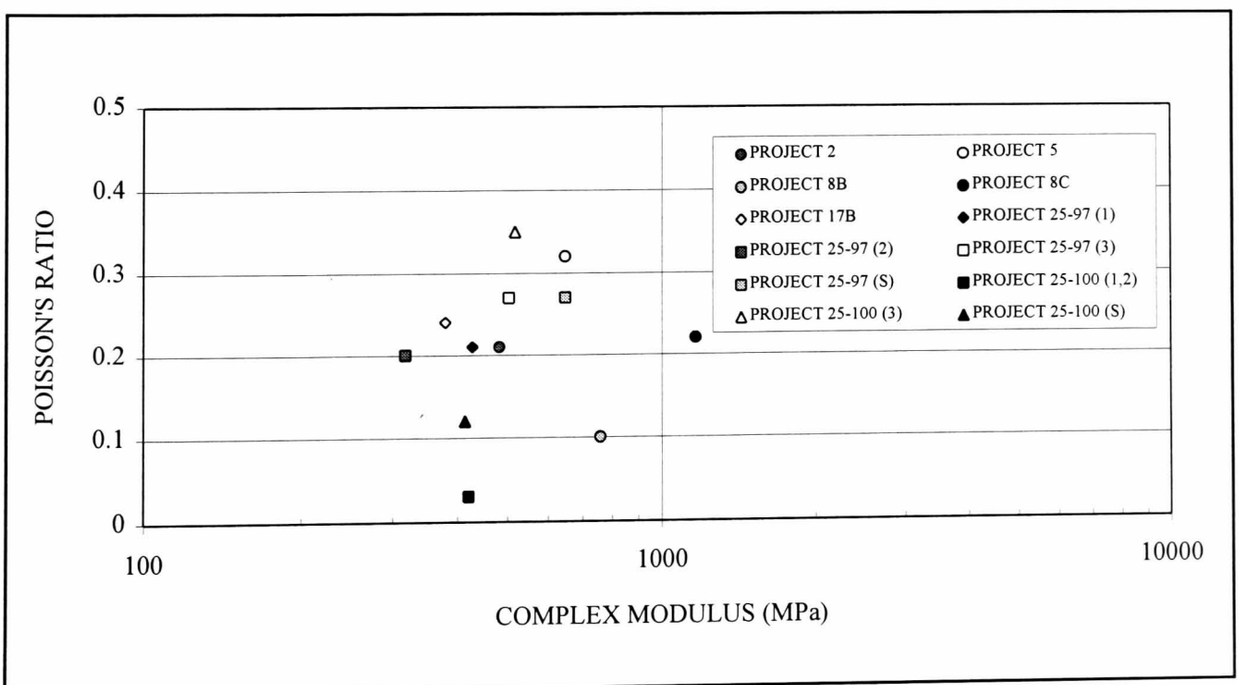


Figure 5.3 - Poisson's Ratio Against Stiffness for Various Asphaltic Concrete Mixtures - Static Loading, After Navarro and Kennedy (3).

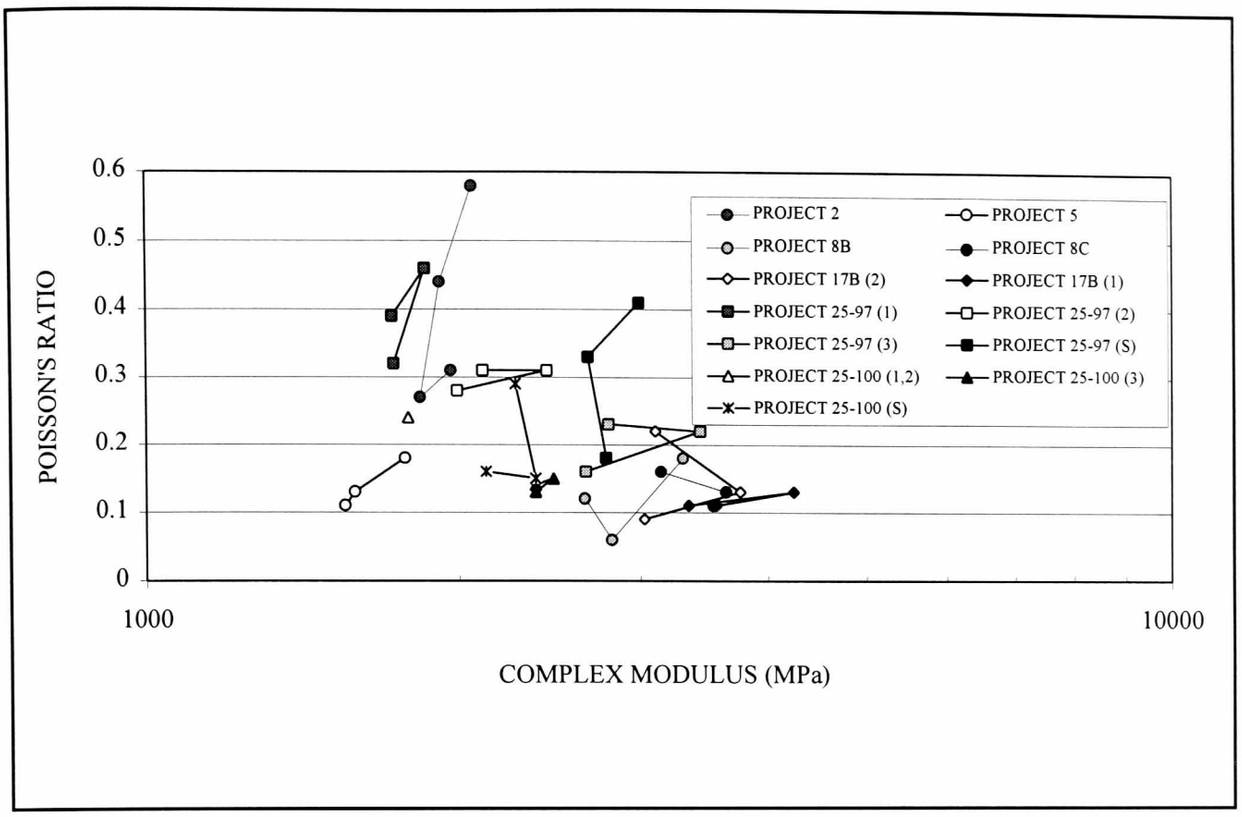


Figure 5.4 - Poisson's Ratio Against Stiffness for Various Asphaltic Concrete Mixtures - Dynamic Loading, After Navarro and Kennedy (3).

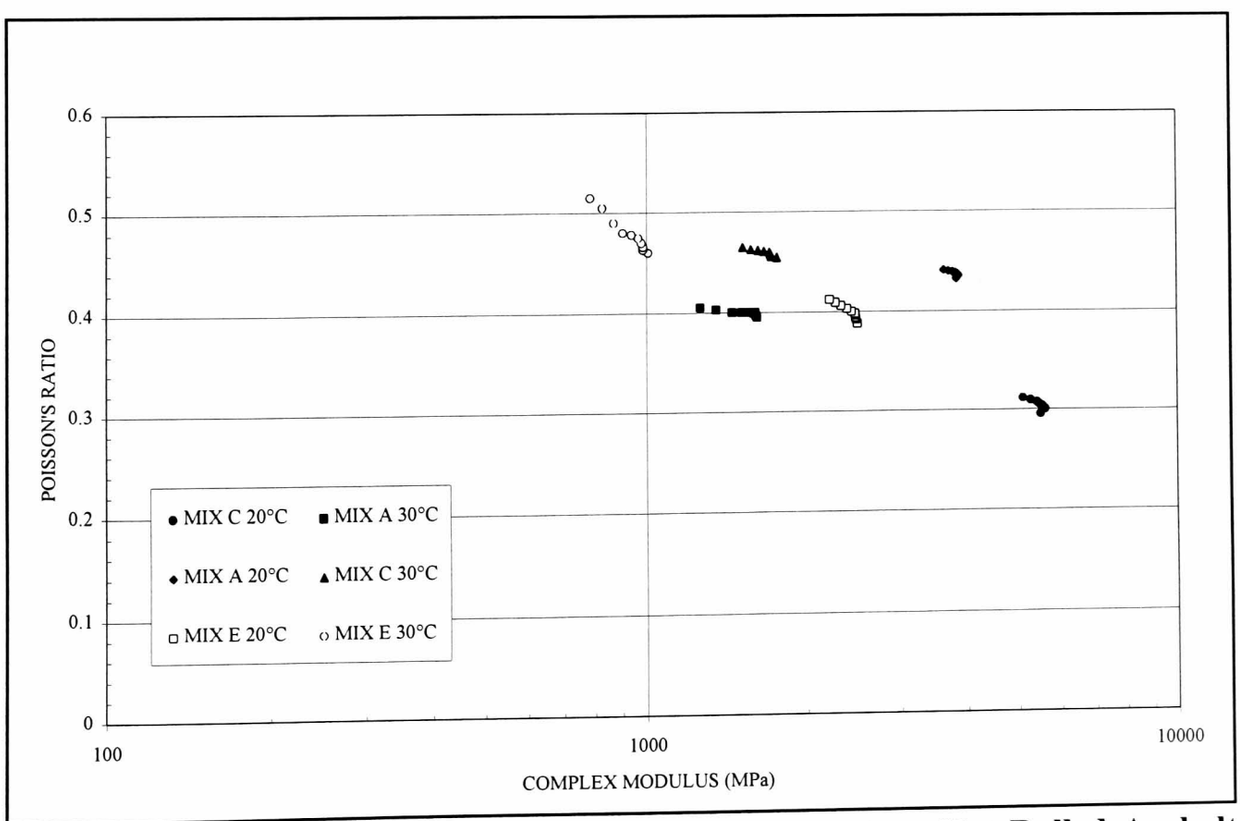


Figure 5.5 - Poisson's Ratio Against Stiffness for Various Hot Rolled Asphalt Mixtures - Dynamic Loading, After Cragg and Pell (4).

Nunn (5) has reported values of Poisson's ratio for bituminous materials related to the temperature of the material (Table 5.1), the exact details of how these results were obtained, however, are not publicly available.

Table 5.1 - Values for Poisson's Ratio at Various Temperatures, as Recommended by TRL.

Temperature (°C)[Note 1]	Poisson's Ratio
0	0.25
10	0.25
20	0.35
30	0.45

Note 1 It is recommended that linear interpolation be used between the values given in this table. Outside of the temperature range given in the table the values of 0.25 and 0.45 should be used for low and high temperatures respectively.

Due to the scatter in the values for Poisson's ratio shown here and need for knowing Poisson's ratio shown at the beginning of this Chapter it was considered necessary to obtain good quality data for Poisson's ratio under the range of conditions likely to be found in-service.

5.2 Test Programme

The initial test program consisted of testing a typical sand-asphalt mixture complying with B.S. 594 (6). This mixture was selected as it was considered to be the most homogenous standard material. Cylindrical specimens, with the same geometry as the ITFT specimens, were manufactured at two void contents in order to have different stiffnesses under the same test conditions, to investigate whether Poisson's ratio is dependent on temperature or stiffness.

Unfortunately, as can be seen in the next section, what seemed unrealistic values for Poisson's ratio were obtained when cylindrical specimens were tested in the NAT and it

became necessary to carry out some validation work on both the measurement and analysis systems being employed.

To do this, 100mm cubes of the same sand-asphalt material and a 30/14 HRA (as described in Chapters 3 and 4) were manufactured and tested, the results of which are shown in the next section. These again produced unrealistic results at the start of the test. It was, therefore, decided to validate the entire measurement system, by manufacturing a cube of aluminium for which the Poisson's ratio was known and to test it in a servo-hydraulic apparatus (as the NAT cannot produce a large enough stress to deform aluminium) using the same measurement system as that which had been used on both the cores and cubes of bituminous material in the NAT.

Assuming the aluminium cube results were correct, the next stage was to test a cylindrical specimen made of the same aluminium, in the indirect tensile mode, to see if the elastic theory, which gave Equation 5.7, works for a material which is linearly elastic at small strains.

5.3 Results

Figure 5.6 shows typical results for a cylindrical specimen tested in the NAT using equation 5.7 for the calculation of Poisson's ratio. This was a core of sand-asphalt with a high void content. The specimen was tested at 0°C and at varying levels of compressive deformation and loading time. The results show that the level of compressive deformation does not have an effect on Poisson's ratio but that changing the loading time does have an effect on the stiffness, as expected, but not Poisson's ratio.

However, these points are really secondary to the fact that the testing produced high values for Poisson's ratio between 0.62 and 0.66 for this specimen and between 0.60 and 0.70 for all the cores of material tested.

It was, therefore, necessary to test cubes of the same material with the same measurement system and the same temperatures to try to explain the reason for the high values of Poisson's ratio.

Figure 5.7 shows the results of tests on a sand-asphalt cube at 0°C, tested at various strain levels and frequencies, and from this it can be seen that, after an initial period the Poisson's ratio settles down to realistic values. However, it is not clear why, during the first few hundred pulses, the values were very high. This trend of high values during the initial part of the test was apparent in all the experiments carried out on cubes of material (e.g. Figure 5.8). However, Figure 5.9 shows results from the cube used for Figure 5.7, retested at 32°C demonstrating uniform values for Poisson's ratio. Hence, the initial high values appeared to only be generated when a specimen is initially tested. This would seem to indicate that there is some internal restructuring under applied load but with no measurable permanent deformation taking place. This effect has also been found by Deshpande (7) who explains the phenomenon by the thickening of the bitumen films normal to the applied load and thinning of the films in the direction of the applied load. He also found that, eventually, a steady state condition occurs.

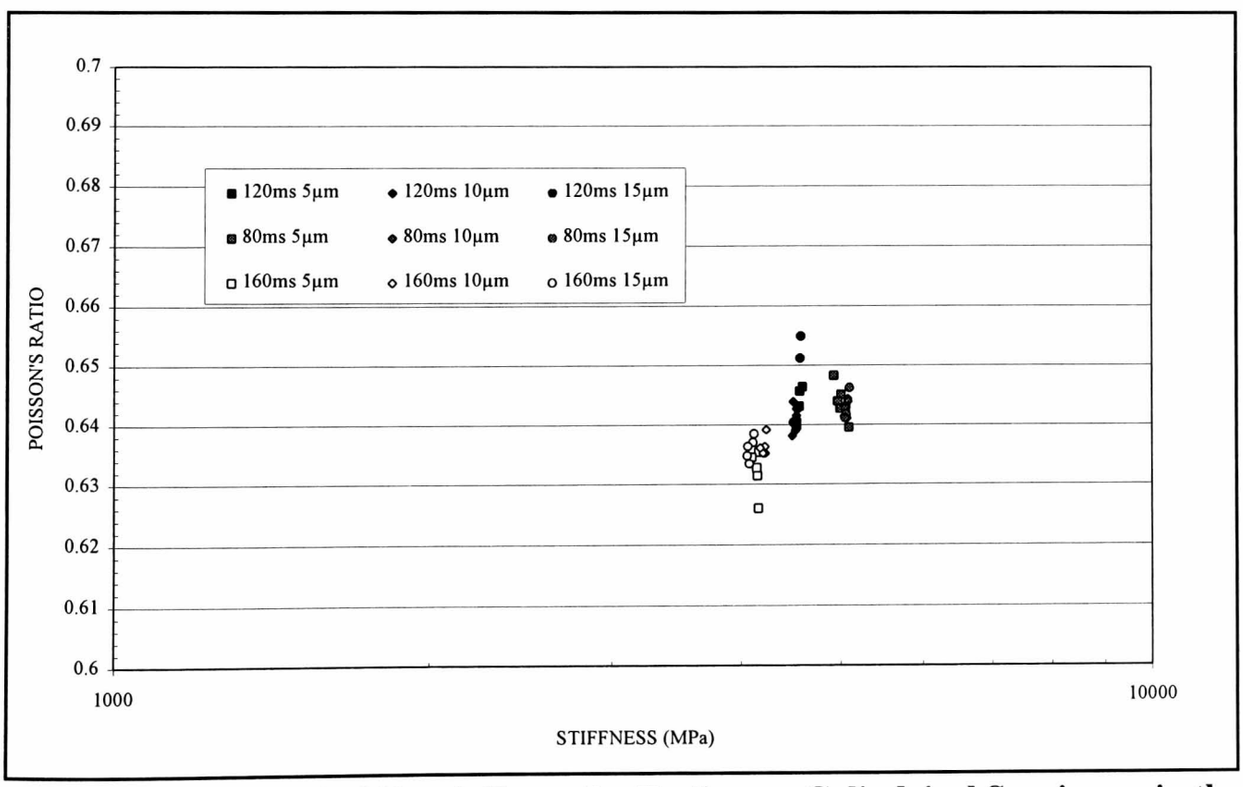


Figure 5.6 - A Typical Result From the Testing on Cylindrical Specimens in the Indirect Tensile Mode, in the NAT.

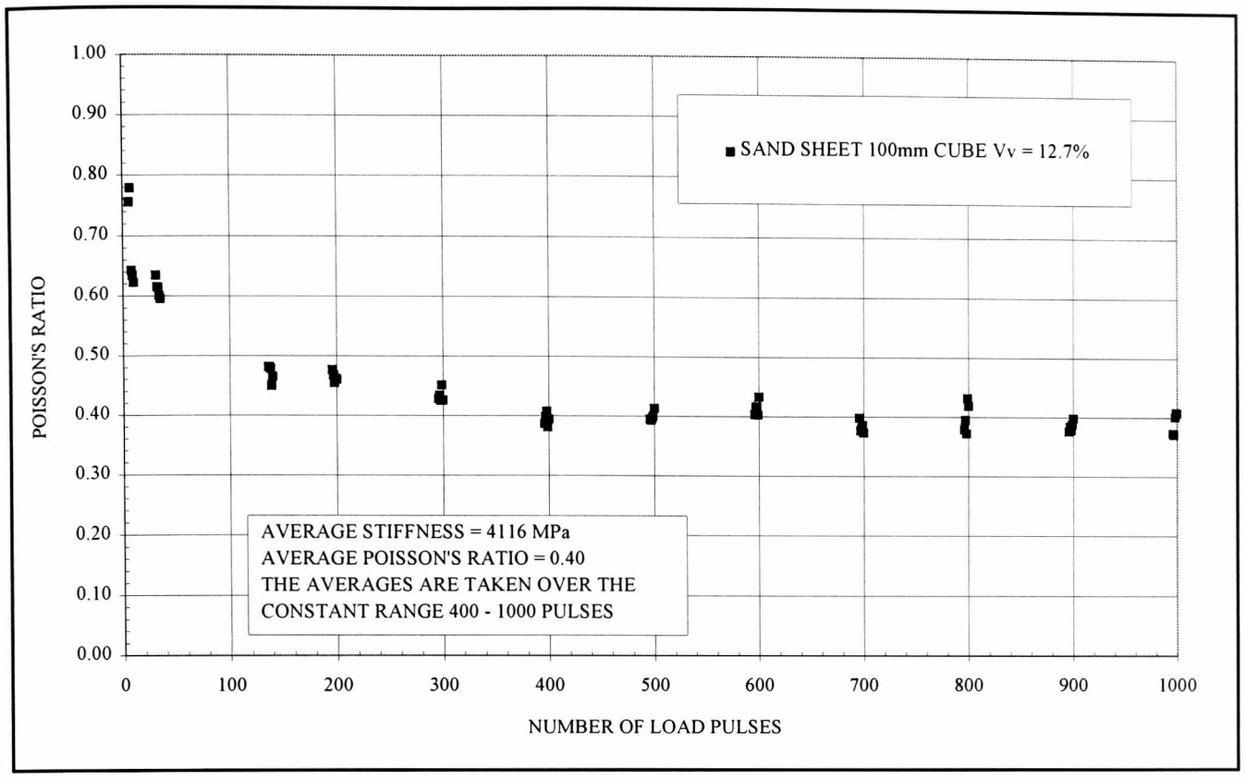


Figure 5.7 - Poisson's Ratio Measured on a 100mm Cube of Sand-Asphalt @ 0°C.

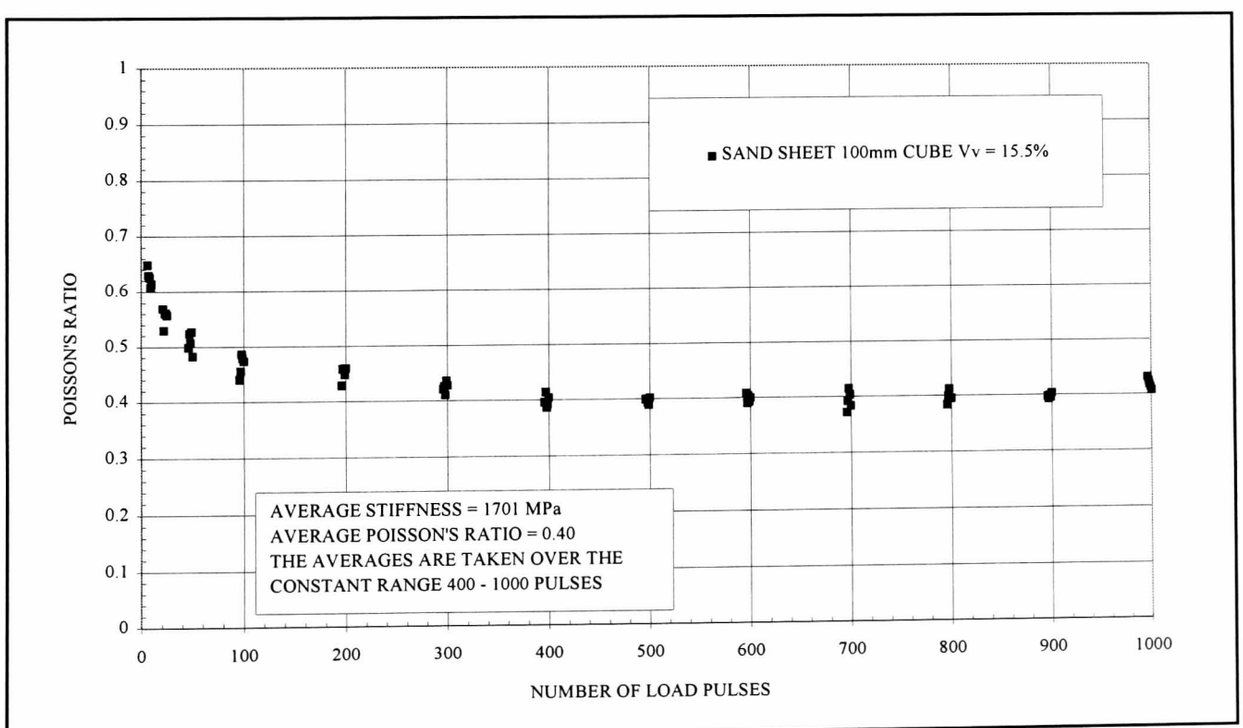


Figure 5.8 - Poisson's Ratio Measured on a 100mm Cube of Sand-Asphalt @ 20°C.

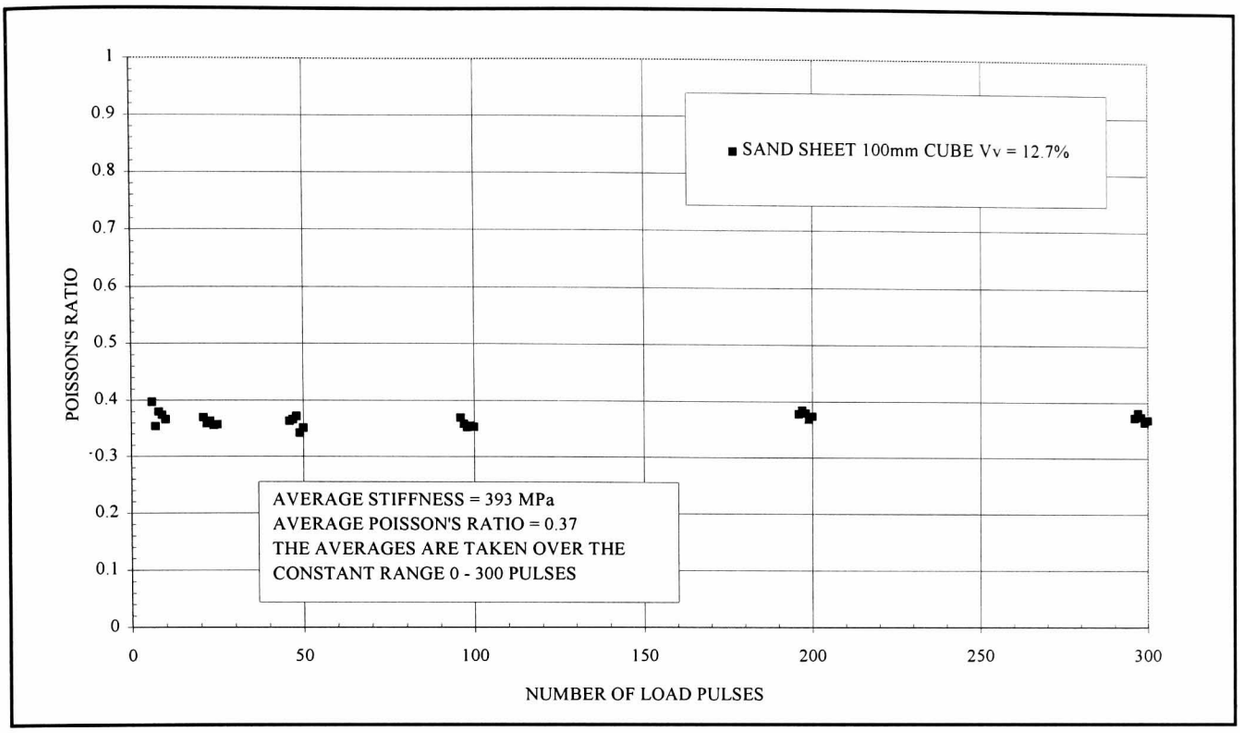


Figure 5.9 - 100mm Cube of Sand-Asphalt Retested @ 32°C Demonstrating that the Restructuring Only Happens During the First Set of Applied Loads.

Figure 5.10 is a summary graph showing values of Poisson's ratios against stiffness modulus for all the cubes tested at a variety of temperatures, including one of a 30/14 HRA . The results indicate that there is no relationship between Poisson's ratio and either temperature or stiffness modulus and that a single value, of the order of 0.35, would seem to be appropriate for use under all conditions. However, there was still a necessity to ascertain if this is a true material effect or merely a manifestation of the testing method. It is for this reason that the aluminium specimens were tested as they should provide consistent values for Poisson's ratio under all temperatures, speeds of loading and during the entire testing period.

5.3.1 Aluminium Cube

Figure 5.11 shows the arrangement of the LVDT's for testing the cube of aluminium. The aluminium was accurately machined to have 100mm sides and flat parallel faces. The LVDT mounting pips were manufactured out of aluminium in order to minimise the weight and, therefore, should have had no effect on the response of the material to the applied loading.

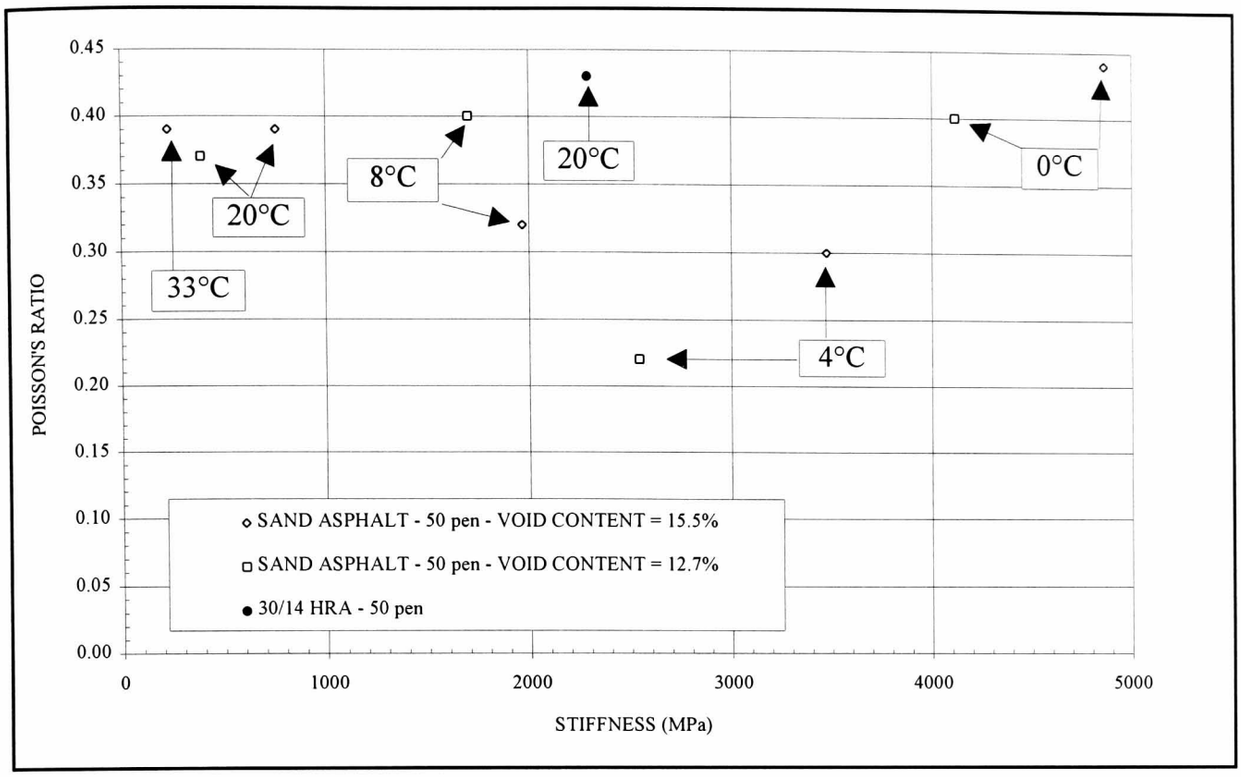


Figure 5.10 - Summary Graph of Poisson's Ratio Against Stiffness Modulus for Cubes of Different Materials and Test Conditions.

From Figure 5.11 it can be seen that two identical measurement systems were used, mounted on opposite faces, ensuring that the response to the applied loading was uniform for the entire cube.

The calculation of Poisson's ratio for a cube is simply the negative ratio of the horizontal strain to the vertical strain. Since the gauge lengths were equal in both directions the data can be presented in terms of the measured deformations and this is done in Table 5.2.

The value of Poisson's ratio for aluminium lies between 0.31 and 0.34 dependent upon the grade of material used. As this testing gave a value in the correct range it indicates that the measurement system works correctly. This demonstrates that the trend which was found when testing bituminous cubes of material (Figure 5.7) was a real material effect and not caused by any external influence. This in turn indicates that in order to achieve correct stiffness results in the indirect tensile test a number of conditioning pulses (500 at low stress and high frequency) should be applied to the specimen.

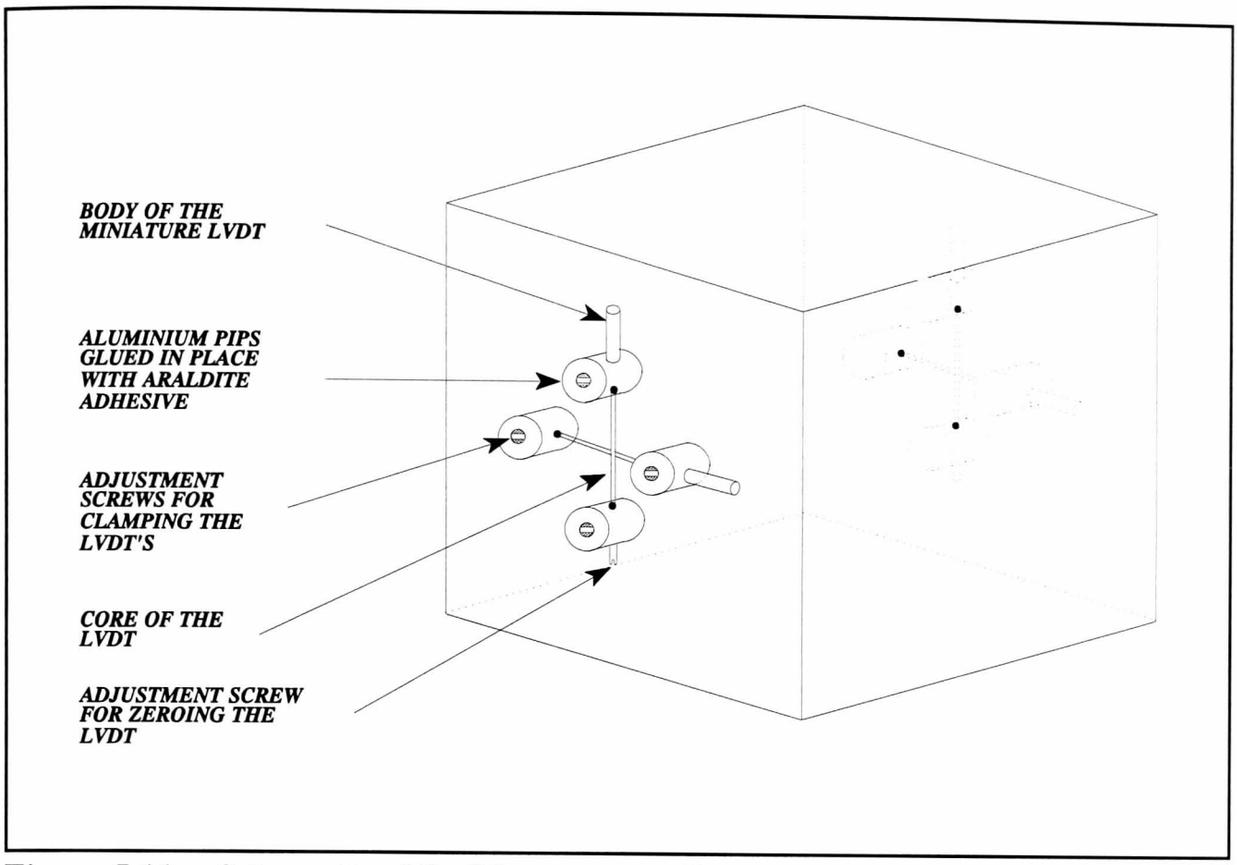


Figure 5.11 - Schematic of the Measurement System Used for the Validation Work on Poisson's Ratio.

Table 5.2 - Poisson's Ratio for the Aluminium Cube.

	LVDT Readings (μm)				Poisson's Ratio (υ)		
Load (kN)	Side 1 Vertical	Side 1 Horizontal	Side 2 Vertical	Side 2 Horizontal	Side 1	Side 2	Average
500	37	8	18	5	0.22	0.28	0.25
1000	67	19	35	11	0.28	0.31	0.30
1500	101	29	53	18	0.29	0.34	0.31
2000	138	43	76	25	0.31	0.33	0.32
					Average Value for last 3 readings *Note 1*		**0.31**

Note 1 The first reading was not included in the average as the sensitivity of the signal conditioning used with the LVDT's was not sufficiently high for the reading to be reliable.

5.3.2 Aluminium Core

A 100mm diameter cylinder 40mm thick was machined out of aluminium and the measurement system, described and validated in section 5.3.1, was mounted on its two

flat faces. The core was tested in the ITFT frame mounted in a servo-hydraulic apparatus. This testing was carried out in order to validate the linear elastic theory used for both the stiffness test and the ITFT. This linear elastic theory gives rise to equation 5.7 for the calculation of Poisson's ratio, the derivation of which is given in Section 5.1.

As all the gauge lengths over which reading were taken were identical the measured deformations can be directly substituted for the strains in the above equation. Table 5.3 presents the results of the testing on the aluminium core.

Table 5.3 - Poisson's Ratio for the Aluminium Core.

	LVDT Readings (μm)				Poisson's Ratio (υ)		
Load (kN)	Side 1 Vertical	Side 1 Horizontal	Side 2 Vertical	Side 2 Horizontal	Side 1	Side 2	Average
1000	110	64	102	61	0.31	0.33	0.32
1500	162	96	166	96	0.32	0.30	0.31
2000	221	130	215	129	0.32	0.33	0.33
						Average Value	**0.32**

As this testing also gives a value of Poisson's ratio in the expected range of 0.31 to 0.34, the linear elastic theory has been validated. This means that, provided the assumption that bituminous materials behave as linear elastic materials under certain conditions (relatively low temperatures and/or fast loading times) is valid, then the stiffness and fatigue measurements made with the NAT are correct. However, it must be restated that Equation 5.7 used for these calculations is based upon point strains at the centre of the specimen and the measurements shown in Table 5.3 are over a gauge length of 25mm. Figure 3.1 indicates that the average strain over the centre 25mm will be marginally lower than the maximum point strain but this is the case for both ϵ_{xmax} and ϵ_{ymax} and, therefore, the quotient of the two will still give approximately the correct answer. This is borne out by the results shown in Table 5.3.

These two pieces of validation work verify the conclusion, from the work reported earlier, that a value of 0.35 is appropriate, for Poisson's ratio, for bituminous materials under the conditions of test likely to be encountered during normal testing.

5.4 Summary

This work has shown that for some bituminous materials, under a wide range of conditions of test, a value of 0.35 can be assumed for Poisson's ratio. It has also shown that during the initial loading of a bituminous specimen some internal restructuring takes place which is thought to be associated with the thickening and thinning of the films of bitumen around the aggregate.

It has also been shown that the linear elastic theory for a cylindrical specimen loaded on a diameter is correct for a linear elastic material. Therefore, assuming that, under certain conditions of test (up to 30°C, risetimes less than 130ms), a bituminous material behaves linear elastically the theory for the indirect tensile stiffness modulus and fatigue test is valid.

5.5 References

1. Roque, R. and Buttlar, W.G., "The Development of a Measurement and Analysis System to Accurately Determine Asphalt Concrete Properties Using the Indirect Tensile Mode," Proceedings of the Association of Asphalt Paving Technologists (AAPT), Volume 61, pp 304-332, 1992.
2. Navarro, D. and Kennedy, T.W., "Fatigue and Repeated-Load Elastic Characteristics of Inservice Asphalt-Treated Materials," Research Report 183-2, Project 3-9-72-183, Centre for Highway Research, University of Texas at Austin, January 1975.
3. Alavi, S.H. and Monismith, C.L., "Time and Temperature Dependent Properties of Asphalt Concrete Mixtures Tested as Hollow Cylinders and Subjected to Dynamic Axial and Shear Loads," Proceedings of the Association of Asphalt Paving Technologists (AAPT), Volume 63, pp , 1994.

4. Cragg, R. and Pell, P.S., "The Dynamic Stiffness of Bituminous Road Materials," Proceedings of the Association of Asphalt Paving Technologists (AAPT), Volume 40, pp 126-193, 1969.

5. Nunn, M.E., "The Characterisation of Bituminous Macadams by Indirect Tensile Stiffness Modulus," TRL Project Report 160, 1995.

6. British Standards Institution, "Hot Rolled Asphalt for Roads and Other Paved Areas," B.S. 594 : Part 1, 1992.

7. Deshpande, V.S., "Deformation Behaviour of Idealised Bituminous Mixes," M.Phil Thesis, Cambridge University Engineering Department, August 1995.

CRACK PROPAGATION

6.1 Introduction

Once crack initiation has taken place in a bituminous road layer the pavement is still capable of sustaining traffic loading. Crack initiation is followed by a period of crack propagation which can be significantly longer than the time required to initiate a crack (1). Therefore, crack propagation is an important phenomenon which needs to be assessed and, if possible, quantified as it is the cracks, when propagated, which cause weakening of the pavement structure. To do this in-situ, as with all fatigue characterisation, is very difficult, hence, surrogate testing methods are needed. Two generic methods have been adopted in previous research; a theoretical approach, based on metallurgy theory (fracture mechanics), and a practical experimental approach, simulating crack propagation. Both methods have merit, but for the purposes of this research it was decided to carry out simulative testing, due to the inherent difficulties encountered by a number of researchers when using fracture mechanics for a 2 or 3 phase bituminous material instead of for continuous material for which the theory was developed (detailed in Section 6.2).

The test method developed for this project is shown schematically in Figure 6.1 and a photograph is given in Plate 6.1. It was developed from apparatus used in previous research into reflective cracking (2) and used a beam of material with two steel plates glued to the bottom. A 10mm gap was left between the plates to act as a crack initiator and the beam was supported at both ends and hinged to allow flexure to take place without imposing restrictive forces. Load was applied by a pneumatic actuator situated above the beam directly above the gap in the steel plates with a second actuator beneath the beam to return it to the normal position after each load pulse.

The system was controlled by a computer to apply the load with the same waveform used in the NAT, with a 120ms risetime, thus, allowing the stiffness data gathered, for the

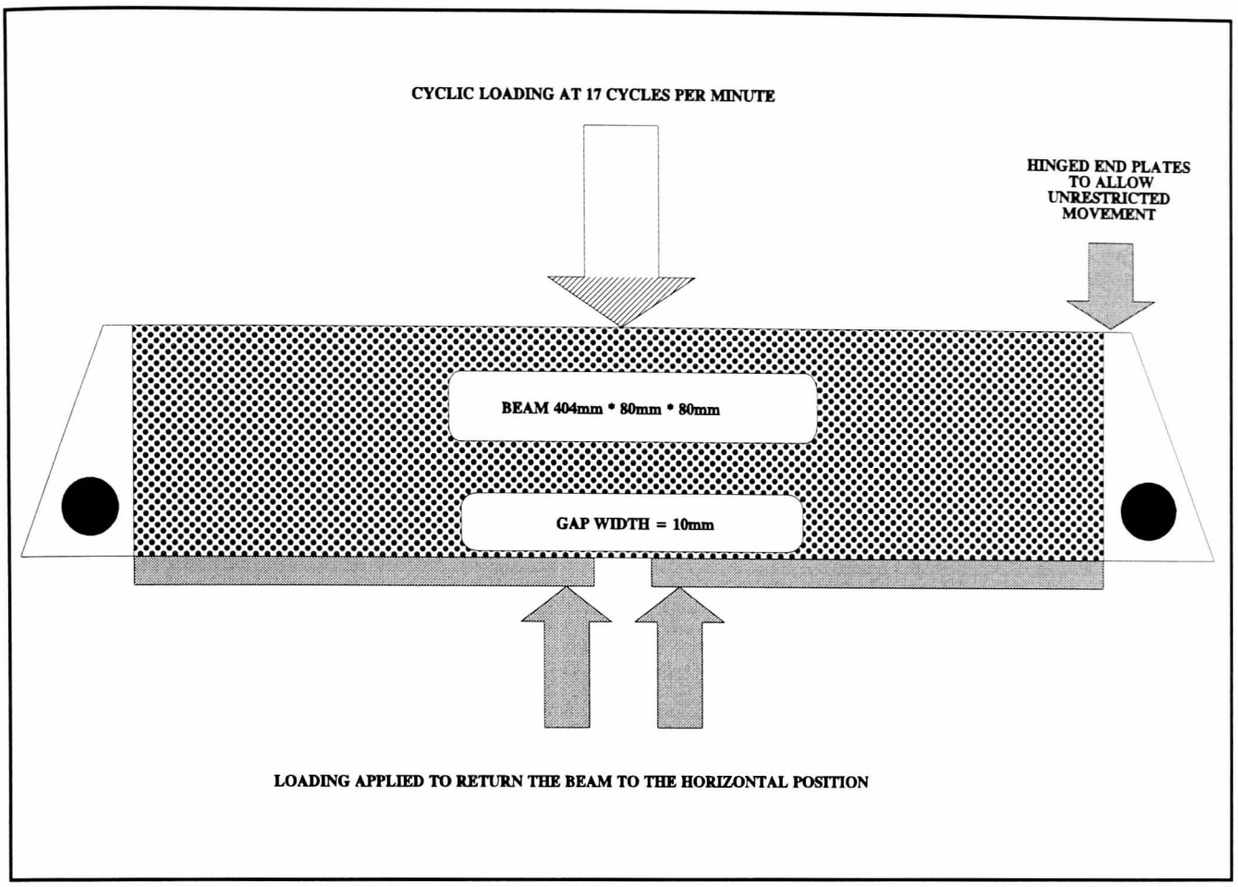


Figure 6.1 - Schematic Showing the Test Configuration for Crack Propagation.

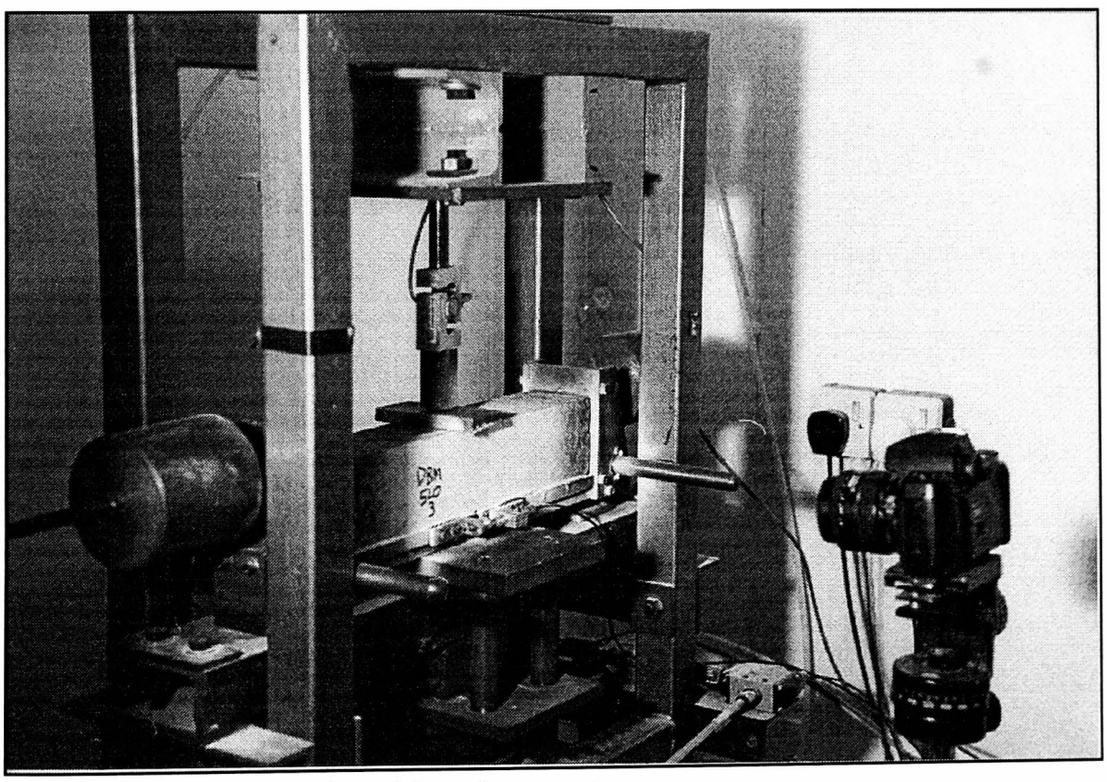


Plate 6.1 - Beam Cracking Apparatus.

same mixtures, in the ITFT programme to be used. The controlling parameter was the strain measured across the gap between the steel plates. The displacement, over the gauge length of 10mm, was monitored using LVDT's mounted on either side of the beam, the outputs of which were averaged and the value used for the control of the test. The crack that developed on the surface of the beam, as the test progressed, was photographed using a computer controlled camera and these images were then analysed using state-of-the-art image analysis equipment and software (Section 6.3). The crack was made more visible by the application of white paint to the surface of the beam. The second form of analysis examined the fall off of the load as the test progressed. It was decided to stop the test once the load reached 25% of its' original value, as little change occurred after this reduction due to the crack tip approaching the neutral axis of the beam. The level of strain across the gap in the steel plates, in the main test program, was 8,500 microstrain. This value was selected, after analysis of the specimens tested in the pilot programme, because the average length of test for each specimen was required to be of the order of 24 hours in order to complete the main test program in the time available. The number of load applications to failure, as defined above, then allowed a ranking of the materials and assessment of the material parameters which had an effect on the resistance to crack propagation.

6.2 Fracture Mechanics

Fracture mechanics for bituminous materials has been developed from theory originating in the field of metallurgy, notably by Paris (3) and Rice (4). The theory has allowed metallurgists to predict the rate of crack propagation up to the end of stage III cracking.

The definitions of the four stages of cracking, in metals, are:

Stage I	Nucleation event during which microstructurally small cracks form,
Stage II	Period of small crack growth in which the path can be strongly influenced by microstructure,

Stage III The crack has become sufficiently large for continuum mechanics to apply. Growth rate behaviour is now quantified by linear elastic fracture mechanics and

Stage IV Final stage of unstable rapid growth as the fracture toughness of the material is approached.

Stage III cracking is the area of particular interest for crack propagation. When the observed crack propagation rate (dc/dN) is plotted against the stress intensity factor (K_1) on a log-log scale (Figure 6.2) a sigmoidal variation curve is usually obtained. The central part of such a curve is approximately linear and may be described by Paris's law:

$$\frac{dc}{dN} = A \cdot \Delta K_1^n \qquad \textbf{(6.1)}$$

Equation 6.1 may be integrated to allow the calculation of the number of load applications (N) to reach the unstable fast fracture stage IV cracking:

$$N = \int_{c_1}^{c_2} \frac{dc}{A \cdot \Delta K_1^n} \qquad \textbf{(6.2)}$$

Where:

c	=	Crack length (mm),
c_1	=	Crack length at start of integration period (mm),
c_2	=	Crack length at end of integration period (mm),
N	=	Number of stress cycles for crack to propagate between c_1 and c_2,
A	=	Regression constant,
n	=	Regression constant and
ΔK_1	=	Stress intensity factor range (Mpa·mm^{½}).

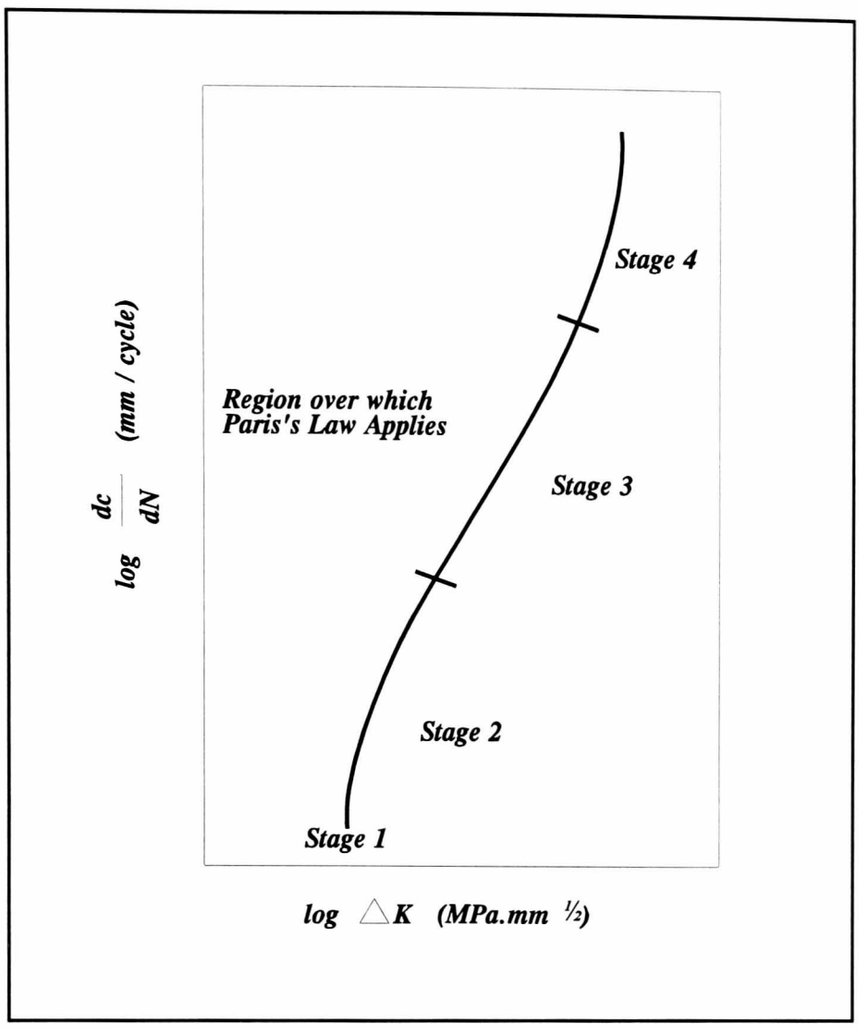


Figure 6.2 - Graph Demonstrating the Region Over Which Paris's Law Applies.

The stress intensity factor range for finite plates can be expressed in the form:

$$\Delta K_1 = K_{max} - K_{min} = Y \cdot \Delta\sigma \cdot \sqrt{\pi c} \qquad \textbf{(6.3)}$$

K_{max} = Stress intensity factor at the maximum applied stress level,

K_{min} = Stress intensity factor at the minimum applied stress level,

$\Delta\sigma$ = Applied stress ($\sigma_{max} - \sigma_{min}$) and

Y = Dimensionless factor dependent upon geometry.

For the flexure test used in the main test programme, Y the geometric factor is given by Equation 6.4 (5):

$$Y = \frac{1}{\sqrt{\pi}}\left[2.17 - 4.24\left(\frac{c}{L}\right) + 20.53\left(\frac{c}{L}\right)^2 - 35.21\left(\frac{c}{L}\right)^3 + 29.51\left(\frac{c}{L}\right)^4\right] \qquad \textbf{(6.4)}$$

Where:

L = Beam Height (mm).

The stress intensity factor is used to define the stress field near a crack tip and when it reaches a critical value, K_{1c}, the crack growth becomes unstable (stage IV). The crack growth velocity then tends toward infinity and the specimen collapses. K_{1c} is called the plane strain fracture toughness.

For Equation 6.2 to apply, certain assumptions must be made:

- The material behaves as a homogenous single phase solid,
- The material behaves isotropically,
- The material is continuous,
- Non-linear deformation is restricted to a small zone near the crack tip and
- The bulk material outside of the non-linear deformation zone behaves in a linear elastic manner.

Bituminous materials are not homogenous and contain more than one phase (bitumen, different aggregate types, sand, filler, air and even fibres) and research has shown that they do not behave isotropically (6) and that they are discontinuous. Due to the difficulties in analysing bituminous materials at the microscopic level, it is difficult to ascertain whether there is small or large scale yielding in the region of the crack tip.

Bituminous materials are visco-elastic and, therefore, the last assumption is also incorrect, unless the material is loaded very quickly and/or at low temperature. However, elastic-plastic fracture mechanics has been developed (4) for non-linear materials which

allows the intensity of the crack tip fields to be characterised and, hence, the strain concentration around the crack tip. When the elastic strains are negligible compared to the non-linear strains near the crack tip, this theory uses the path independent J-Integral. This theory also makes certain assumptions:

- The crack tip is subject to a two dimensional deformation field (plane strain, generalised plane stress, antiplane strain),
- The zone around the crack tip is elastic, plastic or elasto-plastic,
- The crack tip is rounded, as the analysis is not meaningful for a sharp crack tip and
- Only small-scale yielding, in relation to the size of the elastic or plastic zone, occurs.

Although this method takes plasticity into consideration, it makes no allowance for viscous flow. It is not known whether the zone around the crack tip for a bituminous material is elastic, plastic, viscous or a combination of these which changes with temperature and/or loading time and, therefore, it is difficult to apply the theory with any confidence. The assumption that a two dimensional deformation field exists around the crack tip has not been verified for bituminous materials and whether the crack tip is sharp or rounded (this affects the magnitude of the deformation zone around the crack tip) is unknown making the theory difficult to apply with any confidence. It is also difficult to assess whether the assumption concerning small scale yielding is correct, again making the theory difficult to apply with any confidence.

All of these incorrect assumptions give an indication of why researchers (5, 7, 8) have failed to generally apply linear elastic or elastic-plastic fracture mechanics for crack propagation computations in bituminous materials, although they have had limited success in applying it to discrete sets of data under ideal conditions. The unsuccessful attempts to apply fracture mechanics are indicated by comparing the critical stress intensity factors obtained by the researchers (5, 7, 8) which show a large variation between 2 and 35 $MPa \cdot mm^{1/2}$. However, during the early seventies, Schapery developed, during a series of papers in the International Journal of Fracture, 'A theory of crack

initiation and growth in viscoelastic media' (9, 10, 11) allowing the calculation of both time to crack initiaition and for crack propagation. This theory was originally developed for visco-elastic polymers but Jacobs (12) has had success in applying a modified version to bituminous materials. This theory also has a number of assumptions but in this case many can be ignored as they are either relatively insignificant or realistic. However, there are five which are necessary for the theory to be developed into a useable form:

- There is a sharp crack tip
- The effect of shear stress on the crack tip is negligible
- The crack cannot decrease in size ($dc/dn \geq 0$)
- The stress normal to the surface of the crack (σ_y) must be independent of stiffness and Poisson's ratio
- Poisson's ratio must be constant

The geometry of the crack tip is unknown and as the assumption that there is a sharp crack tip is required in order to neglect the effect of shear stress, it is important to be able to accurately define the geometry. The assumption that the crack tip cannot decrease in size is not shown in practice as cracks heal over time due to viscous flow of the binder and stress reversal due to traffic. It has been shown that, for a bituminous material, stress and stiffness are mutually dependent and, therefore, it would appear that the fourth assumption may be incorrect. Finally, it is demonstrated in Chapter 5 that Poisson's ratio can very with time although, as this only appears to happen over the first few load applications, the final assumption is probably valid.

Although there appear to be a number of incorrect assumptions in this theory, as far as bituminous materials are concerned, it is the author's opinion that this final methodology offers significant promise as a future method of modelling crack propagation and the work carried out by Jacobs (12) has made a significant start.

If fracture mechanics had of been used in this work the methodology would have followed that presented in Figure 6.3 which shows five graphs. Graphs I and IV require finite element analysis and graph II is generated from the testing (Figures 6.5-6.10). By

combining graphs I and II graph III is developed and then combining graph III with graph IV produces the final graph which allows the constants, A and n, for Paris's law to be calculated, as depicted in Figure 6.2. However, as the tools and time were not available to the author to carry out the finite element work the fracture mechanics calculations were not carried out and no further use will be made of fracture mechanics other than as a recommendation for future work.

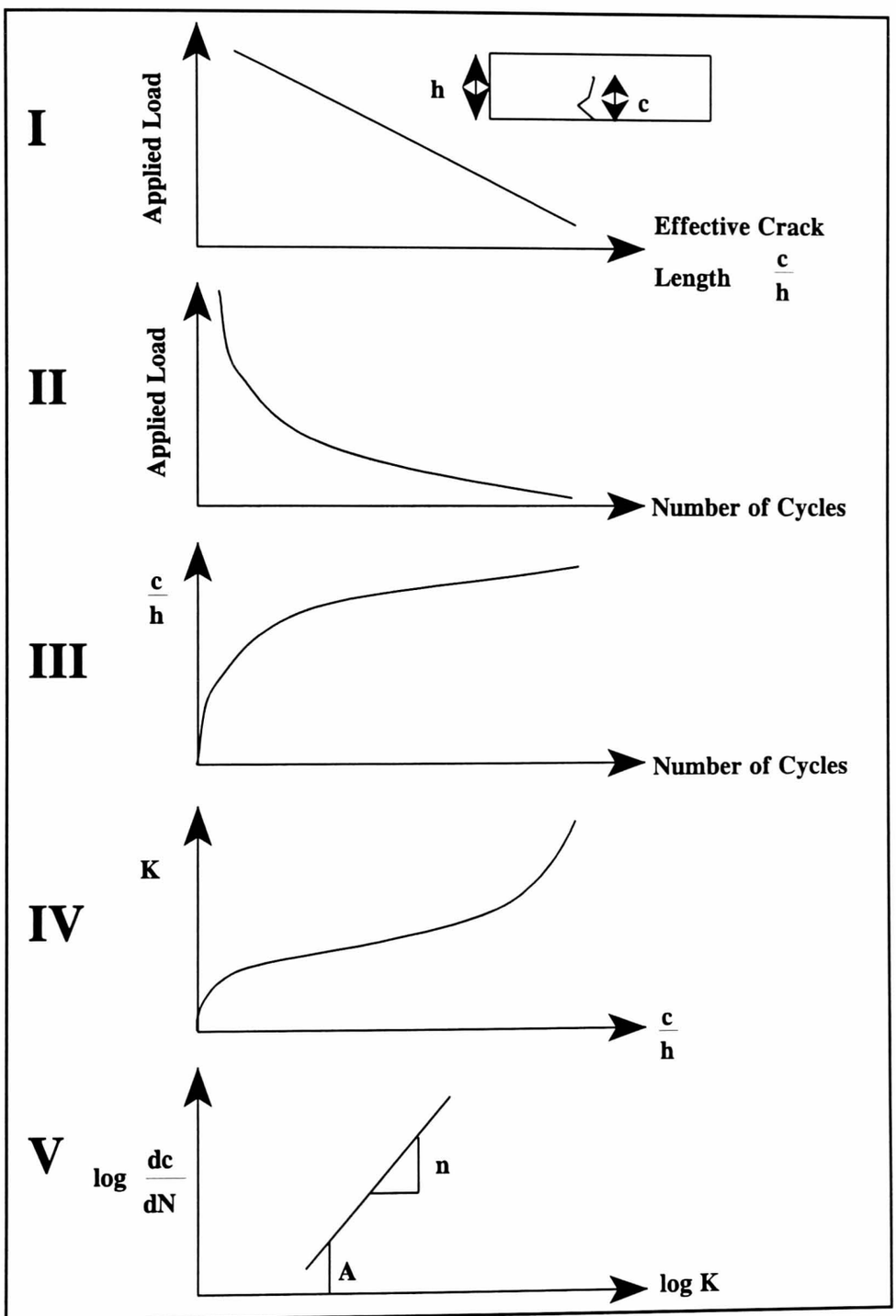


Figure 6.3 - Schematic Demonstrating the Five Steps in Calculating the Paris Law Constants for Use in Fracture Mechanics Calculations.

6.3 Image Analysis

Image analysis equipment was used for one method of determining of the rate of crack propagation. The equipment was used to analyse photographs of the beams, which were taken at specific reductions in the stiffness of the beam showing varying stages of cracking, and consisted of:

- A high quality servo-controlled CCD camera, the functions of which (focus, zoom, aperture and iris) were controlled via the computer. The camera had the red, green and blue colours on separate chips allowing exceptionally high quality images to be obtained for subsequent analysis.
- A Neotech frame grabber, installed in the computer, which digitised the image received from the camera. The controlling software for the frame grabber also allowed some manipulation of the image (sharpening, smoothing, Fourier transforms etc.) in order to ensure the correct image was obtained prior to analysis.
- A high specification Apple Macintosh computer (model 8100/80 Powermac) which allowed high speed processing, essential as each image contained up to 8Mb of information. The computer had a specially designed monitor which had the resolution required for the high quality images produced by the camera.

The software obtained for use with the above system was "Optilab Pro" which is a state-of-the-art package capable of processing and analysing in excess of thirty images at the same time. Therefore, processing and analysing all the images from one specimen was able to be done at the same time, reducing work and increasing the speed of analysis. Some additional software, "Adobe Photoshop", was also obtained which allowed the processed images to be annotated and to be exported to PC based systems.

The overall system, as described above, allowed the measurement of the true crack length on the surface of the beam, as opposed to the methods which have been applied previously (2, 5). These only measured the linear distance the crack had travelled and did not take into account the actual distance, Figure 6.4. It was, therefore, expected that this

novel method of crack length measurement would allow a better assessment of the rate of crack propagation in the test specimens.

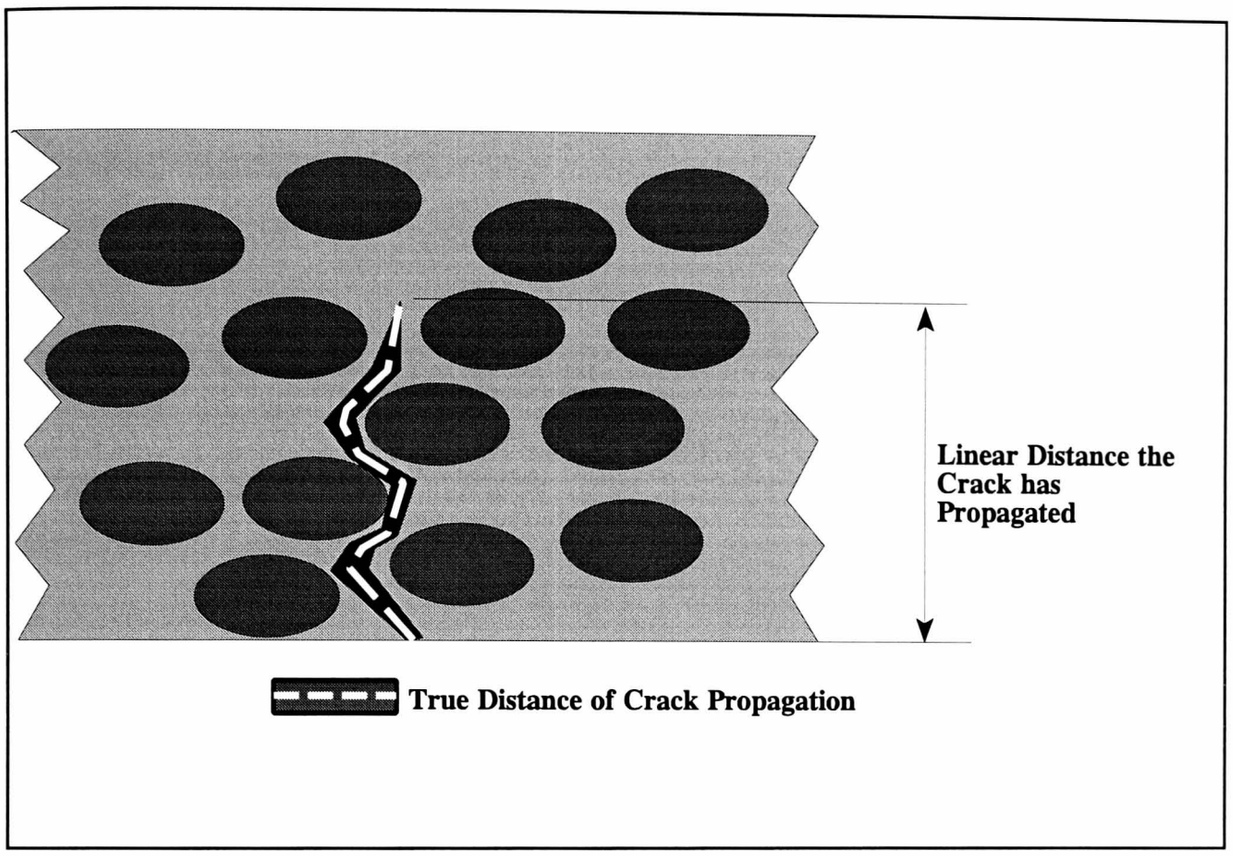


Figure 6.4 - Schematic Showing that the True Distance of Crack Propagation is Longer than the Linear Distance Measured by Previous Research.

6.4 Pilot Test Programme

This was carried out to investigate the test parameters and conditions which should be used for the main test programme. It consisted of testing eighteen beams of a 20mm DBM material, the details of which are shown in Table 6.1. This material was chosen as it was expected that it would have crack propagation properties between those of the other two mixtures to be evaluated.

The test parameters and conditions evaluated were:

- Method of test control (stress, strain or crack opening),
- Strain level,
- Temperature susceptibility,

- Method of volumetric measurement (sealed, unsealed and geometric),
- Beam geometry,
- Method of image capture and storage and
- Method of monitoring the position of the crack.

6.4.1 Results

Evaluating the method of test control was carried out, in a third year undergraduate project under the supervision of the author, prior to the pilot test programme (13). After reviewing the available literature and carrying out some validation tests, the method of control considered most suitable was the strain developed across the gap between the steel plates. The deflection across the gauge length of 10mm was sufficiently large to measure accurately and the LVDT's were easy to position. The beam geometry was investigated. A beam 404mm (length of the compaction mould) long with an 80mm square section was found suitable. All beams were sawn from a slab of material 404 × 280 × 127mm produced in accordance with the protocol given in Appendix A.

The average level of applied strain, in order to fail the beams, on average, in 24 hours, was 8,500 microstrain. Figure 6.5 shows results from a test at 7,500 microstrain indicating that the failure condition had not been reached in 24 hours. By contrast, Figure 6.6 demonstrates that the chosen level of strain (8,500 microstrain) fails the beam within an acceptable time period.

Initially the testing apparatus was not temperature controlled and it was found that this led to a high variability in the response of the beams to the applied load. Therefore, the decision was taken to house the apparatus inside a temperature controlled room. Testing was then carried out at 0°C, 10°C and 20°C and this indicated that temperature influenced the magnitude of the difference between results but did not change the ranking and, hence, all further testing was carried out at 20°C. This prevented further variability in the results due to temperature.

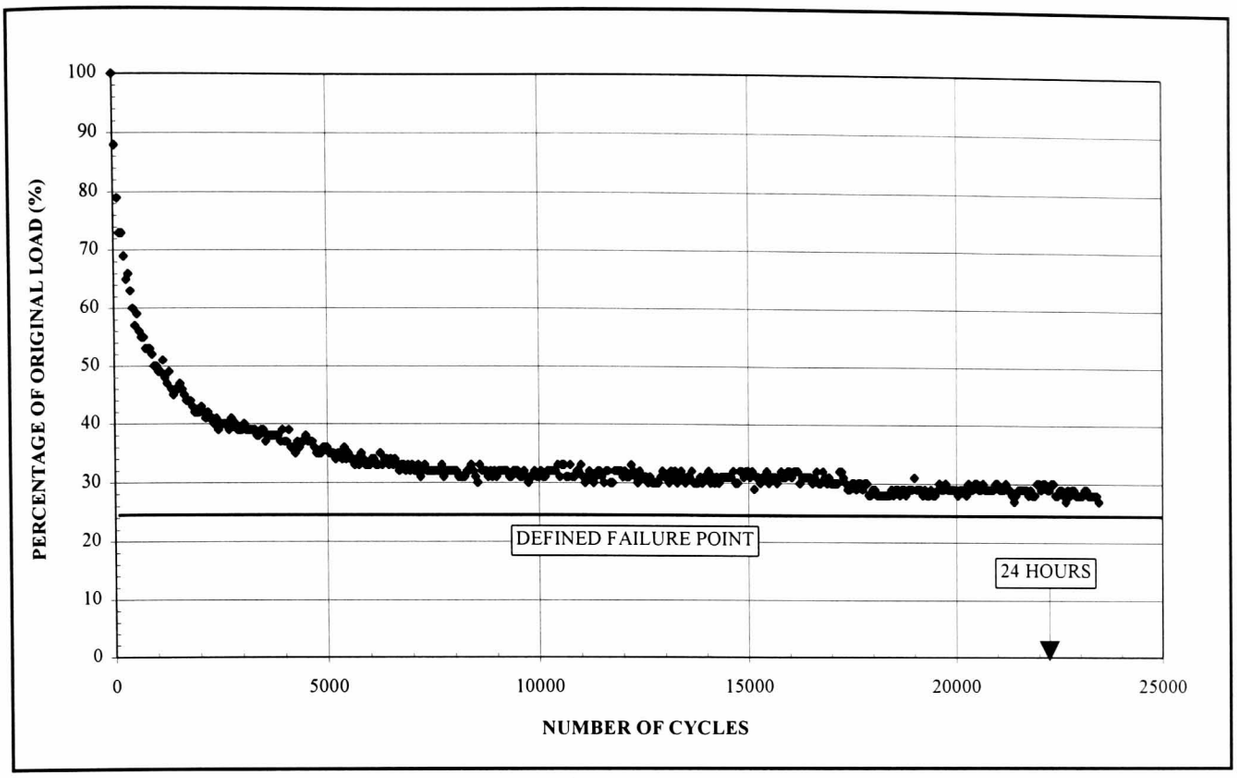


Figure 6.5 - Typical Beam Tested @ 7,500 microstrain.

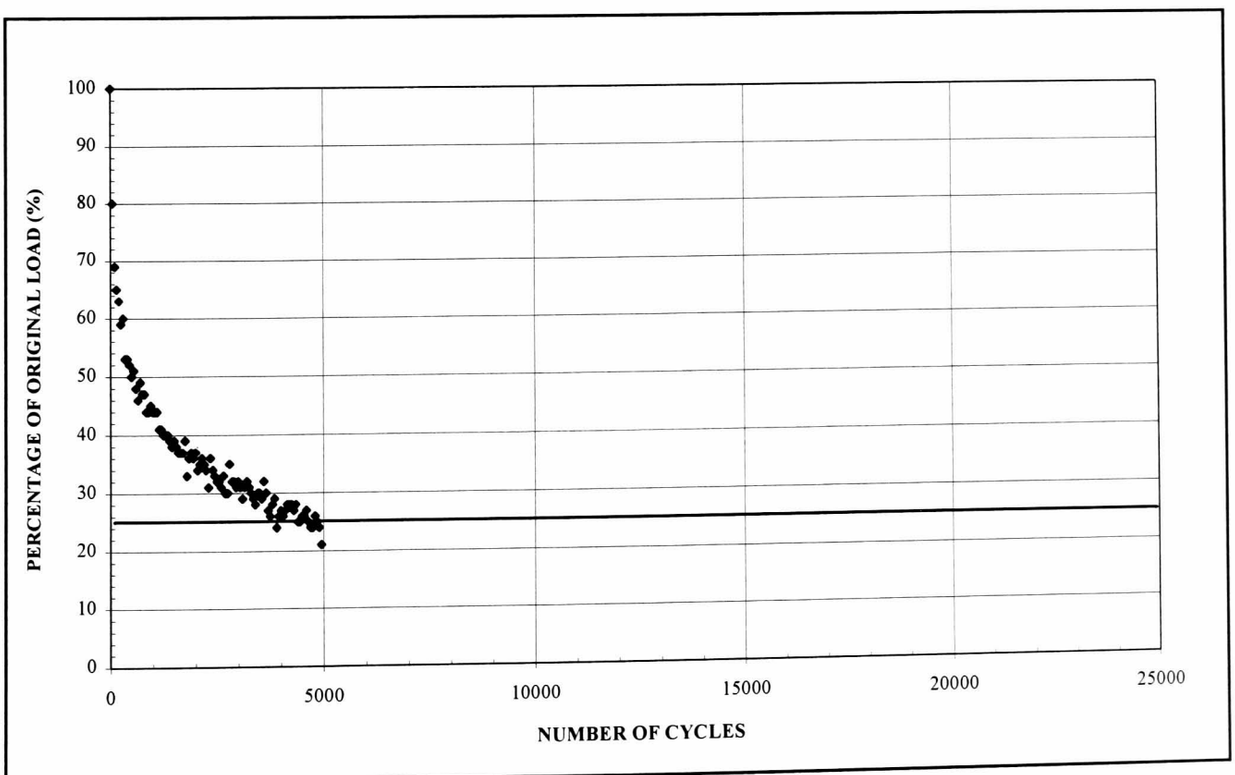


Figure 6.6 - Typical Beam Tested @ 8,500 microstrain.

The method of volumetric measurement was investigated, as the work involved in sealing the 216 beams, for the main test programme, prior to density measurement and stripping them afterwards, was considerable (approximately 1 hour per beam). It was hoped that accurate geometric measurements, on a large specimen, would allow the calculation of the density with an acceptable accuracy. However as can be seen in Table 6.1, and graphically in Figure 6.7, the differences between the three proposed methods was large and it was, therefore, decided that all the density measurements would have to be carried out using the sealed method.

The majority of the beam tests, in the pilot study, were used to ascertain how best to capture images, at what rate and under what lighting conditions. The ideal method of capturing the images would have been to use the image analysis equipment controlled by the same computer as the test itself. This was not feasible as it would have required sole use of the image analysis equipment which had demands from other research projects. Therefore, a high quality camera, with a databack for image referencing, was used. The rate of image capture was chosen to be 12 photographs per beam as this allowed the three replicates of each beam type to be stored on one film. The lighting conditions proved to be the greatest problem as external lighting, needed at fast shutter speeds, raised the temperature of the beam, interfering with the temperature control. To overcome this, the background lighting in the temperature controlled room was made as bright as possible, while the beam was placed as far from the light source as was practical. After many attempts, an appropriate configuration, aperture, shutter speed and level of background illumination was achieved which provided clear, sharp and bright images suitable for image analysis, an example of which is shown in Plate 6.2. Monitoring the crack also proved to be a difficult problem. In order to observe the crack clearly a suitable coating needed to be found. Various white coatings were tried and the best was found to be a car primer. This did not shatter as both Plaster of Paris and whitewash did and did not disguise crack growth, as polymer modified paints did. The car primer was applied by aerosol allowing a good surface finish to be obtained.

Table 6.1 - Geometries and Volumetrics of the Specimens Used for the Pilot Test Programme.

SPECIMEN NAME	LENGTH (mm)	WIDTH (mm)	HEIGHT (mm)	Bulk Specific Gravity (Geometric)	Bulk Specific Gravity (Sealed)	Bulk Specific Gravity (Unsealed)	Maximum Specific Gravity	V_V (%)[Note 1]	VMA (%)[Note 1]	V_B (%)[Note 1]
1A	404.0	81.2	80.7	2.379	2.416	2.423	2.539	4.8	16.0	11.2
1B	404.0	79.8	81.0	2.378	2.409	2.415	2.539	5.1	16.2	11.1
1C	404.0	81.7	81.0	2.329	2.403	2.422	2.539	5.4	16.4	11.0
2A	404.0	81.6	80.9	2.385	2.409	2.415	2.539	5.1	16.2	11.1
2B	404.0	79.9	79.7	2.387	2.408	2.412	2.539	5.2	16.2	11.0
2C	404.0	82.5	81.1	2.390	2.408	2.414	2.539	5.2	16.2	11.0
3A	404.0	80.5	80.9	2.377	2.400	2.411	2.539	5.5	16.5	11.0
3B	404.0	80.0	80.6	2.383	2.400	2.404	2.539	5.5	16.5	11.0
3C	404.0	82.6	81.1	2.346	2.387	2.405	2.539	6.0	17.0	11.0
4A	404.0	81.3	81.5	2.375	2.405	2.410	2.539	5.3	16.4	11.1
4B	404.0	81.3	79.9	2.382	2.410	2.414	2.539	5.1	16.2	11.1
4C	404.0	80.1	80.6	2.390	2.401	2.407	2.539	5.4	16.5	11.1
5A	404.0	80.0	81.3	2.403	2.436	2.445	2.541	4.1	15.3	11.2
5B	404.0	80.9	80.1	2.417	2.447	2.453	2.541	3.7	14.9	11.2
5C	404.0	80.6	82.5	2.410	2.434	2.443	2.541	4.2	15.3	11.1
6A	404.0	80.2	81.1	2.417	2.432	2.443	2.541	4.3	15.4	11.1
6B	404.0	80.5	80.5	2.432	2.447	2.452	2.541	3.7	14.9	11.2
6C	404.0	80.5	80.6	2.426	2.435	2.444	2.541	4.2	15.3	11.1

Note 1 All volumetric calculations were carried out using the sealed specific gravity measurement.

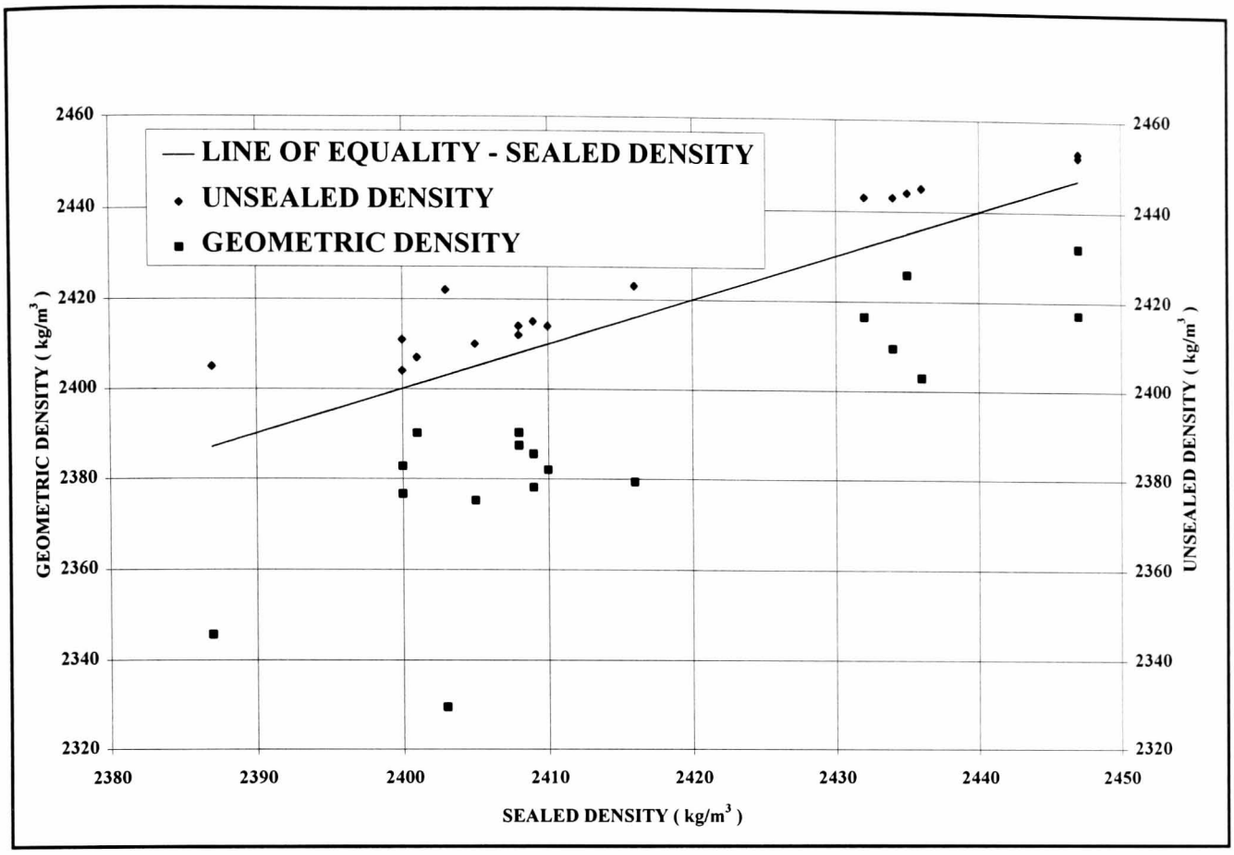


Figure 6.7 - Comparison of Different Methods of Volumetric Determination.

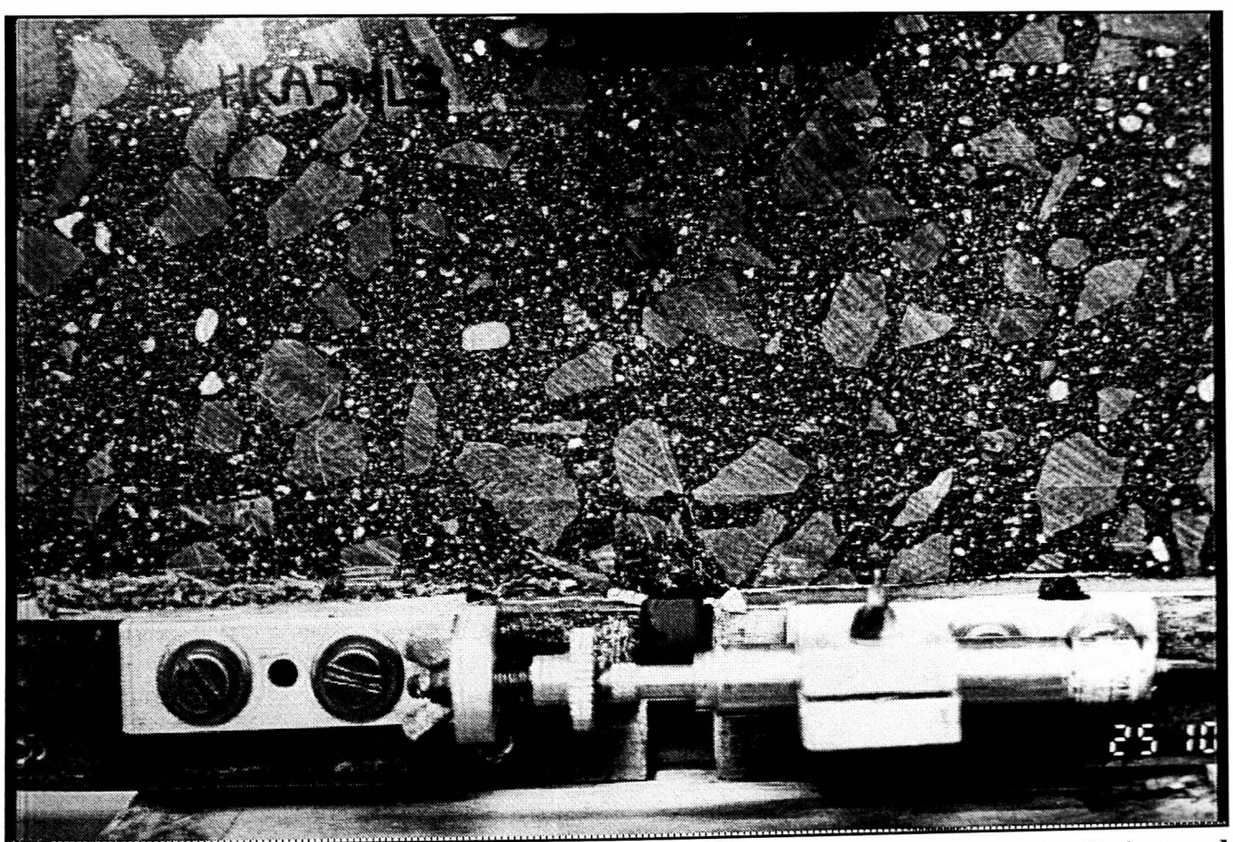


Plate 6.2 - Digitised Image of Beam - Prior to Application of White Paint and Testing.

6.5 Main Test Programme

The main test programme was designed to determine which material properties affect the resistance to crack propagation in a bituminous mixture.

Three material types were selected:

- Hot Rolled Asphalt - 30/14 (HRA) - Mid specification grading (14),
- Dense Bitumen Macadam - 20mm (DBM) - Mid Specification grading (15) and
- Heavy Duty Macadam - 40mm (HDM) - Mid specification grading (15).

Four binder types were selected:

- 50 pen,
- 100 pen,
- SBS modified bitumen[Note 1] and
- EVA modified bitumen[Note 1].

Note 1 The two polymer modified bitumens were supplied pre-blended.

Three binder contents were selected:

- Optimum[Note 1] less one percent,
- Optimum and
- Optimum plus one percent.

Note 1 Optimum is defined as the Marshall optimum for the HRA and as the middle of the British Standard for the two continuously graded mixtures.

Two void contents were selected:

- A void content in the middle of the normal operating range and
- A high void content 2% above the middle of the operating range.

These various combinations entailed the manufacture of 72 slabs of material with 3 beams (replicate testing) being taken from each slab. Thus, there were 216 beams to

manufacture and test. These beams were tested under the experimental conditions described in Section 6.4.1.

Figures 6.8-6.10 are shown here to demonstrate that the method of testing was appropriate. They also show that beam 2 of each set of replicates generally gave longer lives than the other two. Beam 2 is the centre beam cut from the slab and as such is not subject to edge restraints during compaction. Therefore, the aggregate structure is allowed to find its' preferred orientation. The two outside beams are subject to restraint from the mould which, it is thought, affects the particle structuring.

Plate 6.3 shows a digitised image of the beam in Plate 6.1, coated with primer with a crack through it. Plate 6.4 shows the ability of the image analysis system, as the crack has been superimposed onto the uncoated image. This allows the path taken by the crack to be analysed, which was not previously possible.

The main test programme described here was streamlined due to the extremely high performance, long test time, of the SBS modified materials. This streamlining has meant that only two material types have been evaluated (HRA and DBM) and for the majority of the polymer modified materials only one out of the three beams manufactured has been tested. Although it would have been desirable to have completed the test programme as planned the data still had the following variations:

- Two materials types (30/14 HRA and 20mm DBM),
- Two bitumen types (50pen and 100pen),
- Three binder contents (optimum, optimum +1% and optimum -1%),
- Two compaction levels (normal and normal +2%) and
- Three replicates of each material.

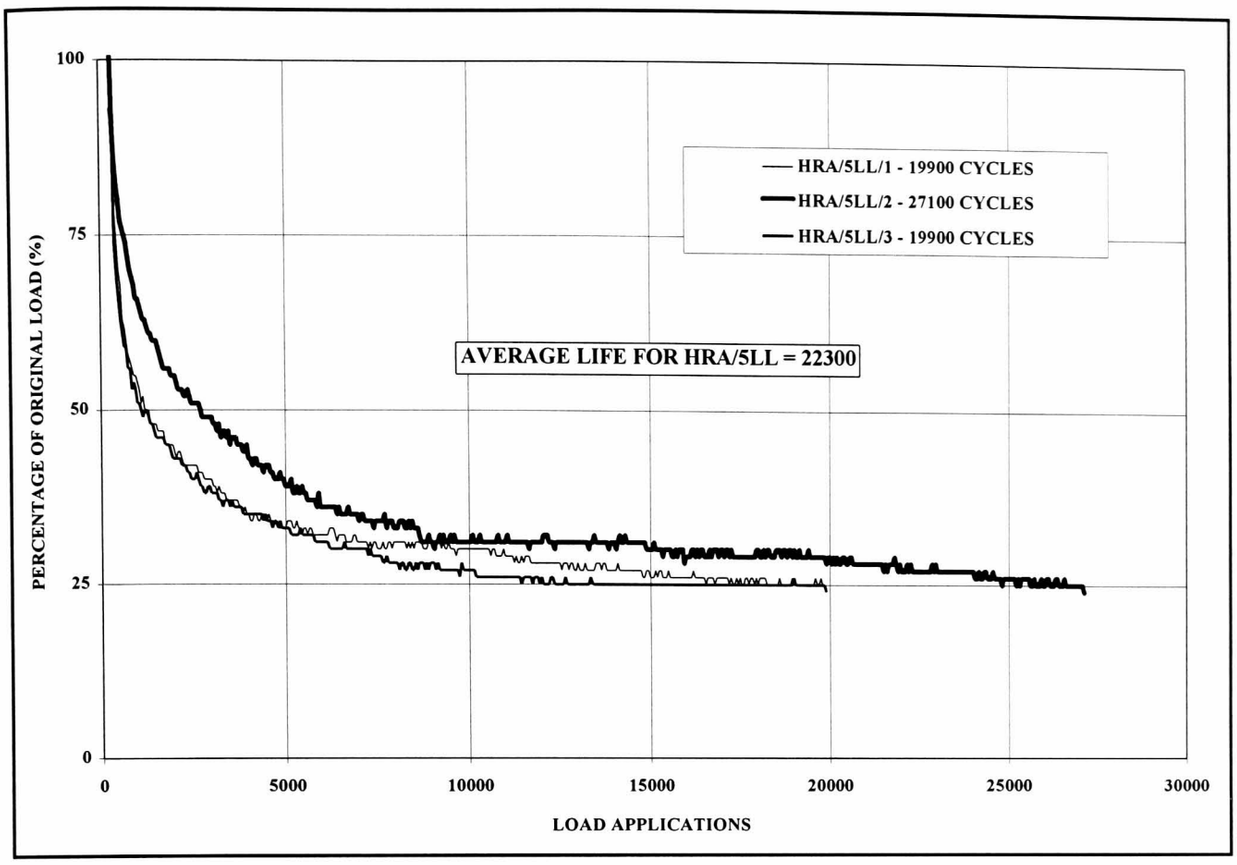


Figure 6.8 - Beam Test Result for Specimens HRA/5LL - Hot Rolled Asphalt, 50 pen Bitumen, Low Void Content and Low Binder Content.

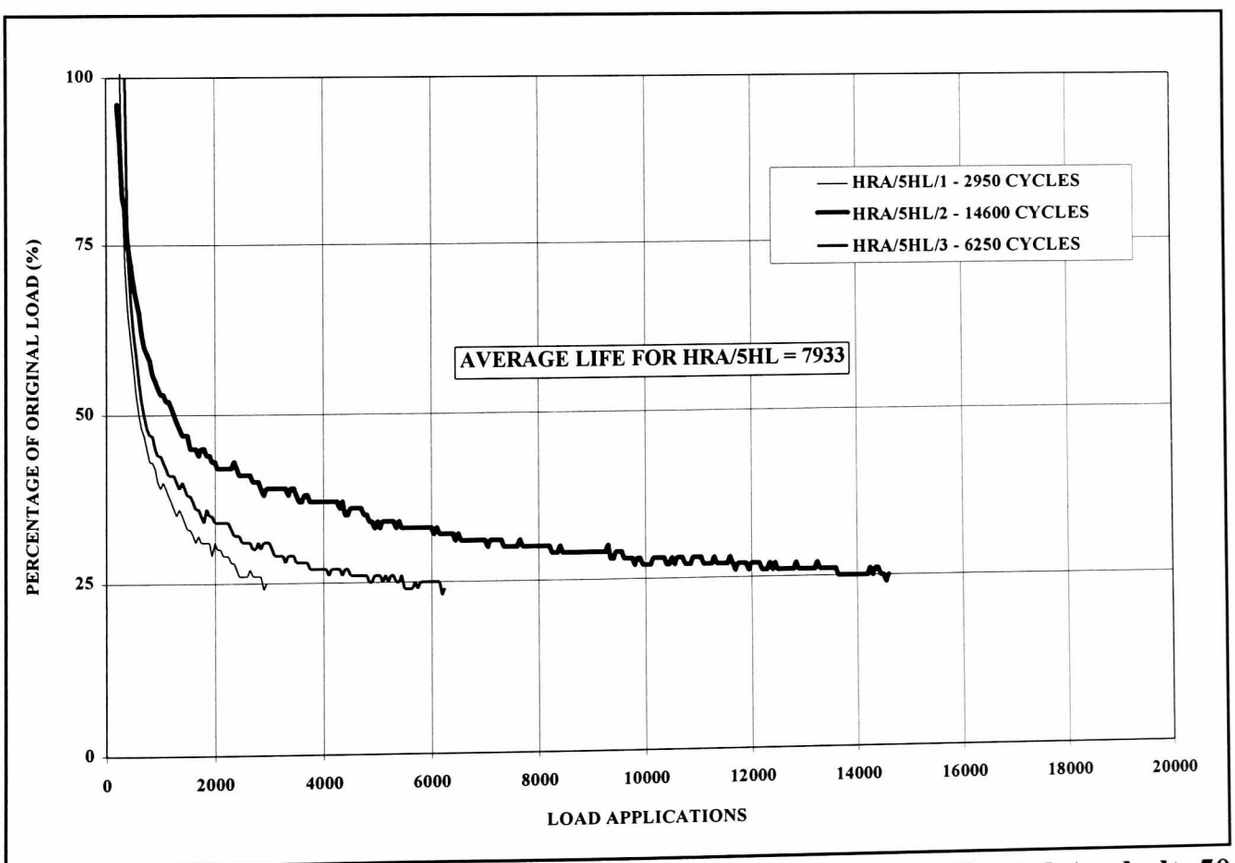


Figure 6.9 - Beam Test Result for Specimens HRA/5HL - Hot Rolled Asphalt, 50 pen Bitumen, High Void Content and Low Binder Content.

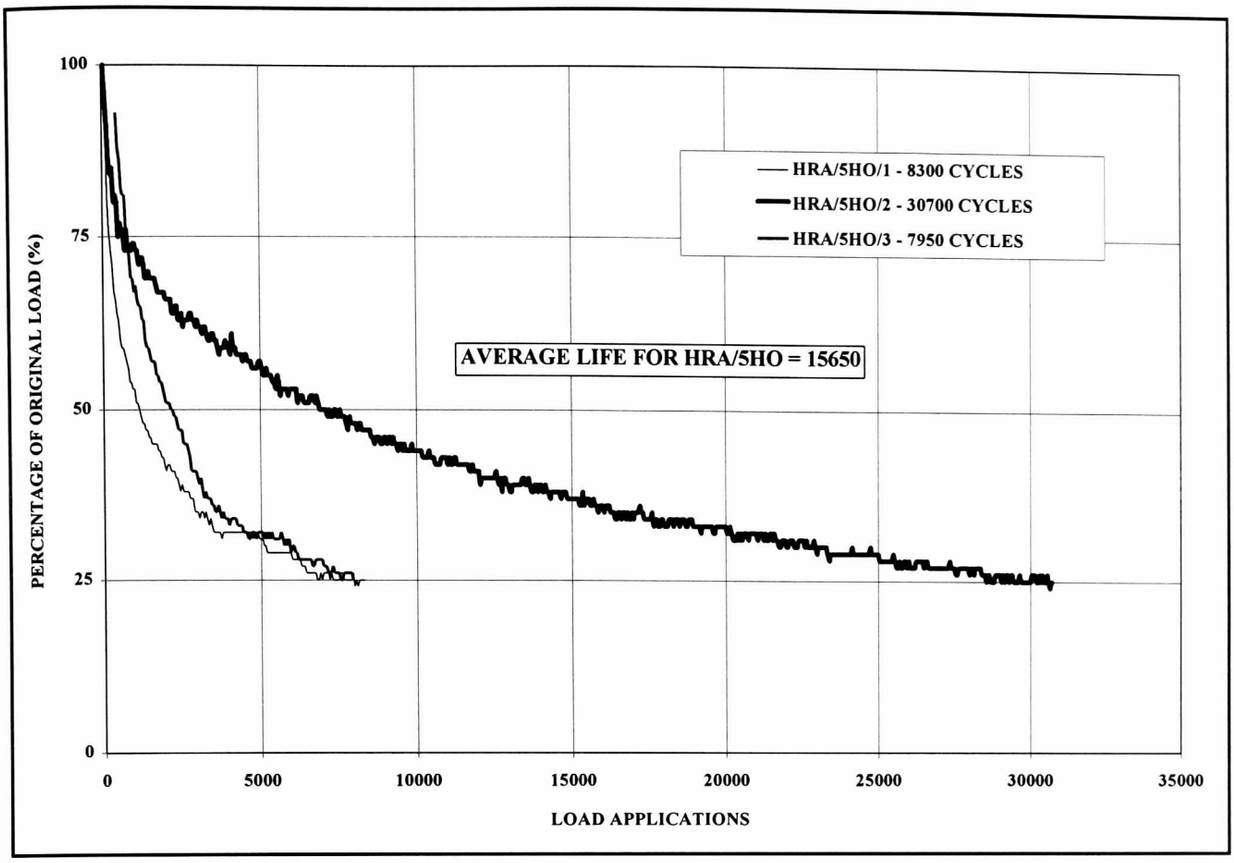


Figure 6.10 - Beam Test Result for Specimens HRA/5HO - Hot Rolled Asphalt, 50 pen Bitumen, High Void Content and Optimum Binder Content.

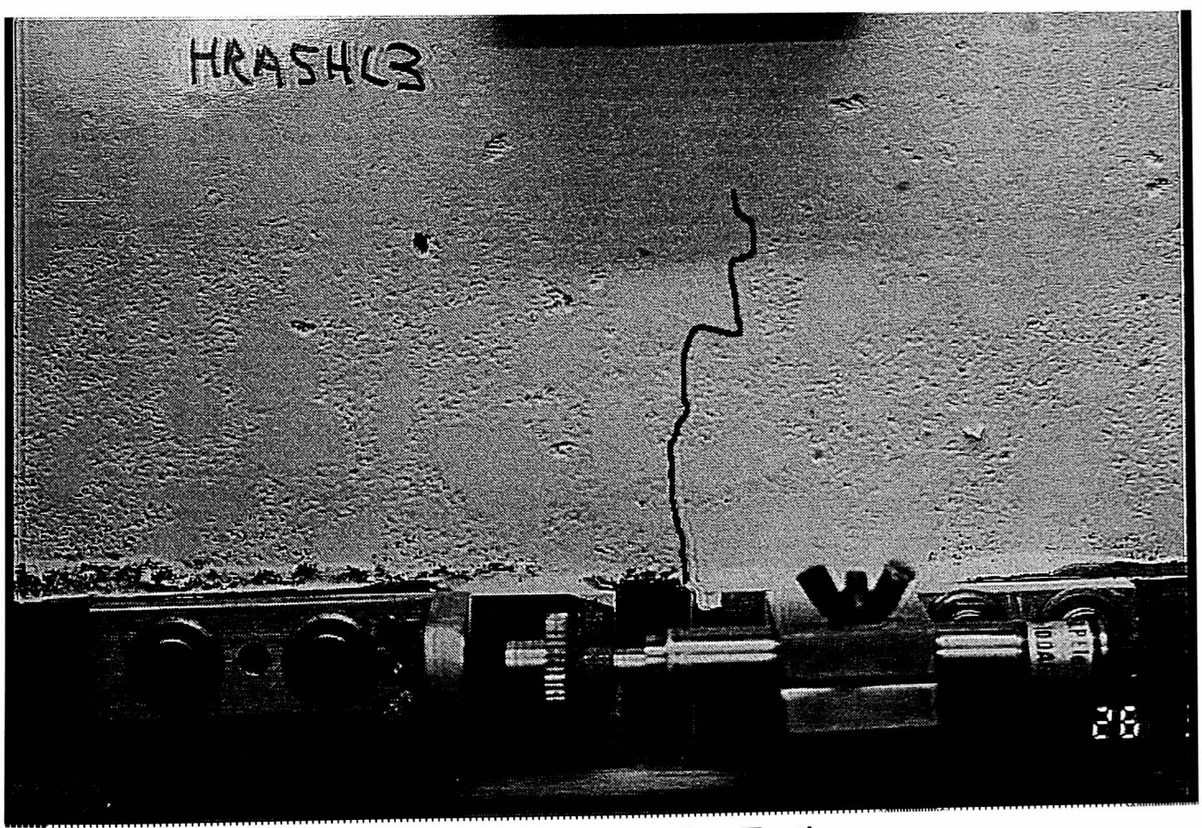


Plate 6.3 - Digitised Image of a Beam - After Testing.

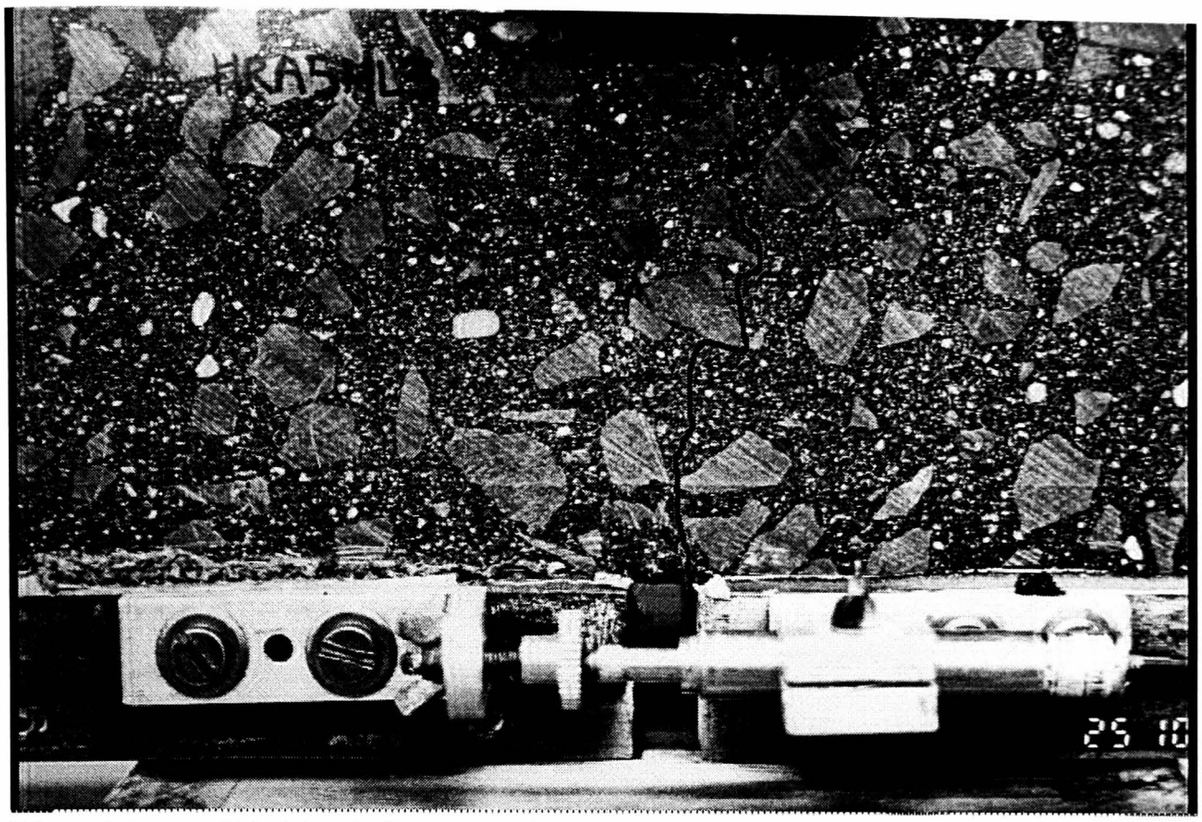


Plate 6.4 - Digitised Image of a Beam in Plate 6.3 With the Crack Electronically Superimposed - Showing the Path Taken Around the Aggregate Structure.

This gave 24 different mixtures and 71 beams (1 beam failed prematurely due to a power surge):

- Two materials types (30/14 HRA and 20mm DBM),
- Two bitumen types (SBS and EVA modified),
- Three binder contents (optimum, optimum +1% and optimum -1%),
- Two compaction levels (normal and normal +2%) and
- Generally one beam of each material.

This gave 16 different mixtures and 23 beams:

This gave a total of 40 different mixtures and 112 beams: 94 from the main test programme with 18 beams from the pilot test programme.

6.6 References

1. Brunton, J.M., "Developments in the Analytical Design of Asphalt Pavements Using Computers," PhD Thesis, University of Nottingham, Department of Civil Engineering, May 1983.
2. Caltabriano, B.E., "Reflection Cracking in Asphalt Overlays," M.Phil Thesis, University of Nottingham, Department of Civil Engineering, March 1990.
3. Paris, P.C., "Fracture Mechanics in the Elastic-Plastic Regime," Flaw Growth and Fracture, ASTM STP 631, American Society for Testing and Materials, pp 3-27, 1977.
4. Rice, J.R., "A Path Independent Integral and the Approximate Analysis of Strain Concentration by Notches and Cracks," Journal of Applied Mechanics, pp 379-386, 1968.
5. Krans, R.L., Van der Ven, M.F.C., Molenaar, J.M.M. and Kunst, P.A.J.C., "Crack Growth experiments on Asphalt Concrete Beams," Proceedings of the Conference Strategic Highway Research Program (SHRP) and Traffic Safety on Two Continents, Hague, Netherlands, September 22-24, 1993.
6. Dehlen G.L., "The Effect of Non-Linear Material Response on the Behaviour of Pavements Subjected to Traffic Loads," PhD Thesis, University of California, Berkeley, 1969.
7. Majidzadeh, K., Kauffman, E.M. and Chang, C.W., "Verification of Fracture Mechanics Concepts to Predict Cracking of Flexible Pavements," Federal Highway Administration, Offices of Research and development, Report No. FHWA-RD-73-91, June 1973.
8. Molenaar, A.A.A., "Structural Performance and Design of Flexible Road Construction and Asphalt Concrete Overlays," Delft University of Technology, 1983.
9. Schapery, R.A., "A Theory of Crack Initiation and Growth in Viscoelastic Media - I Theoretical Development," International Journal of Fracture, Volume 11 No. 1, pp 141-159, February 1975.

10. Schapery, R.A., "A Theory of Crack Initiation and Growth in Viscoelastic Media - II Approximate Methods of Analysis," International Journal of Fracture, Volume 11 No. 3, pp 369-388, June 1975.

11. Schapery, R.A., "A Theory of Crack Initiation and Growth in Viscoelastic Media - III Analysis of Continuous Growth," International Journal of Fracture, Volume 11 No. 4, pp 549-563, August 1975.

12. Jacobs, M.M.J., "Crack Growth in Asphaltic Mixes," PhD. Thesis, Delft University of Technology, Netherlands, 1995.

13. Bolton, T., "Reflective Cracking in Asphaltic Overlays," Dissertation Submitted in part Consideration of the Degree of M.Eng (Hons) in Civil Engineering, University of Nottingham, Department of Civil Engineering, May 1994.

14. British Standards Institution, "Hot Rolled Asphalt for Roads and Other Paved Areas," B.S. 594 : Part 1, 1992.

15. British Standards Institution, "Coated Macadams for Roads and Other Paved Areas," B.S. 4987 : Part 1, 1993.

RESULTS OF THE CRACK PROPAGATION TEST PROGRAMME

7.1 Introduction

The work on crack propagation did not go entirely as planned, since only 40 out of a possible 72 mixtures were evaluated and only 112 out of 234 beams were tested. This was largely due to the length of time of test of the SBS modified mixtures and it was this data set which was reduced most, with only 5 different mixtures and 7 beams being tested. Testing of the SBS beams typically took about 8 days plus 2 days to set up this, therefore, meant that testing the 7 beams took about 10 weeks. To have tested the whole set of SBS beams would, therefore, have taken nearly two years. Despite these limitations the testing which was carried out produced some very interesting results with practical significance.

7.2 Image Analysis

It was hoped that the use of image analysis to measure the cracks would produce a new way to quantify crack propagation rates. This was not possible, however, as only about 50 of the beams tested had visible cracks (Appendix E), with no measurable cracks apparent on any of the polymer modified beams. Typical graphs and Plates are given in Figures 7.1 to 7.3 and Plates 7.1 to 7.3. These show very clearly that the method has potential but that further work into this area is required, particularly in monitoring polymer modified mixtures. Measurement of the true crack length is considered worthwhile as it should allow a new definition of failure in future testing since it is this parameter which the author considers has given rise to much of the variation in the data shown later in this Chapter. This method has also shown, by the electronic superimposition of the crack onto the unpainted beam, the way in which cracks grow and which route they take. By examining the images in Appendix E, it is clear that cracks always propagate around the coarse aggregate passing as close to the aggregate as possible. The cracks also try and travel the shortest route between the point of crack initiation and the point of applied load.

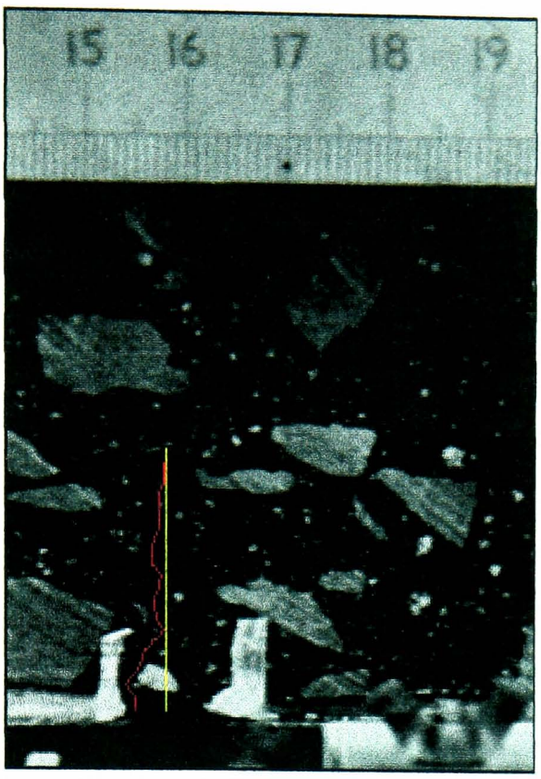


Plate 7.1 - Electronically Superimposed Crack on Unpainted Beam - Specimen HRA5HH3.

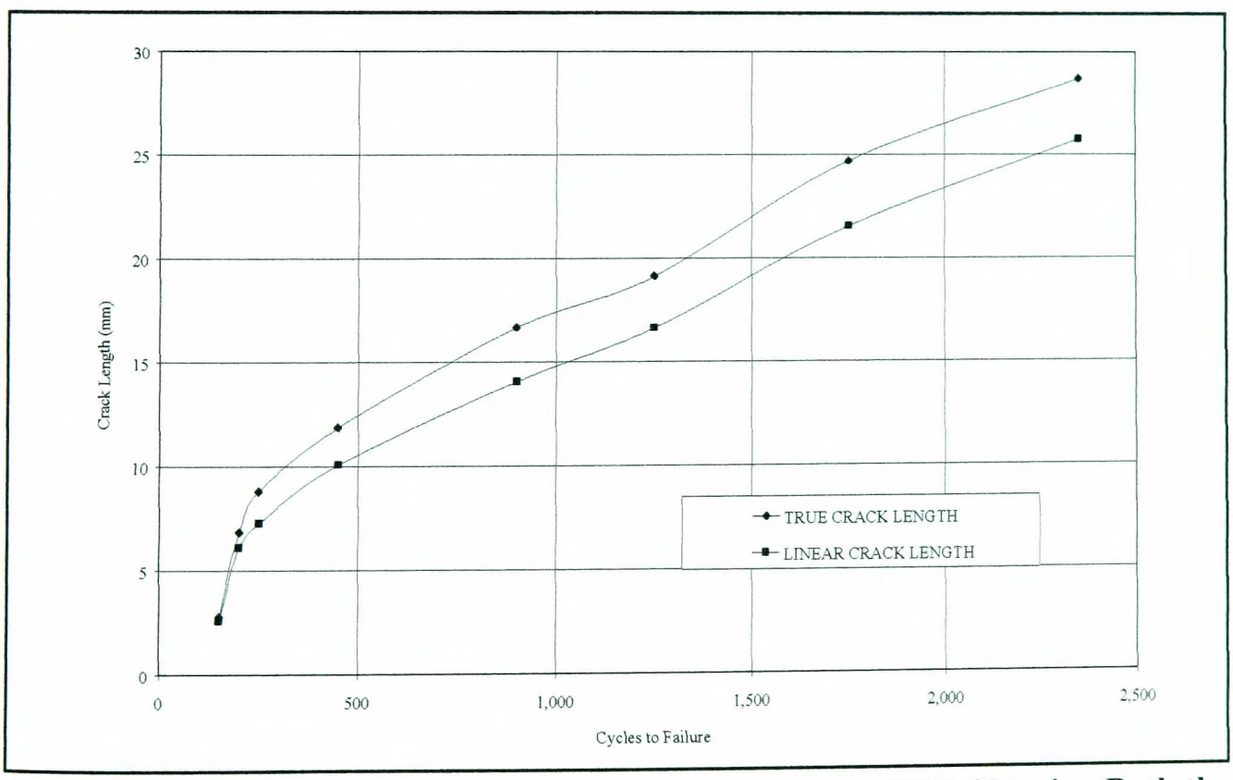


Figure 7.1 - Rates of Crack Growth for Specimen HRA5HH3 Showing Both the Linear and the True Crack Lengths.

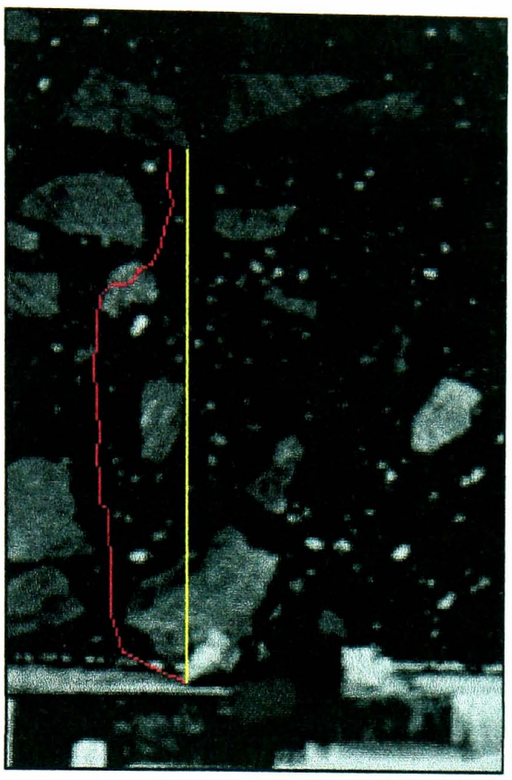


Plate 7.2 - Electronically Superimposed Crack on Unpainted Beam - Specimen HRA5HH1.

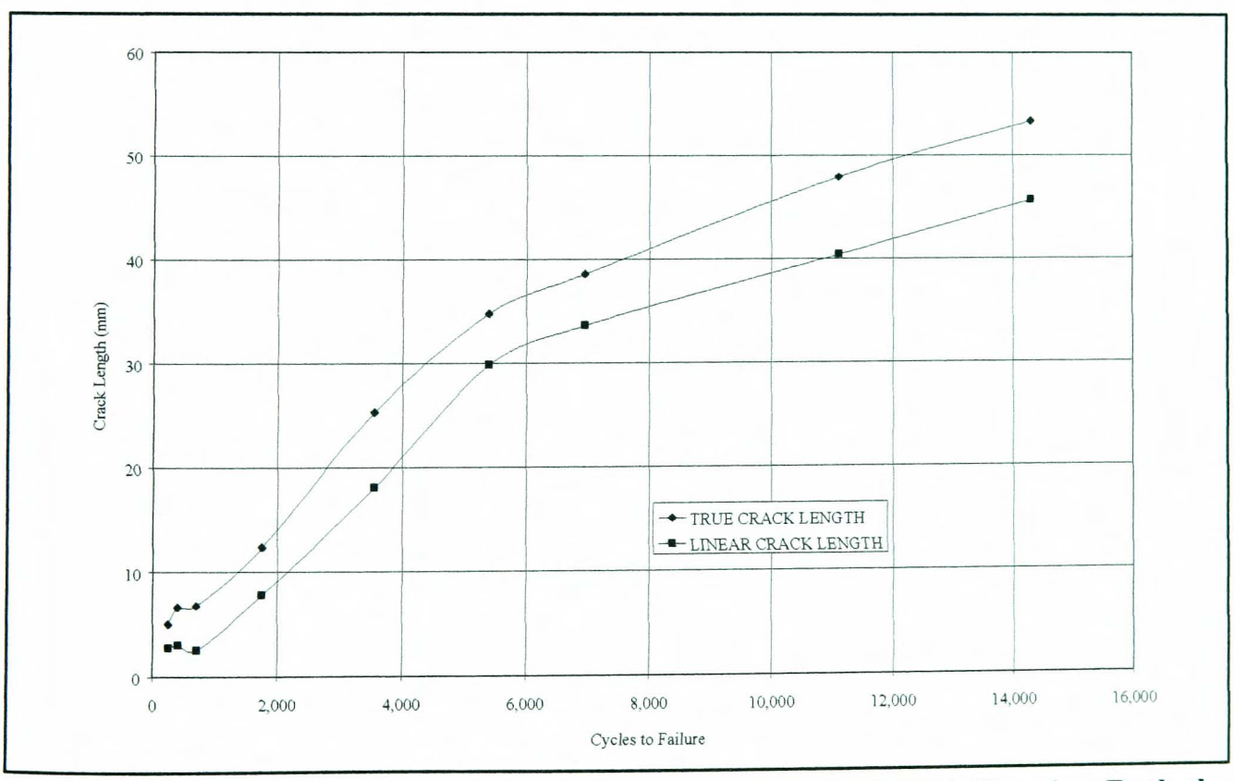


Figure 7.2 - Rates of Crack Growth for Specimen HRA5HH1 Showing Both the Linear and the True Crack Lengths.

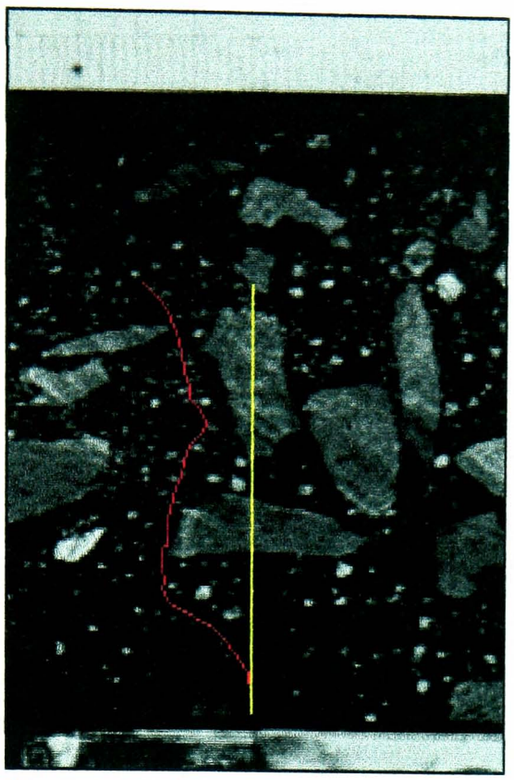


Plate 7.3 - Electronically Superimposed Crack on Unpainted Beam - Specimen HRA5HO2.

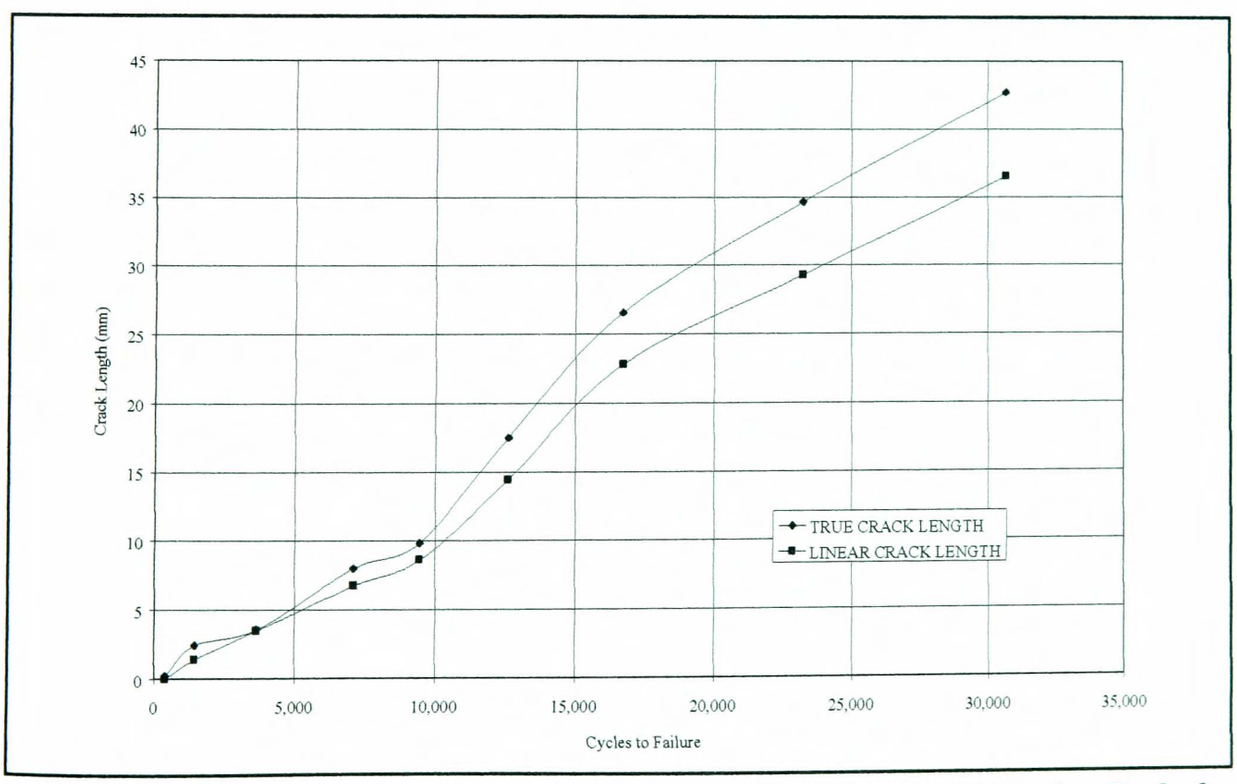


Figure 7.3 - Rates of Crack Growth for Specimen HRA5HO2 Showing Both the Linear and the True Crack Lengths.

These findings suggest the need for future work where, it is envisaged, the route of propagation will be predicted, by the use of image analysis, prior to the test taking place. As it is considered that a crack will always take the weakest path, the results would imply that the interface between the aggregate and the matrix is less resistant to cracking. Therefore, the lower the amount of coarse aggregate the better and, hence, this partially explains the better performance of HRA materials in comparison to continuously graded ones. However, if a continuously graded material is to be used then the higher the quantity of coarse aggregate the better as it makes the propagation route of the crack longer, thus, increasing the life.

Further work is required on the use of image analysis in crack propagation work, particularly in the control of the test, the definition of failure and to monitor the progression of cracks in real time. It is felt by the author that if this had been the case during the test programme described in the previous Chapter, that quantification of crack propagation for all the materials would have been possible.

7.3 Analysis of Crack Propagation Data

When analysing the data it became clear that one important parameter of the mixture, with regard to crack propagation, was stiffness. The stiffness of the beams was ascertained by comparing the magnitude of the initial load with stiffness data from the ITSM testing carried out in the ITFT work. This resulted in a good correlation and although the applied stress was significantly higher in the beam tests than that applied during the ITSM tests, both values of stress were in the area where the dependence is far less important (Figure 3.17). Hence, it was considered that this was an acceptable method of estimating the stiffness of the beams.

During the main test programme many variables were examined but none of these could explain the variations in performance found during the testing. However, each of the variables did have an influence on the stiffness which in turn was able to explain the variation in performance. The data when presented in the form of stiffness against number of cycles to failure fell into four distinct groups:

- Unmodified HRA,
- Unmodified DBM,
- SBS modified mixtures and
- EVA modified mixtures.

These results are presented in Figures 7.4 to 7.7 . It can be seen that crack propagation appears to be related to the stiffness of the mixture in a power relationship. The equations of the 4 best fit lines are given in equations 7.1 to 7.4 and these all indicate that the lower the stiffness of a bituminous mixture the better its resistance to crack propagation. This is in direct contradiction to the requirements for prevention of crack initiation in a thick bituminous pavement but in agreement for a thin bituminous pavement.

Unmodified DBM $$N = \left(\frac{S_m}{6563} \right)^{-8.482} \quad (7.1)$$

Unmodified HRA $$N = \left(\frac{S_m}{16843} \right)^{-5.063} \quad (7.2)$$

SBS Modified $$N = \left(\frac{S_m}{138380} \right)^{-2.548} \quad (7.3)$$

EVA Modified $$N = \left(\frac{S_m}{6101} \right)^{-7.770} \quad (7.4)$$

Where:

N = Number of cycles to failure and

S_m = Stiffness modulus at 20°C and a risetime of 120ms or frequency of 1Hz.

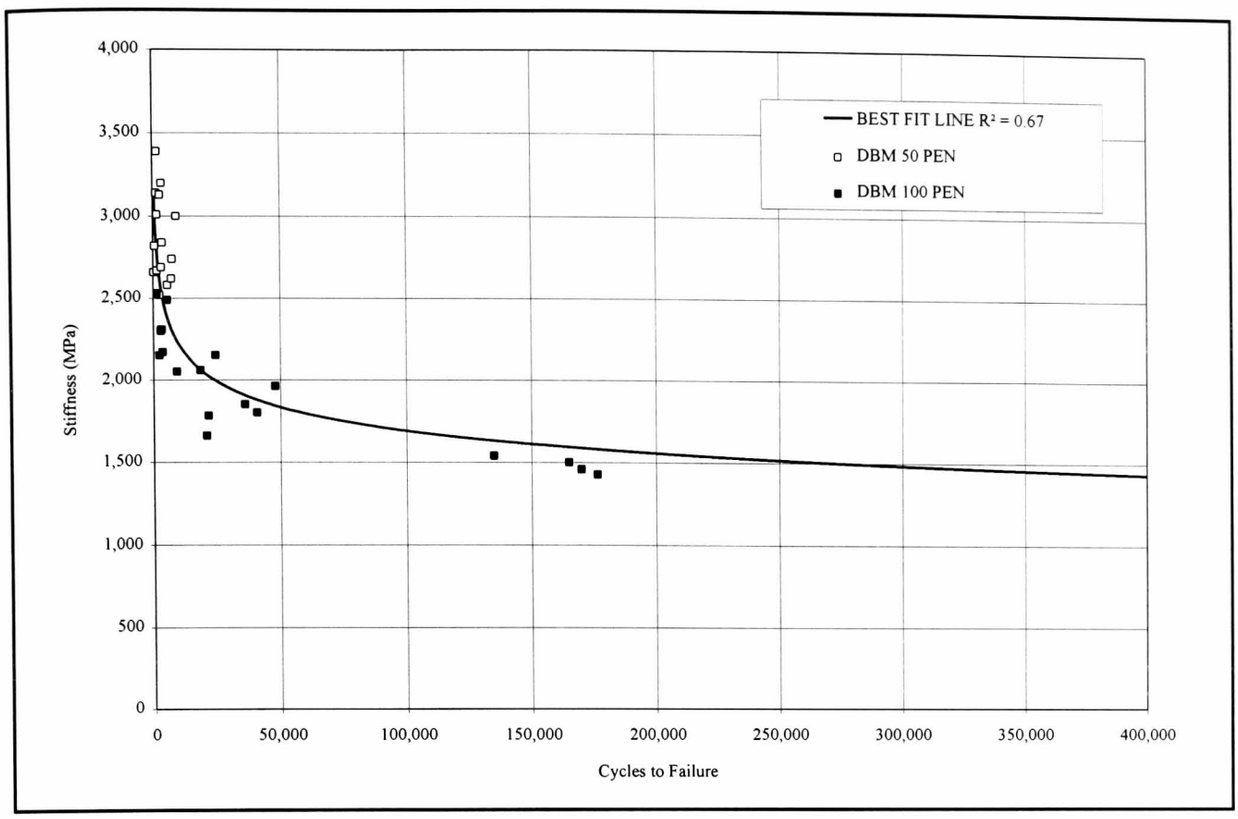


Figure 7.4 - Unmodified DBM Data Demonstrating the Power Relationship with Stiffness.

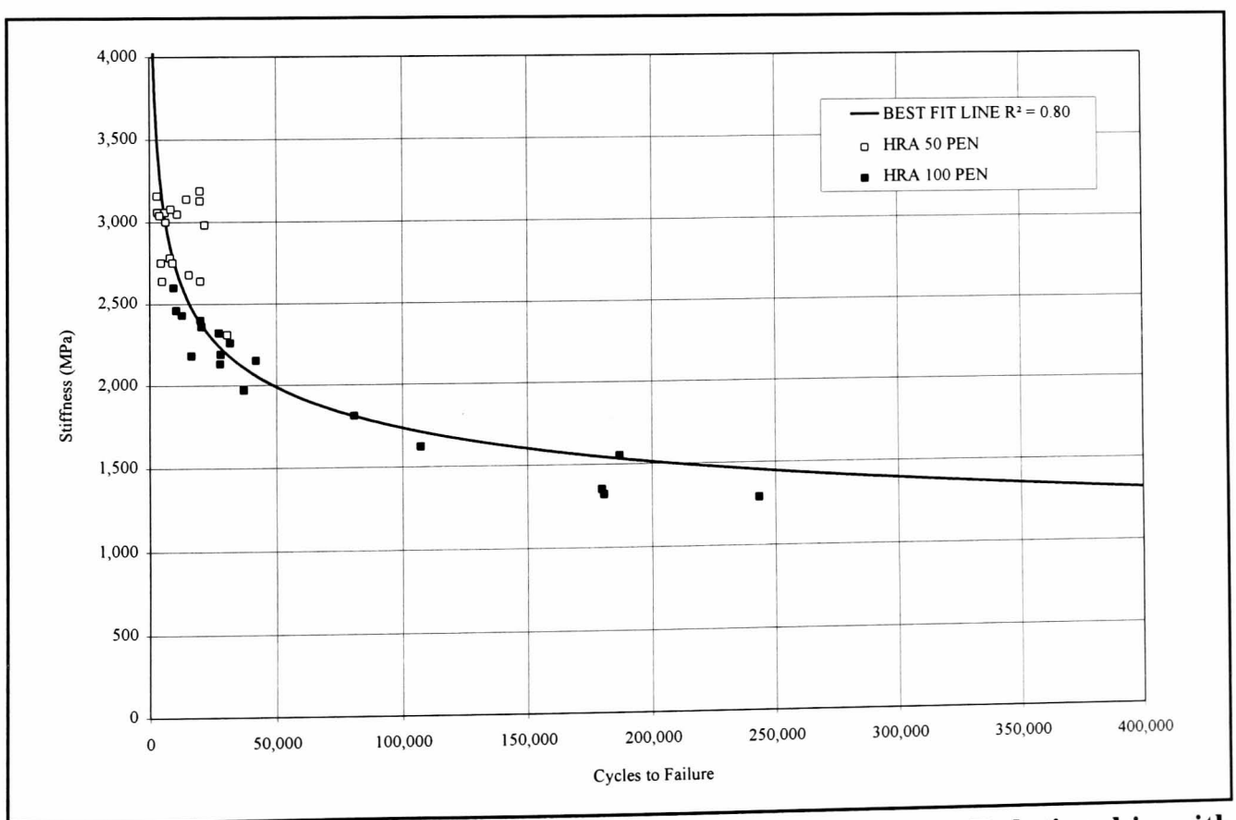


Figure 7.5 - Unmodified HRA Data Demonstrating the Power Relationship with Stiffness.

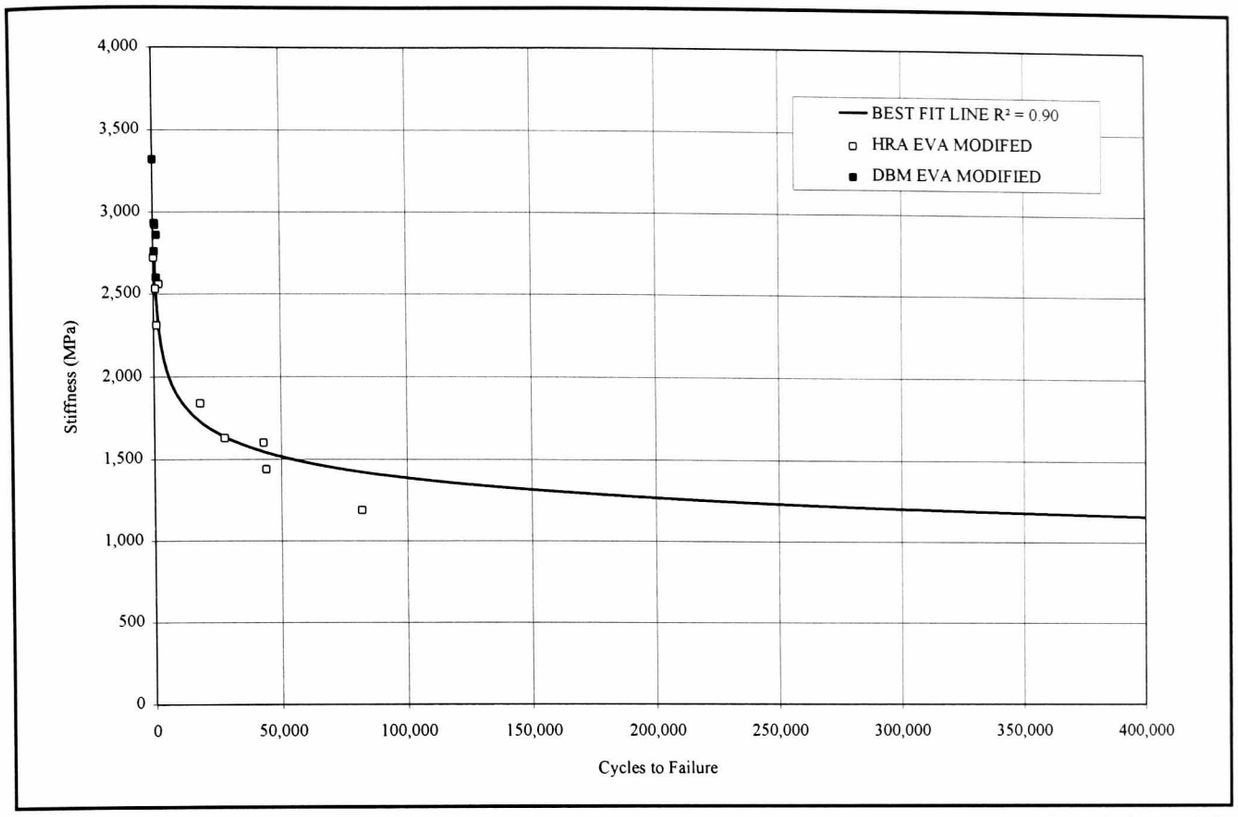


Figure 7.6 - EVA Modified Data Demonstrating the Power Relationship with Stiffness.

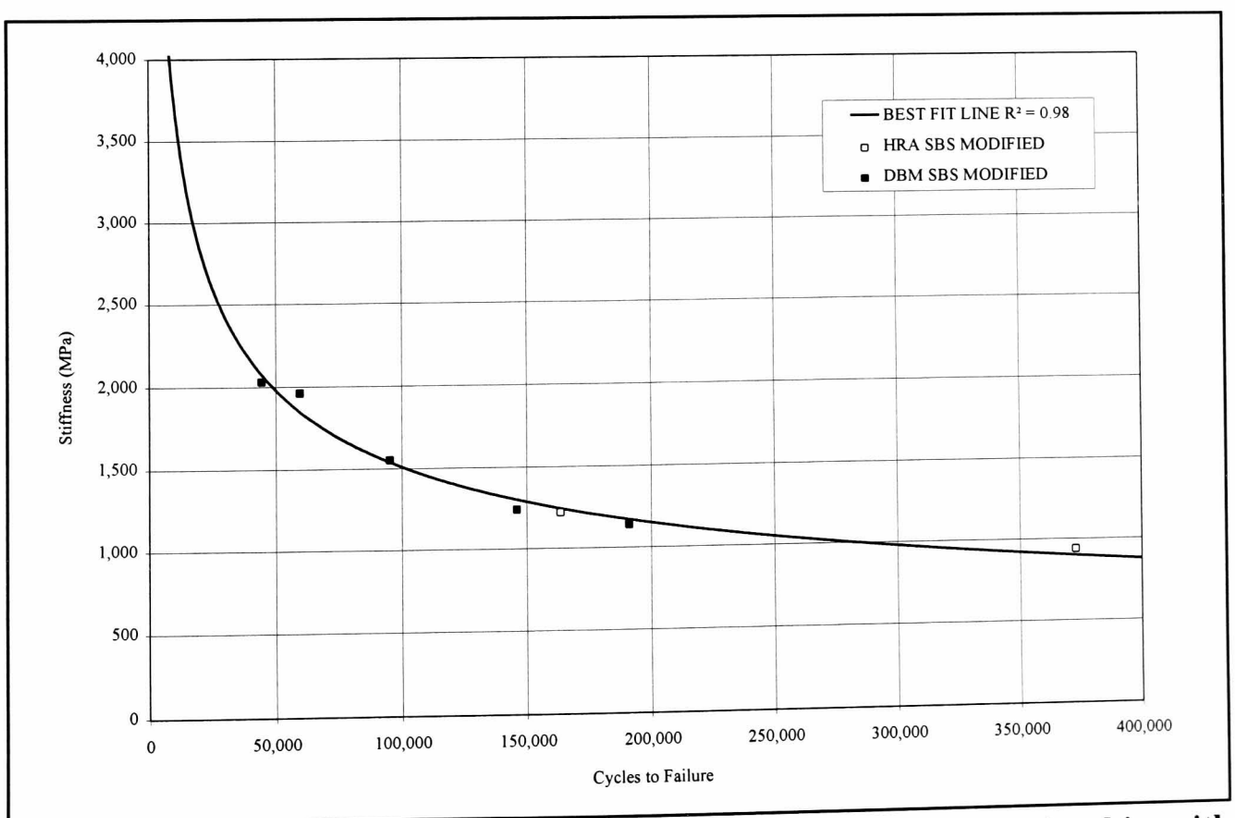


Figure 7.7 - SBS Modified Data Demonstrating the Power Relationship with Stiffness.

These four equations allow calculation of the number of cycles for crack propagation, for any material encompassed in the range of mixtures tested, provided that an appropriate value of stiffness modulus is available for the material. This will, in turn, allow a design shift factor for crack propagation for the material to be developed provided one material is selected as the datum to which all others are compared. This work on a shift factor is shown in the next Chapter and demonstrates that the research described in this and the previous Chapter has advanced the way in which crack propagation can be treated in pavement design and evaluation. However, it is important to reiterate that the equations are only valid for the conditions under which they were established, the extrapolation shown on the graphs is included only to show the overall shape of the equations and predictions outside of the data ranges cannot be expected to be accurate. This leads to a question over their applicability as it is very unlikely that a tensile strain of 8,500 microstrain will be developed in the pavement. Therefore, this is an area where further work is required to see if the rankings which were obtained remain the same at lower levels of strain and also under the controlled stress mode of loading. If the rankings do remain the same, then the concept outlined in the next Chapter remains valid as the data is normalised by the 20mm DBM datum material and although the magnitude of the numbers will change the ratios should still be correct.

7.4 Summary

The work on crack propagation has shown that crack propagation measurements can be obtained using image analysis. However, it would appear that to achieve a good result for all material types requires the use of image analysis equipment in the real time control and analysis of the test.

The images given in Appendix E show that cracks always propagate around coarse aggregate and that there appears to be a preferential path at the interface between the matrix and the coarse aggregate. This separating of the coarse aggregate from the matrix has been reported previously by Jacobs (1) who carried out a large amount of work into crack propagation using a variety of techniques. It would also appear that cracks try and take the shortest route between the point of crack initiation and the point of applied load.

This is as expected but it does not appear to have been demonstrated previously. This, in the pavement, leads to the conclusion that as a wheel load travels over a pavement, the crack must always be changing direction as opposed to always growing in one direction. Another conclusion which may be drawn from this is that the shape and orientation of the aggregate may help reduce the rate of crack propagation. Aggregate with a high flakiness index may act as a crack growth inhibitor if the general orientation is perpendicular to the growth of the crack whereas the converse is true if the general orientation is perpendicular to the growth of the crack. This has implications for the mixture design process, which generally excludes the use of high flakiness aggregate, indicating that for certain mixtures under certain service conditions flaky aggregate may have a rôle to play.

The analysis of the data produced during the testing has lead to the development of four groups of materials, although it can be seen from Figures 7.4 and 7.5 that the HRA and DBM mixtures have similar curves and could, perhaps, be grouped together under a generic heading of unmodified mixtures.

- Unmodified HRA,
- Unmodified DBM,
- SBS modified mixtures and
- EVA modified mixtures.

These all demonstrate a power relationship between the number of load applications for crack propagation and the initial stiffness of the material. It is not fully understood why the materials group in this fashion but it is the authors opinion that the crack propagation response of the polymer modified materials is dominated by the binder properties. Hence, all other parameters are of secondary importance, whereas the unmodified mixtures ostensibly have the same base binder (stiffness varies but not the way in which the binder responds) and hence other parameters are now of primary importance.

The next Chapter will demonstrate how these findings can be used to modify the shift factors applied to the life to crack initiation in order to allow different crack propagation times for different materials.

7.5 References

1. Jacobs, M.M.J., "Crack Growth in Asphaltic Mixes," PhD. Thesis, Delft University of Technology, The Netherlands, February 1995.

PRACTICAL APPLICATION OF THE RESEARCH RESULTS

8.1 Introduction

This Chapter is intended to show how the research described in this thesis may be applied, provided that it can be shown that the level of applied strain in the testing is valid, to mixture design, pavement evaluation and pavement design. The first two are probably the most important in the U.K. as very few new road schemes are being carried out and the majority of the money invested in the transport infrastructure is used to maintain that which already exists. However, there are many schemes all over the world, particularly in less developed countries, where a simple tool like the Nottingham Asphalt Tester (NAT) and simple economic tests for stiffness (Indirect Tensile Stiffness Modulus, ITSM), permanent deformation (Repeated Load Axial Test, RLAT, and static creep) and fatigue cracking (Indirect Tensile Fatigue Test, ITFT) would be an invaluable asset for the design engineer as well as the maintenance engineer.

8.2 Mixture Design

It is not proposed that the ITFT be used as one of the general tests for mixture design as it would be too expensive and time consuming to use for all the mixture variations which are generally considered when designing a bituminous mixture. However, it is proposed that when other variables have been optimised (volumetrics, stiffness and possibly permanent deformation) and the final mixture has been selected, then its fatigue properties can be evaluated in order to ensure that the mixture has an adequate level of fatigue performance. It is considered that this would be done by comparing the mixture against standard mixtures such as those presented in Figure 8.1 which have a known level of performance. The equations of the lines shown in Figure 8.1 are given here for ease of reference:

30/14 *HRA Equations are* $\epsilon = 4322\ N^{-0.264}$ $N = 5.93 \times 10^{13}\ \epsilon^{-3.788}$

20mm DBM Equations are $\epsilon = 1406\ N^{-0.248}$ $N = 6.06 \times 10^{13}\ \epsilon^{-4.032}$

28mm DBM 50 Equations are $\epsilon = 2595\ N^{-0.255}$ $N = 2.45 \times 10^{13}\ \epsilon^{-3.923}$

SBS Modified 30/14 HRA Equations are $\epsilon = 4388\ N^{-0.241}$ $N = 1.30 \times 10^{15}\ \epsilon^{-4.149}$

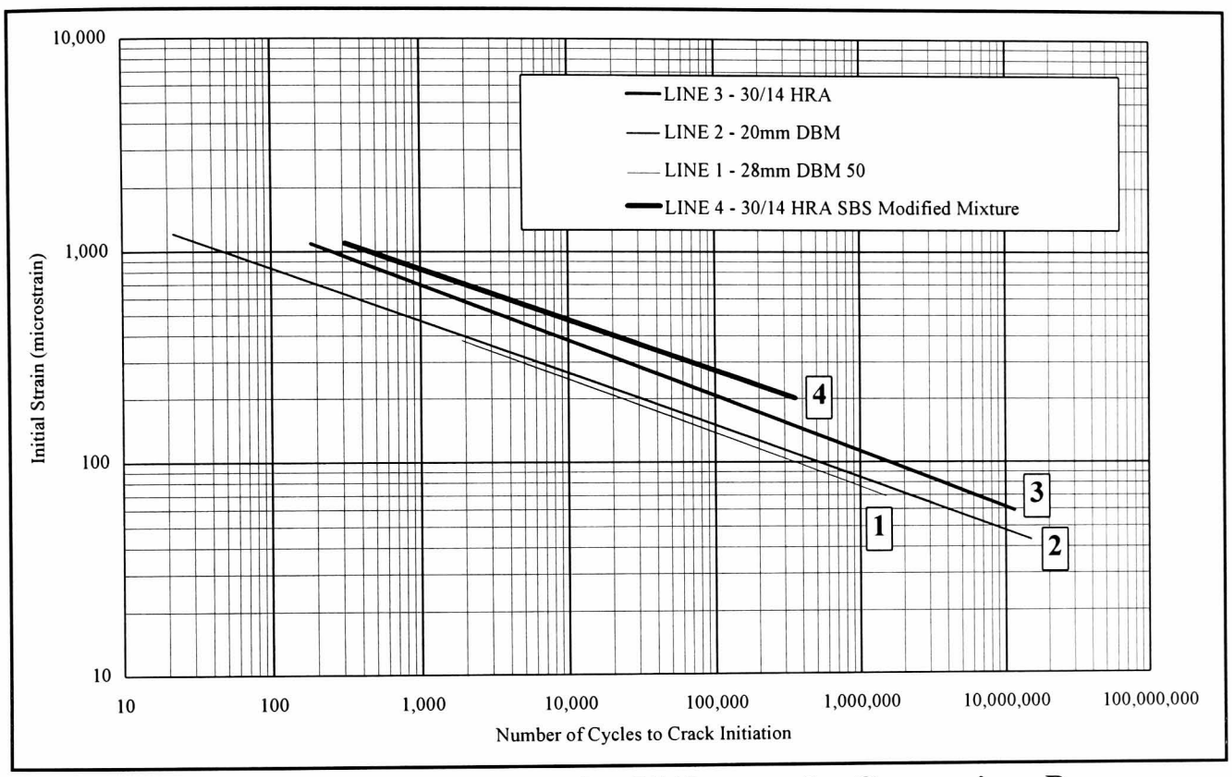


Figure 8.1 - Four Examples of Standard Mixtures for Comparison Purposes.

It must be noted here that these equations include the data for the trapezoidal cantilever testing.

It must be borne in mind that the ITFT only examines the life to crack initiation and that if the total life to failure needs to be considered then a method such as that proposed in Section 8.4 should be utilised as this will allow a better comparison than just the ITFT result.

8.3 Pavement Evaluation

Pavement evaluation is a difficult task as it requires non-destructive testing of the pavement to ascertain the remaining life of the structure and to decide upon a suitable

maintenance strategy. Traditional methods of fatigue testing are not suitable for this task as they would require large pieces of pavement to be extracted in order to produce the correct specimen geometries. However, the ITFT uses 100mm diameter cores which can easily be removed from the pavement without damaging it. Therefore, provided that the original properties of the road are known then an exercise of the sort described in Chapters 3 and 4 can be carried out to evaluate how the properties have changed over time showing either an increase or decrease in life dependent upon the amount of traffic and ageing which have taken place. When testing cores from an existing pavement, the core may be from an "undamaged" position and, hence, only reflect environmental effects on life. To ascertain the effect of traffic, the core would need to embrace potential cracked zones at the surface or base and be correctly oriented in the ITFT.

The work shown in Chapters 3 and 4 demonstrates that for that particular pavement there is a reduction in life, probably due to environmental factors, however, it is very important to emphasise that it is necessary to evaluate each pavement individually as different materials and structures will behave differently over time.

The second type of evaluation work for which the ITFT has been shown to be appropriate is in resolving contractual disputes where certain materials are thought to have poor performance. The ITFT is particularly relevant where areas of material have low binder contents and it is considered that the fatigue performance of the structure may be significantly reduced. The example given in Section 3.8.4 demonstrates that although a material may have a low binder content it does not necessarily follow that it will have poorer fatigue performance and, hence, a large amount of money can be saved as material which would otherwise have been removed is allowed to remain in the pavement. The converse is also true and having a simple fatigue test should help to prevent the occurrence of premature pavement failure. However, it is important, at this point, to reiterate the fact that fatigue must not be considered in isolation and that the stiffness and the pavement structure must be considered at the same time when evaluating a material.

8.4 Pavement Design

It is the intention of this section to show how the results of the research can be applied to the improved design of pavements. It has been shown that the ITFT is a suitable test method for rapidly evaluating the life to crack initiation of bituminous paving mixtures and it has also been shown that, for certain groups of materials, the crack propagation rate can be related to their initial stiffness. Combining these two results allows a method for quickly assessing the overall fatigue performance of a bituminous paving mixture which can cope with any mixture type, including polymer modified ones which traditional methods cannot. The four equations for crack propagation are repeated here for ease of reference:

Unmodified DBM
$$N = \left(\frac{S_m}{6{,}563} \right)^{-8.482} \quad \textbf{(8.1)}$$

Unmodified HRA
$$N = \left(\frac{S_m}{16{,}843} \right)^{-5.063} \quad \textbf{(8.2)}$$

SBS Modified
$$N = \left(\frac{S_m}{138{,}380} \right)^{-2.548} \quad \textbf{(8.3)}$$

EVA Modified
$$N = \left(\frac{S_m}{6{,}101} \right)^{-7.770} \quad \textbf{(8.4)}$$

For bituminous materials, there are 3 factors which have been derived to allow for the differences between laboratory test conditions and those in the pavement where longer lives are obtained:

- Lateral wander,
- Rest periods between load applications and
- Crack propagation time.

Brunton (1) analysed various sets of data and obtained the following values for the 3 factors:

- Lateral wander - 1.1
- Rest periods - 20
- Crack propagation time to critical condition - 3.5
- Crack propagation time to failure conditions - 20

The consideration of rest periods, lateral wheel distribution and crack propagation time, therefore, gives the following shift factors:

- $1.1 \times 20 \times 3.5 = 77$ for critical condition and
- $1.1 \times 20 \times 20 = 440$ for failure condition.

Brunton's analysis for crack propagation was based on Van Dijk's work (2) which used a 20mm asphaltic concrete. It is, therefore, considered that if the 20mm DBM material from the data reported in this thesis, which is the closest material to that used by Van Dijk, is taken as the datum then the shift factors described here can be modified by equations 8.1 to 8.4 to account for different material performance with regard to crack propagation.

The standard material is now defined as a 20mm DBM with a stiffness of 1750 MPa. If this value for stiffness is used in equation 8.1 it gives a standard life of 74,000 load applications. This value can now be used to normalise each of the four equations:

Unmodified DBM

$$\textit{Shift Factor} = \frac{\left(\frac{S_m}{6{,}563}\right)^{-8.482}}{74{,}000} \qquad \textbf{(8.5)}$$

Unmodified HRA

$$\textit{Shift Factor} = \frac{\left(\frac{S_m}{16{,}843}\right)^{-5.063}}{74{,}000} \qquad \textbf{(8.6)}$$

$$\textit{SBS Modified} \qquad \textit{Shift Factor} = \frac{\left(\frac{S_m}{138{,}380}\right)^{-2.548}}{74{,}000} \tag{8.7}$$

$$\textit{EVA Modified} \qquad \textit{Shift Factor} = \frac{\left(\frac{S_m}{6{,}101}\right)^{-7.770}}{74{,}000} \tag{8.8}$$

This now means that if a stiffness value of 1750 MPa, typical for a 20mm DBM basecourse, is used in Equation 8.5 a value of unity is returned which equates to a shift factor of 20 for failure and 3.5 for critical condition, according to the shift factors developed by Brunton (1). These equations can now be normalised further by multiplying by the value of 20 for failure and 3.5 for critical condition, which means that a 20mm DBM basecourse with a stiffness of 1750MPa will have shift factors of 20 for failure condition and 3.5 for critical condition. Equation 8.9 shows the crack propagation equation for DBM materials to critical condition:

$$\textit{Unmodified DBM Critical} \qquad \textit{Shift Factor } (SF_{cp}) = \frac{\left(\frac{S_m}{6563}\right)^{-8.482}}{21{,}143} \tag{8.9}$$

As there are eight different equations for the four material groups and two conditions the generalised form is given in Equation 8.10 with key parameters given in Table 8.1:

$$\textit{Shift Factor } (SF_{cp}) = \frac{\left(\frac{S_m}{\alpha}\right)^{\beta}}{\delta} \tag{8.10}$$

Table 8.1 - Key Parameters for Use in Equation 8.10.

	DBM Unmodified Materials		HRA Unmodified Materials		SBS Modified Materials		EVA Modified Materials	
	Critical	Failure	Critical	Failure	Critical	Failure	Critical	Failure
α	6,563	6,563	16,843	16,843	138,380	138,380	6,101	6,101
β	-8.482	-8.482	-5.063	-5.063	-2.548	-2.548	-7.770	-7.770
δ	21,143	3,700	21,143	3,700	21,143	3,700	21,143	3,700

Using these equations it is now possible to calculate the shift factor for crack propagation according to the actual material type. This coupled to actually testing for the life to crack initiation allows, in the author's opinion, an improved method for calculating the life to failure of a bituminous paving mixture. The method of calculating the life to failure is now to ascertain the life to crack initiation from the ITFT at the tensile strain experienced in the material and to multiply this by 1.1 for lateral wander, 20 for rest periods and by the appropriate shift factor for crack propagation calculated from equation 8.10:

$$\textit{Fatigue Life } (N_f) = N_i \times 1.1 \times 20 \times SF_{cp} \qquad \textbf{(8.11)}$$

Where:

N_i = Life to crack initiation in the ITFT at calculated level of tensile strain and

SF_{cp} = Shift factor calculated from equation 8.10.

A comparison of the proposed method described above and two other commonly used methods will now be presented. The two methods selected for comparison are the Nottingham analytical design method (3) and the Asphalt Institute MS-1 method (4, 5, 6, 7). An example of all three calculations will be given for a typical 20mm DBM material and then Table 8.2 will show the number of Standard axles calculated, for each method, for four materials:

- 20mm DBM 100 pen,
- 30/14 HRA 50 pen,
- 28mm DBM 50 and
- 30/14 HRA SBS Modified.

The equation in the Nottingham analytical design method is:

$$\log N = 15.8 \log \epsilon_t - k - ((5.13 \log \epsilon_t - 14.39) \log V_b) - ((8.63 \log \epsilon_t - 24.2) \log SP_i)$$

where:

ϵ_t = Tensile strain at the bottom of the asphalt layer, microstrain,

N = Millions of standard axles,

V_B = Volume of Binder (%),

Sp_i = Initial Softening Point,

k = 46.06 for life to failure and

k = 46.82 for life to critical condition.

The equation for the Asphalt Institute method is:

$$N = 18.4 \times 10^{\left[4.84 \times \left(\frac{V_b}{V_v + V_b} - 0.69\right)\right]} \times \left(6.167 \times 10^{-5} \times \epsilon_t^{-3.291} \times S_m^{-0.854}\right)$$

where:

ϵ_t = Tensile strain in asphalt layer (mm/mm),

V_v = Volume of voids (%) and

S_m = Stiffness modulus (MPa).

The 20mm DBM used for this comparison is as detailed in Chapters 3 and 4 of this thesis and the input parameters are:

ϵ_t = 100 microstrain or 0.0001 mm/mm,

V_b = 10.6 %,

V_v = 3.6 %,

Sp_i = 44.5°C and

S_m = 2,000 MPa.

The first method of analysis is the new one described in this thesis, which requires the equation for crack initiation generated using the ITFT:

$$N_i = 6.06 \times 10^{13} \epsilon_t^{-4.032}$$

This gives a life to crack initiation (N_i) of 522,965 standard axles.

The shift factor for crack propagation for critical and failure condition, calculated using equation 8.10, are 1.1 and 6.4 respectively. Therefore, the lives to critical and failure condition are:

$$\textit{Critical Fatigue Life } (N_f) = 522{,}965 \times 1.1 \times 20 \times 1.1 = 12{,}655{,}753 \approx 13 \textit{ MSA}$$

$$\textit{Failure Fatigue Life } (N_f) = 522{,}965 \times 1.1 \times 20 \times 6.4 = 73{,}633{,}472 \approx 74 \textit{ MSA}$$

The Nottingham Analytical Design method gives:

$$\textit{Critical Fatigue Life } (N_f) = 2{,}845{,}324 \approx 3 \textit{ MSA}$$

$$\textit{Failure Fatigue Life } (N_f) = 16{,}373{,}130 \approx 16 \textit{ MSA}$$

The Asphalt Institute method gives:

$$\textit{Fatigue Life } (N_f) = 21{,}280{,}550 \approx 21 \textit{ MSA}$$

It should be stated here that there is only one value given in the Asphalt Institute method which is defined as the life to approximately 20% or greater fatigue cracking (based on total pavement area. This condition probably lies close to the critical condition used in the other two methods.

The values given in Table 8.2 take the following data for each material

20mm DBM as described previously

30/14 HRA

ϵ_t = 100 microstrain or 0.0001 mm/mm,

V_b = 17.5 %,

V_v = 3.2 %,

Sp_i = 54.5°C and

S_m = 2,000 MPa.

28mm DBM50

ϵ_t = 100 microstrain or 0.0001 mm/mm,

V_b = 8.9 %,

V_v = 11.5 %,

Sp_i = 53.5°C and

S_m = 2,000 MPa.

30/14 HRA SBS modified

ϵ_t = 100 microstrain or 0.0001 mm/mm,

V_b = 17.5 %,

V_v = 3.8 %,

Sp_i = 84°C and

S_m = 1,000 MPa.

Table 8.2 - Comparison of Fatigue Lives Based Upon Three Different Methods of Analysis.

	New Method (MSA)		Nottingham Method (MSA)		Asphalt Institute (MSA)
	Critical	Failure	Critical	Failure	
20mm DBM	13	74	3	16	21
30/14 HRA	80	454	91	525	142
28mm DBM 50	8	49	5	28	2
30/14 HRA SBS	110	625	13	73	19

The values of the tensile strain are typical values for the mixtures described here with the value for the SBS material being higher due to a considerably lower stiffness.

From Table 8.2 it can be seen that for unmodified mixtures the results are comparable, however, the SBS modified material shows that the traditional empirical methods cannot cope with polymer modification but that the new method gives a far more realistic life to critical or failure condition. It is, therefore, considered that the new method provides a significant improvement in the fatigue analysis of bituminous paving mixtures particularly with regard to polymer modified mixtures. It is, however, important to reiterate the point that the equations for generating the shift factors for crack propagation do not cover every mixture type and that further testing and analysis will be required in order to avoid extensive extrapolation of the data and also the equations are only valid over the range of stiffnesses measured during the course of the crack propagation work. It is also necessary to state here that the validity of this novel method needs verification in either full scale trials or at the least in a large scale testing facility.

8.5 References

1. Brunton, J.M., "Developments in the Analytical Design of Asphalt Pavements Using Computers," PhD Thesis, University of Nottingham, Department of Civil Engineering, May 1983.
2. Van Dijk, W., "Practical Fatigue Characterisation of Bituminous Mixes," Proceedings of the Association of Asphalt Paving Technologists (AAPT), Volume 44, pp 38-74, 1975.
3. Brown, S.F. and Brunton, J.M., "An introduction to the analytical design of bituminous pavements - 3rd edition," University of Nottingham, Department of Civil Engineering, U.K., 1992.
4. Anon, "Thickness Design - Asphalt Pavements for Highways and Streets," The Asphalt Institute, Manual Series No. 1, MS-1, September 1981.
5. Finn, F., *et al*, "The Use of Distress Prediction Subsystems for the Design of Pavement Structures," 4th International Conference on Structural Design of Asphalt Pavements (ISAP), Ann Arbor, Volume 1, pp 3-38, 1977.

6. Shook, J.F., *et al*, "Thickness Design of Asphalt Pavements - The Asphalt Institute Method," 5th International Conference on Structural Design of Asphalt Pavements (ISAP), Delft, pp 17-44, 1982.

7. Monismith, C.L., Finn, F.N., Kasianchuk, D.A. and McLean, D.B., "Asphalt Mixture Behaviour in Repeated Flexure," Report No. TE 70 - 5, University of California, Berkeley, 1970.

DISCUSSION AND CONCLUSIONS

9.1 Introduction

This section discusses the results of the three areas of work and draws conclusions based upon the findings. It is intended to demonstrate that each of the pieces of work is independently of use but that they can be used together to form a coherent method of assessing the overall fatigue resistance of a bituminous paving mixture.

9.2 Indirect Tensile Fatigue

The results show that the Indirect tensile fatigue test is a suitable method for assessing the life to crack initiation of a bituminous paving mixture. This was achieved by comparing the ITFT with two other methods of fatigue test; the trapezoidal cantilever test and the uniaxial tension-compression test. A comparison of the maximum allowable strain at 10^6 cycles was performed demonstrating that the variation between the individual tests was typically about 15%. Thus, it may be concluded that the ITFT gives results equivalent to the other test methods and, hence, the problems raised by other researchers over the shorter lives predicted by the ITFT have been resolved. However, it must be stated that this agreement has only been evaluated under certain sets of conditions and agreement under conditions outside of those used in this work cannot be inferred. This section of work also demonstrated that the ITFT was capable of evaluating polymer modified mixtures, showing that SBS materials exhibited superior crack initiation properties compared to the identical mixture manufactured with conventional bitumen. During the course of this initial work it was found that test temperature and/or air void content (within the ranges tested) did not affect the position of the fatigue line but did affect the position of the data point on the line. These parameters, therefore, affected the stiffness which affected the magnitude of the tensile strain generated in the specimen and, hence, the life to crack initiation of the specimen.

From the initial work it was evident that the ITFT was capable of generating the fatigue line for life to crack initiation in as little as four hours. This is considerably quicker than any other method, hence, making the ITFT a commercially viable test. However, care must be taken to ensure that tensile failure is achieved and not compressive or shear failure as described in Chapter 3. Based upon the evidence presented in this dissertation the author has drafted a British Standard based upon the protocol. This means that there is now a national reference for fatigue testing, a considerable step forward from the previous position of generally no fatigue testing being performed in the U.K..

Following this initial work a programme of testing was undertaken to assess the repeatability and reproducibility of the ITFT. The repeatability work was performed on three mixtures: 30/14 HRA, 20mm DBM and a crumb rubber modified Marshall asphalt. The results, based on comparisons within the data set, showed that the variability was unlikely to be more than 8% and that the variability of extrapolated data was unlikely to be more than 10%; this provided a very high level of confidence in the test. Based on these results a series of reproducibility trials were conducted involving six laboratories, each testing three different materials: 30/14 HRA, 20mm DBM and a 40mm HDM. The results showed that the reproducibility of the ITFT was also very good and that the variation in data between any two different laboratories was likely to be less than 17%. It is envisaged that the variability for both repeatability and reproducibility will be considerably reduced when full precision trials involving much larger data sets are carried out by the British Standards Institution.

The results section also described the practical use of the ITFT for evaluating the fatigue resistance of various bituminous layers in a pavement. This showed that, during the initial life of this particular pavement, changes in fatigue performance were caused by a mechanism other than traffic loading, and it was surmised that the change was probably due to environmental factors. This practical work led onto the first contractual use of the ITFT to evaluate a bituminous layer which had areas of material with a low binder content. By using the ITFT to measure the fatigue resistance it was possible to show that:

- There appeared to be no significant difference between the disputed areas and the control areas in terms of fatigue life.
- As the control areas were not in dispute then neither should the areas with low binder content.

The final outcome was to leave the disputed material in place, thus, saving hundreds of thousands of pounds and, to date, there have been no problems with the material. This contractual use of the ITFT again demonstrates the value and commercial viability of the test.

Towards the end of the research into the ITFT it was decided to evaluate mixtures which were not of U.K. origin in order to assess whether the ITFT was a valid test for mixtures outside of typical U.K. experience. To this end two French continuously graded mixtures were tested in the ITFT and compared to fatigue lines generated in the uniaxial tension compression test, these tests showed that the ITFT was valid for these mixtures under the conditions of test utilised in the comparison. In addition an SMA was tested and also showed the ITFT to be suitable, hence, continuing the evolution and validation of the test and test method.

The conclusions drawn from the work on the ITFT are:

1. There is a good correlation, under certain conditions of test, between fatigue results obtained with the Indirect Tensile Fatigue Test and the more fundamental Trapezoidal test when comparing them on the basis of applied maximum tensile strain.

2. There is a good correlation, under certain conditions of test, between fatigue results obtained with the Indirect Tensile Fatigue Test and the more fundamental uniaxial tension-compression test when comparing them on the basis of applied maximum tensile strain.

3. On the basis of maximum tensile strain (ϵ_{xmax}) against life to failure using the methods outlined in this dissertation and the relevant protocols, over the range of materials studied, the temperature of test can be changed without affecting the resulting fatigue characterisation.

4. The ITFT is able to characterise the fatigue performance of a material by testing:
   - A small number of specimens ($\approx$10)
   - At convenient test temperatures (20 to 30°C)
   - Under conditions of high tensile stress (>450 kPa)

   This implies that the fatigue testing time needed to produce an adequate fatigue relationship for a bituminous material could be as little as 4 hours. However, care must be taken to ensure tensile failure occurs as opposed to either compressive of shear failure.

5. Specimens, of nominally identical material, with different void contents (28mm DBM 50) produced a single fatigue line. The void content does, however, affect the stiffness of the specimen and hence, determines the position of the data point on the fatigue line.

6. The ranking of the materials tested in the main programme indicated that the 30/14 HRA SBS modified mixture performed better than the other mixtures tested with respect to resistance to fatigue cracking.

7. The 30/14 HRA unmodified mixture performed less well than the modified mixture but performed very well in comparison to the continuously graded mixtures.

8. The two continuously graded mixtures (20mm DBM and 28mm DBM 50) exhibited approximately the same fatigue characteristics.

9. The ITFT proved to be a highly repeatable test.

10. The ITFT proved to be a highly reproducible test.

11. The ITFT has been shown to be capable of testing most bituminous mixtures.

12. The comprehensive evaluation of the ITFT show that it is:

- **Experimentally sensible**
- **Simple**
- **Inexpensive**
- **Commercially viable**

9.3 Poisson's Ratio

The work found that, for bituminous materials, Poisson's ratio is generally greater than 0.50 during early loading cycles, this then decreases until it reaches 0.35 and steady state conditions are achieved. This phenomenon has been attributed to the thickening and thinning of the bitumen films around the aggregates during each load cycle until no further change takes place. The number of load applications to achieve steady state conditions was found to be in the region of 500 under all conditions of test which were investigated. The value of 0.35 appeared to be consistent despite variations of temperature, void content or mixture type. This has implications for both the Indirect Tensile Stiffness Modulus (ITSM) and for the ITFT and would seem to indicate that at least 500 conditioning pulses should be applied to a specimen prior to taking a measurement of stiffness. However, it was found that neither the speed nor the magnitude of the conditioning pulses had much effect on the final value for Poisson's ratio and, hence, provided that the load pulses are low stress and applied quickly the stiffness test should still be fast and non-destructive. Following stiffness testing the specimen should be oriented in the same way in the ITFT so that the value of 0.35 for Poisson's ratio will still be valid.

Due to the high initial values for Poisson's ratio it was decided to ascertain whether it was a true material effect or an error induced by the test or measuring equipment. To check this the measurement and testing system was used on a cube of aluminium. This gave

a correct value, for Poisson's ratio, for aluminium and, hence, the effect was deemed to be a true material phenomenon. The only other possible variable which could have caused such an error was that the linear elastic theory was incorrect. To evaluate this aluminium was again used but this time in the form of a cylinder subject to the same loading regime as the bituminous specimens in the ITFT. This gave a correct value for Poisson's ratio and not only allowed the measurement and test system to be validated but also the linear elastic theory used for the calculation of the stresses and strains in both the ITSM and the ITFT.

The conclusions drawn from the work on Poisson's ratio are:

1. Poisson's ratio is a difficult parameter to measure as bituminous materials are visco-elastic and, therefore, able to accumulate permanent deformation. Thus, only small strains can be generated before the aggregate structure begins to change.

2. The measurement system developed for Poisson's ratio appears to be able to cope with the small strains needed to avoid damaging the specimen.

3. There appears to be some internal restructuring of the mixture as indicated by the high values of Poisson's ratio obtained during the early stages of the tests on the cubes and cores of material.

4. The variation of Poisson's ratio under the initial 500 load applications has been shown to be a true material effect.

5. The use of linear elastic theory for calculation of indirect tensile parameters has been shown to be appropriate under certain conditions: fast loading times and/or low temperatures.

6. When carrying out indirect tensile stiffness tests a large number of conditioning pulses should be applied to the specimen in order to ensure that Poisson's ratio has achieved a constant value.

7. Test frequency appears to have little or no effect on the measured value of Poisson's ratio.

8. Test temperature appears to have little or no effect on the measured value of Poisson's ratio.

9. Material stiffness appears to have little or no effect on the measured value of Poisson's ratio.

10. Based on the testing carried out in this research, it appears appropriate to use a value of 0.35 for Poisson's ratio under all conditions of test. Although it must be stated that this was evaluated for only two mixture types, a sand asphalt and a 30/14 HRA, and, therefore, further testing is required in order to validate the use of 0.35 for all mixtures.

9.4 Crack Propagation

The main finding of the work on crack propagation was that the life for crack propagation appears to be heavily dependent upon the magnitude of the initial stiffness. The relationship between the life and the initial stiffness was found to be a power relationship and the 40 different mixtures tested fell into four groups:

- SBS modified mixtures
- EVA modified mixtures
- HRA unmodified mixtures
- DBM unmodified mixtures

From these relationships a general equation was developed for estimating the shift factors which need to be applied to the measured life to crack initiation (ITFT testing) to account

for the crack propagation phase. However, there is some concern that the power relationship is too sensitive to small changes in stiffness for practical use and this needs to be further evaluated. The work went on to demonstrate how the work on the ITFT, Poisson's ratio and crack propagation may be combined to give a fatigue procedure which can be used for:

- Mixture Design
- Pavement Evaluation
- Pavement Design

It was found that image analysis is a very promising tool for the evaluation of crack propagation rates but that during this work it could not be used for an overall analysis of the results as generally there were only cracks visible on the unmodified beams. This being said it is envisaged that if a larger strain was developed across the crack initiation gap then the cracks in the polymer modified materials would be far more visible. This however may be a problem in itself as concerns have already been highlighted over the relatively large strains used in the work presented in this dissertation.

The image analysis was used for a qualitative assessment of the crack propagation route and it was found that cracks always propagate around the coarse aggregate trying to separate it from the matrix. This gives an indication that the interface between the coarse aggregate and the matrix is weak compared to the rest of mixture and forms a preferential path for cracks. The image analysis work also found that increasing the local presence of coarse aggregate helped to retard the linear crack growth due to the more circuitous path that the cracks takes. However, it was noted that the cracks tried to take the shortest route between the point of crack initiation and the point of applied load via the interface between the coarse aggregate and the matrix. It is envisaged that further development of the image analysis system and software should allow an automated system which will predict the path of cracks, monitor and control the test system and measure the length of the cracks.

The conclusions drawn from the work on crack propagation, therefore, are:

1. Crack propagation rate appears to be heavily influenced by the initial stiffness of the material and can be described by a power relationship that is mixture specific.

2. The lower the initial stiffness the better the materials resistance to crack propagation, however, it is envisaged that there will be a threshold stiffness at which the material will no longer be capable of supporting the applied loading.

3. SBS modified materials considerably outperform materials made with 50pen, 100pen and EVA modified bitumen.

4. Cracks attempt to follow the shortest route, around the interface between the coarse aggregate and the matrix, between the point of crack initiation and the point of the applied load.

5. The path of least resistance to cracks appears to be the interface between the coarse aggregate and the matrix.

6. Increasing the quantity of coarse aggregate, provided there is no increase in initial stiffness, improves the resistance to crack propagation due to more tortuous path of the crack

7. A method has been established for calculating the shift factors to be applied to the life to crack initiation which combines all the work described in this dissertation.

RECOMMENDATIONS FOR FUTURE RESEARCH

10.1 Indirect Tensile Fatigue

1. Numerical quantification of the repeatability and reproducibility of the ITFT needs to be obtained in order for the test method to become a full national standard and eventually a European standard.

2. Further testing of unusual and new mixtures is required to ensure that the ITFT continues to be applicable to all mixture types, including cold mixtures.

3. Validation of the test method by comparison with realistic conditions is needed. It is envisaged that, initially, this will be done in a large scale wheel tracking apparatus and subsequently in the field by continuous monitoring.

4. Development of a method of measuring the horizontal deformation which will not be damaged when a specimen fails is essential for the continued evolution of the test and test method. This will allow a much more accurate determination of the point of crack initiation and will also allow the stiffness to be measured during the test. This will negate the need for Indirect Tensile Stiffness Modulus (ITSM) testing, hence, reduce the overall testing time making the test even more economically viable than it is at present.

5. Establishment of a large database of ITFT information from which specification criteria can be produced which will be statistically acceptable and mixture specific.

10.2 Poisson's Ratio

1. Now that a simple and reliable method of test has been established testing needs to be carried out on a much greater range of mixtures, binder contents, gradations,

compaction levels, temperatures, stresses and frequencies to ensure that the single value of 0.35 is correct for all mixtures under all conditions.

2. Fundamental research into the mechanism causing the initial decrease of Poisson's ratio over the first 500 load applications is required in order to fully understand why the material behaves as it does.

3. Triaxial testing should be undertaken to ascertain whether different levels of confinement have an effect on Poisson's ratio. Dependent upon the results an appropriate value of Poisson's ratio should be obtained for use in pavement design at the level of confinement provided by the pavement structure.

10.3 Crack Propagation

1. Continuation of the testing is required in order to evaluate whether the power relationship between the crack propagation rate and stiffness is true for all materials. Assuming that this is shown to be the case then a model, dependent upon the different parameters of each relationship, may be able to be developed which can predict the crack propagation characteristics of any mixture under any condition. An assessment of the sensitivity of the power relationship is also required to determine its suitability for practical use.

2. Further development of the testing apparatus is required to allow images from both sides of the beam to be analysed, thus allowing an average crack propagation rate for the beam to be measured.

3. Testing at higher strains is needed to generate cracks in modified materials which can be monitored using image analysis, since this research failed to generate measurable cracks in most of the modified materials.

4. Validation of the use of high strains is required to demonstrate the suitability of the methods outlined in Chapter 8.

5. It is considered that it may be possible to monitor the deformation zone around the crack tip by placing, or drawing, a very fine grid on the surface of the beam prior to testing and then analysing the grid displacement during testing using the image analysis equipment. This may lead to a better understanding of the material and it may be feasible to apply fracture mechanics to the system with a higher degree of confidence than is currently possible.

6. Validation of the general equation (equation 8.10) for crack propagation is necessary. It is envisaged that, initially, this will be done in a large scale wheel tracking apparatus and subsequently in the field by continuous monitoring.

7. Development of the work done by Schapery and Jacobs on visco-elastic fracture mechanics is required along with development of the apparatus to enable the required parameters to be measured. This should allow a fundamental assessment of crack propagation to carried out along with the development of suitable mathematical models.

APPENDIX A



PROTOCOL FOR MANUFACTURE AND STORAGE

This protocol was written to ensure that all of the samples used in the research described in this thesis have been manufactured, stored and handled in the same manner.

APPARATUS AND CALIBRATION DETAILS

Below is listed all the apparatus and calibration information required by this protocol.

Equipment	N°	Calibration Organisation	Calibration Parameter	Calibration Method	Calibration Frequency
Forced Draft Oven	4	U.N.*	Temperature	Five Point Sand Test on Each Shelf	6 Months
Heated Sun & Planet Mixer	2	U.N.	Temperature	Comparison Against NPL Traceable Thermocouple	6 Months
Aluminium Mould (404 × 280 × 127mm)	4	U.N.	Length	Comparison Against NPL Traceable Ruler	6 Months
Pneumatic Roller Compactor	1	U.N.	Pressure	Comparison Against a Calibrated Pressure Meter	6 Months
Sartorius Balance	1	European Instruments	Mass	-	12 Months
75mm Paint Scraper	1	-	-	-	-
Spherical Headed Tamping Rods	2	-	-	-	-
Divider	1	-	-	-	-
Thermometers (K-Type)	2	U.N.	Temperature	Comparison Against NPL Traceable Thermocouple	6 Months
Stop clock	2	U.N.	Time	Comparison Against NPL Traceable Time Piece	6 Months

*** This means calibrated internally at the University of Nottingham (U.N.)**

SPECIMEN MANUFACTURE

1. On receipt, the aggregate shall be dried in preparation for batching and mixing in accordance with the grading requirements.

2. The target mixing temperature shall be selected in order to give a viscosity of 170 ± 20 centistokes based on the initial binder properties.

MIXING

1. The aggregate shall be weighed into clean metal trays in the required proportions to give the required individual batch sizes. The trays shall then be placed in a thermostatically controlled oven and the aggregate heated to within 5°C of the mixing temperature.

2. The required mass of bitumen shall be heated, at the same time as the aggregate, in an air jacketed container, again to within 5°C of the mixing temperature.

3. When at the correct temperature, the aggregate shall be placed in a sun and planet mixer and a small hollow formed in the centre of the loose material to receive the bitumen. The bitumen shall be weighed into the mixer in accordance with the batch weights. Mixing temperature shall be maintained by means of a heated oil jacket around the mixing pan.

4. The bitumen and aggregate shall then be mixed for 120 seconds or until uniform bitumen coverage is achieved. On completion of mixing the material shall be discharged into a heated metal tray which is placed in an oven set at the compaction temperature, until all five trays are mixed and at the compaction temperature.

COMPACTION

1. The compaction temperature shall be determined to give a viscosity in the unaged binder of 280 ± 30 centistokes.

2. The specimens shall be manufactured in aluminium moulds with plan dimensions of 404 by 280mm. The batch weights shall be calculated so that a slab, compacted to a final thickness of 127mm, will have a specified void content.

3. The height of the jambs on the roller compactor shall be set using a block of mild steel, machined to a height of 127mm, positioned under the rolling section of the compactor. This allows the play in the frame and trolley to be removed when full pressure is applied, therefore ensuring that the final height of the compacted slab is precisely 127mm.

4. The aluminium mould, which has been oven heated to the compaction temperature, shall be fixed to the trolley of the roller compactor.

5. Five trays of mixed material shall be taken from the oven and placed in the mould in a single layer, guide slots shall be used during placing to ensure even distribution across the mould. The material shall be tamped with a heated, spherical headed, tamping rod. After tamping the guide slots shall be removed and the surface levelled with a spatula.

6. The material shall then be compacted, under the action of the rolling section, to the required depth using a pneumatic roller compactor.

7. The finished surface level shall be achieved by forcing a heated aluminium plate, fitted inside the mould and on top of the partially compacted material, down to the required level which is fixed by the jambs of the roller compactor.

SPECIMEN PREPARATION

1. Following compaction, the slabs shall be allowed to cool before being stripped from the compaction moulds. The slab shall then be sawn and cored into the appropriate geometries using the clipper saw and coring rig.

2. Once prepared the samples shall be stored for a defined period of time, as specified by the operator, at 5°C. The exact time between mixing and testing shall be recorded for future reference.

Any deviation from this protocol shall be reported with the test results.

British Standard Draft for Development

DD ABF Method for the determination of the fatigue characteristics of bituminous mixtures using indirect tensile fatigue

This publication is a Draft for Development and is therefore not to be regarded as a British Standard.

Comments should be returned to

Mr J M READ
RESEARCH OFFICER
DEPARTMENT OF CIVIL ENGINEERING
UNIVERSITY OF NOTTINGHAM
UNIVERSITY PARK
NOTTINGHAM
NG7 2RD.

Foreword

This Draft for Development has been prepared under the direction of Working Group 2 of Technical Committee B/510/1. It describes a procedure for determining the fatigue characteristics of a bituminous mixture using the indirect tensile fatigue test.

CONTENTS

	Page No.
1. SCOPE	A8
2. DEFINITIONS	A8
3. SUMMARY OF TEST METHOD	A8
4. APPARATUS	A8
5. SAMPLE PREPARATION	A9
8. CALCULATION	A11
9. PRECISION	A12
10.REPORTING OF RESULTS	A13

Method

1. SCOPE

This test describes a method to estimate the resistance to fatigue failure of bituminous mixtures. The method is applicable to wearing courses, base courses and roadbases containing penetration grade bitumens or modified binders.

The results should only be considered as indicating the fatigue characteristics of bituminous mixtures. Caution should be exercised when quoting finite values or when comparing results of different materials tested under different conditions or tested by different methods.

2. DEFINITIONS

2.1 For the purposes of this Draft for Development, the definitions given in BS 598: Part 100 apply together with the following.

2.2 *Failure of a test specimen* is when there is 9 mm of vertical deformation of the top loading strip.

3. SUMMARY OF TEST METHOD

3.1 The dimensions of the test specimens shall be measured and recorded. The specimens are then conditioned at the test temperature before being placed in the test frame, centred on and with the flat faces of the specimen perpendicular to the bottom loading strip. The top loading strip is then be placed on the frame so that it is located centrally on the specimen. The loading is then applied via the test apparatus. Each specimen is tested at a different target level of the maximum tensile stress at the centre of the specimen.

3.2 For each specimen, the maximum tensile horizontal strain at the centre of the specimen is calculated from Poisson's ratio, the maximum tensile stress at the centre of the specimen and the indirect tensile stiffness modulus at the maximum tensile stress at the centre of the specimen.

3.3 The indirect tensile stiffness modulus is stress related due to the non-linear visco-elastic nature of bitumen. Preferably, this parameter at the indirect tensile fatigue test stress level is obtained using a controlled stress version of the stiffness test. If this test is unavailable, the parameter is obtained from a series of indirect tensile stiffness moduli measurements at different stress levels for each specimen.

4. APPARATUS

The apparatus shall consist of:

4.1 *Test system* capable of imparting 0 to 4 kN through a spherical seating with a rise-time of between 80 and 160 ms. A schematic diagram of the testing apparatus is shown in Figure 1.

4.2 *Fatigue testing frame* of a sufficiently rigid nature to ensure that all the applied load is transmitted to the specimen and with top and bottom loading strips. The frame shall have a safety system which ensures that, upon violent failure of the samples, the top loading strip does not drop and damage the bottom loading strip.

4.3 *Top and bottom loading strips* made of hardened steel and machined to a width of 12.5 ± 2 per cent over the range.

4.4 *Linear Variable Differential Transformers* having a gauge length of at least 10 mm and an accuracy of 0.1 per cent over the range.

4.5 *Data logging equipment* capable of capturing data on the applied force, transient deformation, overall deformation and the pulse number from every load pulse.

5. SAMPLE PREPARATION

5.1 General

The samples shall be either laboratory prepared or cut from a pavement, but all the samples taken to generate one fatigue relationship shall be from one method or the other.

5.2 Sample Geometry

The samples shall be cylindrical with a thickness of 40 ± 5 mm and a diameter of 100 ± 3 mm. The parallel flat ends shall be trimmed to a tolerance of ± 0.5 mm.

Note. 150 mm diameter samples can be used for the stiffness testing and then 100 mm samples cored out of the centre of them. However, it is preferable to carry out the stiffness test on the actual 100 mm core that is to be used in the indirect tensile fatigue test.

5.3 Measurement of the Sample

5.3.1 Take four determinations of the diameter at approximately equal distances around the circumference of each sample (Figure 2). The diameter of the sample, d (mm), shall be the mean of these determinations calculated to the nearest whole millimetre.

5.3.2 Take eight measurements of the thickness at the same points as the diametral measurements (Figure 2). The thickness of the sample, t (mm), shall be the mean of these determinations to the nearest whole millimetre.

Note. The sample geometry for the stiffness testing shall comply with all requirements of DD 213 current at the time of testing.

6. PROCEDURE FOR INDIVIDUAL DETERMINATIONS

6.1 Test Temperatures

The test temperature shall be 20°C ± 1°C. Both the stiffness modulus and fatigue testing shall be carried out at this temperature.

Note. Test temperatures other than 20°C may be used but the chosen temperature must fall in the range 0 to 30°C. Operators should be aware that, if testing at the low temperatures in this range, tests may progress for extended periods. They should also take care when testing above 25°C that the loading strips do not dig into the specimen by more than 2 mm, measured by placing a straight edge over the indentation and measuring the maximum value. If this does occur then the test specimen and result is void.

6.2 Indirect Tensile Stiffness Modulus

6.2.1 Determine the indirect tensile stiffness modulus of each specimen in accordance with DD 213.

6.2.2 If the controlled stress version of the software is available, the target stress level

for the indirect tensile fatigue test shall be used for the controlling value of stress during the stiffness test.

6.2.3 If the controlled stress version of the software is not available, the target deformation shall be 5 μm, 9 μm, 13 μm and 17 μm on each of two axes of the sample.

Note. These deformations are intended as general guidance and it may be necessary, due to the type of material being tested, to adjust the actual target deformations in order to achieve a spread of stress levels. It is suggested that this spread be at least 200 kPa where possible. As the deformations are variable and only used to achieve a range of stress levels, no tolerances need be applied.

6.2.4 Tabulate the resulting eight stiffness measurements and their corresponding stress levels and calculate the average stiffness modulus for the sample.

Note. A suitable table is given as Table 1.
Table 1: Standard Result Sheet

Horiz-ontal deform-ation (μm)	Axis 1		Axis 2	
	Stress (kPa)	Stiffness (MPa)	Stress (kPa)	Stiffness (MPa)
5				
9				
13				
17				

6.3 Indirect Tensile Fatigue Testing

6.3.1 Position the specimen on the lower loading strip so that it seats itself properly without excessive movement and so that the two faces of the specimen are perpendicular to the loading strip. Place the upper loading strip on the top of the specimen and seat it such that there is no excessive movement.

6.3.2 Adjust the linear variable differential transformers so that they are at the minimum limit of their linear range, thus allowing them to measure over a range of at least 9 mm.

6.3.3 Apply the loading at a rate of 40 ± 1 pulses per minute at the test stress level.

6.3.4 Record the number of load applications to failure of the test specimen.

7. PROCEDURE FOR FATIGUE ANALYSIS

7.1 Number of Determinations

7.1.1 For a full test, carry out determinations on not less than ten specimens for mixtures with a maximum nominal aggregate size of 20 mm and below and on not less than twelve specimens for mixtures with a maximum nominal aggregate size greater than 20 mm.

7.1.2 For a restricted test, carry out determinations on not less than five specimens for mixtures with a maximum nominal aggregate size of 20 mm and below and on not less than ten specimens for mixtures with a maximum nominal aggregate of grater than 20 mm.

7.2 Target Test Stress Level

7.2.1 The target test stress level for the first specimen to be tested shall be 600 kPa unless this cannot reliably be obtained, when the first target stress level shall be 500 kPa.

7.2.2 The target test stress level for the second, third and fourth specimens are given in Table 2.

Table 2: Target test stress level for second, third and fourth specimens

Test Stress Level	N_{500} ≤200	200< N_{500} ≤500	500< N_{500} ≤1000	1000< N_{500}
2nd Specimen	400	425	450	475
3rd Specimen	300	350	400	450
4th Specimen	200	250	300	400
Test Stress Level	N_{600} ≤200	200< N_{600} ≤500	500< N_{600} ≤1000	1000< N_{600}
2nd Specimen	500	525	550	575
3rd Specimen	400	450	500	550
4th Specimen	300	350	400	500

where N_{500} is the number of load applications applied to the first specimen tested at a stress level of 500 kPa; and
N_{600} is the number of load applications applied to the first specimen tested at a stress level of 600 kPa.

Note. The values given in Table 2 are for guidance only and it is envisaged that, as operators become experienced, they will be better able to choose test stress levels.

7.2.3 The target test stress levels for the fifth and subsequent specimens shall be selected to give as wide a range of lives as possible. The minimum spread of lives must be one order of magnitude so that the maximum value of N_{600} or N_{500} is at least ten times greater the minimum value.

8. CALCULATION

8.1 Maximum Tensile Stress at the Centre of the Specimen

Calculate the maximum tensile stress at the centre of the specimen, $\sigma_{x,max}$ (kPa), from:

$$\sigma_{x,max} = \frac{2 \times P_L}{\pi \times d \times t}$$

where P_L is the vertically applied line loading (kN);
d is the diameter of the test specimen (mm); and
t is the thickness of the test specimen (mm).

8.2 Maximum Tensile Horizontal Strain at the Centre of the Specimen

Calculate the maximum tensile strain generated at the centre of each specimen, $\epsilon_{x,max}$ (microstrain), from:

$$\epsilon_{x,max} = \frac{\sigma_{x,max} \times (1 + 3\nu)}{S_m} \times 1000$$

where $\sigma_{x,max}$ is the maximum tensile stress at the centre of the specimen (kPa);
ν is Poisson's ratio (assumed to be 0.35); and
S_m is the indirect tensile stiffness modulus at $\sigma_{x,max}$ (MPa).

8.3 Tabulation of Results

Tabulate the results for each test specimen.

Table 3: Typical format for tabulating results

Specimen number	Diameter (mm)	Thickness (mm)	$\sigma_{x,max}$ (kPa)	S_m (MPa)	$\epsilon_{x,max}$ (microstrain)	Number of cycles to failure (N)
1						
2						
3						
4						
...						
N						

Note. A suitable table is given as Table 3.

8.4 Generation of the Fatigue Relationship for the Bituminous Mixture

8.4.1 Plot the maximum tensile horizontal strain at the centre of the specimen ($\epsilon_{x,max}$) against the number of cycles to failure (N_f) using logarithmic horizontal and vertical axes.

8.4.2 Apply linear regression analysis using the Least Squares method to the paired data of $\log_{10}(\epsilon_{x,max})$ and $\log_{10}(N_f)$ in order to obtain the equation of the line.

Note 1. An example of such a fatigue line with the linear regression is shown in Figure 4.

Note 2. It should be noted that specimens of the same material tested at different temperatures should lie on the same line.

8.5 Statistical Significance

8.5.1 Calculate the square of the correlation coefficient (R^2) for the linear regression analysis.

8.5.2 If the value of R^2 is below 0.90, test additional specimens and incorporate the results into the data set until, when repeating the linear regression analysis, the value of R^2 is greater than 0.90.

8.5.3 If, after ten specimens have been added to the data set, the R^2 value is still less than 0.90, the result shall be reported with a statement concerning the statistical significance of the data.

Note. If further specimens are unavailable, then the result shall be reported with a statement concerning the statistical significance of the data.

9. PRECISION

The precision of the test method has still to be determined.

10. REPORTING OF RESULTS

10.1 Information

The test report shall include the following information for each test specimen:

(a) The name and address of the testing laboratory;

(b) A unique serial number for the test report;

(c) The number of specimens tested and whether it was a full or a restricted test;

(d) Descriptions and identifications of the specimens, and the date of receipt;

(e) A completed version of Table 3;

(f) A graphical representation of the fatigue line;

(g) The square of the correlation coefficient and the constants of the equation obtained by linear regression analysis for the number of cycles to failure in terms of the maximum tensile horizontal strain at the centre of the specimen;

(h) the number of cycles to failure (N_f) at a maximum tensile horizontal strain at the centre of a specimen of 100 microstrain calculated from the linear regression analysis equation;

(i) the signature of the person accepting technical responsibility for the test report;

(j) the date of issue;

(k) the number and date of this Draft for Development, i.e. DD ABF;

(l) any test conditions and operational details not provided in this Draft for Development, and anomalies, if any, likely to have affected the results.

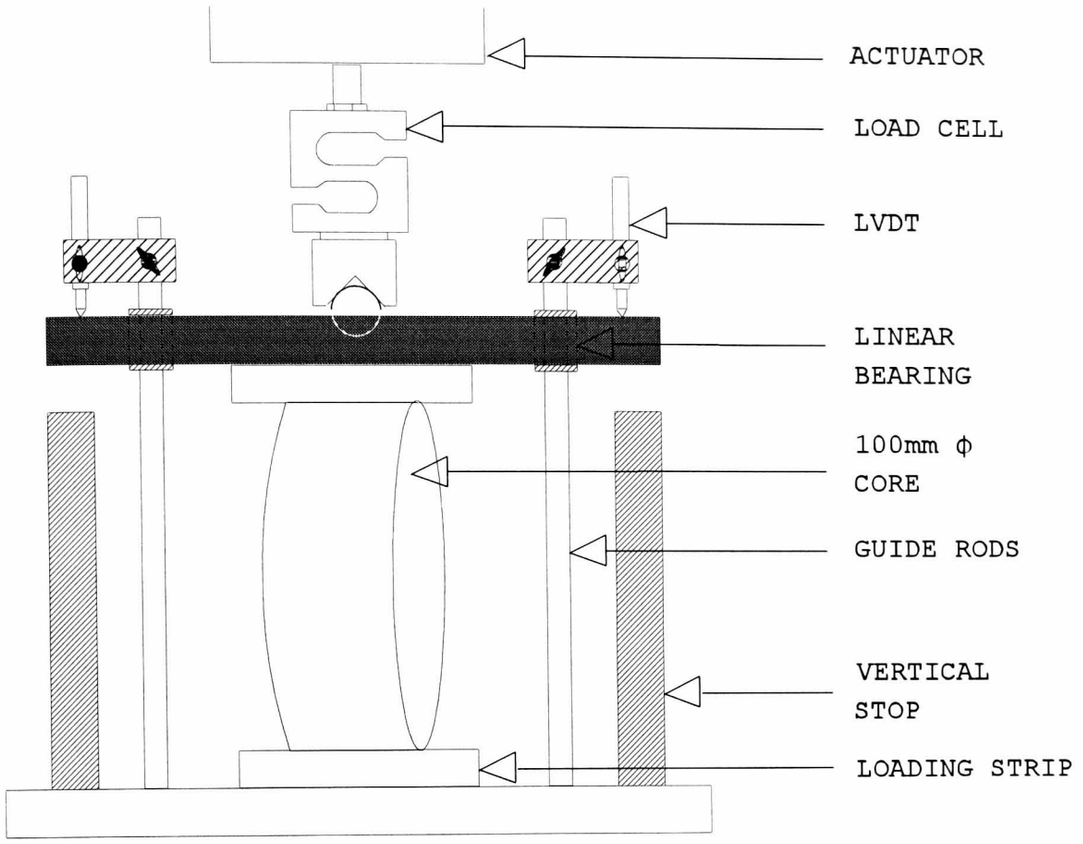


Figure 1: Schematic of one possible apparatus configuration

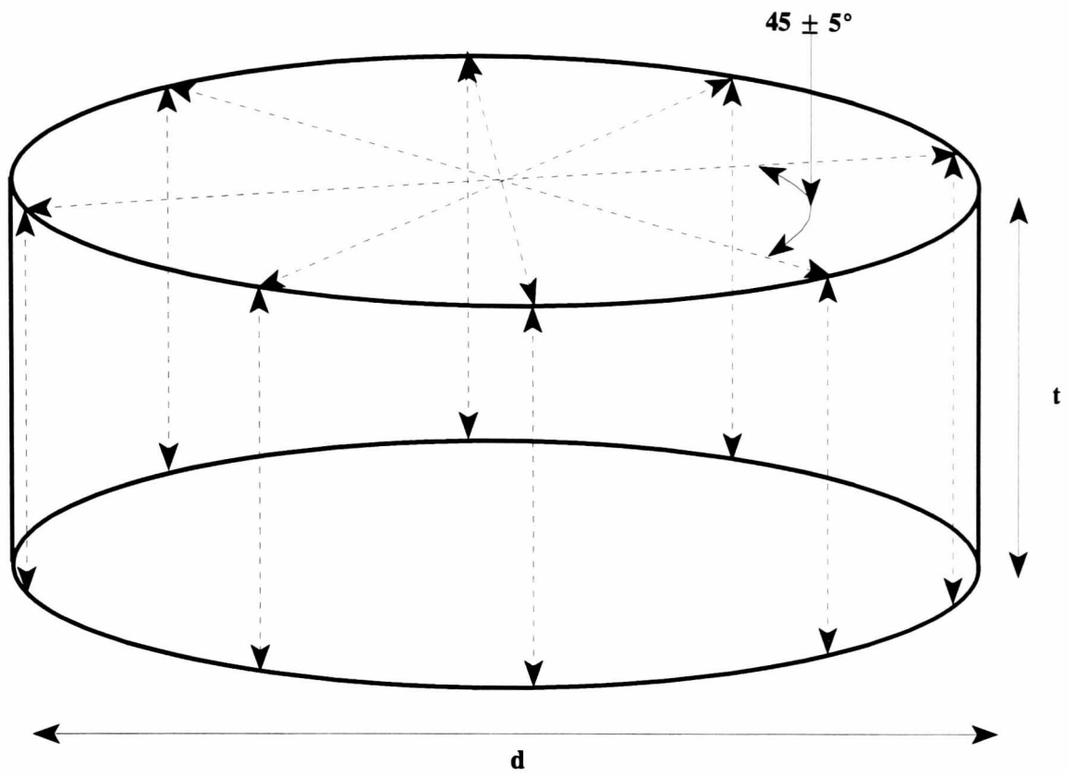


Figure 2: Schematic showing the position of measurement

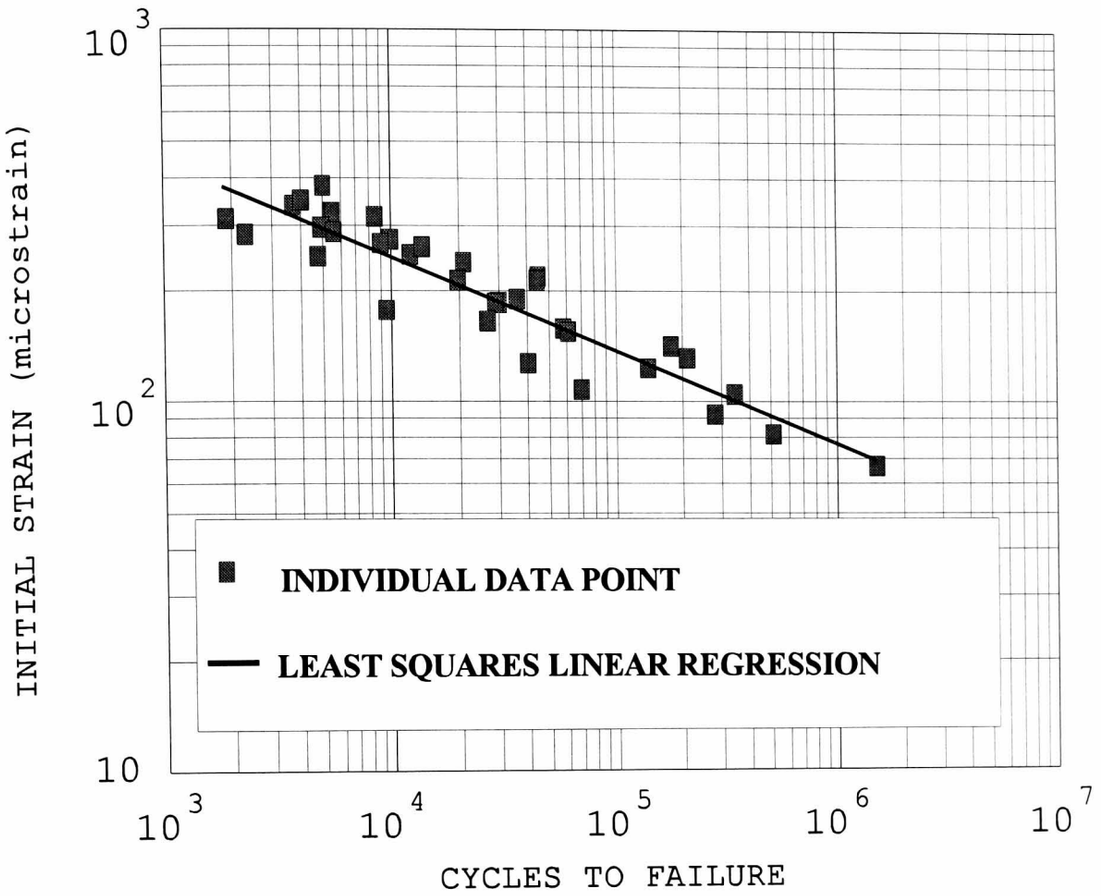


Figure 3: Example of a fatigue graph

APPENDIX B

DATA FOR ITFT WORK

The tables given in this Appendix have the following notation:

Φ	Diameter of a cylindrical specimen (mm),
Width	Width of either an ITFT of trapezoidal specimen (mm),
G_{mm}	Maximum specific gravity of the mixture,
G_{mb}	Bulk specific gravity of the mixture,
VMA	Volume of voids in the mineral aggregate (%),
V_v	Volume of air voids in the mixture (%),
V_b	Volume of bitumen in the mixture (%),
Temp	Temperature at which the testing was carried out (°C),
Frequency	Frequency at which the testing was carried out, for the trapezoidal and uniaxial tension compression tests this is conventional (Hz). For the ITFT a risetime is given of 120ms which equates to approximately 1Hz,
σ	Level of stress used in the test (kPa),
E	Stiffness modulus of the test specimen (MPa),
ϵ	Level of initial strain in the test specimen (microstrain) and
N	Number of cycles to failure.

Figure B.1 shows a typical ITFT raw data file.

FATIGUE TEST RESULT

Date	12-Oct-93
Specimen Name	B-VP-44
Temperature (°C)	20
Diameter (mm)	100
Thickness (mm)	40
Target Stress (kPa)	125
Failure Deformation (mm)	9

Cycles	Force (kN)	Stress (kPa)	Transient Deformation (mm)	Cumulative Deformation (mm)	Risetime (ms)	Estimate of Stiffness (MPa)
10	0.79	123	0.0602	0.2487	120	1,156
20	0.80	125	0.0559	0.3345	120	1,257
30	0.80	125	0.0544	0.3966	118	1,291
40	0.80	125	0.0517	0.4495	118	1,361
50	0.81	126	0.0524	0.4937	122	1,354
60	0.81	126	0.0525	0.5332	120	1,351
70	0.80	125	0.0502	0.5711	118	1,398
80	0.81	125	0.0511	0.6056	122	1,382
90	0.81	126	0.0521	0.6364	122	1,362
100	0.80	124	0.0498	0.6679	118	1,407
200	0.80	124	0.0502	0.9084	120	1,399
276	0.80	125	0.0505	1.0500	118	1,394
300	0.80	125	0.0518	1.0905	122	1,359
400	0.81	125	0.0535	1.2452	122	1,324
403	0.81	125	0.0522	1.2504	120	1,354
500	0.81	125	0.0526	1.3836	120	1,342
551	0.81	125	0.0511	1.4505	120	1,385
600	0.80	125	0.0539	1.5115	120	1,307
700	0.80	124	0.0540	1.6320	118	1,299
716	0.80	124	0.0539	1.6513	120	1,302
800	0.80	125	0.0551	1.7467	120	1,279
894	0.81	125	0.0551	1.8518	120	1,279
900	0.80	125	0.0552	1.8581	120	1,274
1,000	0.80	125	0.0556	1.9663	120	1,264
1,078	0.81	125	0.0573	2.0503	122	1,232
1,267	0.81	126	0.0582	2.2504	120	1,221
1,459	0.80	125	0.0585	2.4504	120	1,201
1,647	0.81	125	0.0608	2.6506	120	1,160
1,833	0.81	126	0.0629	2.8515	120	1,128
2,000	0.81	126	0.0637	3.0432	120	1,114
2,007	0.80	124	0.0637	3.0508	118	1,101
2,170	0.80	125	0.0649	3.2506	122	1,085
2,321	0.80	125	0.0683	3.4507	120	1,029
2,457	0.80	125	0.0708	3.6503	120	993
2,579	0.81	125	0.0742	3.8506	120	953
2,686	0.81	125	0.0781	4.0530	120	903
2,776	0.80	125	0.0839	4.2509	120	839
2,849	0.80	125	0.0858	4.4507	120	821
2,906	0.80	124	0.0850	4.6511	118	824
2,949	0.81	125	0.0912	4.8519	120	773
2,981	0.81	125	0.1002	5.0509	122	705
3,000	0.81	125	0.1088	5.2129	120	648
3,004	0.81	125	0.1113	5.2569	120	636
3,018	0.80	124	0.1269	5.4537	118	551
3,029	0.62	97	0.1168	5.6551	120	466
3,036	0.26	40	0.0555	5.7491	119	404

Unable to apply required load

Figure B.1 - Typical ITFT Raw Data File.

Table B.1 - Data for 30/14 HRA Used in the Main Test Programme.

	Φ (mm)	Width (mm)	G_{mm}	G_{mb}	VMA (%)	V_v (%)	V_b (%)	Temp (°C)	Frequency	σ (kPa)	E (Mpa)	ε	N
3/2/C	98	42	2.392	2.312	20.8	3.3	17.5	13.5	120ms	450	4,082	226	52,987
3/3/C	98	41	2.392	2.324	20.4	2.8	17.6	13.5	120ms	350	4,147	173	133,529
3/4/C	98	41	2.392	2.325	20.4	2.8	17.6	13.5	120ms	400	4,121	199	86,174
3/5/C	98	41	2.392	2.310	20.9	3.4	17.5	13.5	120ms	425	4,110	212	51,916
3/6/C	98	40	2.392	2.312	20.8	3.3	17.5	13.5	120ms	475	4,074	239	32,284
4/1/C	99	39	2.391	2.304	21.1	3.6	17.5	13.5	120ms	500	4,051	253	22,349
4/2/C	99	40	2.391	2.302	21.2	3.7	17.5	13.5	120ms	525	4,046	266	24,396
4/3/C	99	40	2.391	2.313	20.8	3.3	17.5	13.5	120ms	550	4,027	280	12,782
4/4/C	99	40	2.391	2.313	20.8	3.3	17.5	13.5	120ms	575	4,009	294	12,106
4/5/C	99	40	2.391	2.310	20.9	3.4	17.5	13.5	120ms	584	4,004	299	19,386
4/6/C	99	40	2.391	2.319	20.6	3.0	17.6	13.5	120ms	425	4,110	212	52,039
4/7/C	99	38	2.391	2.316	20.7	3.1	17.6	13.5	120ms	600	3,994	308	15,038
4/8/C	99	38	2.391	2.318	20.6	3.1	17.5	13.5	120ms	375	4,133	186	116,358
4/9/C	99	40	2.391	2.318	20.6	3.1	17.5	13.5	120ms	300	4,241	145	124,822
5/1/C	98	40	2.390	2.313	20.8	3.2	17.6	25.5	120ms	600	976	1,260	184
5/2/C	98	40	2.390	2.313	20.8	3.2	17.6	25.5	120ms	500	1,010	1,015	279
5/3/C	98	40	2.390	2.303	21.1	3.6	17.5	25.5	120ms	400	1,043	786	587
5/4/C	98	38	2.390	2.314	20.8	3.2	17.6	25.5	120ms	300	1,077	571	1,062
5/5/C	98	38	2.390	2.316	20.7	3.1	17.6	25.5	120ms	200	1,111	369	12,087
5/6/C	98	38	2.390	2.309	20.9	3.4	17.5	25.5	120ms	550	993	1,135	206
6/1/C	98	41	2.388	2.303	21.2	3.6	17.6	25.5	120ms	450	1,026	899	1,053
6/2/C	98	41	2.388	2.309	20.9	3.3	17.6	25.5	120ms	350	1,061	676	1,905
6/3/C	98	41	2.388	2.310	20.9	3.3	17.6	25.5	120ms	250	1,095	468	3,632
6/4/C	99	40	2.388	2.312	20.8	3.2	17.6	25.5	120ms	150	1,126	273	14,744
6/5/C	98	41	2.388	2.317	20.6	3.0	17.6	25.5	120ms	350	1,061	676	1,327
6/6/C	99	41	2.388	2.314	20.8	3.1	17.7	25.5	120ms	225	1,103	418	4,798
6/7/C	98	39	2.388	2.315	20.7	3.1	17.6	25.5	120ms	450	1,026	899	1,143
6/8/C	98	39	2.388	2.312	20.8	3.2	17.6	25.5	120ms	300	1,077	571	2,894
6/9/C	98	38	2.388	2.312	20.8	3.2	17.6	25.5	120ms	475	1,019	956	448
3/1/T	-	40	2.392	2.320	20.6	3.0	17.6	20	20Hz	1,000	4,199	238	41,865
3/2/T	-	40	2.392	2.318	20.6	3.1	17.5	20	20Hz	500	5,112	98	7,578,751
3/3/T	-	40	2.392	2.318	20.6	3.1	17.5	20	20Hz	1,500	4,726	317	39,170
4/2/T	-	40	2.391	2.309	20.9	3.4	17.5	20	20Hz	750	4,661	161	513,704
5/1/T	-	40	2.390	2.314	20.8	3.2	17.6	30	20Hz	1,000	1,929	518	31,907
5/2/T	-	40	2.390	2.310	20.9	3.3	17.6	30	20Hz	500	1,878	266	31,280
5/3/T	-	40	2.390	2.310	20.9	3.3	17.6	30	20Hz	250	2,003	125	1,053,470
6/1/T	-	40	2.388	2.312	20.8	3.2	17.6	30	20Hz	125	2,006	62	11,500,010

Table B.2 - Data for 20mm DBM Used in the Main Test Programme.

	Φ (mm)	Width (mm)	G_{mm}	G_{mb}	VMA (%)	V_v (%)	V_b (%)	Temp (°C)	Frequency	σ (kPa)	E (Mpa)	ε	N
7/1/C	98	40	2.543	2.427	15.5	4.6	10.9	16.3	120ms	600	2,330	528	935
7/2/C	98	40	2.543	2.427	15.5	4.6	10.9	16.3	120ms	100	2,412	85	208,449
7/3/C	99	40	2.543	2.427	15.5	4.6	10.9	16.3	120ms	500	2,346	437	1,361
7/4/C	99	41	2.543	2.437	15.2	4.2	11.0	16.3	120ms	400	2,363	347	2,080
7/5/C	98	41	2.543	2.440	15.1	4.1	11.1	16.3	120ms	300	2,384	258	5,405
7/6/C	99	41	2.543	2.420	15.8	4.8	11.0	16.3	120ms	200	2,398	171	25,183
8/1/C	98	40	2.556	2.427	15.5	5.0	10.5	16.3	120ms	250	2,395	214	28,338
8/2/C	98	40	2.556	2.450	14.7	4.1	10.6	16.3	120ms	350	2,376	302	7,659
8/3/C	99	39	2.556	2.436	15.2	4.7	10.5	16.3	120ms	450	2,353	392	1,919
8/4/C	99	40	2.556	2.418	15.8	5.4	10.4	16.3	120ms	550	2,334	483	1,025
8/5/C	99	40	2.556	2.413	16.0	5.6	10.4	16.3	120ms	550	2,334	483	1,481
8/6/C	99	39	2.556	2.412	16.1	5.6	10.5	16.3	120ms	150	2,402	128	39,714
9/1/C	98	39	2.559	2.413	16.0	5.7	10.3	27.5	120ms	500	744	1,377	64
9/2/C	98	39	2.559	2.418	15.8	5.5	10.3	27.5	120ms	450	764	1,207	22
9/3/C	98	40	2.559	2.437	15.1	4.8	10.3	27.5	120ms	350	803	893	97
9/4/C	98	40	2.559	2.436	15.2	4.8	10.4	27.5	120ms	250	844	607	170
9/5/C	98	40	2.559	2.404	16.3	6.1	10.2	27.5	120ms	150	884	348	828
9/6/C	98	40	2.559	2.442	15.0	4.6	10.4	27.5	120ms	75	915	168	3,489
10/1/C	98	41	2.557	2.423	15.7	5.2	10.5	27.5	120ms	575	714	1,650	31
10/2/C	98	41	2.557	2.421	15.7	5.3	10.4	27.5	120ms	400	784	1,046	67
10/3/C	98	41	2.557	2.419	15.8	5.4	10.4	27.5	120ms	100	903	227	1,642
10/4/C	98	41	2.557	2.430	15.4	5.0	10.4	27.5	120ms	300	823	747	136
10/5/C	98	41	2.557	2.424	15.6	5.2	10.4	27.5	120ms	200	865	474	758
10/6/C	98	41	2.557	2.429	15.5	5.0	10.5	27.5	120ms	600	704	1,747	68
7/1/T	-	40	2.543	2.419	15.8	4.9	10.9	20	20Hz	500	4,633	108	138,953
7/2/T	-	40	2.543	2.416	15.9	5.0	10.9	20	20Hz	1,000	4,087	245	7,556
7/3/T	-	40	2.543	2.412	16.1	5.2	10.9	20	20Hz	250	4,759	53	11,570,532
8/1/T	-	41	2.556	2.415	15.9	5.5	10.4	20	20Hz	750	4,374	171	34,100
8/2/T	-	41	2.556	2.429	15.4	5.0	10.4	20	20Hz	1,250	4,170	300	3,361
8/3/T	-	40	2.556	2.420	15.8	5.3	10.5	20	20Hz	375	4,686	80	936,451
9/1/T	-	41	2.559	2.399	16.5	6.3	10.2	30	20Hz	500	1,218	411	7,060
9/2/T	-	40	2.559	2.412	16.0	5.7	10.3	30	20Hz	250	1,484	168	262,516
9/3/T	-	40	2.559	2.419	16.0	5.5	10.5	30	20Hz	150	1,962	76	15,247,241
10/1/T	-	41	2.557	2.437	15.2	4.7	10.5	30	20Hz	625	1,529	409	6,683
10/2/T	-	41	2.557	2.428	15.5	5.0	10.5	30	20Hz	375	1,810	207	37,818
10/3/T	-	41	2.557	2.434	15.3	4.8	10.5	30	20Hz	200	2,471	81	3,256,565

Table B.3 - Data for 28mm DBM 50 Used in the Main Test Programme.

	Φ (mm)	Width (mm)	G_{mm}	G_{mb}	VMA (%)	V_v (%)	V_b (%)	Temp (°C)	Frequency	σ (kPa)	E (Mpa)	ϵ	N
SSM3T	99	40	2.600	2.352	18.6	9.5	9.1	13.5	120ms	550	4,287	263	13,708
SSL3T	98	40	2.600	2.326	19.5	10.5	9.0	13.5	120ms	600	4,286	287	5,589
SSL2T	98	40	2.600	2.328	19.5	10.5	9.0	13.5	120ms	400	4,316	190	36,134
SSL1T	99	39	2.600	2.345	18.9	9.8	9.1	13.5	120ms	500	4,307	238	20,913
SSK3T	98	40	2.600	2.364	18.2	9.1	9.1	13.5	120ms	450	4,311	214	44,224
SSM1T	99	40	2.600	2.332	19.3	10.3	9.0	13.5	120ms	350	4,348	165	26,645
SSI2T	99	39	2.600	2.372	18.0	8.8	9.2	13.5	120ms	300	4,362	141	176,515
SSN1T	99	40	2.600	2.377	17.8	8.6	9.2	13.5	120ms	575	4,286	275	9,900
SSM3M	99	40	2.600	2.281	21.1	12.3	8.8	13.5	120ms	600	3,796	324	5,457
SSM2M	99	40	2.600	2.265	21.7	12.9	8.8	13.5	120ms	550	3,809	296	4,919
SSL3M	98	39	2.600	2.266	21.6	12.8	8.8	13.5	120ms	350	3,878	185	28,832
SSL1M	99	40	2.600	2.280	21.1	12.3	8.8	13.5	120ms	500	3,825	268	8,988
SSK3M	99	41	2.600	2.318	19.8	10.8	9.0	13.5	120ms	300	3,892	158	58,051
SSM1M	99	39	2.600	2.315	19.9	11.0	8.9	13.5	120ms	625	3,779	339	3,705
SSI2M	98	39	2.600	2.308	20.2	11.2	9.0	13.5	120ms	200	3,905	105	340,811
SSN2M	98	40	2.600	2.295	20.6	11.7	8.9	13.5	120ms	400	3,850	213	19,709
SSN1M	99	39	2.600	2.310	20.1	11.2	8.9	13.5	120ms	250	3,912	131	209,341
SSM3B	99	39	2.600	2.247	22.3	13.6	8.7	13.5	120ms	600	3,220	382	5,027
SSM2B	99	39	2.600	2.253	22.1	13.3	8.8	13.5	120ms	500	3,233	317	8,486
SSL3B	98	40	2.600	2.220	23.2	14.6	8.6	13.5	120ms	400	3,267	251	12,087
SSL2B	98	40	2.600	2.242	22.4	13.8	8.6	13.5	120ms	300	3,306	186	29,823
SSL1B	99	40	2.600	2.265	21.6	12.9	8.7	13.5	120ms	550	3,231	349	4,025
SSK3B	98	39	2.600	2.276	21.3	12.5	8.8	13.5	120ms	150	3,342	92	277,711
SSM1B	99	41	2.600	2.269	21.5	12.7	8.8	13.5	120ms	350	3,291	218	44,864
SSI2B	98	40	2.600	2.232	22.8	14.2	8.6	13.5	120ms	450	4,633	283	2,274
SSN2B	99	40	2.600	2.236	22.6	14.0	8.6	13.5	120ms	250	4,087	155	60,865
SSN1B	99	40	2.600	2.252	22.1	13.4	8.7	13.5	120ms	200	4,759	123	139,475
SS/1/T	-	40	2.600	2.329	19.4	10.4	9.0	20	20Hz	1,000	5,646	177	9,463
SS/2/T	-	40	2.600	2.325	19.6	10.6	9.0	20	20Hz	375	5,608	67	1,507,118
SS/3/T	-	40	2.600	2.340	19.0	10.0	9.0	20	20Hz	500	6,135	81	511,382
SS/4/T	-	41	2.600	2.332	19.3	10.3	9.0	20	20Hz	750	5,902	127	40,368
SS/5/T	-	40	2.600	2.320	19.7	10.8	8.9	20	20Hz	1,500	4,808	312	1,877
SS/6/T	-	40	2.600	2.330	19.4	10.4	9.0	20	20Hz	1,250	5,048	248	4,757
SS/7/T	-	40	2.600	2.319	19.8	10.8	9.0	20	20Hz	625	5,797	108	69,656

Table B.4 - Data for SBS Modified 30/14 HRA Used in the Main Test Programme.

	Φ (mm)	Width (mm)	G_{mm}	G_{mb}	VMA (%)	V_v (%)	V_b (%)	Temp (°C)	Frequency	σ (kPa)	E (Mpa)	ϵ	N
M1/1/C	98	42	2.397	2.296	21.4	4.2	17.2	20	120ms	550	1,202	938	482
M1/2/C	98	42	2.397	2.287	21.7	4.6	17.1	20	120ms	300	1,046	588	3,987
M1/3/C	98	42	2.397	2.303	21.1	3.9	17.2	20	120ms	200	986	416	30,279
M1/4/C	98	42	2.397	2.294	21.5	4.3	17.2	20	120ms	250	1,015	505	6,104
M1/5/C	98	42	2.397	2.288	21.6	4.5	17.1	20	120ms	600	1,234	997	310
M1/6/C	98	42	2.397	2.308	21.0	3.7	17.3	20	120ms	150	955	322	99,985
M2/1/C	98	42	2.390	2.308	20.9	3.4	17.5	20	120ms	125	1,124	228	355,469
M2/2/C	98	41	2.390	2.311	20.9	3.3	17.6	20	120ms	450	1,090	846	1,018
M2/3/C	98	41	2.390	2.295	21.4	4.0	17.4	20	120ms	500	1,085	945	544
M2/4/C	98	42	2.390	2.306	21.0	3.5	17.5	20	120ms	350	1,100	652	3,081
M2/5/C	98	41	2.390	2.301	21.2	3.7	17.5	20	120ms	400	1,096	748	1,367
M2/6/C	98	41	2.390	2.306	21.0	3.5	17.5	20	120ms	225	1,114	414	16,459
M3/1/C	98	41	2.385	2.297	21.3	3.7	17.6	20	120ms	600	1,114	1,104	530
M3/2/C	99	41	2.385	2.287	21.7	4.1	17.6	20	120ms	500	1,165	880	1,574
M3/3/C	98	40	2.385	2.293	21.5	3.9	17.6	20	120ms	400	1,224	670	2,598
M3/4/C	98	41	2.385	2.296	21.4	3.7	17.7	20	120ms	300	1,273	483	6,847
M3/5/C	99	41	2.385	2.280	21.9	4.4	17.5	20	120ms	200	1,318	311	23,693
M3/6/C	98	41	2.385	2.276	22.1	4.6	17.5	20	120ms	125	1,356	189	191,357
M2/1/T	-	41	2.390	2.315	20.7	3.1	17.6	20	20Hz	250	1,515	165	1,115,000
M2/2/T	-	41	2.390	2.321	20.5	2.9	17.6	20	20Hz	300	1,796	167	563,000
M2/3/T	-	40	2.390	2.315	20.7	3.1	17.6	20	20Hz	750	1,825	411	65,485

Table B.5 - Data for Repeatability Testing on 30/14 HRA Used in Main Test Programme.

	Φ (mm)	Width (mm)	G_{mm}	G_{mb}	VMA (%)	V_v (%)	V_b (%)	Temp (°C)	Frequency	σ (kPa)	E (Mpa)	ε	N
1/1/C	98	40	2.394	2.253	22.8	5.9	16.9	25.5	120ms	600	968	1,271	176
1/2/C	98	40	2.394	2.277	22.0	4.9	17.1	25.5	120ms	400	1,002	818	612
1/3/C	99	40	2.394	2.260	22.6	5.6	17.0	25.5	120ms	375	1,057	727	1,007
1/4/C	99	41	2.394	2.245	23.1	6.2	16.9	25.5	120ms	250	1,107	463	3,768
1/5/C	99	37	2.394	2.236	23.4	6.6	16.8	25.5	120ms	200	1,242	330	12,149
2/1/C	99	40	2.398	2.323	20.4	3.1	17.3	25.5	120ms	125	1,119	229	61,205
2/2/C	98	40	2.398	2.315	20.7	3.5	17.2	25.5	120ms	100	1,025	200	101,006
2/3/C	99	40	2.398	2.313	20.8	3.5	17.3	25.5	120ms	50	861	119	245,867
2/4/C	98	39	2.398	2.314	20.8	3.5	17.3	25.5	120ms	100	967	212	48,677
2/6/C	99	40	2.398	2.307	21.0	3.8	17.2	25.5	120ms	150	1,174	262	23,486

Table B.6 - Data for Repeatability Testing on 20mm DBM Used in Main Test Programme.

	Φ (mm)	Width (mm)	G_{mm}	G_{mb}	VMA (%)	V_v (%)	V_b (%)	Temp (°C)	Frequency	σ (kPa)	E (Mpa)	ε	N
11/1/C	98	40	2.550	2.399	16.4	5.9	10.5	27.5	120ms	400	816	1,005	51
11/2/C	98	41	2.550	2.419	15.5	5.1	10.4	27.5	120ms	225	870	530	570
11/3/C	98	39	2.550	2.413	15.9	5.4	10.5	27.5	120ms	200	851	482	1,274
11/4/C	98	41	2.550	2.420	15.6	5.1	10.5	27.5	120ms	100	792	259	5,909
11/5/C	99	39	2.550	2.415	15.9	5.3	10.6	27.5	120ms	100	837	245	11,578
12/1/C	98	41	2.548	2.404	15.9	5.7	10.2	27.5	120ms	50	861	119	33,469
12/2/C	98	40	2.548	2.401	16.0	5.8	10.2	27.5	120ms	50	854	120	60,039
12/3/C	98	40	2.548	2.399	16.1	5.8	10.3	27.5	120ms	50	915	112	118,794
12/4/C	98	30	2.548	2.409	16.0	5.5	10.5	27.5	120ms	50	1,046	98	87,512
12/6/C	98	40	2.548	2.414	15.5	5.3	10.2	27.5	120ms	275	807	699	213

Table B.7 - Data for Repeatability Testing on Crumb Rubber.

	Temp (°C)	Frequency	ϵ	N	ϵ	N
Crumb 1	20	120ms	189	180,641	-	-
Crumb 2	20	120ms	303	19,414	-	-
Crumb 3	20	120ms	278	22,245	-	-
Crumb 4	20	120ms	214	24,600	-	-
Crumb 5	20	120ms	413	1,572	-	-
Crumb 6	20	120ms	365	1,168	-	-
Repeat 1	20	120ms	-	-	397	1,490
Repeat 2	20	120ms	-	-	199	122,067
Repeat 3	20	120ms	-	-	235	46,504
Repeat 4	20	120ms	-	-	296	7,126
Repeat 5	20	120ms	-	-	578	238

Table B.8 - Data for Reproducibility Testing on 30/14 HRA - Northamptonshire.

	Φ (mm)	Width (mm)	G_{mm}	G_{mb}	VMA (%)	V_v (%)	V_b (%)	Temp (°C)	Frequency	σ (kPa)	E (Mpa)	ε	N
1/1	100	40	2.398	2.309	21.3	3.7	17.6	13.5	120ms	600	5,234	235	14,121
1/2	100	40	2.398	2.316	21.0	3.4	17.6	13.5	120ms	450	5,766	160	92,498
1/3	100	40	2.398	2.318	21.0	3.3	17.7	13.5	120ms	350	5,562	129	235,535
1/4	100	40	2.398	2.318	20.9	3.3	17.6	13.5	120ms	400	4,970	165	110,706
1/5	100	40	2.398	2.316	20.8	3.4	17.4	13.5	120ms	425	5,657	154	69,014
1/6	100	40	2.398	2.304	21.5	3.9	17.6	13.5	120ms	475	5,440	179	39,204
1/7	100	40	2.398	2.302	21.5	4.0	17.5	13.5	120ms	500	5,230	196	19,374
1/8	100	40	2.398	2.313	21.1	3.5	17.6	13.5	120ms	525	5,436	198	26,219
1/9	100	40	2.398	2.316	21.0	3.4	17.6	13.5	120ms	550	5,244	215	16,151
1/10	100	40	2.398	2.319	21.0	3.3	17.7	13.5	120ms	575	6,171	191	18,190
1/11	100	40	2.398	2.310	21.2	3.7	17.5	13.5	120ms	584	5,274	227	16,195
1/12	100	40	2.398	2.332	20.0	2.8	17.2	13.5	120ms	425	6,136	142	57,880
1/13	100	40	2.398	2.324	20.6	3.1	17.5	13.5	120ms	600	5,125	240	8,582
1/14	100	40	2.398	2.312	21.1	3.6	17.5	13.5	120ms	375	4,960	155	79,148
1/15	100	40	2.398	2.318	20.8	3.3	17.5	13.5	120ms	300	4,805	128	396,682
2/1	100	40	2.394	2.318	20.4	3.2	17.2	25.5	120ms	500	1,275	804	274
2/2	100	40	2.394	2.320	20.4	3.1	17.3	25.5	120ms	400	1,684	487	756
2/3	100	40	2.394	2.310	21.0	3.5	17.5	25.5	120ms	300	1,437	428	1,438
2/4	100	40	2.394	2.324	20.4	2.9	17.5	25.5	120ms	600	1,177	1,045	143
2/5	100	40	2.394	2.332	20.2	2.6	17.6	25.5	120ms	200	1,454	282	4,744
2/6	100	40	2.394	2.309	21.0	3.6	17.4	25.5	120ms	550	1,425	791	177
2/7	100	40	2.394	2.317	20.6	3.2	17.4	25.5	120ms	450	1,314	702	370
2/8	100	40	2.394	2.315	20.5	3.3	17.2	25.5	120ms	350	1,560	460	586
2/9	100	40	2.394	2.314	20.7	3.3	17.4	25.5	120ms	250	1,597	321	2,303
2/10	100	40	2.394	2.303	21.0	3.8	17.2	25.5	120ms	150	1,464	210	12,290
2/11	100	40	2.394	2.313	21.0	3.4	17.6	25.5	120ms	350	1,816	395	972
2/12	100	40	2.394	2.315	20.7	3.3	17.4	25.5	120ms	225	1,532	301	3,200
2/13	100	40	2.394	2.312	21.0	3.4	17.6	25.5	120ms	450	1,502	614	387
2/14	100	40	2.394	2.312	20.9	3.4	17.5	25.5	120ms	300	1,864	330	2,779
2/15	100	40	2.394	2.311	20.9	3.5	17.4	25.5	120ms	475	1,445	674	324

Table B.9 - Data for Reproducibility Testing on 30/14 HRA - Suffolk.

	Φ (mm)	Width (mm)	G_{mm}	G_{mb}	VMA (%)	V_v (%)	V_b (%)	Temp (°C)	Frequency	σ (kPa)	E (Mpa)	ε	N
3/3	100	40	2.397	2.304	21.5	3.9	17.6	13.5	120ms	350	5,053	142	61,094
3/5	100	40	2.397	2.309	21.4	3.7	17.7	13.5	120ms	425	5,345	163	47,807
3/6	100	40	2.397	2.303	21.5	4.0	17.5	13.5	120ms	475	5,728	170	13,398
3/7	100	40	2.397	2.311	21.5	3.6	17.9	13.5	120ms	500	5,230	196	21,297
3/8	100	40	2.397	2.320	21.2	3.3	17.9	13.5	120ms	525	4,937	218	20,361
3/9	100	40	2.397	2.318	21.0	3.3	17.7	13.5	120ms	550	5,447	207	9,052
3/10	100	40	2.397	2.308	21.5	3.8	17.7	13.5	120ms	575	5,147	229	8,743
3/11	100	40	2.397	2.310	21.0	3.7	17.3	13.5	120ms	584	5,568	215	11,546
3/12	100	40	2.397	2.311	21.1	3.6	17.5	13.5	120ms	425	6,406	136	34,529
3/13	100	40	2.397	2.312	20.9	3.6	17.3	13.5	120ms	600	5,642	218	9,695
3/14	100	40	2.397	2.305	21.5	3.9	17.6	13.5	120ms	375	5,737	134	81,255
3/15	100	40	2.397	2.305	21.6	3.9	17.7	13.5	120ms	300	5,256	117	200,848
4/3	100	40	2.397	2.315	21.0	3.5	17.5	25.5	120ms	300	1,158	531	865
4/4	100	40	2.397	2.316	21.1	3.4	17.7	25.5	120ms	600	1,068	1,152	261
4/5	100	40	2.397	2.321	20.8	3.2	17.6	25.5	120ms	200	1,158	354	2,513
4/6	100	40	2.397	2.323	20.5	3.1	17.4	25.5	120ms	550	1,325	851	250
4/7	100	40	2.397	2.322	20.7	3.2	17.5	25.5	120ms	450	1,052	877	299
4/8	100	40	2.397	2.320	20.7	3.3	17.4	25.5	120ms	350	1,072	669	390
4/9	100	40	2.397	2.315	21.0	3.5	17.5	25.5	120ms	250	1,291	397	1,236
4/10	100	40	2.397	2.317	21.0	3.4	17.6	25.5	120ms	150	1,147	268	5,482
4/11	100	40	2.397	2.314	21.0	3.5	17.5	25.5	120ms	350	1,288	557	390
4/12	100	40	2.397	2.322	20.5	3.2	17.3	25.5	120ms	225	1,156	399	2,011
4/13	100	40	2.397	2.320	20.8	3.3	17.5	25.5	120ms	450	1,149	803	257
4/14	100	40	2.397	2.318	20.9	3.3	17.6	25.5	120ms	300	1,328	463	993
4/15	100	40	2.397	2.317	21.0	3.4	17.6	25.5	120ms	475	1,387	702	204

Table B.10 - Data for Reproducibility Testing on 20mm DBM - Kent.

	Φ (mm)	Width (mm)	G_{mm}	G_{mb}	VMA (%)	V_v (%)	V_b (%)	Temp (°C)	Frequency	σ (kPa)	E (Mpa)	ε	N
D1/4	100	41	2.525	2.421	15.7	4.1	11.6	20	120ms	600	1,694	726	312
D1/5	100	40	2.525	2.365	17.7	6.3	11.4	20	120ms	575	1,481	796	225
D1/6	100	40	2.525	2.418	15.8	4.2	11.6	20	120ms	550	1,804	625	752
D2/4	100	40	2.525	2.445	14.9	3.2	11.7	20	120ms	525	1,833	587	601
D2/5	100	40	2.525	2.416	15.9	4.3	11.6	20	120ms	500	1,938	529	496
D2/6	100	40	2.525	2.403	16.4	4.8	11.6	20	120ms	475	1,817	536	863
D3/6	100	41	2.525	2.406	16.3	4.7	11.6	20	120ms	400	1,798	456	801
D4/4	100	40	2.525	2.389	16.8	5.4	11.4	20	120ms	375	1,519	506	801
D4/6	100	41	2.525	2.411	16.1	4.5	11.6	20	120ms	325	1,810	368	2,149
D5/6	100	40	2.525	2.349	18.2	7.0	11.2	20	120ms	200	1,559	263	4,660

Table B.11 - Data for Reproducibility Testing on 20mm DBM - Surrey.

	Φ (mm)	Width (mm)	G_{mm}	G_{mb}	VMA (%)	V_v (%)	V_b (%)	Temp (°C)	Frequency	σ (kPa)	E (Mpa)	ε	N
D1/7	100	39	2.525	2.420	15.8	4.2	11.6	20	120ms	600	1,981	621	80
D1/8	100	41	2.525	2.421	15.7	4.1	11.4	20	120ms	575	1,936	609	81
D1/9	100	41	2.525	2.422	15.7	4.1	11.6	20	120ms	550	1,964	574	152
D2/7	100	40	2.525	2.436	15.2	3.5	11.7	20	120ms	525	2,148	501	105
D2/8	100	41	2.525	2.416	15.9	4.3	11.6	20	120ms	500	2,669	384	120
D2/9	100	41	2.525	2.423	15.7	4.0	11.7	20	120ms	475	2,297	424	116
D3/7	100	40	2.525	2.406	16.3	4.7	11.6	20	120ms	450	2,010	459	206
D3/8	100	41	2.525	2.416	15.9	4.3	11.6	20	120ms	425	2,099	415	141
D3/9	100	41	2.525	2.395	16.6	5.1	11.5	20	120ms	400	1,911	429	168
D4/7	100	40	2.525	2.387	16.9	5.5	11.4	20	120ms	375	1,671	460	165
D4/8	100	42	2.525	2.416	15.9	4.3	11.6	20	120ms	350	2,424	296	493
D4/9	100	40	2.525	2.408	16.2	4.6	11.6	20	120ms	325	2,063	323	277
D5/7	100	41	2.525	2.414	16.0	4.4	11.6	20	120ms	300	2,480	248	722
D5/8	100	41	2.525	2.416	15.9	4.3	11.6	20	120ms	250	2,669	192	991
D5/9	100	41	2.525	2.390	16.8	5.3	11.5	20	120ms	200	2,010	204	1,802

Table B.12 - Data for Reproducibility Testing on 20mm DBM - Buckinghamshire.

	Φ (mm)	Width (mm)	G_{mm}	G_{mb}	VMA (%)	V_v (%)	V_b (%)	Temp (°C)	Frequency	σ (kPa)	E (Mpa)	ε	N
D1/10	100	40	2.525	2.425	15.6	4.0	11.6	20	120ms	600	1,806	681	97
D1/11	100	40	2.525	2.417	15.9	4.3	11.4	20	120ms	575	1,731	681	82
D1/12	100	41	2.525	2.410	16.1	4.6	11.5	20	120ms	550	1,639	688	150
D2/10	100	40	2.525	2.421	15.7	4.1	11.6	20	120ms	525	1,445	745	109
D2/11	100	41	2.525	2.418	15.8	4.2	11.6	20	120ms	500	1,468	698	120
D2/12	100	41	2.525	2.423	15.7	4.0	11.7	20	120ms	475	1,531	636	118
D3/10	100	39	2.525	2.416	15.9	4.3	11.6	20	120ms	450	1,764	523	205
D3/11	100	40	2.525	2.412	16.0	4.5	11.5	20	120ms	425	1,958	445	143
D3/12	100	40	2.525	2.400	16.5	5.0	11.6	20	120ms	400	1,589	516	170
D4/10	100	41	2.525	2.384	17.0	5.6	11.4	20	120ms	375	1,805	426	165
D4/11	100	40	2.525	2.423	15.7	4.0	11.7	20	120ms	350	1,676	428	500
D4/12	100	41	2.525	2.406	16.3	4.7	11.6	20	120ms	325	1,887	353	301
D5/10	100	40	2.525	2.414	16.0	4.4	11.6	20	120ms	300	1,892	325	722
D5/11	100	40	2.525	2.403	16.4	4.8	11.6	20	120ms	250	2,002	256	985
D5/12	100	41	2.525	2.406	16.3	4.7	11.6	20	120ms	200	2,147	191	1,900

Table B.13 - Data for Reproducibility Testing on 40mm HDM - Northamptonshire.

	Φ (mm)	Width (mm)	G_{mm}	G_{mb}	VMA (%)	V_v (%)	V_b (%)	Temp (°C)	Frequency	σ (kPa)	E (Mpa)	ε	N
H1/1	100	41	2.587	2.446	13.9	5.5	8.5	20	120ms	600	3,555	346	330
H1/2	100	40	2.587	2.467	13.1	4.6	8.5	20	120ms	575	4,318	273	1,571
H1/11	100	41	2.587	2.480	12.7	4.1	8.6	20	120ms	550	3,591	314	1,373
H2/1	100	41	2.587	2.456	13.5	5.1	8.4	20	120ms	525	4,937	218	1,897
H2/2	100	41	2.587	2.453	13.6	5.2	8.4	20	120ms	500	4,343	236	1,583
H3/1	100	41	2.587	2.472	12.9	4.4	8.5	20	120ms	475	4,007	243	2,959
H3/2	100	41	2.587	2.475	12.8	4.3	8.5	20	120ms	450	3,976	232	2,651
H4/1	98	41	2.587	2.430	14.4	6.1	8.3	20	120ms	425	2,632	331	2,261
H4/2	98	41	2.587	2.438	14.1	5.8	8.3	20	120ms	400	2,222	369	2,523
H5/1	100	41	2.587	2.429	14.5	6.1	8.4	20	120ms	375	3,417	225	4,552
H5/2	100	41	2.587	2.459	13.4	4.9	8.5	20	120ms	350	3,417	210	5,451
H6/1	100	41	2.587	2.459	13.4	4.9	8.5	20	120ms	325	3,266	204	10,365
H6/2	100	41	2.587	2.455	13.5	5.1	8.4	20	120ms	300	3,683	167	14,394
H7/1	98	40	2.587	2.459	13.4	4.9	8.5	20	120ms	250	3,486	147	14,619
H7/2	98	41	2.587	2.446	13.9	5.5	8.5	20	120ms	200	3,534	116	40,495

Table B.14 - Data for Reproducibility Testing on 40mm HDM - Norfolk.

	Φ (mm)	Width (mm)	G_{mm}	G_{mb}	VMA (%)	V_v (%)	V_b (%)	Temp (°C)	Frequency	σ (kPa)	E (Mpa)	ε	N
H1/3	100	40	2.587	2.446	13.9	5.5	8.5	20	120ms	600	4,198	293	826
H1/4	100	41	2.587	2.431	14.4	6.0	8.4	20	120ms	575	3,339	353	1,489
H2/11	100	41	2.587	2.444	13.9	5.5	8.4	20	120ms	550	3,970	284	1,886
H2/3	100	41	2.587	2.448	13.8	5.4	8.4	20	120ms	525	3,599	299	931
H2/4	100	41	2.587	2.459	13.4	4.9	8.5	20	120ms	500	3,233	317	1,606
H3/4	100	41	2.587	2.466	13.2	4.7	8.5	20	120ms	450	3,342	276	3,837
H4/3	100	41	2.587	2.448	13.8	5.4	8.4	20	120ms	425	2,570	339	768
H4/4	100	41	2.587	2.413	15.0	6.7	8.3	20	120ms	400	1,826	449	174
H5/3	100	41	2.587	2.480	12.7	4.1	8.6	20	120ms	375	3,643	211	7,558
H5/4	100	41	2.587	2.445	13.9	5.5	8.4	20	120ms	350	2,941	244	9,199
H6/4	100	40	2.587	2.463	13.3	4.8	8.5	20	120ms	300	3,820	161	34,776
H7/3	98	41	2.587	2.451	13.7	5.3	8.4	20	120ms	250	4,133	124	131,959

Table B.15 - Data for Reproducibility Testing on 40mm HDM - Shell.

	Φ (mm)	Width (mm)	G_{mm}	G_{mb}	VMA (%)	V_v (%)	V_b (%)	Temp (°C)	Frequency	σ (kPa)	E (Mpa)	ε	N
H1/5	100	41	2.587	2.396	15.6	7.4	8.2	20	120ms	600	3,083	399	278
H1/6	100	41	2.587	2.434	14.3	5.9	8.4	20	120ms	575	3,094	381	229
H3/11	100	41	2.587	2.385	16.0	7.8	8.2	20	120ms	550	3,591	314	452
H2/5	100	41	2.587	2.453	13.6	5.2	8.4	20	120ms	525	3,552	303	1,357
H2/6	100	41	2.587	2.453	13.6	5.2	8.4	20	120ms	500	3,522	291	742
H3/5	100	40	2.587	2.448	13.8	5.4	8.4	20	120ms	475	3,554	274	3,449
H3/6	100	41	2.587	2.460	13.4	4.9	8.5	20	120ms	450	3,942	234	2,451
H4/5	100	41	2.587	2.403	15.4	7.1	8.3	20	120ms	425	2,427	359	213
H4/6	98	41	2.587	2.406	15.3	7.0	8.3	20	120ms	400	2,595	316	485
H5/5	100	41	2.587	2.437	14.2	5.8	8.4	20	120ms	375	3,190	241	2,089
H5/6	100	40	2.587	2.462	13.3	4.8	8.5	20	120ms	350	3,737	192	5,960
H6/5	100	41	2.587	2.483	12.6	4.0	8.6	20	120ms	325	3,507	190	11,570
H6/6	100	41	2.587	2.481	12.6	4.1	8.5	20	120ms	300	3,942	156	19,579
H7/5	98	41	2.587	2.443	14.0	5.6	8.4	20	120ms	250	3,973	129	23,542
H7/6	98	41	2.587	2.422	14.7	6.4	8.3	20	120ms	200	3,694	111	60,440

Table B.16 - Data for Reproducibility Testing on 40mm HDM - Suffolk.

	Φ (mm)	Width (mm)	G_{mm}	G_{mb}	VMA (%)	V_v (%)	V_b (%)	Temp (°C)	Frequency	σ (kPa)	E (Mpa)	ϵ	N
H1/7	100	40	2.587	2.471	13.0	4.5	8.5	20	120ms	600	4,377	281	898
H1/8	100	40	2.587	2.401	15.4	7.2	8.2	20	120ms	575	4,516	261	698
H4/11	100	41	2.587	2.346	17.4	9.3	8.1	20	120ms	550	5,318	212	1,764
H2/7	100	41	2.587	2.421	14.7	6.4	8.3	20	120ms	525	3,816	282	782
H2/8	100	41	2.587	2.419	14.8	6.5	8.3	20	120ms	500	4,790	214	2,865
H3/7	100	40	2.587	2.425	14.6	6.3	8.3	20	120ms	475	4,943	197	3,184
H3/8	100	41	2.587	2.429	14.5	6.1	8.4	20	120ms	450	4,212	219	5,620
H4/7	98	41	2.587	2.401	15.4	7.2	8.2	20	120ms	425	2,021	431	980
H4/8	98	41	2.587	2.355	17.1	9.0	8.1	20	120ms	400	1,424	576	95
H5/7	100	41	2.587	2.456	13.5	5.1	8.4	20	120ms	375	3,576	215	10,168
H5/8	100	41	2.587	2.410	15.1	6.8	8.3	20	120ms	350	3,606	199	11,018
H6/7	100	41	2.587	2.432	14.3	6.0	8.3	20	120ms	325	3,158	211	9,501
H6/8	100	41	2.587	2.414	15.0	6.7	8.3	20	120ms	300	3,455	178	6,922
H7/7	98	41	2.587	2.420	14.8	6.5	8.3	20	120ms	250	5,452	94	23,700
H7/8	98	41	2.587	2.433	14.3	6.0	8.3	20	120ms	200	4,227	97	60,937

Table B.17 - Data for Reproducibility Testing on 40mm HDM - SWK (PE).

	Φ (mm)	Width (mm)	G_{mm}	G_{mb}	VMA (%)	V_v (%)	V_b (%)	Temp (°C)	Frequency	σ (kPa)	E (Mpa)	ϵ	N
H1/9	100	41	2.587	2.469	13.0	4.6	8.4	20	120ms	600	5,616	219	1,057
H1/10	100	40	2.587	2.468	13.1	4.6	8.5	20	120ms	575	3,194	369	1,917
H5/11	100	41	2.587	2.414	15.0	6.7	8.3	20	120ms	550	3,502	322	1,432
H2/9	100	41	2.587	2.397	15.6	7.3	8.3	20	120ms	525	3,363	320	900
H2/10	100	41	2.587	2.401	15.4	7.2	8.2	20	120ms	500	2,351	436	1,617
H3/9	100	41	2.587	2.423	14.7	6.3	8.4	20	120ms	475	3,323	293	1,480
H3/10	100	41	2.587	2.432	14.3	6.0	8.3	20	120ms	450	3,117	296	133
H4/10	100	41	2.587	2.361	16.8	8.7	8.1	20	120ms	400	2,492	329	681
H5/9	100	41	2.587	2.442	14.0	5.6	8.4	20	120ms	375	2,078	370	1,764
H5/10	100	41	2.587	2.407	15.2	7.0	8.2	20	120ms	350	2,708	265	6,370
H6/9	100	41	2.587	2.413	15.0	6.7	8.3	20	120ms	325	3,298	202	12,980
H6/10	100	40	2.587	2.369	16.6	8.4	8.2	20	120ms	300	2,412	255	11,049
H7/9	98	41	2.587	2.448	13.8	5.4	8.4	20	120ms	250	1,786	287	4,283
H7/10	98	41	2.587	2.415	14.9	6.6	8.3	20	120ms	200	3,905	105	166,817

Table B.18 - Data for Repeat Reproducibility Testing on 20mm DBM - Buckinghamshire.

	Φ (mm)	Width (mm)	G_{mm}	G_{mb}	VMA (%)	V_v (%)	V_b (%)	Temp (°C)	Frequency	σ (kPa)	E (Mpa)	ϵ	N
A1	99	41	2.556	2.413	16.0	5.6	10.4	20	120ms	600	3,324	370	329
A2	99	41	2.556	2.437	15.0	4.7	10.3	20	120ms	500	3,024	339	480
A3	99	41	2.556	2.404	16.1	5.9	10.2	20	120ms	400	3,071	267	1,318
A4	99	40	2.556	2.399	16.1	6.1	10.0	20	120ms	600	2,894	425	313
A5	99	40	2.556	2.419	16.0	5.4	10.6	20	120ms	550	3,915	288	253
A6	99	40	2.556	2.412	15.9	5.6	10.3	20	120ms	450	3,576	258	1,118
A7	99	40	2.556	2.415	15.7	5.5	10.2	20	120ms	350	2,953	243	1,448
A8	99	40	2.556	2.420	15.8	5.3	10.5	20	120ms	250	3,463	148	9,461
A9	99	40	2.556	2.427	15.5	5.0	10.5	20	120ms	300	3,705	166	7,837
A10	99	41	2.556	2.436	14.9	4.7	10.2	20	120ms	200	3,228	127	899

Table B.19 - Data for Repeat Reproducibility Testing on 20mm DBM - Kent.

	Φ (mm)	Width (mm)	G_{mm}	G_{mb}	VMA (%)	V_v (%)	V_b (%)	Temp (°C)	Frequency	σ (kPa)	E (Mpa)	ϵ	N
A11	99	41	2.556	2.434	15.2	4.8	10.4	20	120ms	600	2,505	491	426
A12	99	41	2.556	2.421	15.7	5.3	10.4	20	120ms	500	2,748	373	333
A13	99	41	2.556	2.428	15.5	5.0	10.5	20	120ms	400	3,094	265	1,828
A14	99	41	2.556	2.437	15.1	4.7	10.4	20	120ms	300	3,254	189	3,818
A15	99	40	2.556	2.429	15.5	5.0	10.5	20	120ms	200	3,130	131	106,671
B1	99	40	2.550	2.419	15.6	5.1	10.5	20	120ms	550	3,316	340	1,047
B2	99	41	2.550	2.430	15.0	4.7	10.3	20	120ms	450	2,746	336	451
B3	99	41	2.550	2.424	15.4	4.9	10.5	20	120ms	350	3,624	198	2,954
B4	99	41	2.550	2.423	15.4	5.0	10.4	20	120ms	250	3,285	156	10,331
B5	99	41	2.550	2.427	15.3	4.8	10.5	20	120ms	600	3,465	355	433

Table B.20 - Data for Repeat Reproducibility Testing on 20mm DBM - Northamptonshire.

	Φ (mm)	Width (mm)	G_{mm}	G_{mb}	VMA (%)	V_v (%)	V_b (%)	Temp (°C)	Frequency	σ (kPa)	E (Mpa)	ε	N
B6	99	41	2.550	2.425	15.6	4.9	10.7	20	120ms	600	2,356	522	201
B7	99	41	2.550	2.412	16.0	5.4	10.6	20	120ms	500	2,887	355	472
B8	99	41	2.550	2.416	16.0	5.3	10.7	20	120ms	400	3,154	260	2,394
B9	99	41	2.550	2.419	15.8	5.1	10.7	20	120ms	300	3,289	187	6,511
B10	99	41	2.550	2.420	15.7	5.1	10.6	20	120ms	200	3,661	112	19,741
B11	99	41	2.550	2.440	15.0	4.3	10.7	20	120ms	550	3,115	362	631
B12	99	41	2.550	2.420	15.6	5.1	10.5	20	120ms	450	2,795	330	254
B13	99	40	2.550	2.427	15.4	4.8	10.6	20	120ms	350	2,728	263	1,031
B14	99	40	2.550	2.416	15.8	5.3	10.5	20	120ms	600	3,994	308	708
B15	99	40	2.550	2.427	15.5	4.8	10.7	20	120ms	250	3,635	141	14,700

Table B.21 - Data for Repeat Reproducibility Testing on 20mm DBM - Shell.

	Φ (mm)	Width (mm)	G_{mm}	G_{mb}	VMA (%)	V_v (%)	V_b (%)	Temp (°C)	Frequency	σ (kPa)	E (Mpa)	ε	N
C1	99	41	2.558	2.399	16.7	6.2	10.5	20	120ms	600	2,922	421	161
C2	99	42	2.558	2.442	14.9	4.5	10.4	20	120ms	600	2,645	465	119
C3	99	42	2.558	2.412	16.0	5.7	10.3	20	120ms	400	2,908	282	1,048
C6	99	41	2.558	2.414	16.1	5.6	10.5	20	120ms	550	2,869	393	200
C7	99	41	2.558	2.415	16.0	5.6	10.4	20	120ms	450	3,318	278	469
C8	99	42	2.558	2.404	16.5	6.0	10.5	20	120ms	350	2,544	282	578
C10	99	42	2.558	2.418	16.0	5.5	10.5	20	120ms	500	3,350	306	211

Table B.22 - Data for Repeat Reproducibility Testing on 20mm DBM - SWK (PE).

	Φ (mm)	Width (mm)	G_{mm}	G_{mb}	VMA (%)	V_v (%)	V_b (%)	Temp (°C)	Frequency	σ (kPa)	E (Mpa)	ε	N
C11	99	41	2.558	2.434	15.4	4.8	10.6	20	120ms	600	2,828	435	413
C12	99	41	2.558	2.428	15.6	5.1	10.5	20	120ms	500	2,642	388	461
C13	99	41	2.558	2.437	15.3	4.7	10.6	20	120ms	400	2,789	294	1,197
C14	99	41	2.558	2.429	15.5	5.0	10.5	20	120ms	300	2,915	211	4,826
C15	99	42	2.558	2.424	15.7	5.2	10.5	20	120ms	200	2,662	154	21,592
D1	99	40	2.551	2.423	15.5	5.0	10.5	20	120ms	550	3,015	374	337
D2	99	40	2.551	2.419	15.7	5.2	10.5	20	120ms	450	3,035	304	621
D3	99	40	2.551	2.421	15.6	5.1	10.5	20	120ms	350	2,708	265	2,143
D4	99	41	2.551	2.430	15.3	4.7	10.6	20	120ms	250	2,340	219	6,327
D5	99	41	2.551	2.427	15.4	4.9	10.5	20	120ms	600	2,393	514	147

Table B.23 - Data for Repeat Reproducibility Testing on 20mm DBM - Tarmac.

	Φ (mm)	Width (mm)	G_{mm}	G_{mb}	VMA (%)	V_v (%)	V_b (%)	Temp (°C)	Frequency	σ (kPa)	E (Mpa)	ϵ	N
D6	99	41	2.551	2.427	15.4	4.9	10.5	20	120ms	500	2,550	402	409
D7	99	40	2.551	2.413	16.0	5.4	10.6	20	120ms	582	2,238	533	190
D8	99	40	2.551	2.420	15.6	5.1	10.5	20	120ms	300	3,170	194	3,134
D9	99	40	2.551	2.419	15.7	5.2	10.5	20	120ms	400	2,523	325	937
D10	99	40	2.551	2.450	14.5	4.0	10.5	20	120ms	200	3,154	130	5,791
D11	99	40	2.551	2.418	15.6	5.2	10.4	20	120ms	550	2,665	423	430
D12	99	40	2.551	2.429	15.3	4.8	10.5	20	120ms	450	4,174	221	840
D13	99	41	2.551	2.412	15.9	5.4	10.5	20	120ms	350	2,500	287	1,106
D14	99	41	2.551	2.436	15.0	4.5	10.5	20	120ms	250	3,033	169	6,095
D15	99	42	2.551	2.437	15.1	4.5	10.6	20	120ms	556	2,669	427	298

Table B.24 - Data for Practical Application of ITFT - 40/14 HRA W/C SBS Modified - Tracked.

	Φ (mm)	Width (mm)	G_{mm}	G_{mb}	VMA (%)	V_v (%)	V_b (%)	Temp (°C)	Frequency	σ (kPa)	E (Mpa)	ε	N
1	99	41	2.379	2.284	20.4	4.0	16.4	20	120ms	300	274	2,245	295
2	99	41	2.379	2.285	20.4	4.0	16.4	20	120ms	400	272	3,015	108
3	99	41	2.379	2.288	20.3	3.8	16.5	20	120ms	500	279	3,674	80
4	99	42	2.379	2.277	20.7	4.3	16.4	20	120ms	450	259	3,562	102
5	99	40	2.379	2.287	20.3	3.9	16.4	20	120ms	533	276	3,959	64
18	99	42	2.379	2.223	22.5	6.6	15.9	20	120ms	500	337	3,042	80
19	99	40	2.379	2.257	21.4	5.1	16.3	20	120ms	400	373	2,198	130
20	98	38	2.379	2.247	21.7	5.5	16.2	20	120ms	650	430	3,099	36
21	99	40	2.379	2.295	20.0	3.5	16.5	20	120ms	300	487	1,263	362
22	98	39	2.379	2.278	20.6	4.2	16.4	20	120ms	200	563	728	1,231
30	99	41	2.382	2.256	21.4	5.3	16.1	20	120ms	500	569	1,801	59
31	99	41	2.382	2.224	22.5	6.6	15.9	20	120ms	400	305	2,689	119
32	99	40	2.382	2.229	22.3	6.4	15.9	20	120ms	300	467	1,317	372
33	99	36	2.382	2.245	21.8	5.8	16.0	20	120ms	200	390	1,051	1,004
34	99	40	2.382	2.246	21.7	5.7	16.0	20	120ms	250	705	727	811

Table B.25 - Data for Practical Application of ITFT - 40/14 HRA W/C SBS Modified - Untracked.

	Φ (mm)	Width (mm)	G_{mm}	G_{mb}	VMA (%)	V_v (%)	V_b (%)	Temp (°C)	Frequency	σ (kPa)	E (Mpa)	ε	N
7	99	40	2.373	2.281	20.5	3.9	16.6	20	120ms	550	215	5,244	37
8	100	41	2.373	2.294	20.1	3.3	16.8	20	120ms	300	386	1,593	262
9	99	39	2.373	2.296	20.0	3.2	16.8	20	120ms	400	225	3,644	94
10	100	41	2.373	2.309	19.6	2.7	16.9	20	120ms	200	247	1,660	404
11	99	41	2.373	2.308	19.6	2.7	16.9	20	120ms	100	191	1,073	4,686
12	99	42	2.386	2.311	19.5	3.1	16.4	20	120ms	500	297	3,451	67
13	99	40	2.386	2.286	20.3	4.2	16.1	20	120ms	400	333	2,462	137
14	99	38	2.386	2.305	19.7	3.4	16.3	20	120ms	600	312	3,942	59
15	99	40	2.386	2.317	19.3	2.9	16.4	20	120ms	200	316	1,297	1,191
16	99	39	2.386	2.283	20.5	4.3	16.2	20	120ms	300	308	1,997	335
24	99	42	2.400	2.313	19.4	3.6	15.8	20	120ms	300	981	627	664
25	99	34	2.400	2.280	20.6	5.0	15.6	20	120ms	500	786	1,304	166
26	99	39	2.400	2.268	21.0	5.5	15.5	20	120ms	600	657	1,872	70
27	99	41	2.400	2.269	20.9	5.5	15.4	20	120ms	400	740	1,108	258
28	99	40	2.400	2.280	20.6	5.0	15.6	20	120ms	200	880	466	1,485

Table B.26 - Data for Practical Application of ITFT - 40/14 HRA W/C Unmodified - Tracked.

	Φ (mm)	Width (mm)	G_{mm}	G_{mb}	VMA (%)	V_v (%)	V_b (%)	Temp (°C)	Frequency	σ (kPa)	E (Mpa)	ϵ	N
36	97	39	2.409	2.333	18.4	3.2	15.2	20	120ms	500	2,054	499	563
37	99	40	2.409	2.323	18.8	3.6	15.2	20	120ms	400	1,708	480	560
38	99	40	2.409	2.332	18.5	3.2	15.3	20	120ms	300	2,043	301	1,292
39	99	40	2.409	2.341	18.1	2.8	15.3	20	120ms	200	2,092	196	4,344
40	99	41	2.409	2.333	18.4	3.2	15.2	20	120ms	100	2,050	100	41,765
41	99	41	2.409	2.340	18.2	2.9	15.3	20	120ms	550	1,944	580	423
48	99	40	2.395	2.332	18.5	2.6	15.9	20	120ms	500	1,700	603	302
49	99	40	2.395	2.338	18.3	2.4	15.9	20	120ms	400	1,647	498	496
50	99	41	2.395	2.325	18.7	2.9	15.8	20	120ms	300	1,631	377	849
51	99	41	2.395	2.321	18.8	3.1	15.7	20	120ms	200	1,872	219	1,763
52	99	41	2.395	2.344	18.0	2.1	15.9	20	120ms	550	1,845	611	211
53	99	41	2.395	2.334	18.4	2.5	15.9	20	120ms	100	1,667	123	9,373
60	99	41	2.408	2.314	19.1	3.9	15.2	20	120ms	100	2,887	71	21,351
61	99	41	2.408	2.336	18.3	3.0	15.3	20	120ms	200	2,808	146	3,117
62	99	40	2.408	2.338	18.2	2.9	15.3	20	120ms	300	3,000	205	836
63	99	40	2.408	2.351	17.8	2.4	15.4	20	120ms	400	2,908	282	727
64	99	40	2.408	2.330	18.5	3.2	15.3	20	120ms	500	2,412	425	374
65	99	39	2.408	2.334	18.4	3.1	15.3	20	120ms	585	2,192	547	330

Table B.27 - Data for Practical Application of ITFT - 40/14 HRA W/C Unmodified - Untracked.

	Φ (mm)	Width (mm)	G_{mm}	G_{mb}	VMA (%)	V_v (%)	V_b (%)	Temp (°C)	Frequency	σ (kPa)	E (Mpa)	ϵ	N
42	99	40	2.400	2.316	19.0	3.5	15.5	20	120ms	550	1,444	781	148
43	99	41	2.400	2.364	17.3	1.5	15.8	20	120ms	500	1,870	548	376
44	99	40	2.400	2.329	18.6	3.0	15.6	20	120ms	400	1,680	488	598
45	99	40	2.400	2.306	19.4	3.9	15.5	20	120ms	300	1,464	420	794
46	99	41	2.400	2.342	18.1	2.4	15.7	20	120ms	200	1,653	248	2,370
47	99	41	2.400	2.310	19.2	3.8	15.5	20	120ms	100	1,541	133	15,417
54	99	40	2.399	2.322	18.8	3.2	15.6	20	120ms	500	1,622	632	147
55	99	40	2.399	2.333	18.4	2.8	15.6	20	120ms	400	1,694	484	262
56	99	42	2.399	2.352	17.8	2.0	15.8	20	120ms	300	952	646	177
57	99	41	2.399	2.331	18.5	2.8	15.7	20	120ms	200	1,475	278	1,670
58	99	40	2.399	2.320	18.9	3.3	15.6	20	120ms	100	2,181	94	13,612
59	99	42	2.399	2.329	18.6	2.9	15.7	20	120ms	150	2,196	140	10,890

Table B.28 - Data for Practical Application of ITFT - 50/20 HRA B/C SBS Modified - Tracked.

	Φ (mm)	Width (mm)	G_{mm}	G_{mb}	VMA (%)	V_v (%)	V_b (%)	Temp (°C)	Frequency	σ (kPa)	E (Mpa)	ϵ	N
74	99	35	2.411	2.279	21.3	5.5	15.8	20	120ms	500	391	2,621	24
75	99	32	2.411	2.274	21.5	5.7	15.8	20	120ms	300	358	1,718	97
76	99	36	2.411	2.247	22.4	6.8	15.6	20	120ms	100	317	647	699
89	99	37	2.401	2.278	21.4	5.1	16.3	20	120ms	500	295	3,475	39
90	99	40	2.401	2.310	20.3	3.8	16.5	20	120ms	400	357	2,297	62
91	99	37	2.401	2.295	20.8	4.4	16.4	20	120ms	300	311	1,977	130
92	99	42	2.401	2.314	20.1	3.6	16.5	20	120ms	200	427	960	453
93	99	40	2.401	2.295	20.8	4.4	16.4	20	120ms	50	362	283	6,693
101	99	40	2.385	2.304	20.5	3.4	17.1	20	120ms	500	323	3,173	51
102	99	41	2.385	2.294	20.8	3.8	17.0	20	120ms	400	293	2,799	77
103	98	39	2.385	2.316	20.1	2.9	17.2	20	120ms	300	358	1,718	247
104	99	41	2.385	2.292	20.9	3.9	17.0	20	120ms	200	311	1,318	983
105	99	41	2.385	2.284	21.2	4.2	17.0	20	120ms	50	272	377	12,738

Table B.29 - Data for Practical Application of ITFT - 50/20 HRA B/C SBS Modified - Untracked.

	Φ (mm)	Width (mm)	G_{mm}	G_{mb}	VMA (%)	V_v (%)	V_b (%)	Temp (°C)	Frequency	σ (kPa)	E (Mpa)	ϵ	N
78	99	33	2.394	2.198	24.1	8.2	15.9	20	120ms	500	370	2,770	34
79	99	41	2.394	2.278	21.4	4.8	16.6	20	120ms	400	330	2,485	54
80	99	38	2.394	2.274	21.5	5.0	16.5	20	120ms	300	321	1,916	97
81	99	31	2.394	2.288	21.0	4.4	16.6	20	120ms	200	278	1,475	298
82	99	35	2.394	2.254	22.2	5.8	16.4	20	120ms	100	251	817	487
83	99	41	2.412	2.268	21.7	6.0	15.7	20	120ms	500	379	2,704	32
84	99	41	2.412	2.321	19.9	3.8	16.1	20	120ms	400	586	1,399	155
85	99	41	2.412	2.325	19.7	3.6	16.1	20	120ms	300	327	1,881	196
86	99	40	2.412	2.307	20.4	4.4	16.0	20	120ms	200	317	1,293	384
87	99	41	2.412	2.304	20.5	4.5	16.0	20	120ms	50	238	431	10,345
95	99	40	2.390	2.338	19.3	2.2	17.1	20	120ms	500	539	1,902	45
96	99	41	2.390	2.326	19.7	2.7	17.0	20	120ms	400	246	3,333	47
97	99	38	2.390	2.322	19.8	2.8	17.0	20	120ms	300	268	2,295	143
98	99	41	2.390	2.334	19.4	2.3	17.1	20	120ms	200	355	1,155	876
99	99	41	2.390	2.341	19.2	2.1	17.2	20	120ms	50	317	323	47,486

Table B.30 - Data for Practical Application of ITFT - 50/20 HRA B/C Unmodified - Tracked.

	Φ (mm)	Width (mm)	G_{mm}	G_{mb}	VMA (%)	V_v (%)	V_b (%)	Temp (°C)	Frequency	σ (kPa)	E (Mpa)	ϵ	N
107	98	41	2.422	2.331	19.3	3.8	15.5	20	120ms	550	2,557	441	513
108	99	42	2.422	2.323	19.6	4.1	15.5	20	120ms	500	2,669	384	849
109	99	41	2.422	2.334	19.2	3.6	15.6	20	120ms	450	2,312	399	1,338
110	99	40	2.422	2.324	19.5	4.0	15.5	20	120ms	400	2,867	286	2,223
111	99	41	2.422	2.328	19.4	3.9	15.5	20	120ms	350	2,440	294	2,396
112	99	42	2.422	2.346	18.8	3.1	15.7	20	120ms	300	1,737	354	2,043
119	99	40	2.430	2.346	18.8	3.5	15.3	20	120ms	550	2,198	513	259
120	99	40	2.430	2.344	18.8	3.5	15.3	20	120ms	450	2,514	367	600
121	99	41	2.430	2.361	18.2	2.8	15.4	20	120ms	350	2,814	255	1,875
122	99	41	2.430	2.352	18.6	3.2	15.4	20	120ms	250	1,530	335	2,341
123	99	40	2.430	2.351	18.6	3.3	15.3	20	120ms	200	1,806	227	3,505
124	99	42	2.430	2.353	18.5	3.2	15.3	20	120ms	150	1,798	171	8,870
131	99	39	2.425	2.322	19.6	4.2	15.4	20	120ms	600	2,393	514	331
132	99	41	2.425	2.348	18.7	3.2	15.5	20	120ms	500	2,362	434	447
133	99	42	2.425	2.369	18.0	2.3	15.7	20	120ms	400	2,939	279	1,114
134	99	41	2.425	2.364	18.1	2.5	15.6	20	120ms	200	2,908	141	10,174
135	99	42	2.425	2.344	18.8	3.3	15.5	20	120ms	300	2,686	229	3,335
136	99	40	2.425	2.341	18.9	3.5	15.4	20	120ms	100	2,071	99	55,113

Table B.31 - Data for Practical Application of ITFT - 50/20 HRA B/C Unmodified - Untracked.

	Φ (mm)	Width (mm)	G_{mm}	G_{mb}	VMA (%)	V_v (%)	V_b (%)	Temp (°C)	Frequency	σ (kPa)	E (Mpa)	ϵ	N
113	99	41	2.421	2.354	18.5	2.8	15.7	20	120ms	550	2,028	556	295
114	99	40	2.421	2.334	19.2	3.6	15.6	20	120ms	500	2,417	424	619
115	99	40	2.421	2.320	19.7	4.2	15.5	20	120ms	450	2,787	331	842
116	99	41	2.421	2.315	19.8	4.4	15.4	20	120ms	400	2,141	383	1,063
117	99	41	2.421	2.359	18.3	2.6	15.7	20	120ms	350	2,466	291	1,069
118	99	41	2.421	2.371	17.9	2.1	15.8	20	120ms	250	2,010	255	2,791
125	99	41	2.427	2.335	19.1	3.8	15.3	20	120ms	550	1,740	648	326
126	99	41	2.427	2.352	18.6	3.1	15.5	20	120ms	450	1,910	483	648
127	99	40	2.427	2.338	19.0	3.7	15.3	20	120ms	350	2,271	316	1,506
128	99	39	2.427	2.317	19.8	4.5	15.3	20	120ms	600	2,204	558	311
129	99	40	2.427	2.318	19.7	4.5	15.2	20	120ms	250	2,135	240	2,581
130	99	41	2.427	2.334	19.2	3.8	15.4	20	120ms	100	1,934	106	27,874

Table B.32 - Data for Practical Application of ITFT - 40/14 HRA W/C Unmodified - Virgin Properties.

	Φ (mm)	Width (mm)	G_{mm}	G_{mb}	VMA (%)	V_v (%)	V_b (%)	Temp (°C)	Frequency	σ (kPa)	E (Mpa)	ϵ	N
1	100	40	2.377	2.322	18.8	2.3	16.5	20	120ms	500	2,079	493	266
2	100	41	2.377	2.320	18.9	2.4	16.4	20	120ms	400	3,048	269	711
3	100	41	2.377	2.330	18.5	2.0	16.5	20	120ms	300	2,212	278	2,137
4	100	40	2.377	2.317	19.0	2.5	16.5	20	120ms	200	1,367	300	3,372
5	100	40	2.377	2.325	18.7	2.2	16.5	20	120ms	150	2,181	141	38,752
6	100	41	2.377	2.318	19.0	2.5	16.5	20	120ms	550	1,813	622	237
7	100	40	2.377	2.325	18.7	2.2	16.5	20	120ms	450	2,460	375	527
8	100	39	2.377	2.334	18.4	1.8	16.6	20	120ms	350	2,990	240	1,077
9	100	41	2.377	2.331	18.5	1.9	16.6	20	120ms	250	2,092	245	3,075
10	100	40	2.377	2.330	18.5	2.0	16.5	20	120ms	100	2,071	99	83,764
11	100	40	2.377	2.329	18.6	2.0	16.6	20	120ms	300	2,312	266	2,638
12	100	39	2.377	2.334	18.4	1.8	16.6	20	120ms	600	2,557	481	175
13	100	39	2.377	2.322	18.8	2.3	16.5	20	120ms	500	2,563	400	285
14	100	39	2.377	2.337	18.3	1.7	16.6	20	120ms	400	2,405	341	693
15	100	40	2.377	2.319	18.9	2.4	16.5	20	120ms	200	2,412	170	7,475

Table B.33 - Data for Practical Application of ITFT - 40/14 HRA W/C SBS Modified - Virgin Properties.

	Φ (mm)	Width (mm)	G_{mm}	G_{mb}	VMA (%)	V_v (%)	V_b (%)	Temp (°C)	Frequency	σ (kPa)	E (Mpa)	ϵ	N
16	100	40	2.355	2.313	19.4	1.8	17.6	20	120ms	500	870	1,178	202
17	100	39	2.355	2.294	20.1	2.6	17.5	20	120ms	550	751	1,501	141
18	100	39	2.355	2.291	20.2	2.7	17.5	20	120ms	450	918	1,005	188
19	100	40	2.355	2.293	20.1	2.6	17.5	20	120ms	400	821	999	309
20	100	40	2.355	2.283	20.4	3.1	17.3	20	120ms	350	656	1,094	469
21	100	40	2.355	2.282	20.5	3.1	17.4	20	120ms	300	692	889	909
22	100	40	2.355	2.287	20.3	2.9	17.4	20	120ms	250	738	694	1,604
23	100	40	2.355	2.296	20.0	2.5	17.5	20	120ms	200	672	610	3,987
24	100	40	2.355	2.296	20.0	2.5	17.5	20	120ms	150	904	340	29,766
25	100	40	2.355	2.291	20.2	2.7	17.5	20	120ms	100	995	206	386,023
26	100	39	2.355	2.286	20.4	2.9	17.5	20	120ms	600	988	1,245	267
27	100	39	2.355	2.300	19.9	2.3	17.6	20	120ms	575	843	1,398	140
28	100	40	2.355	2.293	20.1	2.6	17.5	20	120ms	475	951	1,024	535
29	100	40	2.355	2.299	19.9	2.4	17.5	20	120ms	375	910	845	1,342
30	100	39	2.355	2.317	19.3	1.6	17.7	20	120ms	175	972	369	47,387

Table B.34 - Data for Practical Application of ITFT - 50/20 HRA B/C Unmodified - Virgin Properties.

	Φ (mm)	Width (mm)	G_{mm}	G_{mb}	VMA (%)	V_v (%)	V_b (%)	Temp (°C)	Frequency	σ (kPa)	E (Mpa)	ε	N
31	100	40	2.403	2.295	20.5	4.5	16.0	20	120ms	550	850	1,326	63
32	100	40	2.403	2.301	20.3	4.2	16.4	20	120ms	500	1,042	984	54
33	100	40	2.403	2.312	19.9	3.8	16.1	20	120ms	450	1,204	766	98
34	100	40	2.403	2.300	20.4	4.3	16.1	20	120ms	400	972	844	111
35	100	40	2.403	2.270	21.4	5.5	15.9	20	120ms	350	931	771	145
36	100	40	2.403	2.286	20.8	4.9	15.9	20	120ms	300	907	678	233
37	100	42	2.403	2.292	20.6	4.6	16.0	20	120ms	250	1,100	466	544
38	100	42	2.403	2.276	21.2	5.3	15.9	20	120ms	200	840	488	615
39	100	42	2.403	2.276	21.2	5.3	15.9	20	120ms	525	825	1,305	45
40	100	40	2.403	2.288	20.8	4.8	16.0	20	120ms	425	923	944	125
41	100	40	2.403	2.303	20.3	4.2	16.1	20	120ms	325	1,031	646	213
42	100	40	2.403	2.313	19.9	3.7	16.2	20	120ms	225	1,288	358	1,285
43	100	40	2.403	2.274	21.3	5.4	15.9	20	120ms	150	976	315	1,922
44	100	41	2.403	2.277	21.2	5.2	16.0	20	120ms	125	935	274	3,037
45	100	41	2.403	2.294	20.6	4.5	16.1	20	120ms	100	1,242	165	8,556

Table B.35 - Data for Practical Application of ITFT - 50/20 HRA B/C SBS Modified - Virgin Properties.

	Φ (mm)	Width (mm)	G_{mm}	G_{mb}	VMA (%)	V_v (%)	V_b (%)	Temp (°C)	Frequency	σ (kPa)	E (Mpa)	ε	N
46	100	40	2.371	2.289	21.0	3.5	17.5	20	120ms	100	586	350	18,008
47	100	40	2.371	2.293	20.9	3.3	17.6	20	120ms	200	722	568	1,077
48	100	39	2.371	2.302	20.5	2.9	17.6	20	120ms	300	745	826	231
49	100	39	2.371	2.289	21.0	3.5	17.5	20	120ms	400	732	1,120	156
50	100	40	2.371	2.293	20.9	3.3	17.6	20	120ms	500	715	1,434	94
51	100	40	2.371	2.275	21.5	4.0	17.5	20	120ms	50	563	182	263,551
52	100	40	2.371	2.296	20.7	3.2	17.5	20	120ms	75	638	241	55,555
53	100	40	2.371	2.289	21.0	3.5	17.5	20	120ms	503	596	1,730	119
54	100	40	2.371	2.295	20.8	3.2	17.6	20	120ms	550	630	1,790	72
55	100	40	2.371	2.283	21.2	3.7	17.5	20	120ms	350	631	1,137	207
56	100	40	2.371	2.295	20.8	3.2	17.6	20	120ms	450	490	1,883	99
57	100	39	2.371	2.290	21.0	3.4	17.6	20	120ms	538	694	1,589	100
58	100	40	2.371	2.283	21.2	3.7	17.5	20	120ms	250	492	1,042	665
59	100	39	2.371	2.291	20.9	3.4	17.5	20	120ms	150	531	579	3,110
60	100	39	2.371	2.297	20.7	3.1	17.6	20	120ms	600	647	1,901	49

Table B.36 - Data for Practical Application of ITFT - Retested 50/20 HRA B/C Unmodified - Virgin Properties.

	Φ (mm)	Width (mm)	G_{mm}	G_{mb}	VMA (%)	V_v (%)	V_b (%)	Temp (°C)	Frequency	σ (kPa)	E (Mpa)	ϵ	N
1	100	40	2.398	2.339	19.0	2.5	16.5	20	120ms	550	1,277	883	115
2	100	41	2.398	2.324	19.5	3.1	16.4	20	120ms	100	1,444	142	19,972
3	100	40	2.398	2.341	18.9	2.4	16.5	20	120ms	500	1,436	714	109
4	100	40	2.398	2.335	19.1	2.6	16.5	20	120ms	400	1,399	586	362
5	100	40	2.398	2.340	19.0	2.4	16.6	20	120ms	300	1,545	398	1,383
6	100	40	2.398	2.341	18.9	2.4	16.5	20	120ms	200	1,701	241	3,119
7	100	40	2.398	2.331	19.3	2.8	16.5	20	120ms	75	1,507	102	57,537
8	100	40	2.398	2.330	19.3	2.8	16.5	20	120ms	450	1,192	774	148
9	100	40	2.398	2.334	19.2	2.7	16.5	20	120ms	350	1,198	599	451
10	100	39	2.398	2.339	19.0	2.5	16.5	20	120ms	600	1,173	1,049	89
11	100	39	2.398	2.334	19.2	2.7	16.5	20	120ms	575	1,230	958	75
12	100	40	2.398	2.340	19.0	2.4	16.6	20	120ms	250	1,521	337	1,720
13	100	40	2.398	2.323	19.6	3.1	16.5	20	120ms	150	1,610	191	7,914
14	100	41	2.398	2.330	19.3	2.8	16.5	20	120ms	325	1,296	514	550
15	100	41	2.398	2.315	19.8	3.5	16.3	20	120ms	50	1,553	66	589,458

Table B.37 - Data for Further Validation of the ITFT - Comparison with Uniaxial Tension Compression Apparatus - 20mm HDM (1987).

	Φ (mm)	Width (mm)	Temp (°C)	Frequency	σ (kPa)	E (Mpa)	ϵ	N
1	100	40	20	120ms	450	3,404	271	407
2	100	40	20	120ms	475	3,268	298	553
3	100	41	20	120ms	400	3,228	254	575
4	100	42	20	120ms	300	3,203	192	1,739
5	100	39	20	120ms	200	3,796	108	5,789
6	100	39	20	120ms	100	3,475	59	347,756
7	100	39	20	120ms	425	3,444	253	495
8	100	40	20	120ms	450	3,632	254	976
9	100	40	20	120ms	350	3,466	207	996
10	100	40	20	120ms	250	3,768	136	4,779
11	100	40	20	120ms	150	3,576	86	64,595
F1	100	-	10	10Hz	-	-	70	51,600
F2	100	-	10	10Hz	-	-	43	789,000
F3	100	-	10	10Hz	-	-	93	12,600
F4	100	-	10	10Hz	-	-	51	237,000
F5	100	-	10	10Hz	-	-	64	75,000
F6	100	-	10	10Hz	-	-	84	18,600
F7	100	-	10	10Hz	-	-	55	164,400

Table B.38 - Data for Further Validation of the ITFT - Comparison with Uniaxial Tension Compression Apparatus - 0/10mm French Asphaltic Concrete (1992).

	Φ (mm)	Width (mm)	Temp (°C)	Frequency	σ (kPa)	E (Mpa)	ϵ	N
12	100	40	20	120ms	470	2,992	322	758
13	100	40	20	120ms	470	2,753	350	666
14	100	42	20	120ms	400	3,178	258	748
15	100	41	20	120ms	300	2,915	211	2,758
16	100	40	20	120ms	200	2,828	145	15,770
17	100	42	20	120ms	100	2,697	76	123,069
18	100	41	20	120ms	425	3,068	284	584
19	100	41	20	120ms	450	3,106	297	1,054
20	100	40	20	120ms	350	3,040	236	2,035
21	100	40	20	120ms	250	2,588	198	4,133
22	100	40	20	120ms	150	2,651	116	59,436
F8	100	-	10	10Hz	-	-	43	2,484,000
F9	100	-	10	10Hz	-	-	55	504,000
F10	100	-	10	10Hz	-	-	72	63,000
F11	100	-	10	10Hz	-	-	113	10,800
F12	100	-	10	10Hz	-	-	80	51,000
F13	100	-	10	10Hz	-	-	92	34,800
F14	100	-	10	10Hz	-	-	62	186,600

Table B.39 - Data for Further Validation of the ITFT - Comparison with Uniaxial Tension Compression Apparatus - 0/14mm French Asphaltic Concrete (1995).

	Φ (mm)	Width (mm)	Temp (°C)	Frequency	σ (kPa)	E (Mpa)	ϵ	N
23	100	40	20	120ms	450	2,666	346	432
24	100	41	20	120ms	425	2,578	338	480
25	100	40	20	120ms	400	2,620	313	694
26	100	40	20	120ms	300	2,606	236	1,980
27	100	40	20	120ms	200	2,628	156	10,724
28	100	40	20	120ms	100	2,531	81	256,024
29	100	40	20	120ms	400	2,547	322	787
30	100	40	20	120ms	450	2,666	346	618
31	100	40	20	120ms	350	2,544	282	1,401
32	100	40	20	120ms	250	2,440	210	2,483
33	100	39	20	120ms	150	2,651	116	94,741
F15	100	-	10	10Hz	-	-	42	2,187,600
F16	100	-	10	10Hz	-	-	55	273,000
F17	100	-	10	10Hz	-	-	106	10,200
F18	100	-	10	10Hz	-	-	67	100,200
F19	100	-	10	10Hz	-	-	72	87,000
F20	100	-	10	10Hz	-	-	49	805,000
F21	100	-	10	10Hz	-	-	90	23,400

APPENDIX C

DATA FOR THE POISSON'S RATIO WORK

The tables given in this Appendix have the following notation:

Φ	Diameter of the test specimen to the nearest millimetre,
Width	Width of the test specimen to the nearest millimetre,
G_{mm}	Maximum specific gravity of the mixture,
G_{mb}	Bulk specific gravity of the mixture,
VMA	Volume of voids in the mineral aggregate (%),
V_v	Volume of air voids in the mixture (%),
V_b	Volume of bitumen in the mixture (%),
E	Stiffness modulus of the test specimen at 20°C and with a risetime of 120ms.

Table C.1 - Data for the Cores Used for Measuring Poisson's Ratio.

	Φ (mm)	Width (mm)	G_{mm}	G_{mb}	VMA (%)	V_v (%)	V_b (%)	E (MPa)
L1	99	32	2.265	2.045	30.9	9.7	21.2	1489.0
L2	99	32	2.265	2.062	30.3	9.0	21.3	1749.0
L3	99	38	2.265	2.038	31.1	10.0	21.1	1100.0
L4	98	40	2.265	2.043	31.0	9.8	21.2	1267.0
L5	99	40	2.265	2.074	29.9	8.4	21.5	1443.0
L6	99	41	2.265	2.035	31.2	10.2	21.0	1198.0
H7	98	40	2.265	2.053	30.6	9.4	21.2	1149.0
H8	98	39	2.265	2.084	29.6	8.0	21.6	1378.0
H9	98	39	2.265	2.037	31.2	10.1	21.1	1305.0
H10	98	39	2.265	2.087	29.5	7.9	21.6	1248.0
H11	98	39	2.265	2.050	30.7	9.5	21.2	1228.0
H12	98	40	2.265	2.050	30.7	9.5	21.2	1295.0

Table C.2 - Data for Core H7 Sand Asphalt

Stress (kN)	Risetime (ms)	Force (kN)	Hor Def (mm)	Ver Def (mm)	Poisson's	E (MPa)
0°C, 120ms, 5μm						
614.9	128	3.786017	0.00495	0.012409	0.6463	4,587
615.0	126	3.786838	0.00486	0.012478	0.63976	4,528
615.0	130	3.787112	0.004877	0.012496	0.640316	4,525
615.1	128	3.787385	0.004912	0.012461	0.643031	4,553
615.2	128	3.787933	0.004965	0.012478	0.645605	4,560
0°C, 120ms, 10μm						
620.9	128	3.822958	0.004945	0.012617	0.641462	4,528
620.9	126	3.823232	0.004973	0.012635	0.642614	4,528
620.7	128	3.821863	0.005036	0.012739	0.643817	4,495
620.9	130	3.823232	0.0049	0.012617	0.638979	4,515
620.9	130	3.823232	0.004911	0.012687	0.63809	4,486
0°C, 120ms, 15μm						
620.6	128	3.821043	0.004909	0.0126	0.639842	4,521
620.4	130	3.819948	0.004946	0.01267	0.640376	4,498
620.4	128	3.820222	0.004954	0.012583	0.642695	4,542
620.8	130	3.822411	0.005204	0.012652	0.654866	4,575
620.4	130	3.820222	0.005122	0.012617	0.651176	4,566
0°C, 160ms, 5μm						
583.6	188	3.593378	0.005162	0.013	0.645034	4,149
582.9	188	3.589273	0.005084	0.012913	0.642699	4,161
582.9	188	3.589273	0.005134	0.012983	0.643899	4,143
582.9	188	3.589	0.005222	0.013	0.648229	4,157
582.7	188	3.588179	0.005079	0.013053	0.639495	4,098
0°C, 160ms, 10μm						
619.4	130	3.814202	0.005284	0.013505	0.640997	4,219
619.0	130	3.811739	0.005349	0.013505	0.64434	4,233
619.1	130	3.812286	0.005284	0.013488	0.64134	4,224
619.3	130	3.813381	0.005381	0.013609	0.643871	4,200
619.2	132	3.812833	0.005346	0.013644	0.641385	4,176
0°C, 160ms, 15μm						
619.5	188	3.814749	0.005467	0.013871	0.642991	4,118
620.0	188	3.817485	0.005566	0.013958	0.646206	4,110
619.3	190	3.813381	0.005534	0.014062	0.642582	4,058
619.1	188	3.812013	0.005483	0.013975	0.641748	4,077
618.3	130	3.807087	0.005477	0.013992	0.641119	4,064
0°C, 80ms, 5μm						
521.3	80	3.210015	0.003594	0.00952	0.631399	5,000
521.1	80	3.208647	0.003667	0.009572	0.635302	4,991
522.4	80	3.216582	0.003651	0.009624	0.632691	4,961
520.0	82	3.20208	0.003546	0.009589	0.625971	4,919
517.2	80	3.184841	0.003556	0.009311	0.634476	5,087
0°C, 80ms, 10μm						
546.4	80	3.364619	0.003801	0.009885	0.636298	5,065
545.8	80	3.360788	0.003841	0.009885	0.639121	5,076
544.2	80	3.350664	0.003785	0.009885	0.635167	5,037
544.5	80	3.352853	0.003759	0.009816	0.635197	5,077
541.8	80	3.336161	0.003784	0.00985	0.636047	5,040
0°C, 80ms, 15μm						
535.2	80	3.295663	0.003771	0.009729	0.638449	5,058
535.3	80	3.29621	0.003717	0.009641	0.63701	5,096
534.2	80	3.289096	0.003699	0.009676	0.634736	5,053
533.9	80	3.28718	0.003667	0.009641	0.633384	5,060
533.4	80	3.284444	0.003728	0.009694	0.63263	5,045

Table C.3 - Data for Core H12

Stress (kN)	Risetime (ms)	Force (kN)	Hor Def (mm)	Ver Def (mm)	Poisson's	E (MPa)
0°C, 120ms, 5μm						
318.7	114	1.962512	0.005104	0.013174	0.638327	2,223
318.9	114	1.963607	0.005102	0.013261	0.636449	2,205
319.1	116	1.964975	0.005209	0.013209	0.643144	2,230
319.2	116	1.965248	0.005146	0.013105	0.641978	2,245
319.1	114	1.964975	0.005119	0.01314	0.639821	2,233
0°C, 120ms, 10μm						
610.1	120	3.756738	0.009537	0.02339	0.652402	2,427
604.6	120	3.723081	0.009356	0.023147	0.649961	2,423
609.0	120	3.749624	0.009422	0.023129	0.652146	2,448
603.3	120	3.714598	0.009313	0.022903	0.651637	2,447
607.0	120	3.73731	0.009336	0.022694	0.654912	2,494
0°C, 120ms, 15μm						
611.0	126	3.762211	0.009831	0.023773	0.656389	2,400
613.6	124	3.778355	0.009843	0.023843	0.655901	2,401
616.4	128	3.795321	0.009912	0.02393	0.656851	2,405
616.4	126	3.795321	0.009872	0.023947	0.655502	2,400
617.0	126	3.799425	0.009883	0.023895	0.656434	2,410
0°C, 80ms, 5μm						
391.3	80	2.409632	0.00526	0.013366	0.642577	2,702
392.6	80	2.417567	0.005302	0.013766	0.636738	2,614
392.6	80	2.417567	0.005426	0.013923	0.639919	2,594
393.2	80	2.421398	0.005449	0.014097	0.637704	2,559
393.2	80	2.421125	0.005468	0.014114	0.638318	2,557
0°C, 80ms, 10μm						
549.1	80	3.381311	0.008068	0.02071	0.639819	2,438
550.2	80	3.387878	0.008229	0.020797	0.644067	2,444
549.9	80	3.385689	0.008179	0.020658	0.644235	2,458
549.1	80	3.381037	0.008171	0.02071	0.643277	2,446
549.3	80	3.382405	0.008181	0.020606	0.644995	2,464
0°C, 80ms, 15μm						
547.4	80	3.370365	0.007971	0.020484	0.639514	2,455
548.2	82	3.375564	0.008029	0.020275	0.644291	2,498
547.9	82	3.373923	0.007934	0.02024	0.641507	2,492
547.2	82	3.369271	0.007912	0.020188	0.641451	2,495
546.6	80	3.36544	0.00791	0.020084	0.642792	2,508
0°C, 160ms, 5μm						
291.7	204	1.796142	0.005014	0.012757	0.642232	2,106
291.8	208	1.796689	0.005025	0.012617	0.645862	2,139
291.7	208	1.796142	0.005044	0.012548	0.648426	2,156
291.6	204	1.795321	0.004999	0.012617	0.644434	2,133
291.7	208	1.796142	0.004892	0.012496	0.641151	2,146
0°C, 160ms, 10μm						
613.1	192	3.775072	0.010208	0.024417	0.659497	2,351
613.8	192	3.77945	0.010124	0.024469	0.656535	2,340
613.8	192	3.77945	0.01015	0.024434	0.657671	2,346
614.2	192	3.782186	0.010177	0.024434	0.658429	2,350
614.3	192	3.78246	0.010094	0.024434	0.656099	2,343
0°C, 160ms, 15μm						
620.7	196	3.822137	0.010198	0.024504	0.658201	2,367
621.4	196	3.826242	0.010178	0.024835	0.653838	2,326
621.0	196	3.824053	0.010214	0.0244	0.659865	2,383
620.7	194	3.822137	0.010257	0.024452	0.660459	2,378
620.8	196	3.822411	0.010227	0.024417	0.66003	2,380

Table C.4 - Volumetric Data for bituminous Mixture Cubes.

	length (mm)	Width (mm)	Height (mm)	G_{mm}	G_{mb}	VMA (%)	V_v (%)	V_b (%)	Test Temp (°C)	Number of cycles to Steady State	Poisson's Ratio
Sand Asphalt 2	100.2	100.2	100.2	2.266	1.976	33.1	12.8	20.3	0	400	0.40
Sand Asphalt 3	100.2	100.2	100.2	2.266	1.975	33.0	12.8	20.2	4	500	0.22
Sand Asphalt 4	100.3	100.3	100.3	2.266	1.981	33.0	12.6	20.4	8	400	0.40
Sand Asphalt 5	100.3	100.3	100.3	2.266	1.979	33.1	12.7	20.4	20	50	0.37
Sand Asphalt 6	100.1	100.1	100.1	2.266	1.915	35.1	15.5	19.6	0	400	0.44
Sand Asphalt 7	100.4	100.4	100.4	2.266	1.918	35.0	15.4	19.6	8	400	0.32
Sand Asphalt 8	100.3	100.3	100.3	2.266	1.910	35.0	15.7	19.3	20	400	0.39
Sand Asphalt 9	100.2	100.2	100.2	2.266	1.914	35.2	15.5	19.7	33	50	0.39
Sand Asphalt 10	100.6	100.6	100.6	2.266	1.914	35.3	15.5	19.8	4	500	0.30
30/14 HRA	100.4	100.4	100.4	2.388	2.312	20.8	3.2	17.6	20	500	0.43

Cycle	Force (kN)	Hor def (mm)	Ver def (mm)	Stress (kPa)	E (MPa)	Poisson's Ratio
6	3.67	0.001789	0.002367	367	4,651	0.76
7	3.68	0.001762	0.002262	368	4,881	0.78
8	3.67	0.001643	0.002558	367	4,304	0.64
9	3.68	0.001690	0.002663	368	4,146	0.63
10	3.68	0.001700	0.002732	368	4,041	0.62
31	3.55	0.001590	0.002506	355	4,250	0.63
32	3.55	0.001520	0.002471	355	4,310	0.62
33	3.54	0.001496	0.002436	354	4,360	0.61
34	3.53	0.001453	0.002419	353	4,378	0.60
35	3.52	0.001431	0.002402	352	4,396	0.60
136	3.78	0.001407	0.002924	378	3,878	0.48
137	3.78	0.001408	0.002924	378	3,878	0.48
138	3.78	0.001399	0.002924	378	3,878	0.48
139	3.78	0.001338	0.002976	378	3,810	0.45
140	3.78	0.001351	0.002906	378	3,902	0.46
196	3.78	0.001335	0.002802	378	4,047	0.48
197	3.76	0.001367	0.002924	376	3,858	0.47
198	3.76	0.001336	0.002941	376	3,835	0.45
199	3.76	0.001326	0.002872	376	3,928	0.46
200	3.76	0.001345	0.002924	376	3,858	0.46
296	3.76	0.001199	0.002802	376	4,026	0.43
297	3.75	0.001223	0.002819	375	3,991	0.43
298	3.75	0.001206	0.002837	375	3,965	0.43
299	3.75	0.001271	0.002819	375	3,991	0.45
300	3.76	0.001185	0.002785	376	4,050	0.43
396	3.78	0.001116	0.002889	378	3,925	0.39
397	3.75	0.001109	0.002785	375	4,039	0.40
398	3.75	0.001134	0.002785	375	4,039	0.41
399	3.75	0.001067	0.002802	375	4,015	0.38
400	3.76	0.001076	0.002732	376	4,129	0.39
496	3.74	0.001057	0.002680	374	4,187	0.39
497	3.72	0.001060	0.002698	372	4,136	0.39
498	3.72	0.001088	0.002750	372	4,058	0.40
499	3.72	0.001085	0.002715	372	4,110	0.40
500	3.72	0.001114	0.002698	372	4,136	0.41
596	3.73	0.001095	0.002715	373	4,122	0.40
597	3.72	0.001071	0.002576	372	4,332	0.42
598	3.71	0.001058	0.002541	371	4,380	0.42
599	3.71	0.001044	0.002593	371	4,292	0.40
600	3.71	0.001077	0.002489	371	4,472	0.43
696	3.72	0.001066	0.002680	372	4,164	0.40
697	3.72	0.001002	0.002663	372	4,191	0.38
698	3.72	0.001020	0.002680	372	4,164	0.38
699	3.72	0.001033	0.002680	372	4,164	0.39
700	3.71	0.000986	0.002645	371	4,208	0.37
796	3.45	0.000949	0.002506	345	4,130	0.38
797	3.44	0.000989	0.002506	344	4,118	0.39
798	3.42	0.000958	0.002576	342	3,983	0.37
799	3.42	0.001111	0.002576	342	3,983	0.43
800	3.40	0.001078	0.002576	340	3,960	0.42
896	3.71	0.001047	0.002785	371	3,996	0.38
897	3.70	0.001070	0.002785	370	3,986	0.38
898	3.69	0.001065	0.002819	369	3,927	0.38
899	3.69	0.001080	0.002785	369	3,975	0.39
900	3.69	0.001074	0.002698	369	4,103	0.40
996	3.72	0.000985	0.002645	372	4,219	0.37
997	3.70	0.000980	0.002645	370	4,197	0.37
998	3.70	0.001081	0.002698	370	4,114	0.40
999	3.70	0.001079	0.002645	370	4,197	0.41
1000	3.70	0.001069	0.002628	370	4,224	0.41

Figure C.1 - Typical Raw Data for the Measurement of Poisson's ratio on a Cube.

APPENDIX D

DATA FOR CRACK PROPAGATION TEST PROGRAMME

The tables given in this Appendix have the following notation:

Length	Length of the test specimen to the nearest millimetre,
Width	Width of the test specimen to the nearest millimetre (average of 5 measurements along the length of the beam),
Height	Height of the test specimen to the nearest millimetre (average of 5 measurements along the length of the beam at the same points as the width was measured),
G_{mm}	Maximum specific gravity of the mixture,
G_{mb}	Bulk specific gravity of the mixture,
VMA	Volume of voids in the mineral aggregate (%),
V_v	Volume of air voids in the mixture (%),
V_b	Volume of bitumen in the mixture (%),
E	Stiffness modulus of the test specimen at 20°C and with a risetime of 120ms,
N	Number of cycles to failure (25% of initial stiffness).

The specimen identification is made up as follows:

HRA 5 L L 1

The first 3 letters refer to the mixture type:

HRA	Hot Rolled Asphalt
DBM	Dense Bitumen Macadam

The next character refers to the type of bitumen:

5	50 pen
1	100 pen
E	EVA modified
S	SBS modified

The next letter refers to the void content:

H	High void content
L	Low void content

The next letter refers to the binder content:

H	Optimum plus 1%
O	Optimum
L	Optimum minus 1%

The last number refers to the replicate number:

1	First replicate
2	Second replicate
3	Third replicate

Figure D.1 shows a typical beam cracking raw data file.

"BEAM CRACKING RESULT

Date 06/03/1995

Specimen Number DBM 5HO 2

Cycles	Load (kN)	Strain	Percentage of Initial Load (%)	Risetime (ms)	Number of Photographs
50	2.40	0.0536	0	118	0
100	2.29	0.0682	0	124	0
150	2.65	0.1302	105	120	0
200	1.43	0.0909	57	122	4
250	1.27	0.0883	50	118	4
300	1.18	0.0889	47	118	5
350	1.14	0.0897	45	122	5
400	1.09	0.0905	43	122	6
450	1.00	0.0866	40	122	6
500	1.01	0.0878	40	118	6
550	0.98	0.0886	39	120	7
600	0.92	0.0867	37	118	7
650	0.93	0.0871	37	118	7
700	0.92	0.0905	37	124	7
750	0.89	0.0900	35	118	7
800	0.85	0.0883	34	122	8
850	0.83	0.0898	33	126	8
900	0.82	0.0880	32	120	8
950	0.80	0.0865	32	120	8
1,000	0.77	0.0870	31	124	8
1,050	0.78	0.0866	31	122	8
1,100	0.79	0.0929	31	124	8
1,150	0.78	0.0891	31	120	8
1,200	0.78	0.0896	31	122	8
1,250	0.77	0.0876	31	114	8
1,300	0.76	0.0863	30	120	8
1,350	0.75	0.0889	30	122	9
1,400	0.73	0.0876	29	118	9
1,450	0.72	0.0882	28	130	9
1,500	0.69	0.0869	28	122	9
1,550	0.70	0.0878	28	122	9
1,600	0.71	0.0890	28	122	9
1,650	0.70	0.0906	28	118	9
1,700	0.67	0.0914	27	126	9
1,750	0.66	0.0880	26	118	9
1,800	0.66	0.0890	26	118	9
1,850	0.63	0.0848	25	116	9
1,900	0.63	0.0867	25	122	9
1,950	0.63	0.0863	25	114	9
2,000	0.63	0.0862	25	122	9
2,050	0.64	0.0875	25	120	9
2,100	0.64	0.0882	25	124	9
2,150	0.63	0.0864	25	118	9
2,200	0.62	0.0875	25	114	9
2,250	0.61	0.0875	24	114	9
2,300	0.62	0.0883	25	114	9
2,350	0.62	0.0883	25	122	9
2,400	0.63	0.0834	25	124	9
2,450	0.63	0.0880	25	118	9
2,500	0.63	0.0895	25	124	9

Figure D.1 - Typical Beam Cracking Raw Data File.

Table D.1 - Data for the Beams Used in the Pilot Test Programme - DBM 5HO.

	Length (mm)	Width (mm)	Height (mm)	G_{mm}	G_{mb}	VMA (%)	V_v (%)	V_a (%)
1A	404	81	81	2.539	2.416	16.0	4.8	11.2
1B	404	80	81	2.539	2.409	16.2	5.3	10.9
1C	404	82	81	2.539	2.403	16.4	5.5	10.9
2A	404	82	81	2.539	2.409	16.2	5.3	10.9
2B	404	80	80	2.539	2.408	16.2	5.3	10.9
2C	404	83	81	2.539	2.408	16.2	5.3	10.9
3A	404	81	81	2.539	2.400	16.5	5.6	10.9
3B	404	80	81	2.539	2.400	16.5	5.6	10.9
3C	404	83	81	2.539	2.387	17.0	6.1	10.9
4A	404	81	82	2.539	2.405	16.4	5.4	11.0
4B	404	81	80	2.539	2.410	16.2	5.2	11.0
4C	404	80	81	2.539	2.401	16.5	5.6	10.9
5A	404	80	81	2.541	2.436	15.3	4.1	11.2
5B	404	81	80	2.541	2.447	14.9	3.7	11.2
5C	404	81	83	2.541	2.434	15.3	4.2	11.1
6A	404	80	81	2.541	2.432	15.4	4.3	11.1
6B	404	81	81	2.541	2.447	14.9	3.7	11.2
6C	404	81	81	2.541	2.435	15.3	4.2	11.1

Table D.2 - Data for the HRA 50 pen Beams Used in the Main Test Programme.

	Length (mm)	Width (mm)	Height (mm)	G_{mm}	G_{mb}	VMA (%)	V_v (%)	V_b (%)	E (MPa)	N
HRA 5LL 1	404	81	80	2.453	2.297	19.1	6.4	12.7	3,130	19,900
HRA 5LL 2	404	80	80	2.453	2.306	18.8	6.0	12.8	2,980	27,100
HRA 5LL 3	404	81	80	2.453	2.309	18.7	5.9	12.8	3,190	19,900
HRA 5HL 1	404	81	80	2.456	2.304	18.8	6.2	12.6	3,160	2,950
HRA 5HL 2	404	80	80	2.456	2.317	18.4	5.7	12.7	3,140	14,600
HRA 5HL 3	404	81	80	2.456	2.309	18.7	6.0	12.7	3,000	6,250
HRA 5LO 1	404	81	81	2.415	2.338	17.6	3.2	14.4	3,060	6,050
HRA 5LO 2	404	82	81	2.415	2.343	17.5	3.0	14.5	3,050	10,850
HRA 5LO 3	404	81	81	2.415	2.346	17.3	2.9	14.4	3,060	3,050
HRA 5HO 1	404	80	80	2.420	2.312	18.5	4.5	14.0	3,080	8,300
HRA 5HO 2	404	80	81	2.420	2.326	18.1	3.9	14.2	2,310	30,700
HRA 5HO 3	404	82	80	2.420	2.323	18.2	4.0	14.2	2,780	7,950
HRA 5LH 1	404	80	81	2.383	2.333	17.8	2.1	15.7	2,750	4,500
HRA 5LH 2	404	80	79	2.383	2.344	17.4	1.6	15.8	2,750	9,000
HRA 5LH 3	404	81	80	2.383	2.338	17.6	1.9	15.7	3,040	3,900
HRA 5HH 1	404	80	81	2.389	2.321	18.2	2.8	15.4	2,640	20,050
HRA 5HH 2	404	81	80	2.389	2.319	18.3	2.9	15.4	2,680	15,500
HRA 5HH 3	404	81	80	2.389	2.302	18.9	3.6	15.3	2,640	4,900

Table D.3 - Data for the HRA 100 pen Beams Used in the Main Test Programme.

	Length (mm)	Width (mm)	Height (mm)	G_{mm}	G_{mb}	VMA (%)	V_v (%)	V_b (%)	E (MPa)	N
HRA 1LL 1	404	79	80	2.452	2.333	17.8	4.9	12.9	2,460	10,400
HRA 1LL 2	404	81	80	2.452	2.344	17.4	4.4	13.0	2,600	9,450
HRA 1LL 3	404	81	80	2.452	2.338	17.6	4.6	13.0	2,430	12,750
HRA 1HL 1	404	80	80	2.449	2.321	18.2	5.2	13.0	2,180	16,450
HRA 1HL 2	404	80	80	2.449	2.319	18.3	5.3	13.0	2,260	31,700
HRA 1HL 3	404	81	80	2.449	2.302	18.9	6.0	12.9	2,130	27,800
HRA 1LO 1	404	81	80	2.418	2.367	16.6	2.1	14.5	2,360	20,450
HRA 1LO 2	404	81	81	2.418	2.375	16.3	1.8	14.5	2,320	27,300
HRA 1LO 3	404	81	81	2.418	2.374	16.4	1.8	14.6	2,400	20,050
HRA 1HO 1	404	81	82	2.420	2.304	18.8	4.8	14.0	1,970	37,150
HRA 1HO 2	404	80	81	2.420	2.313	18.5	4.4	14.1	2,150	41,950
HRA 1HO 3	404	80	80	2.420	2.308	18.7	4.6	14.1	2,190	28,000
HRA 1LH 1	404	81	80	2.383	2.329	17.9	2.3	15.6	1,620	107,350
HRA 1LH 2	404	80	81	2.383	2.320	18.3	2.6	15.7	1,550	186,950
HRA 1LH 3	404	81	81	2.383	2.328	18.0	2.3	15.7	1,810	80,950
HRA 1HH 1	404	80	81	2.386	2.284	19.5	4.3	15.2	1,320	180,750
HRA 1HH 2	404	80	80	2.386	2.267	20.1	5.0	15.1	1,290	243,550
HRA 1HH 3	404	82	80	2.386	2.276	19.8	4.6	15.2	1,350	179,950

Table D.4 - Data for the HRA EVA Modified Beams Used in the Main Test Programme.

	Length (mm)	Width (mm)	Height (mm)	G_{mm}	G_{mb}	VMA (%)	V_v (%)	V_b (%)	E (MPa)	N
HRA ELL 1	404	81	81	2.455	2.361	16.8	3.8	13.0	2,930	600
HRA ELL 2	404	81	80	2.455	2.363	16.7	3.7	13.0	2,720	150
HRA EHL 1	404	80	81	2.452	2.326	18.1	5.1	13.0	2,560	2,100
HRA EHL 2	404	81	81	2.452	2.335	17.7	4.8	12.9	3,320	100
HRA EHL 3	404	81	81	2.452	2.309	18.7	5.8	12.9	2,310	1,200
HRA ELO 1	404	80	81	2.420	2.344	17.4	3.1	14.3	1,630	27,750
HRA ELO 2	404	81	80	2.420	2.353	17.1	2.8	14.3	1,600	43,150
HRA ELO 3	404	81	81	2.420	2.332	17.8	3.6	14.2	1,440	44,100
HRA EHO 2	404	81	80	2.419	2.305	18.8	4.7	14.1	2,750	750
HRA ELH 2	404	81	79	2.382	2.328	18.0	2.3	15.7	1,190	82,000
HRA EHH 2	404	81	80	2.379	2.269	20.1	4.6	15.5	1,840	18,150

Table D.5 - Data for the HRA SBS Modified Beams Used in the Main Test Programme.

	Length (mm)	Width (mm)	Height (mm)	G_{mm}	G_{mb}	VMA (%)	V_v (%)	V_b (%)	E (MPa)	N
HRA SLL 2	404	80	80	2.448	2.350	17.2	4.0	13.2	1,220	163,650
HRA SHH 2	404	80	81	2.381	2.284	19.5	4.1	15.4	940	372,850

Table D.6 - Data for the DBM 50 pen Beams Used in the Main Test Programme.

	Length (mm)	Width (mm)	Height (mm)	G_{mm}	G_{mb}	VMA (%)	V_v (%)	V_b (%)	E (MPa)	N
DBM 5LL 1	404	81	80	2.587	2.437	15.2	5.8	9.4	3,140	1,250
DBM 5LL 2	404	81	81	2.587	2.440	15.1	5.7	9.4	3,010	1,550
DBM 5LL 3	404	80	81	2.587	2.423	15.7	6.3	9.4	3,390	1,600
DBM 5HL 1	404	80	81	2.587	2.402	16.5	7.2	9.3	2,660	150
DBM 5HL 3	404	81	80	2.587	2.406	16.3	7.0	9.3	2,820	550
DBM 5LO 1	404	79	81	2.543	2.465	14.3	3.1	11.2	3,000	9,200
DBM 5LO 2	404	81	80	2.543	2.476	13.9	2.6	11.3	2,580	5,650
DBM 5LO 3	404	80	80	2.543	2.452	14.7	3.6	11.1	3,130	2,750
DBM 5HO 1	404	80	81	2.543	2.413	16.1	5.1	11.0	2,670	1,450
DBM 5HO 2	404	81	81	2.543	2.415	16.0	5.0	11.0	2,520	2,500
DBM 5HO 3	404	81	79	2.543	2.401	16.5	5.6	10.9	2,690	3,200
DBM 5LH 1	404	81	81	2.496	2.436	15.3	2.4	12.9	2,740	7,450
DBM 5LH 2	404	80	81	2.496	2.449	14.8	1.9	12.9	3,200	3,450
DBM 5LH 3	404	81	81	2.496	2.439	15.2	2.3	12.9	2,840	3,600
DBM 5HH 1	404	81	80	2.496	2.386	17.0	4.4	12.6	2,620	7,100
DBM 5HH 2	404	80	80	2.496	2.394	16.7	4.1	12.6	2,620	7,100
DBM 5HH 3	404	81	80	2.496	2.372	17.5	5.0	12.5	2,300	2,850

Table D.7 - Data for the DBM 100 pen Beams Used in the Main Test Programme.

	Length (mm)	Width (mm)	Height (mm)	G_{mm}	G_{mb}	VMA (%)	V_v (%)	V_b (%)	E (MPa)	N
DBM 1LL 1	404	80	80	2.584	2.437	15.2	5.7	9.5	1,500	165,000
DBM 1LL 2	404	80	80	2.584	2.460	14.4	4.8	9.6	2,530	1,500
DBM 1LL 3	404	81	80	2.584	2.444	15.0	5.4	9.6	2,150	2,250
DBM 1HL 1	404	81	81	2.586	2.399	16.6	7.2	9.4	2,310	3,000
DBM 1HL 2	404	81	80	2.586	2.405	16.4	7.0	9.4	1,540	135,000
DBM 1HL 3	404	80	80	2.586	2.400	16.5	7.2	9.3	2,170	3,650
DBM 1LO 1	404	80	82	2.543	2.453	14.7	3.5	11.2	2,310	3,250
DBM 1LO 2	404	81	80	2.543	2.464	14.3	3.1	11.2	2,490	5,450
DBM 1LO 3	404	82	79	2.543	2.456	14.6	3.4	11.2	1,800	40,800
DBM 1HO 1	404	82	80	2.545	2.412	16.1	5.2	10.9	1,850	36,000
DBM 1HO 2	404	81	80	2.545	2.416	16.0	5.1	10.9	2,050	9,200
DBM 1HO 3	404	80	81	2.545	2.400	16.5	5.7	10.8	2,150	24,450
DBM 1LH 1	404	80	81	2.507	2.437	15.2	2.8	12.4	1,960	48,000
DBM 1LH 2	404	81	81	2.507	2.438	15.2	2.8	12.4	2,060	18,450
DBM 1LH 3	404	81	81	2.507	2.434	15.3	2.9	12.4	1,460	170,050
DBM 1HH 1	404	80	80	2.498	2.387	17.0	4.4	12.6	1,430	176,500
DBM 1HH 2	404	80	79	2.498	2.399	16.6	4.0	12.6	1,780	21,600
DBM 1HH 3	404	80	80	2.498	2.399	16.6	4.0	12.6	1,660	20,900

Table D.8 - Data for the DBM EVA Modified Beams Used in the Main Test Programme.

	Length (mm)	Width (mm)	Height (mm)	G_{mm}	G_{mb}	VMA (%)	V_v (%)	V_b (%)	E (MPa)	N
DBM ELL 2	404	80	79	2.582	2.465	14.3	4.5	9.8	2,600	1,200
DBM ELO 2	404	81	79	2.540	2.485	13.6	2.2	11.4	2,920	750
DBM EHO 2	404	80	80	2.537	2.404	16.4	5.2	11.2	2,860	1,300
DBM ELH 2	404	80	80	2.492	2.457	14.5	1.4	13.1	3,320	50
DBM EHH 2	404	79	80	2.495	2.431	15.4	2.6	12.8	2,760	400

Table D.9 - Data for the DBM SBS Modified Beams Used in the Main Test Programme.

	Length (mm)	Width (mm)	Height (mm)	G_{mm}	G_{mb}	VMA (%)	V_v (%)	V_b (%)	E (MPa)	N
DBM SLL 1	404	80	80	2.591	2.524	12.2	2.6	9.6	1,550	95,400
DBM SLL 2	404	80	80	2.591	2.538	11.7	2.0	9.7	1,960	59,600
DBM SLL 3	404	80	80	2.591	2.531	12.0	2.3	9.7	2,030	44,500
DBM SLH 2	404	79	80	2.503	2.447	14.9	2.2	12.7	1,240	146,050
DBM SHH 2	404	80	82	2.499	2.398	16.6	4.0	12.6	1,140	191,200

APPENDIX E

CRACK PROPAGATION PHOTOGRAPHS

This appendix contains the 47 images which were obtained during the crack propagation test programme. The caption below each image is the specimen identification and is made up as follows:

HRA 5 L L 1

The first 3 letters refer to the mixture type:

HRA	Hot Rolled Asphalt
DBM	Dense Bitumen Macadam

The next character refers to the type of bitumen:

5	50 pen
1	100 pen
E	EVA modified
S	SBS modified

The next letter refers to the void content:

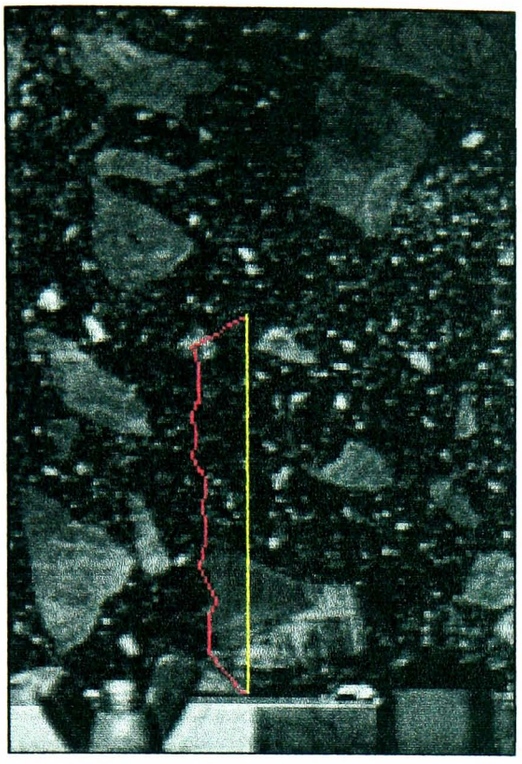
H	High void content
L	Low void content

The next letter refers to the binder content:

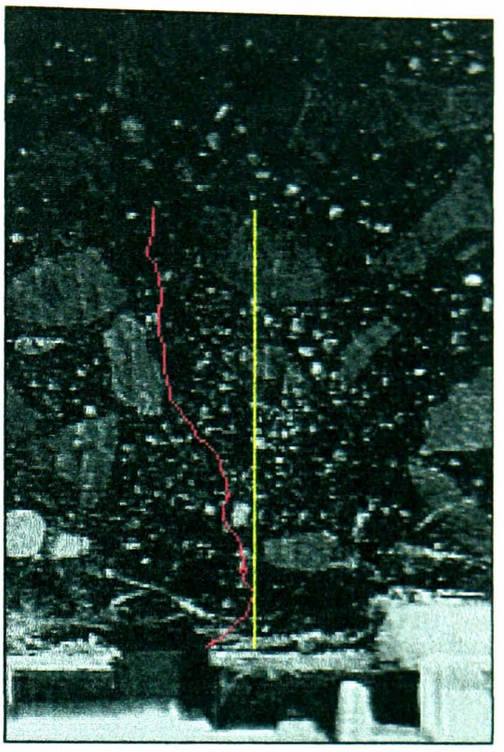
H	Optimum plus 1%
O	Optimum
L	Optimum minus 1%

The last number refers to the replicate number:

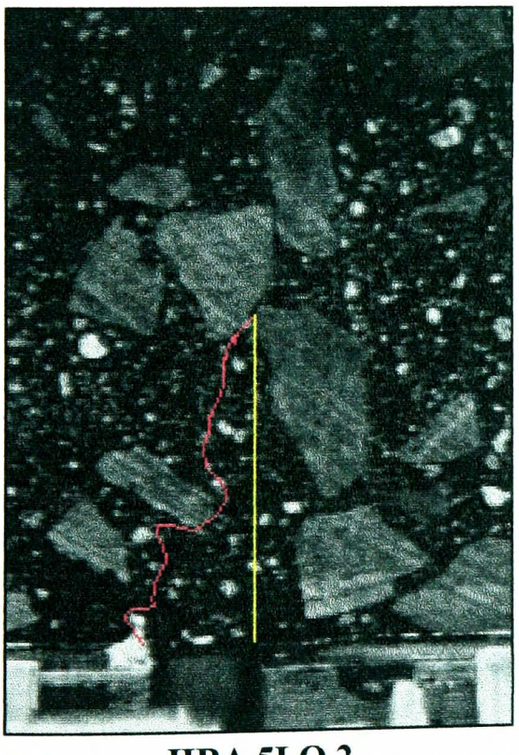
1	1st Replicate
2	2nd Replicate
3	3rd Replicate



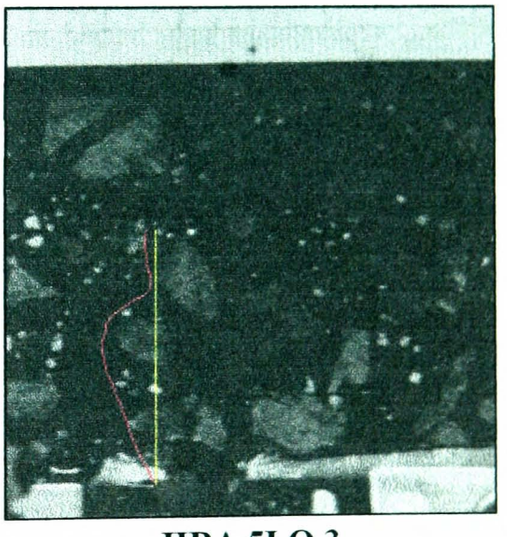
HRA 5LL 1



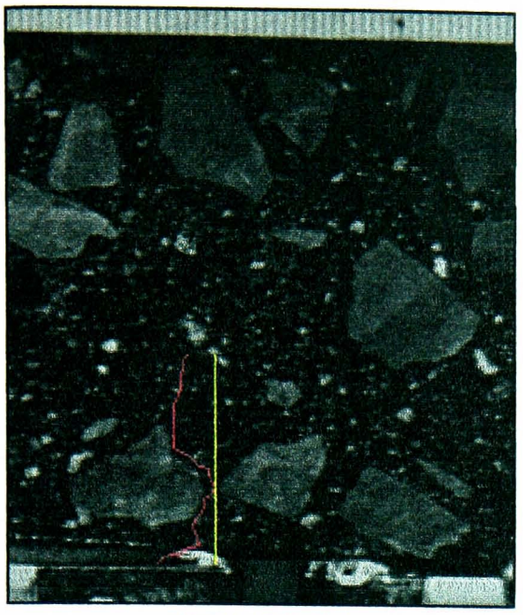
HRA 5LO 1



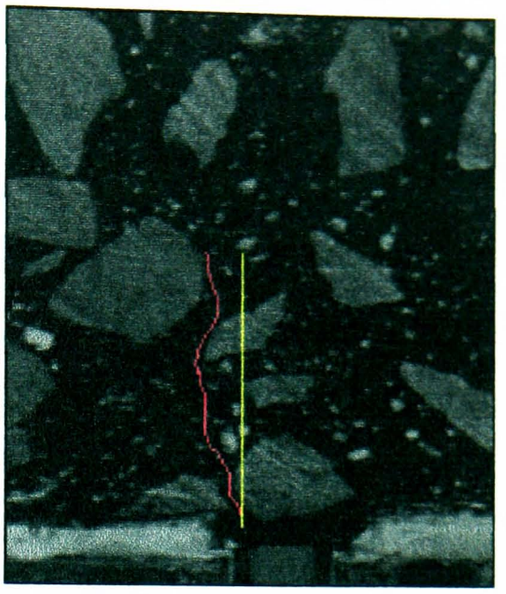
HRA 5LO 2



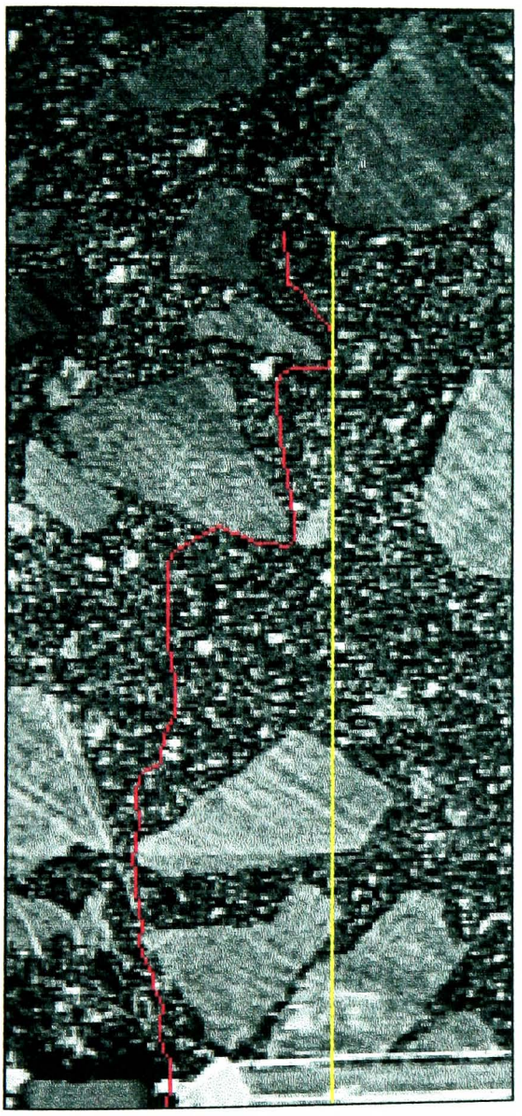
HRA 5LO 3



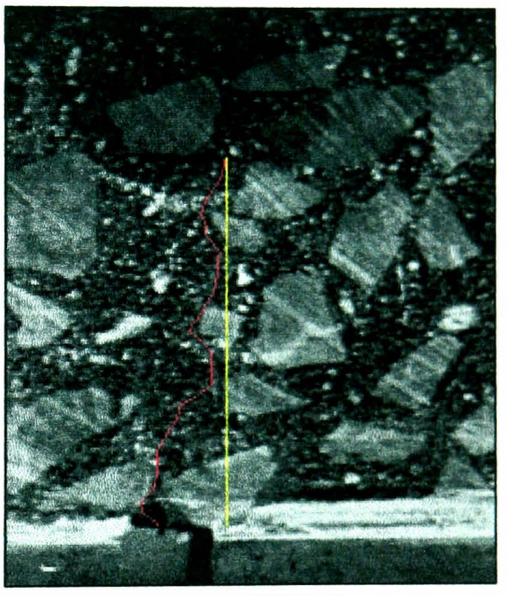
HRA 5LH 1



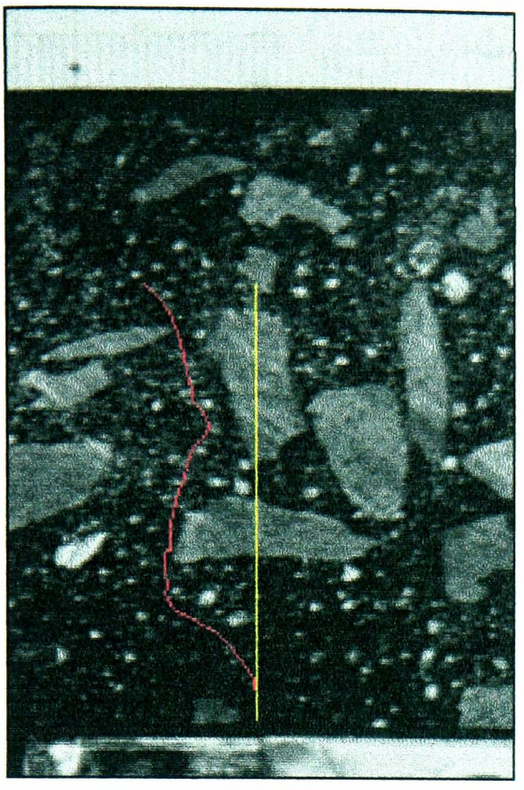
HRA 5LH 2



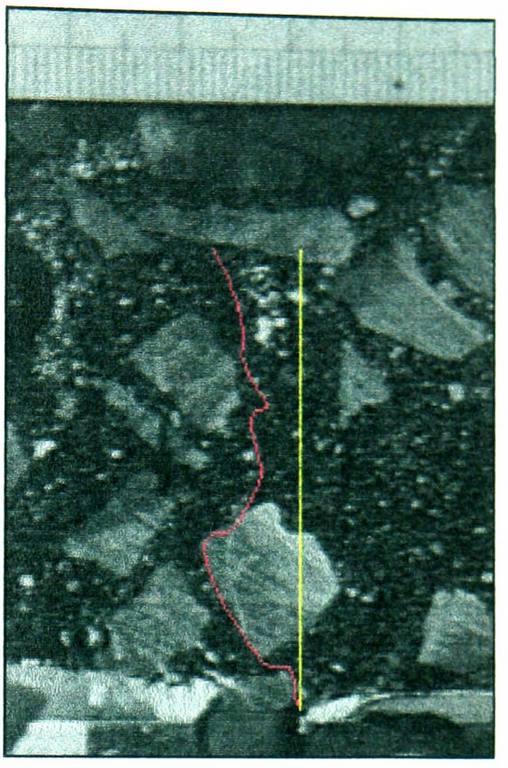
HRA 5HL 3



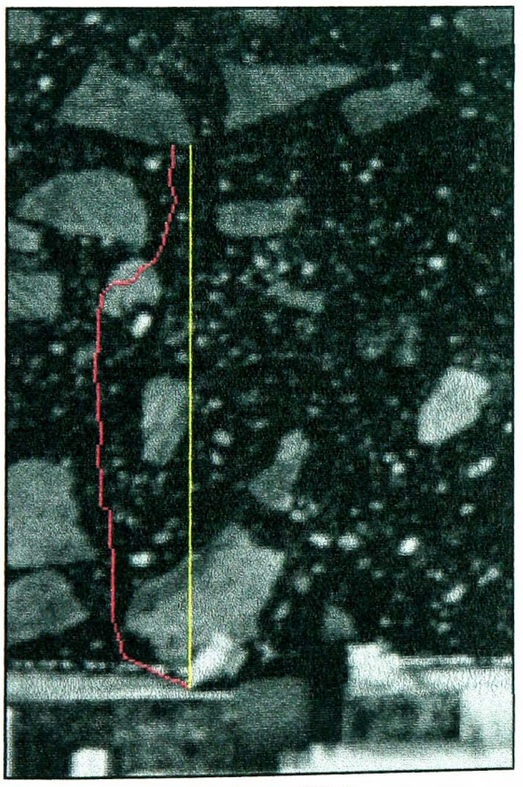
HRA 5HO 1



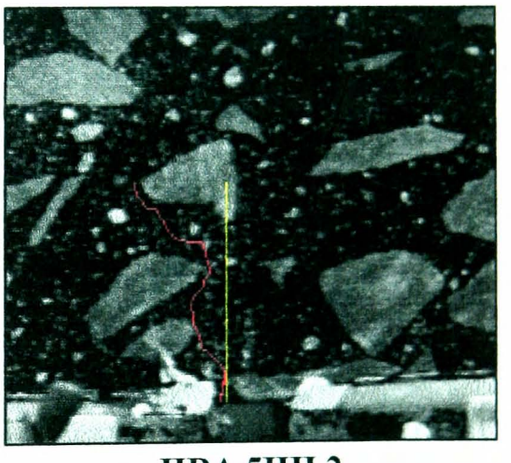
HRA 5HO 2



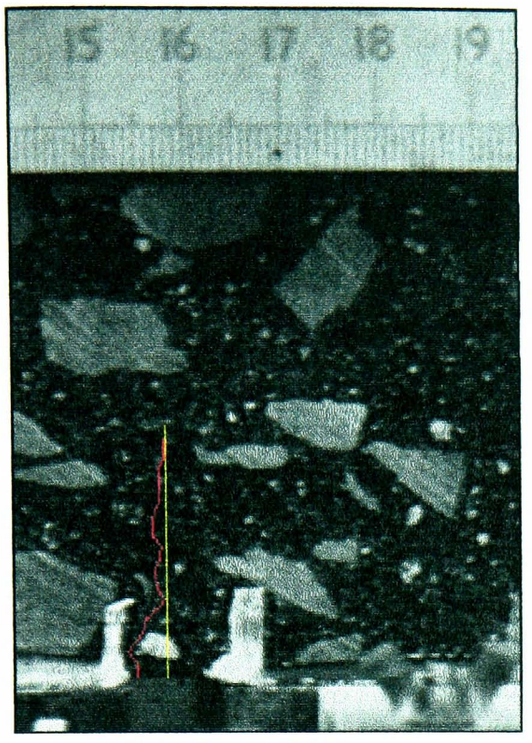
HRA 5HO 3



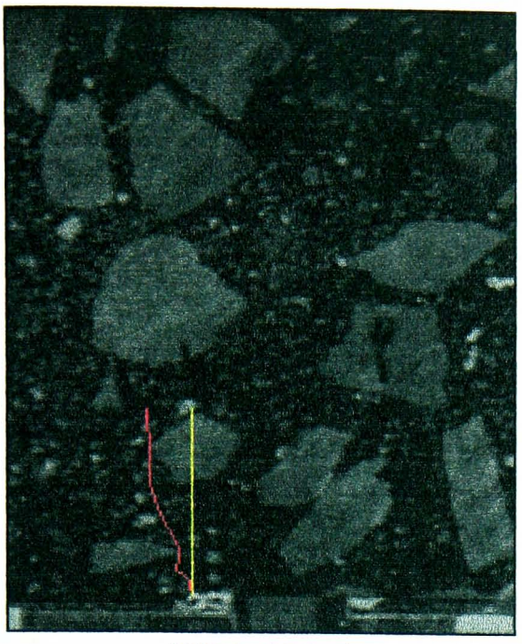
HRA 5HH 1



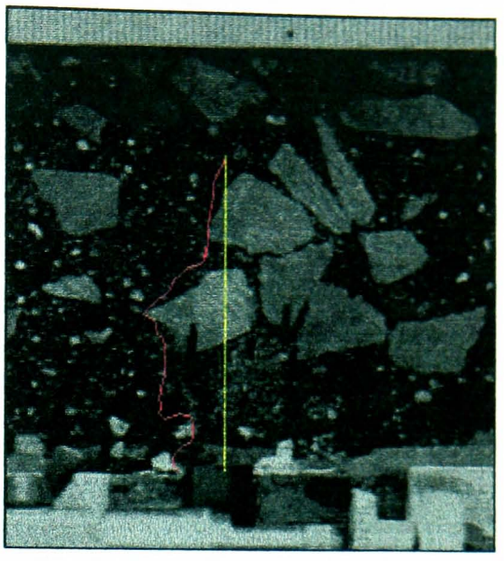
HRA 5HH 2



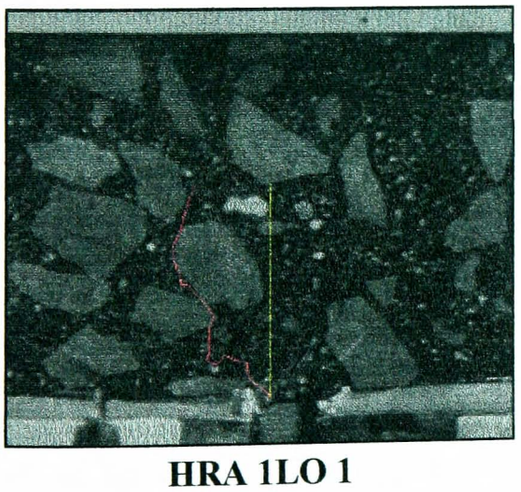
HRA 5HH 3



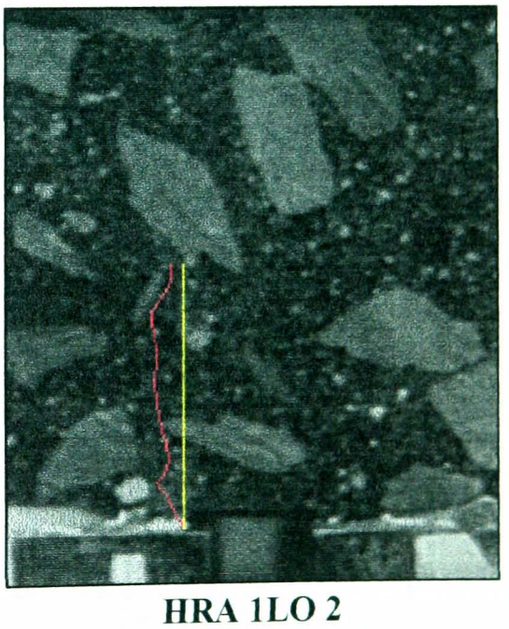
HRA 1LL 1



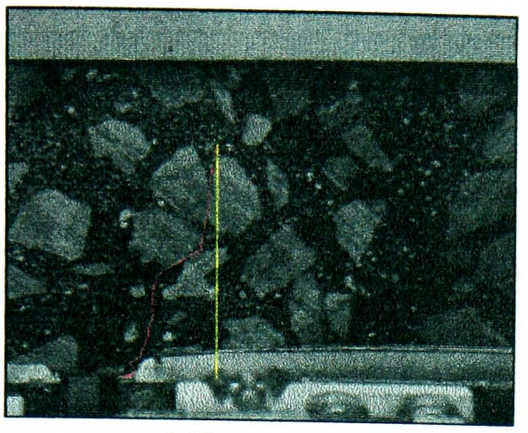
HRA 1LL 2



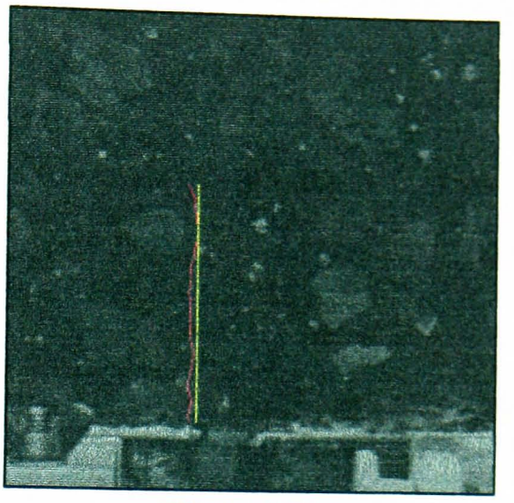
HRA 1LO 1



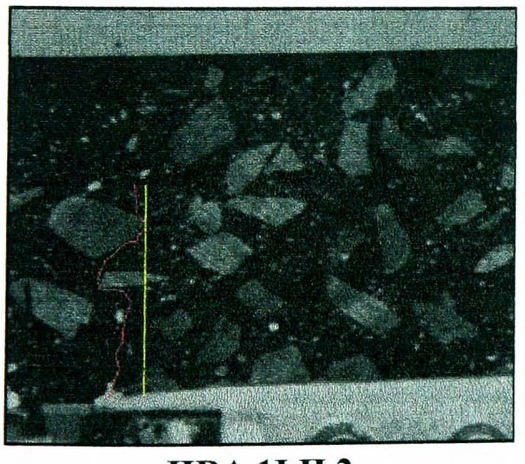
HRA 1LO 2



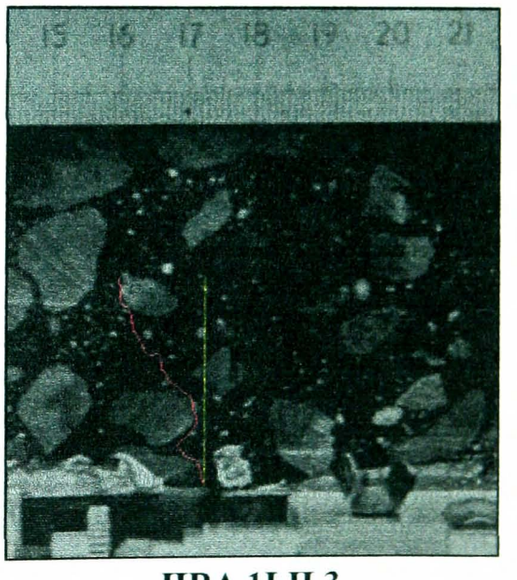
HRA 1LO 3



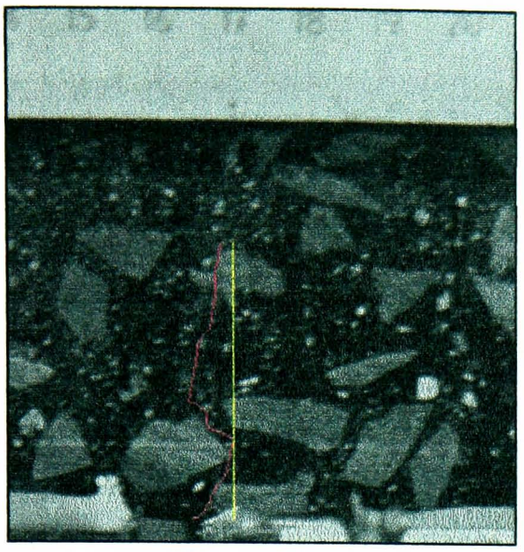
HRA 1LH 1



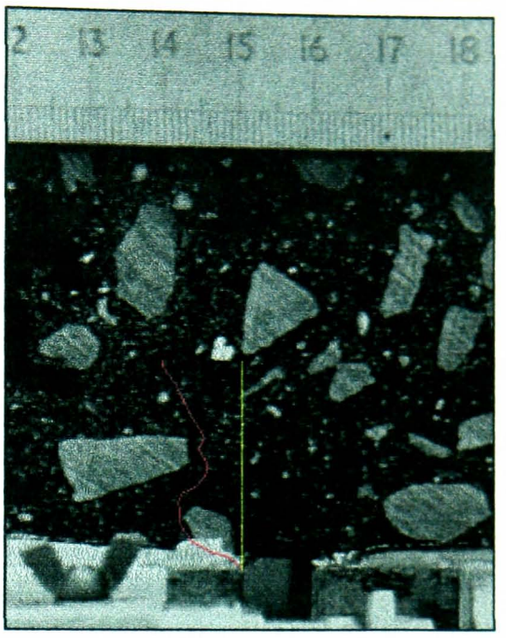
HRA 1LH 2



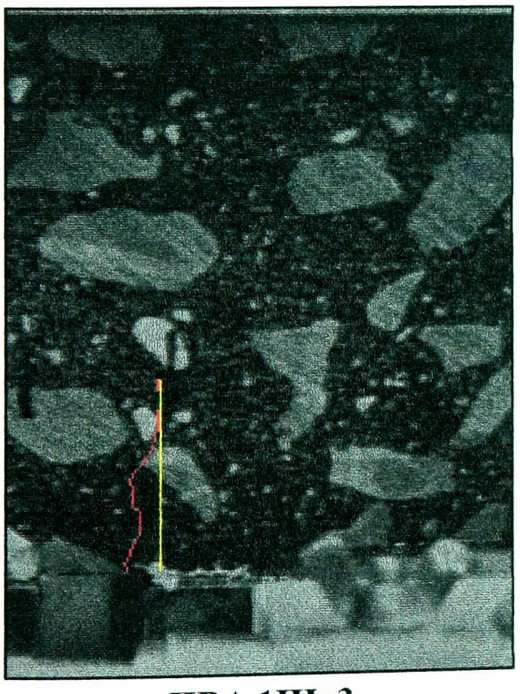
HRA 1LH 3



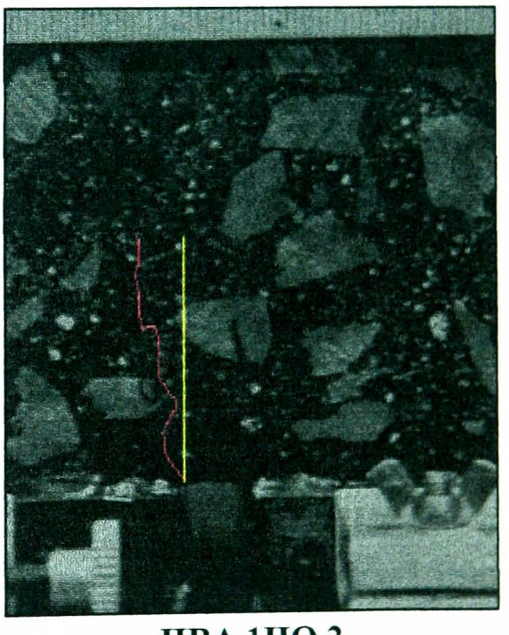
HRA 1HL 1



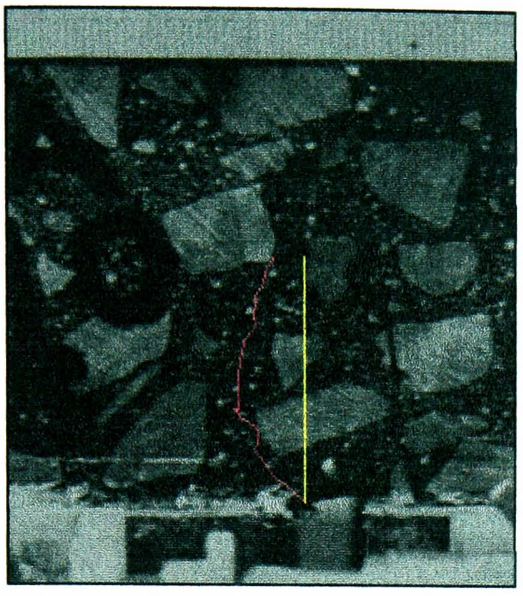
HRA 1HL 2



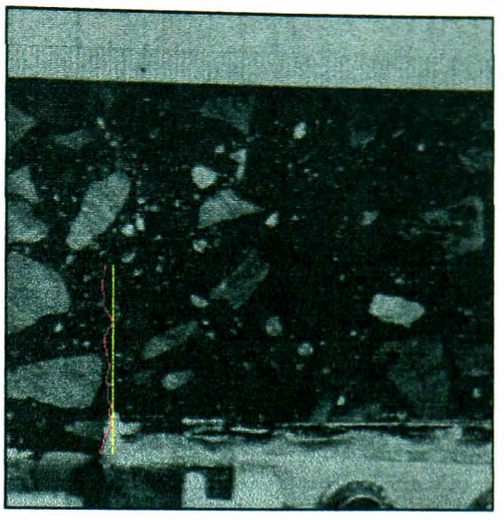
HRA 1HL 3



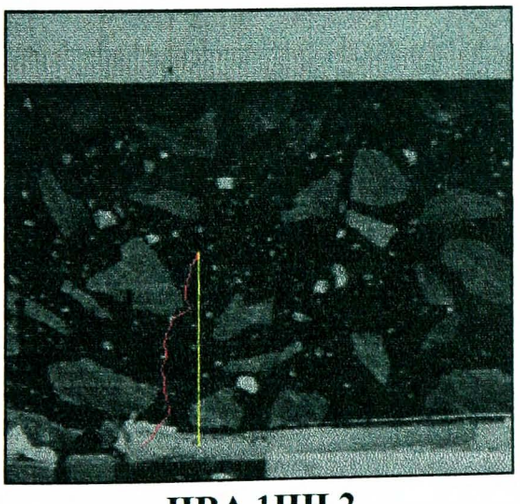
HRA 1HO 2



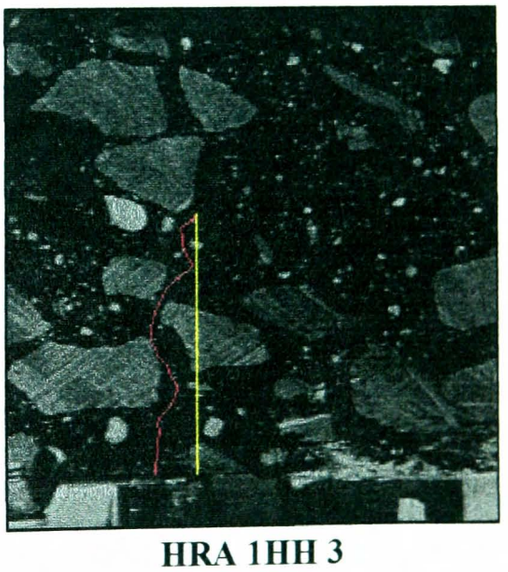
HRA 1HO 3



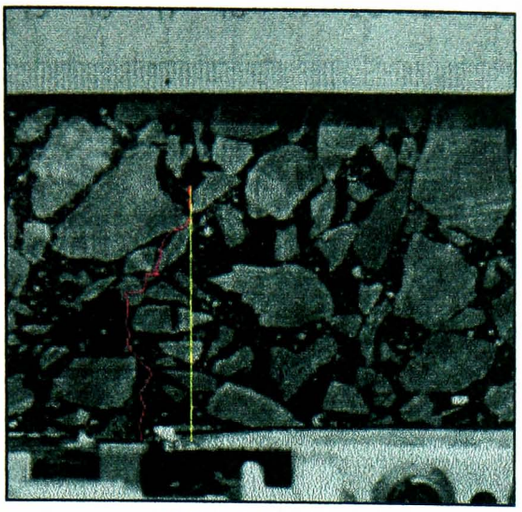
HRA 1HH 1



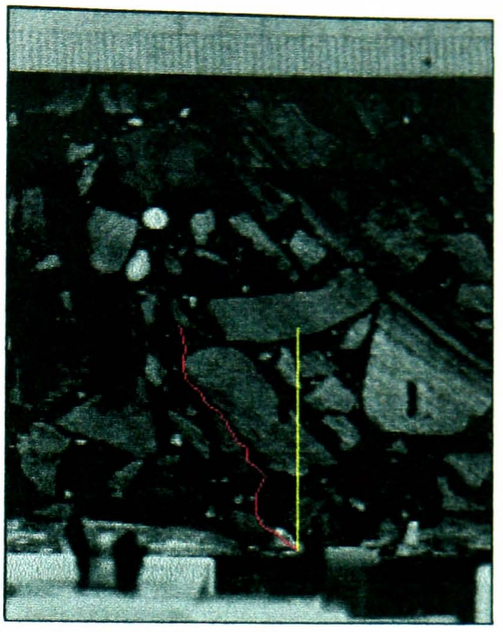
HRA 1HH 2



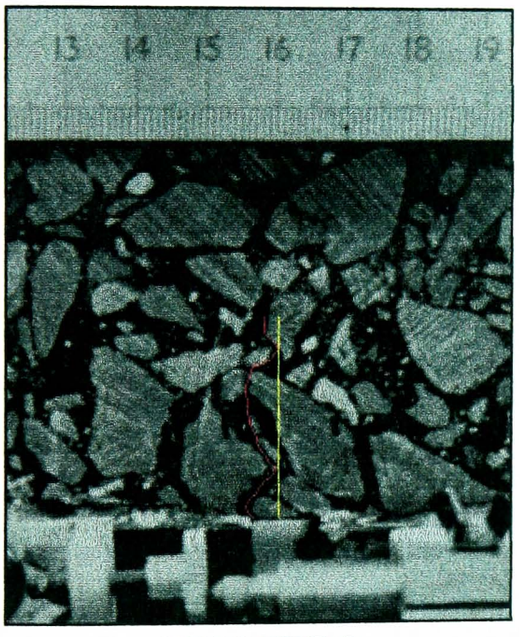
HRA 1HH 3



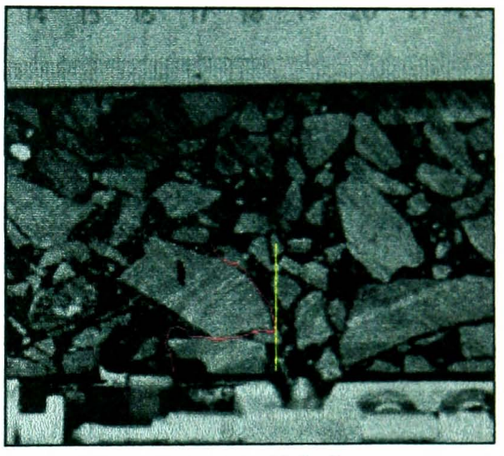
DBM 5LO 2



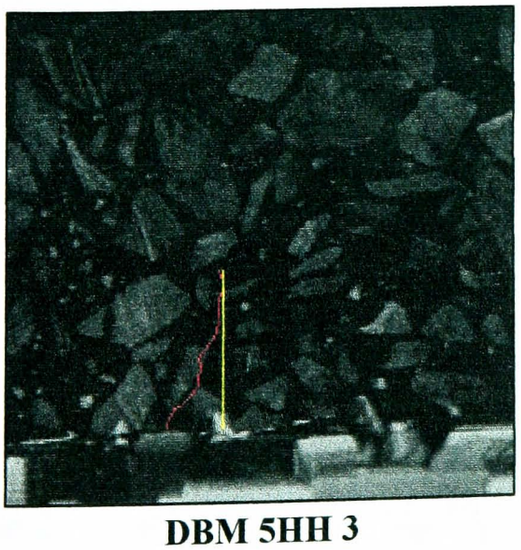
DBM 5LH 3



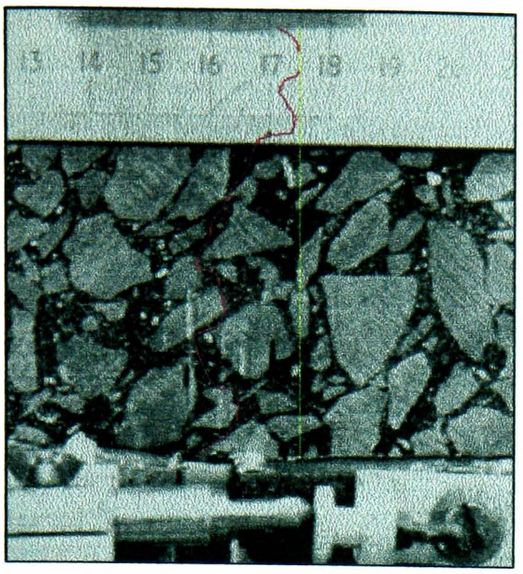
DBM 5HO 2



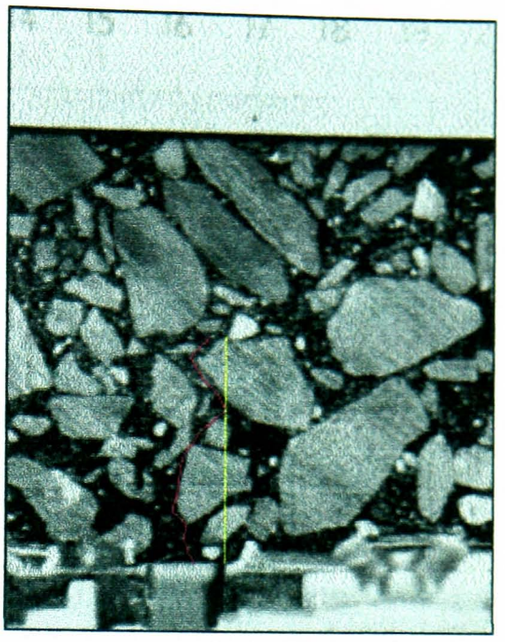
DBM 5HO 3



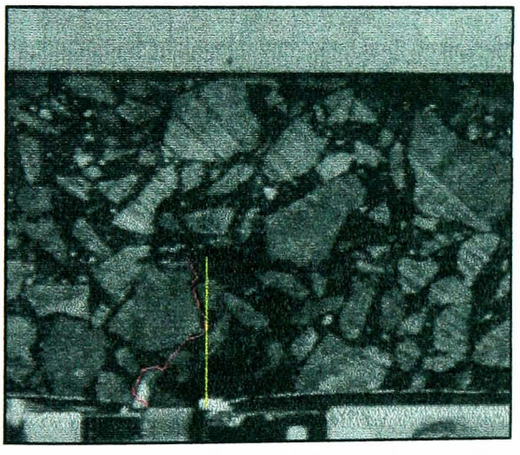
DBM 5HH 3



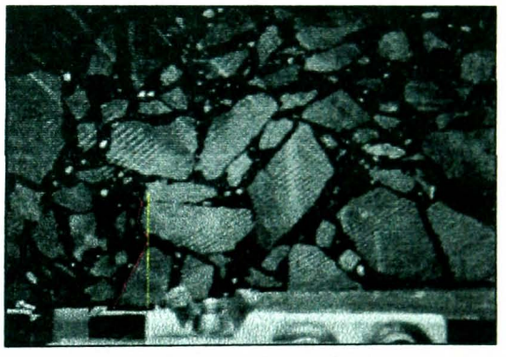
DBM 1LL 1



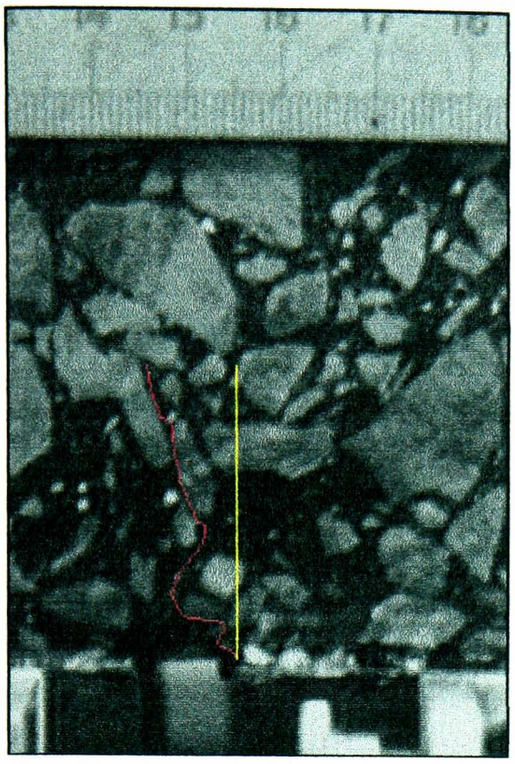
DBM 1LL 3



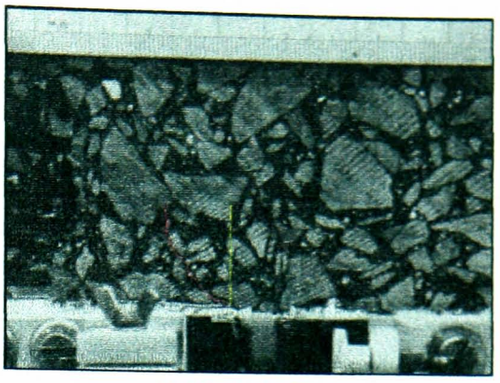
DBM 1LO 1



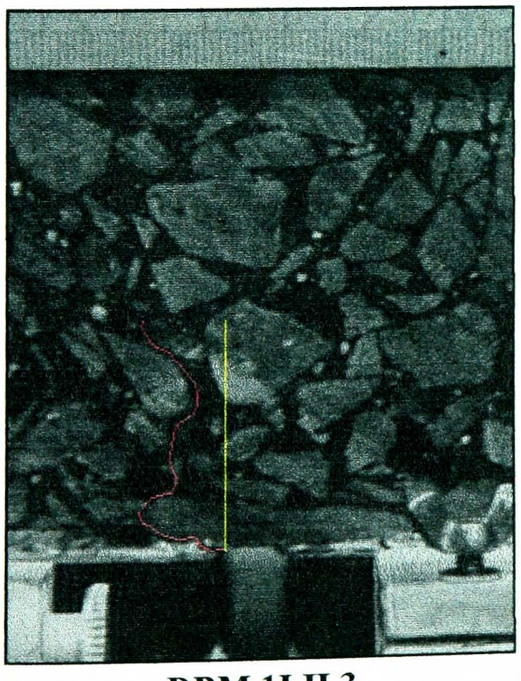
DBM 1LO 3



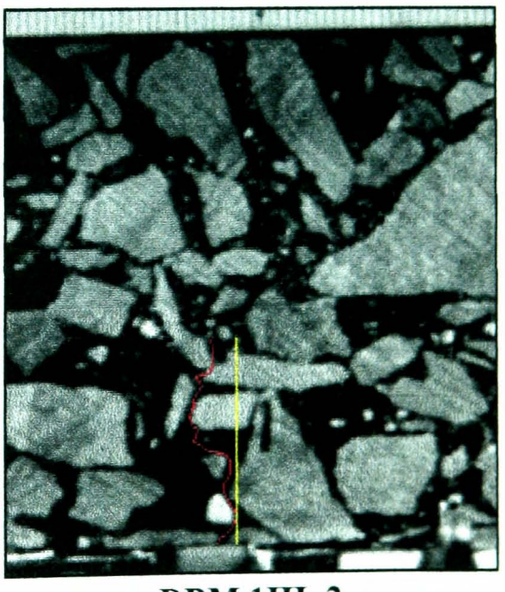
DBM 1LH 1



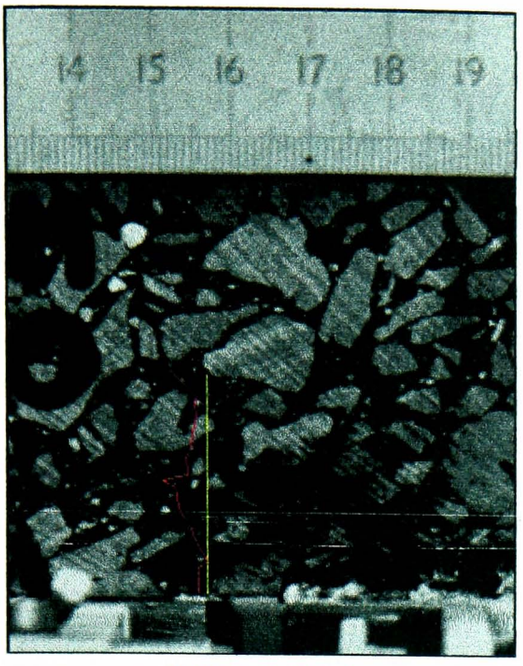
DBM 1LH 2



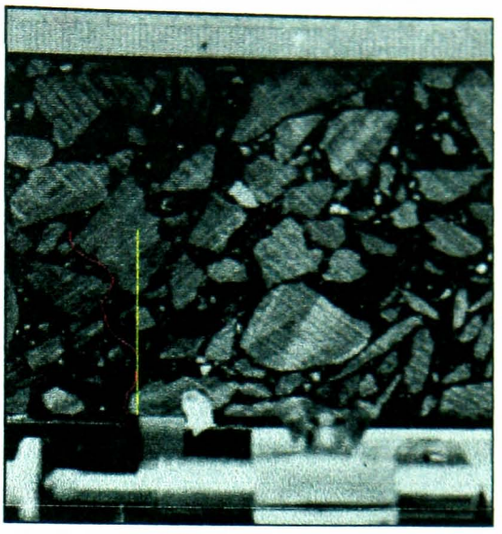
DBM 1LH 3



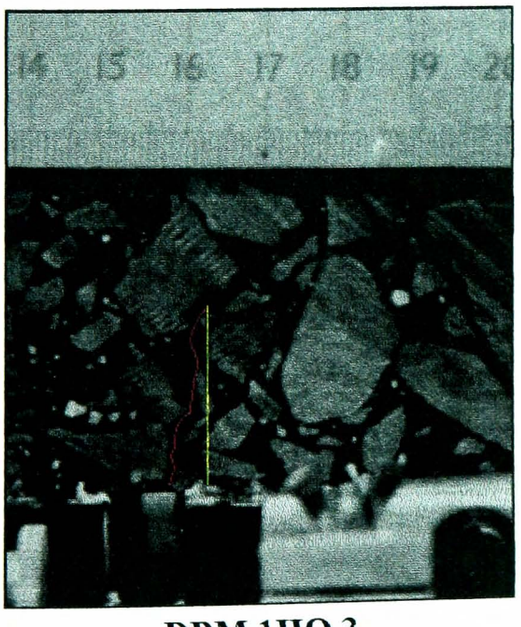
DBM 1HL 2



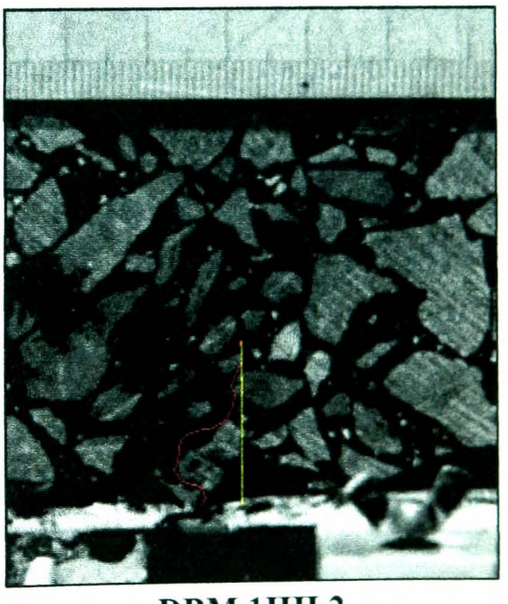
DBM 1HO 1



DBM 1HO 2



DBM 1HO 3



DBM 1HH 2



DBM 1HH 3